Calcareous nannoplankton evolution and the Paleogene greenhouse to icehouse climate-mode transition

Cherry Newsam

Department of Earth Sciences
UCL

Thesis submitted for the degree of Doctor of Philosophy
August 2016

I, Cherry Newsam, confirm that the work presented in this thesis is my own. Where information has been derived from other sources, I confirm that this has been indicated in the thesis.

Signed:

Abstract

This thesis addresses calcareous nannoplankton evolutionary and palaeoecological response across the Paleogene greenhouse to icehouse transition using newly drilled material from Sites U1408 and U1411 (IODP Expedition 342) in the North Atlantic. Calcareous nannoplankton were the dominant oceanic phytoplankton group in the early Paleogene yet declined in diversity and underwent significant assemblage restructuring through the middle Eocene to early Oligocene, coinciding with major climatic reorganisation. However the structure and timing of this nannoplankton response is poorly constrained due to few records of appropriate stratigraphic resolution. Here, exceptionally preserved calcareous nannofossils from stratigraphically expanded packages of Paleogene clay-rich drift sediments from IODP Expedition 342 are used to document diversity loss and population shifts in order to interpret the relationship between plankton evolution and palaeoclimatic and palaeoceanographic change in the North Atlantic across this key interval, with focus on abrupt climatic change at the Middle Eocene Climatic Optimum (MECO) and the Eocene-Oligocene transition (EOT). Results indicate low speciation rates combined with relatively high extinction rates drove calcareous nannoplankton diversity loss through this interval and palaeoecological analysis highlights three key intervals; middle Eocene stability, incorporating muted assemblage response to transient warming at the MECO, the late Eocene transitional phase and the EOT and early Oligocene population restructuring, with major assemblage shifts controlled by intensified surface water cooling and increased nutrient availability. Palaeoclimatic and palaeoceanographic changes through this transition led to reduced optimal habitat space for this phytoplankton group resulting in decline and extinction in many taxa and the proliferation of select opportunists at the onset of the icehouse world.

Acknowledgements

First of all I am extremely grateful to my supervisor Paul Bown for giving me the opportunity to work on this project and for his support and guidance. This PhD would not have been possible without his help, advice and many invaluable discussions. I'd especially like to thank Paul for providing such beautifully preserved nannofossils to work with!

I also owe thanks to both my co-supervisors Bridget Wade, for constant encouragement and advice during my PhD and Tom Dunkley Jones, for sharing his EOT expertise and allowing the use of his data within my thesis. Many thanks as well to Jim Davy for always being on hand to help throughout.

I would like to acknowledge my CASE partner Petrostrat Ltd., with particular thanks to Dave Rutledge and Simon Cole who welcomed me for work experience in Conwy and provided an insight into industry life.

I'm grateful to many people who have shared their expertise throughout this process and I would especially like to thank all those who have provided data which is presented or referenced in this thesis. In particular I would like to acknowledge IODP Expedition 342 shipboard and shore-based participants.

There are far too many people to name from UCL who have contributed to many great PhD years; all of the micropalaeontologists, everyone from the KLB lab coffee club and the PhD students in my office throughout the years – thank you all. Amy especially, I can't thank you enough for always being there from day one to the end.

Finally I am extremely grateful to all my family and friends who have provided continual encouragement over the past four years and above all I thank Mike for his endless support, patience and confidence in me.

This research was funded by a UK Natural Environment Research Council (NERC) studentship and a CASE partnership with Petrostrat Ltd.. Samples were provided by the Integrated Ocean Drilling Program (IODP).

Contents

List of figures

Chapter 3: Calcareous nannoplankton population dynamics and evolution during the Middle Eocene Climatic Optimum in the North Atlantic (IODP Site U1408) 101

Chapter 7: Middle Eocene to early Oligocene calcareous nannoplankton population trends: a proxy for long term surface water palaeoenvironmental change in the North Atlantic 180

List of tables

List of plates

Chapter 1

Introduction

1.1 Overview

The Paleogene greenhouse to icehouse climate-mode transition was a profound interval of long term climatic change in the Cenozoic during which the marine and terrestrial realms saw major shifts in physical, chemical and biological parameters. Following peak warmth during the Early Eocene Climatic Optimum (EECO) (Zachos et al., 2008) there was a protracted period of global cooling through the middle and late Eocene (Zachos et al., 2008, 2001), which culminated at the Eocene-Oligocene transition (EOT) with a sharp cooling and the growth of major Antarctic ice sheets (Coxall and Pearson, 2007). Declining atmospheric carbon dioxide (CO_2) has been proposed as the fundamental driver of this shift in global climatic state from a warm 'greenhouse' world to an 'icehouse' world with glaciated polar regions (DeConto and Pollard, 2003a; Pagani et al., 2011, 2005; Pearson et al., 2009), but other factors such as the opening of the Southern Ocean gateways (Scher and Martin, 2006; Sijp et al., 2014) and orbital forcing are also considered to have amplified the effects (DeConto and Pollard, 2003a). The Eocene cooling trend, ~51-34 million years ago (Ma), was punctuated by transient warming and cooling intervals superimposed on top of the long term background cooling trend (Bohaty and Zachos, 2003; Sexton et al., 2011; Zachos et al., 2001), with the Middle Eocene Climatic Optimum (MECO) event being a particularly notable warming event at ~40 Ma and intensified cooling and ice growth at the EOT. Substantial oceanographic reorganisation took place throughout this long term interval with intensified thermohaline circulation generated by strengthened latitudinal thermal gradients and ocean 'spin up' with elevated wind driven upwelling (Miller et al., 2009) and the development of modern day ocean structure was established by the early Oligocene (Katz et al., 2011).

The high level of climatic and oceanographic change during the Eocene was accompanied by significant marine biotic change, including declining diversity in calcareous plankton groups, high turnover in radiolarians and putative diversity increase in diatoms (Bown, 2005b; Ezard et al., 2011; Kamikuri et al., 2012; Rabosky and

Sorhannus, 2009). The turnover and diversity loss in the major early Paleogene phytoplankton group, calcareous nannoplankton, was particularly profound (Bown et al., 2004). Calcareous nannoplankton are haptophyte algae that produce a cell wall covering of microscopic calcitic plates. These plates, coccoliths, are found preserved throughout the geographically widespread pelagic sedimentary record and provide a wealth of palaeoclimatic and palaeoceanographic information. Individual nannoplankton species or groups exhibit particular preferences for specific ecological niches (Winter et al., 1994) and so reconstructing past environmental conditions using quantitative abundance data is a particularly valuable application (Haq and Lohmann, 1976; Villa et al., 2008). Calcareous nannoplankton appear to have been the dominant oceanic phytoplankton group in the early Paleogene, yet declined in diversity and underwent significant assemblage restructuring throughout the greenhouse to icehouse transition (Aubry, 1992; Bown et al., 2004). A detailed understanding of the structure, timing and cause of this diversity decline has been lacking and records of assemblage response are limited, although the gross trends broadly correlate to palaeoclimatic shifts in low and high resolution studies (Bown et al., 2004; Dunkley Jones et al., 2008; Villa et al., 2008). The principal objective of this research is to address this issue and specifically to produce a detailed record of nannoplankton diversity and palaeoecological response through this interval, alongside comparable records of environmental proxies.

In order to achieve this objective we utilised new ocean drilling material from Integrated Ocean Drilling Program (IODP) Expedition 342. IODP Expedition 342 drilled a series of sites in the Northwest Atlantic ocean, targeting expanded packages of Paleogene drift sediments that provide continuous stratigraphic records with high sedimentation rates. The clay-rich nature of these drift sediments located at mid depths, high above the calcite compensation depth (CCD), has resulted in exceptionally well preserved calcareous microfossils, allowing for high quality diversity and abundance records. The IODP Expedition 342 middle Eocene to late Oligocene successions represent some of the most complete, stratigraphically expanded and well preserved sections yet recovered for this time interval and are ideal for addressing the objective of this research. Furthermore, the North Atlantic Ocean in general is a relatively untapped source of Paleogene palaeoclimatic records and the expedition location at relatively high latitudes and near the flow-path of both deep and shallow water currents is well positioned to document Eocene climate change.

The aims of this thesis are to describe records of calcareous nannoplankton evolutionary and palaeoecological response to the greenhouse to icehouse transition, primarily using successions recovered by IODP Expedition 342. The main records provide a ~13 million year long time series record of quantitative nannoplankton data from a near-continuous composite section using Sites U1408 and U1411. A sampling resolution ranging from ~10-35 thousand years (kyr) allows us to investigate the evolution of surface water environments through this interval at high resolution, to investigate the relationship between biotic evolution and palaeoclimatic change and to test for differences between background- and event-level biotic change, in particular using the MECO and EOT as model intervals of relatively abrupt climatic change.

1.2 Paleogene greenhouse to icehouse transition

The Eocene epoch is characterised as a climatically dynamic interval incorporating the transition from a warm, ice free greenhouse world into a cold icehouse world with expanded ice sheets on Antarctica (Tripati et al., 2005; Villa et al., 2008; Zachos et al., 2001). The early Eocene exhibited sustained warm global temperatures, with a temperature maximum occurring at the EECO, 53-51 Ma (Sexton et al., 2006; Zachos et al., 2008), with sea surface temperatures greater than 30^{o}C in the tropics (Pearson et al., 2007). Global compilations highlight a 17 million year (myr) long term climatic cooling into the earliest Oligocene, represented by an increase in the deep sea benthic foraminiferal oxygen isotope ($\delta^{18}O$) records by 3 per mil (‰) (Figure 1.1; Cramer et al., 2009; Zachos et al., 2008, 2001) but also displayed by other proxies, such as benthic foraminiferal Mg/Ca records (Lear et al., 2000). However, recent studies indicate long term cooling may have been a high latitude phenomenon, with low latitude geochemical proxy records ($\delta^{18}O$ and TEX_{86}) indicating stable warm surface ocean temperatures throughout the Eocene (Bijl et al., 2009; Pearson et al., 2007) and distinct latitudinal temperature gradients (Inglis et al., 2015). Across the Paleogene greenhouse to icehouse transition an overall deepening in the CCD is observed analogous to the long term decline in deep sea $\delta^{18}O$ (Pälike et al., 2012). Fluctuations in the CCD during this interval (Figure 1.1) include prolonged intervals of deepening associated with carbonate accumulation events (CAEs) and transient shoaling events (Pälike et al., 2012). Changing carbon isotope ($\delta^{13}C$) values through the transition at times when there are CCD variations and $\delta^{18}O$ shifts implies a close coupling between the climatic change and the carbon cycle through this interval (Pälike et al., 2012; Tripati et al., 2005). Records of CO_2, although low resolution, indicate decreasing CO_2 values through the greenhouse to icehouse transition (Beerling and Royer 2011; Figure 1.1) with estimates of 1100 parts per million (ppm) in the middle Eocene to 550 ppm by the early Oligocene (Anagnostou et al., 2016; Pearson et al., 2009). This long term climatic disruption (~50-

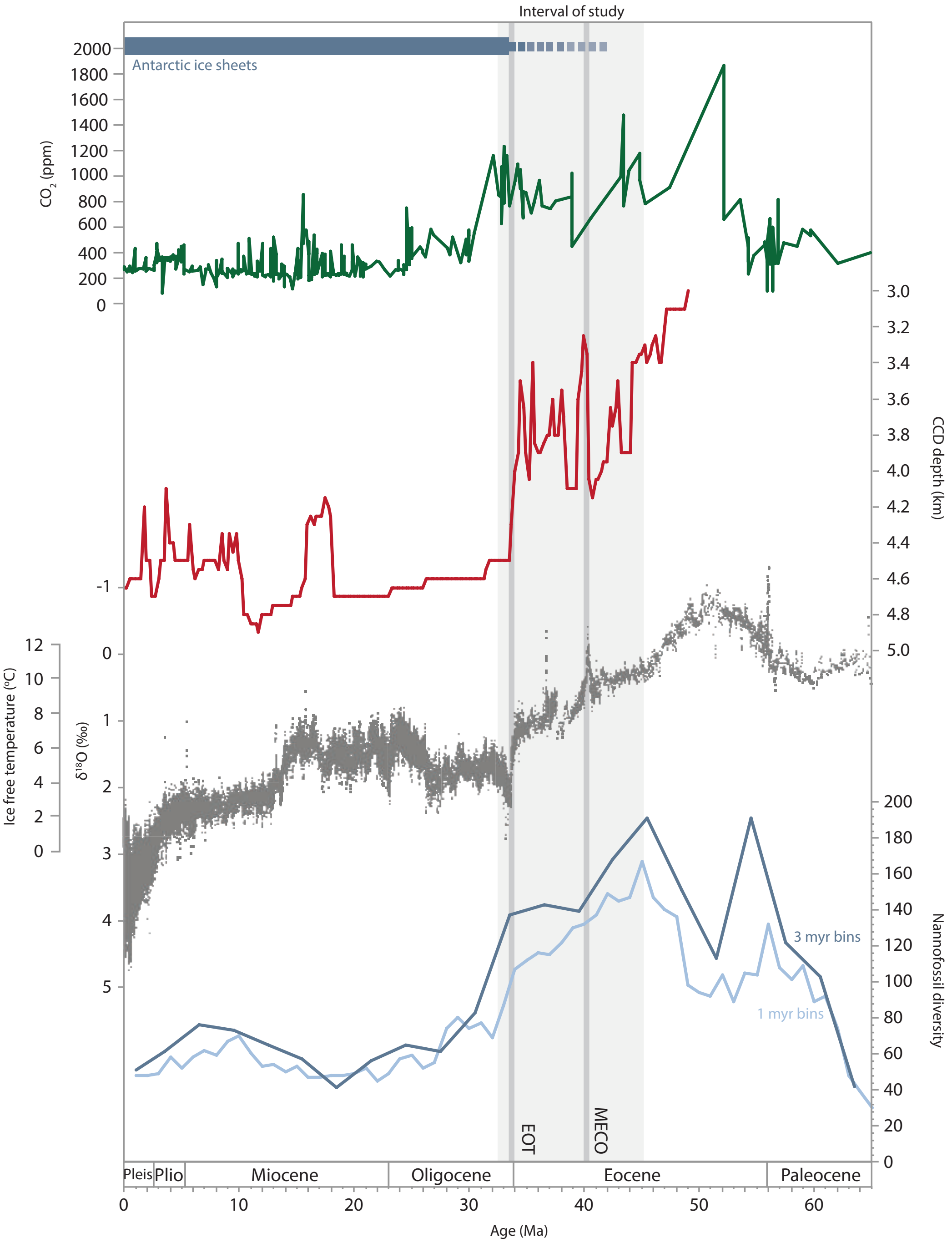

Figure 1.1: Cenozoic palaeorecords; a composite global oxygen isotope compilation (5 point moving average) (Cramer et al., 2009; converted to the Geological Timescale 2012; Gradstein et al., 2012), CCD reconstruction (Pälike et al., 2012); CO_2 reconstruction (Beerling and Royer, 2011; nannofossil diversity records shown in one and three million year time bins (Bown et al., 2004; Bown, pers. comm. 2016). The blue bar indicates presence of Antarctic ice sheets with the dashed blue line representing the possible presence of partial or ephemeral ice sheets. The temperature scale next to the oxygen isotope compilation is only applicable to an ice free world. The interval studied in this thesis is highlighted in grey, with key events the MECO and EOT highlighted in dark grey.

30 Ma) led to significant ecological change, with decreased diversity in marine plankton assemblages (Bown et al., 2004; Ezard et al., 2011; Kamikuri et al., 2012; Rabosky and Sorhannus, 2009) due to high turnover and extinction levels, particularly highlighted at the end event, the EOT (Coxall and Pearson, 2007; Pearson et al., 2008). The cause of the climatic cooling and polar ice sheet formation and expansion is primarily considered to be due to decreasing CO_2 levels, from reduced seafloor spreading and increased carbon burial and siliciclastic weathering (Coxall and Pearson, 2007), with values passing a critical threshold between 560 and 840 ppm (DeConto and Pollard, 2003b). Nevertheless, other parameters such as the opening of the Southern Ocean gateways, leading to the isolation of Antarctica and the initiation of the Antarctic Circumpolar Current (ACC) and orbital configuration creating cold austral summers may also have been important forcing factors accentuating cooling and ice growth (DeConto and Pollard, 2003a; Scher and Martin, 2006; Sijp et al., 2014). Global oxygen and carbon isotope compilations (Cramer et al., 2009; Zachos et al., 2008, 2001) provide a reference reflecting broad-scale Paleogene climatic changes and climatic variability on different timescales, highlighting short significant pulses of warming and cooling interspersed through the long term cooling trend (Bohaty and Zachos, 2003; Miller et al., 1991; Sexton et al., 2006; Villa et al., 2008). Of these significant pulses, two clearly stand out; a transient warming event known as the MECO and the culmination of the climatic cooling at the EOT (Figure 1.2).

1.2.1 Middle Eocene Climatic Optimum (MECO)

The MECO was a transient ocean/atmospheric warming event, globally recognised at ~40 Ma amidst the Eocene cooling trend (Bohaty and Zachos, 2003; Bohaty et al., 2009; Edgar et al., 2010; Sluijs et al., 2013). This reversal in climatic state is highlighted by a negative $\delta^{18}O$ excursion (~1.2 ‰; Bohaty et al., 2009) (Figure 1.2), with temperatures increasing by 4-6^{o}C in the surface and deep waters (Bijl et al., 2010; Bohaty and Zachos, 2003; Bohaty et al., 2009) and peak warming taking place in less than 100 kyr (Bijl et al., 2010; Bohaty et al., 2009; Edgar et al., 2013). Records strongly suggest that the significant climatic change was caused by an increase in CO_2, indicated not only by the rapid significant increase in temperature, but also by the synchronous temporary shoaling of the CCD (Bohaty et al., 2009; Pälike et al., 2012). The source of carbon is unresolved yet proposed mechanisms include increased ridge/arc volcanism and/or metamorphic decarbonation during the Himalayan orogeny (Bohaty and Zachos, 2003). The MECO is often compared to early Paleogene hyperthermals, such as the Paleocene-Eocene Thermal Maximum (PETM), ETM2 and ETM3, yet they exhibit significant

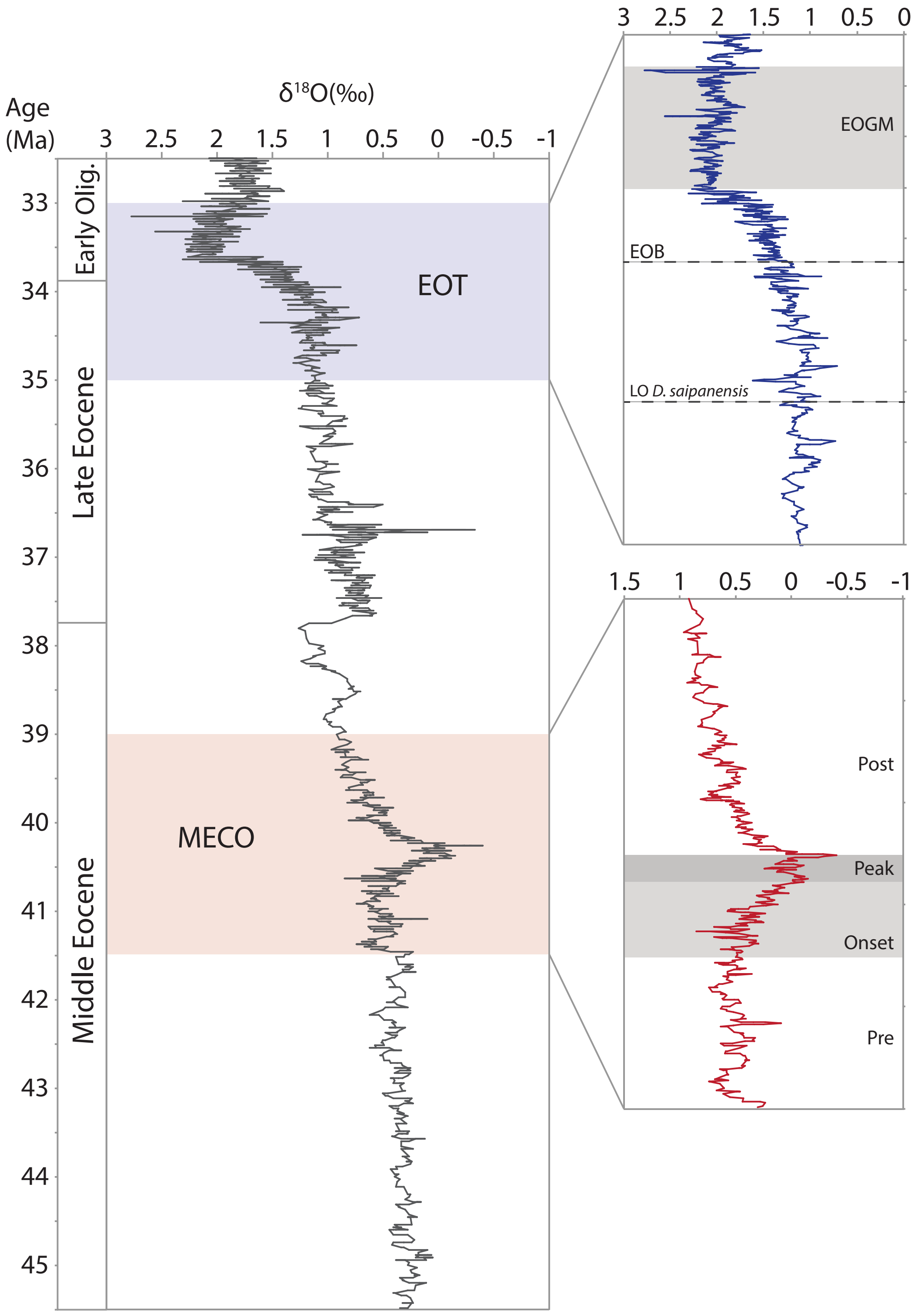

Figure 1.2: Global oxygen isotope compilation (5 point moving average) for the Paleogene greenhouse to icehouse interval studied in this thesis (Cramer et al., 2009; converted to the Geological Timescale 2012 (GTS12); Gradstein et al., 2012). Transient events, the MECO and EOT are highlighted and key intervals within these events are highlighted: the onset and peak MECO, the *Discoaster saipanensis* extinction event (age taken from GTS12), the EOB (age taken from GTS12) and the EOGM.

differences. The MECO is much longer than the early Eocene hyperthermals, sustained over 500-800 kyr (Bohaty et al., 2009; Edgar et al., 2013), with a slower onset and sudden termination in the oxygen isotope excursion, which is not comparable to the short lived early Eocene hyperthermals which exhibit relatively rapid onset (~4 kyr; Zeebe et al., 2016) and recovery (Sexton et al., 2011; Zachos et al., 2005). The lack of a synchronous negative carbon and oxygen isotope excursion through the initial warming further differentiates the MECO from the early Eocene hyperthermals which exhibit a negative $\delta^{13}C$ excursion at the onset, coeval with the negative $\delta^{18}O$ excursion (Sexton et al., 2006; Thomas et al., 2002; Zachos et al., 2005). Across the MECO marine plankton groups exhibit significant response to changing climatic and oceanographic parameters shown by biogeographic range expansions (Bijl et al., 2010; Edgar et al., 2010) and changes in assemblage composition (Luciani et al., 2010; Toffanin et al., 2011; Witkowski et al., 2012). However, due to its recent discovery (Bohaty and Zachos, 2003) the MECO is relatively understudied and requires more detailed analysis.

1.2.2 Eocene-Oligocene transition (EOT)

The EOT marks the culmination of the greenhouse to icehouse long term climatic shift. Considered to have been initiated by CO_2 drawdown (1100 to 760 ppm; Pearson et al., 2009) and subsequent cooling (Pagani et al., 2011; Pearson et al., 2009), the event is characterized by a positive shift in the $\delta^{18}O$ records, which led into the icehouse world (Coxall and Pearson, 2007; Miller et al., 2009) (Figure 1.2). The major shift in $\delta^{18}O$ has been shown to occur as two prominent shifts in a stepwise pattern (Bohaty et al., 2012; Coxall and Wilson, 2011; Coxall et al., 2005; Katz et al., 2008; Lear et al., 2008) signifying global cooling from an initial increase of 0.7 ‰ (Lear et al., 2008; Miller et al., 2009) and further cooling and ice volume increase marked by the second shift of 0.4 ‰ (Lear et al., 2008). The high $\delta^{18}O$ values persisted through the earliest Oligocene in a period referred to as the Early Oligocene Glacial Maximum (EOGM) (Coxall and Pearson, 2007; Liu et al., 2004; Pearson et al., 2008) (Figure 1.2). The term Oi-1, initially coined by Miller et al. (1991) to describe an isotope zone, has been loosely used by subsequent authors and in order to eradicate the improper use of this term, the EOGM is proposed as a better defining interval (Coxall and Pearson, 2007). Significant global change during this interval is not only identified through the isotope shifts but also from evidence of initiation and expansion of Antarctic ice sheets (Coxall et al., 2005; Lear et al., 2008; Zachos et al., 1996) and coincident global sea level fall of approximately 80 m (Miller et al., 2009); >1 km CCD deepening in a stepwise fashion indirectly related to oxygen isotope increases (Miller et al., 2009; Pälike et al., 2012; Zachos et al., 1996);

increased productivity (Diester-Haass and Zachos, 2003; Salamy and Zachos, 1999) and marine biotic disturbance (Coxall and Pearson, 2007; Dunkley Jones et al., 2008; Pearson et al., 2008). Although not regarded as one of the 'Big Five' extinctions (Sepkoski, 1986) the EOT is recognised as the most recent global mass extinction event (Hull, 2015), being the only Cenozoic event with extreme global diversity loss within the marine realm (Bambach, 2006). The Eocene-Oligocene boundary (EOB) is in fact denoted by the extinction of the planktonic foraminifera family Hantkeninidae (Premoli Silva and Jenkins, 1993). Marine plankton groups exhibit severe extinction and turnover, with planktonic foraminifera extinctions in the *Turoborotalia cerroazulensis* group as well as the Hantkeninidae family (Wade and Pearson, 2008), clustered extinction in the radiolarians (Kamikuri et al., 2012) and calcareous nannofossil extinctions including a key genera-equivalent group, the rosette (helio-) discoasters (Dunkley Jones et al., 2008). These plankton extinctions were most likely caused by the interplay of changing climatic and oceanographic parameters (Coxall and Pearson, 2007). Previously, the late Eocene biotic disruption was suggested to be related to major impact events (Popagai and Chesapeake Bay; Keller, 1986; Monechi et al., 2000; Vonhof et al., 2000), though this is now generally disregarded due to significant offsets in timing (Aubry and Bord, 2009; Coxall and Pearson, 2007), however the impacts may have accentuated late Eocene cooling (Coxall and Pearson, 2007).

1.3 Calcareous nannoplankton

Calcareous nannoplankton, calcifying haptophyte algae, are an important phytoplankton group in the modern oceans and were the dominant phytoplankton in the surface waters of the early Paleogene oceans. Their extracellular calcitic structures, coccoliths and nannoliths, form an abundant and continuous fossil record, incorporated into pelagic sediments and allow for detailed palaeoceanographic reconstructions from the preserved nannofossil assemblages (Roth, 1994). Variations in population composition and diversity can be related to many factors; latitude, ocean currents, water masses, salinity and light (Winter et al., 1994), but temperature and nutrients are the key controls (Aubry, 1992; Roth, 1994). Calcareous nannoplankton are typically eurytopic in nature yet some species and groups exhibit specific ecological preferences for warm water oligotrophic or cold water eutrophic conditions and neritic or open ocean environments. However, it is likely that a series of interrelated environmental parameters govern changes to calcareous nannoplankton assemblage compositions rather than a sole driving factor. Preliminary work studying ecological preferences of calcareous nannoplankton species was undertaken by analysing biogeographic ranges of certain species of living coccolithophores (McIntyre and Bé, 1967; Okada and Honjo, 1973) and subsequently applied to the Paleogene fossil record (Haq and Lohmann, 1976; Wei and Wise, 1990).

Records of calcareous nannoplankton population dynamics can be used to determine changes to environmental conditions through the geological timescale from their first appearance in the Triassic (Bown, 2005b; Bown et al., 2004). Following peak Cenozoic diversity the calcareous nannoplankton underwent a severe diversity decline through the greenhouse to icehouse transition, attributed to elevated rates of extinction and low speciation (Figure 1.1; Bown et al., 2004). This is considered to be linked to cooling climate and accompanying palaeoceanographic changes as nannofossil diversity shows a broad correlation to Cenozoic palaeoclimate proxy records with declining species richness as the climate cooled (Aubry, 1992; Bown et al., 2004; Wei and Wise, 1990), likely to have been driven by expanded cold water polar and subpolar environments, restricting the optimal habitats of the calcareous nannoplankton (Bown, 2005b). Nutrient availability no doubt also played a key role, with the contraction of stable oligotrophic environments where calcareous nannoplankton thrive attributing to diversity decline (Aubry, 1992). Quantitative Paleogene records of calcareous nannoplankton assemblages highlight significant population shifts coeval with Paleogene climatic trends (Dunkley Jones et al., 2008; Fioroni et al., 2015; Gibbs et al., 2006; Persico and Villa, 2004; Schneider et al., 2011; Shamrock and Watkins, 2012; Villa et al., 2008; Wei and Wise, 1990). The calcareous nannoplankton display significant assemblage response to key transient events within the greenhouse to icehouse transition, the MECO and EOT, relative to the high degree of climatic change (Dunkley Jones, 2008; Dunkley Jones et al., 2008; O'Dea, 2013; Toffanin et al., 2011), with evolutionary turnover and shifting population compositions globally characterizing these short lived intervals (Dunkley Jones et al., 2008; Toffanin et al., 2011).

Calcareous nannoplankton are often celebrated for their complete and continuous fossil record yet in reality a vast amount of the assemblage is not preserved and within typical deep sea pelagic sediments there is a significant loss of fragile taxa and those species <3 microns (µm) in size, with larger, more robust species having a higher preservation potential (Young et al., 2005). The term Konservat-Lagerstätte has previously been used to refer to the most complete calcareous nannofossil assemblages observed, with preservation of an exceptional standard (Bown et al., 2008), to accentuate the rarity of these assemblages and the new wealth of taxonomic data they provide. The Kilwa Group from coastal Tanzania documented the first of these assemblages recording >60 previously unknown species from the Paleogene (Bown, 2005a; Bown and Dunkley

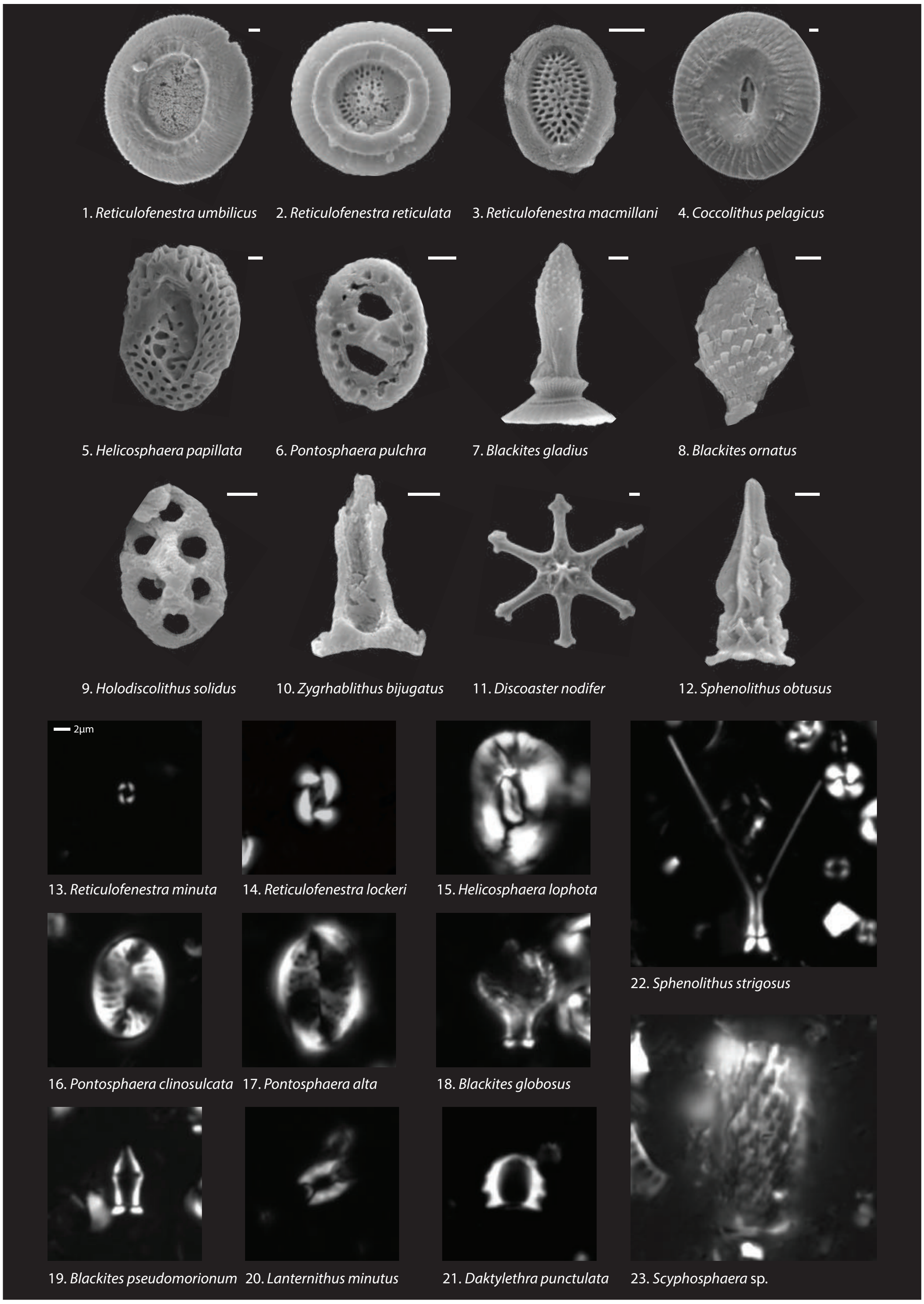

1. *Reticulofenestra umbilicus* 2. *Reticulofenestra reticulata* 3. *Reticulofenestra macmillani* 4. *Coccolithus pelagicus*

5. *Helicosphaera papillata* 6. *Pontosphaera pulchra* 7. *Blackites gladius* 8. *Blackites ornatus*

9. *Holodiscolithus solidus* 10. *Zygrhablithus bijugatus* 11. *Discoaster nodifer* 12. *Sphenolithus obtusus*

13. *Reticulofenestra minuta* 14. *Reticulofenestra lockeri* 15. *Helicosphaera lophota*

22. *Sphenolithus strigosus*

16. *Pontosphaera clinosulcata* 17. *Pontosphaera alta* 18. *Blackites globosus*

19. *Blackites pseudomorionum* 20. *Lanternithus minutus* 21. *Daktylethra punctulata* 23. *Scyphosphaera* sp.

Plate 1.1: Exceptional preservation of calcareous nannofossils from IODP Expedition 342 sediments, shown in SEM (1-12) and LM (13-23) images. A micron scale bar is shown next to each SEM image and a LM scale bar is shown on the first LM image (13). Image sample numbers are detailed in Chapter 2.

Jones, 2006). The supra-CCD clay-rich Paleogene drift sediments from IODP Expedition 342 have facilitated exquisite preservation of calcareous nannofossils and assemblages contain enhanced species richness, with similar diversity values as recorded at the coastal Tanzania sites (Bown, 2005a; Bown et al., 2008), providing a comparable section but from a mid to high latitude, open ocean setting. The high diversity of fragile groups *Helicosphaera, Pontosphaera, Blackites* and holococcoliths, the consistent preservation of micron sized central area grills, nets, bars and crosses and ornamentation on spines and the dominance of small reticulofenestrids <3 µm highlight the exceptional preservation of the Expedition 342 sediments observed under the light microscope (LM) and scanning electron microscope (SEM) (Plate 1.1). The complete assemblages preserved in these North Atlantic sediments allows for a detailed documentation of calcareous nannofossil response across this critical Paleogene greenhouse to icehouse interval.

1.4 Paleogene oceanography and the North Atlantic IODP Expedition 342

Ocean circulation is a key parameter driving global climate changes, with the modern day ocean conveyor belt fundamental in transporting heat around the globe (Broecker, 1991). During the Paleogene significant changes to ocean circulation influenced global cooling and saw the formation of this modern day circulation structure. The initiation of the ACC in the Southern Ocean in the early Oligocene following the opening of the Southern Ocean gateways (Scher and Martin, 2006; Scher et al., 2015), the Tasman gateway and the Drake Passage, led to significant oceanographic and climatic change with the isolation and glaciation of Antarctica and the subsequent initiation of Antarctic bottom waters, creating a source of deep water formation in the southern hemisphere. The equivalent ocean dynamics in the northern hemisphere are not as well understood, yet as an outcome of the ACC onset there was an incursion of an intermediate water mass in the western North Atlantic by the early Oligocene suggesting a modern ocean multilayer structure was establishing (Katz et al., 2011). The formation of a type of North Atlantic Deep Water in the Paleogene has been proposed due the presence of drift sedimentation, yet the onset is poorly constrained and currently estimated between the early middle Eocene through to the early Oligocene (Davies et al., 2001; Hohbein et al., 2012; Via and Thomas, 2006). Major oceanographic reorganisation was enhanced by strengthened thermohaline circulation from increasing latitudinal temperature gradients and wind driven upwelling (Miller et al., 2009).

Today, a southward flowing, deep, cold water current overflows ridges from its northern source in the Arctic Ocean and Labrador Sea and moves down the western Atlantic as the Deep Western Boundary Current and the Gulf Stream, which initiated in the early Paleogene (Pinet et al., 1981), transports warm nutrient rich surface waters northwards up the western boundary and across the Atlantic. The study sites of this thesis are located where the Deep Western Boundary Current flowing southwards intersects with the north-easterly flowing warm Gulf Stream and as palaeogeographic reconstructions from the Eocene indicate the Atlantic margin shape was analogous to today (Figure 1.3), it implies these currents followed similar trajectories in the past (Norris et al., 2014).

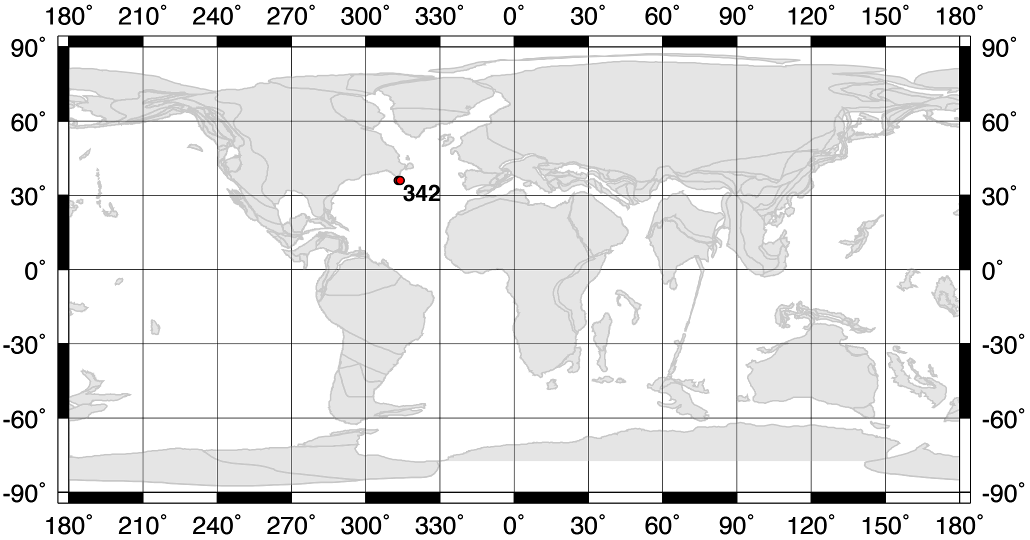

Figure 1.3: Palaeogeographic reconstruction of the late middle Eocene (38 Ma) showing the location of IODP Expedition 342 sites (www.odsn.de.).

IODP Expedition 342 drilled 10 sites in the Northwest Atlantic off the coast of Newfoundland from June to July 2012. Two sites from this expedition (Site U1408 and Site U1411), located on the Southeast Newfoundland Ridge, form the basis of this thesis (Figure 1.4). The Paleogene sediments at these sites were deposited as expanded packages of clay-rich drift sediments, with the morphology indicating the drifts were formed under southward flowing bottom water currents in the Eocene, corroborating previous studies of northern hemisphere deep water formation (Davies et al., 2001; Hohbein et al., 2012). A key objective of IODP Expedition 342 was to target these Paleogene drift sediment sequences with extremely high sedimentation rates, to enable high resolution analysis of greenhouse to icehouse climatic change, with a further aim to recover well preserved microfossils to allow for geochemical analysis and floral and

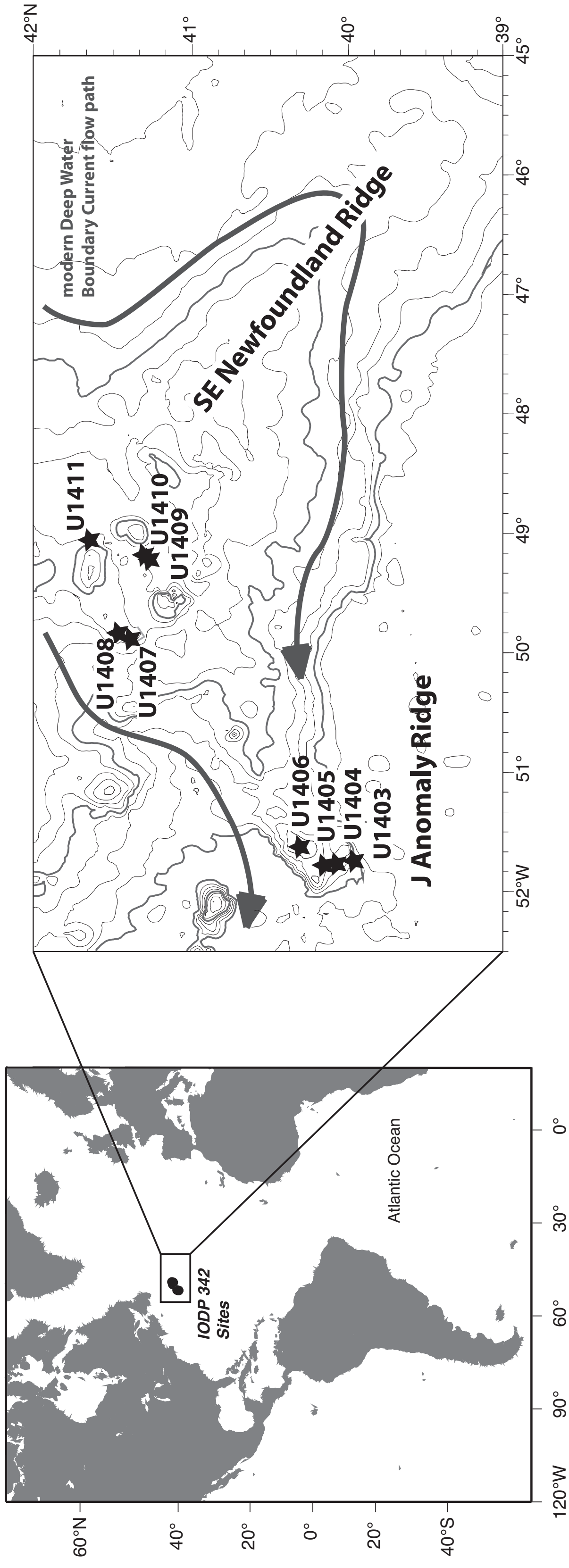

Figure 1.4: Location map of the sites drilled during IODP Expedition 342 in the Northwest Atlantic. Modified from Norris et al. (2014).

faunal assemblage studies (Norris et al., 2014). The clay-rich drift successions facilitated good to exceptional preservation of calcareous microfossils within the continuous stratigraphically expanded Paleogene sediments on the Southeast Newfoundland Ridge, only previously recorded in clay-rich shelf and slope environments, therefore providing a comparable record from an open ocean locality. The spliced composite records formed from high recovery cores at Sites U1408 and U1411, provide a near-continuous expanded middle Eocene to early Oligocene interval comprised of supra-CCD, clay-rich drift sediments containing exceptionally preserved calcareous nannofossils and are ideal sections to address the objectives of this thesis.

1.5 Thesis outline

1.5.1 Themes and objectives

This thesis addresses the evolutionary and ecological response of calcareous nannoplankton and the relationship between this and the striking climatic change through the Paleogene greenhouse to icehouse transition. The calcareous nannoplankton response across this interval is broadly understood but the timing and structure of diversity loss and population shifts are not well constrained, due to few records of appropriate stratigraphic resolution and varying preservational state of calcareous nannofossil assemblages. The exceptionally preserved calcareous nannofossil assemblages from the stratigraphically expanded IODP Expedition 342 Paleogene sediments allow us to address these issues of diversity loss and assemblage restructuring through this key Cenozoic interval. This research is focused in two themes; the response of calcareous nannoplankton to rapid pulses of climatic change and the response of calcareous nannoplankton to the long term transition between the Paleogene greenhouse and icehouse worlds.

The key objectives of the thesis are to:

1. Provide a detailed record of calcareous nannofossil assemblages from the middle Eocene to the earliest Oligocene in the North Atlantic.
2. Analyse calcareous nannoplankton assemblage response across the MECO and EOT, incorporating evolutionary response, originations and extinctions, and establishing palaeoecological indicators and using these to interpret palaeoceanographic and palaeoclimatic changes in the North Atlantic.
3. Compile a long term diversity record throughout the greenhouse to icehouse

transition, detailing species richness and evolutionary rates, and relate this to changing palaeoceanographic and palaeoclimatic parameters.

1.5.2 Thesis structure

This thesis documents long term middle Eocene through to early Oligocene calcareous nannofossil records from IODP Expedition 342 (Sites U1408 and U1411) in the North Atlantic, providing a high resolution northern hemisphere mid to high latitude dataset, from near-continuous sedimentary records containing exceptionally well preserved calcareous nannofossils, allowing for a detailed analysis of calcareous nannoplankton response and adaption to the severe Paleogene greenhouse to icehouse climatic change. Each chapter is presented in the format of a stand alone study using the conclusion to draw together observations and discussions to provide a cohesive overview of calcareous nannoplankton response to this key transition in Cenozoic Earth's history.

Chapter 2 provides a record of middle Eocene to early Oligocene (32.51 to 45.26 Ma) calcareous nannofossils from Sites U1408 and U1411, detailing the exceptional preservation observed within the clay-rich drift sediments from the Southeast Newfoundland Ridge and describing the composition of the assemblages; documenting principal biostratigraphic events and determining zonal boundaries using standard zonation schemes NP and CP zones (Martini, 1971; Okada and Bukry, 1980) and additional CNE/O zones from the recent biozonation scheme of Agnini et al. (2014). A systematic taxonomic list of all species found within the assemblages is provided.

Chapters 3 and 4 present high resolution quantitative nannofossil assemblage records across the MECO (39 to 41.5 Ma) at Site U1408 and EOT (33 to 35 Ma) at Site U1411 documenting significant evolutionary events and using population data and inferred species palaeoecological preferences to interpret palaeoceanographic and palaeoclimatic changes in the North Atlantic. To place these new observations in a wider context we have compiled data from a range of global sites to compare our results from Site U1411 to four key sites from different ocean basins, oceanographic settings and latitudes in order to establish the global response in calcareous nannoplankton across the EOT – Chapter 5.

Chapter 6 investigates the structure and timing of the calcareous nannoplankton diversity decline through the greenhouse to icehouse transition, detailing species richness trends and focussing on evolutionary rates; speciation, extinction, diversification and turnover, comparing diversity measures from the Expedition 342 sites to a global compilation of nannofossil diversity and other proxy records of palaeoclimatic change.

Chapter 7 documents calcareous nannoplankton assemblage data from the middle Eocene to the early Oligocene, using groups of taxa and species trends and their known palaeoecological affinities as a proxy for palaeoceanographic change in the North Atlantic across key palaeoclimatic intervals. We also assess the assemblage structure at the IODP Expedition 342 sites in relation to other global nannofossil records to invoke latitudinal control on nannoplankton populations through this dynamic interval of climatic and oceanographic change.

Chapter 2

Middle Eocene to early Oligocene calcareous nannofossils of IODP Expedition 342, Sites U1408 and U1411

2.1 Introduction

Significant advances in Paleogene calcareous nannofossil taxonomy have been made in recent years, particularly through new research by the Tanzania Drilling Project (Bown, 2005a; Bown and Dunkley Jones, 2006; Bown et al., 2008; Dunkley Jones et al., 2009), which has led to the documentation of many new taxa and previously unknown high diversities, reflecting the nature of the exquisite preservation of nannofossils within these sediments. These records have been supplemented by subsequent Integrated Ocean Drilling Program (IODP) expeditions, such as Expedition 320 (Bown and Dunkley Jones, 2012) and by reassessment of previously drilled sites (e.g. Shamrock and Watkins, 2012). A key objective of IODP Expedition 342 was to target clay-rich Paleogene drift sediments in order to recover well preserved calcareous microfossils for high resolution analysis. On the Southeast Newfoundland Ridge Paleogene sequences were recovered containing good to exceptionally well-preserved calcareous nannofossils which are comparable to those observed in the Paleogene Kilwa Group, Tanzania. These Expedition 342 nannofossil records are the first example of a mid to high latitude open ocean site with such highly diverse and exceptionally preserved nannofossils across the Paleogene greenhouse to icehouse interval and therefore form a complementary dataset to the hemipelagic Tanzanian records, because they are coeval in age but truly oceanic in nature.

IODP Expedition 342 targeted 10 sites (U1402-U1411) in the North Atlantic, off the coast of Newfoundland (Figure 2.1), with the aim to recover high resolution Paleogene sedimentary records. The sedimentary sequences were deposited as highly expanded drift sediment packages. Sites U1408 and U1411 on the Southeast Newfoundland Ridge recovered particularly well represented middle Eocene through to the earliest Oligocene sequences and have been used here as a long time series composite section. These sequences are characterized by rapid accumulation rates, on average 2-3 cm/kyr across the interval of interest, which compares with ~0.5-1 cm/kyr for typical pelagic sedimentation. Near-continuous stratigraphic records are available at both sites using spliced composite sections from multiple holes with Site U1408 contributing a middle Eocene section (1408A-25X to 1408C-4H) and U1411 a late Eocene to early Oligocene section (1411B-28X to 1411B-10H). The high clay content, typically 25-50 %, has facilitated extremely high quality preservation of calcareous nannofossils within these shallowly buried deep sea pelagic sediments. High sampling resolution (~10 to 35 kyr) has enabled us to produce detailed taxonomic, population and biostratigraphic records, which are documented herein.

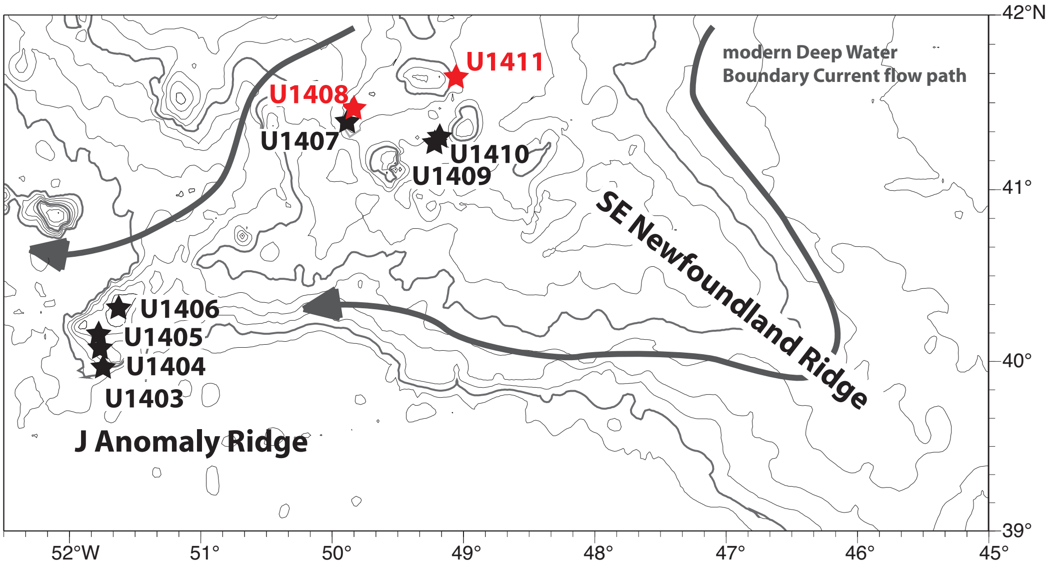

Figure 2.1: Location map for IODP Expedition 342 sites. Sites U1408 (41°26’N 49°47’W) and U1411 (41°37’N 48°6’W) are shown in red. Modified from Norris et al. (2014).

2.2 Materials and methods

2.2.1 Materials

At Site U1408 three holes, A-C, form a splice, which is 280.62 m thick. A post cruise working version U1408 splice has been used for this study. The studied section is from 32.88 to 228.62 metres composite depth (mcd) (samples 1408B-5H-3W, 63-64 cm to 1408B-24X-5W, 123-124 cm) spanning the middle Eocene, including the Middle Eocene Climatic Optimum (MECO - peak MECO at 64.6 to 66.85 mcd), across nannofossil NP Zones 15b to 18 (Martini, 1971). 232 samples were analysed with sampling resolution of ~35 kyr increased to ~17 kyr across the MECO interval (41.38-87.47 mcd). Two holes from Site U1411, B and C, form a splice of 274.02 m thickness (Hole A was abandoned due to poor recovery). The studied section spans the late Eocene to early Oligocene and ranges from 107.87 to 273.25 mcd (samples 1411B-12H-6W, 135-136 cm to 1411B-28X-7H, 22 cm), including the Eocene-Oligocene transition (EOT - with the Eocene-Oligocene boundary (EOB) at 159.14 mcd), across NP Zones 18 to 22 (Martini, 1971). There is a minor coring gap between 195.66 to 213.46 mcd (1411B-20H-4W, 96-97cm to 1411C-15X-1W, 10-11 cm). 198 samples were analysed with sampling resolution of ~30 kyr increased to ~10 kyr across the EOT (145.95-169.18 mcd).

The Paleogene drift sediments at Sites U1408 and U1411 are predominantly clay-rich nannofossil oozes with exceptionally well preserved microfossils (Figure 2.2) (Norris et al., 2014). Site U1408 comprises greenish grey nannofossil clays with light interbedded nannofossil ooze from lithological Unit III across the middle Eocene (32.88 to 228.62 mcd). There is well-defined cyclicity with clear colour banding across the MECO at a decimetre scale. The sediments studied from Site U1411 from the upper Eocene succession are from lithological Unit III (233.63 to 273.25 mcd) comprising greenish grey to dark greenish grey clayey nannofossil chalk and clayey nannofossil chalk with foraminifera. Lithological Unit II found across the lower Oligocene to upper Eocene interval (107.87 to 233.63 mcd) is predominantly clayey nannofossil ooze with increased carbonate content across the EOT. Both sites exhibit a moderate degree of bioturbation, typically *Zoophycos, Planolites* and *Chondrites* burrows, creating a mottled surface appearance.

Calcareous nannofossils are abundant, have exceptional preservation and are highly diverse throughout the entire study interval. Planktonic foraminifera are diverse and exceptionally well preserved (in places ‘glassy’) and, unusually for deep sea sediments, a complete succession of *Hantkenina* is present leading up to the EOB (Norris et al., 2014). There is little evidence of reworking through most of the succession but several discrete intervals with reworking do occur in the upper Eocene Site U1411 Unit III and are associated with plane parallel laminae, foraminiferal sands and pebble sized clasts of nannofossil chalks. The reworking is easily identified with poorly preserved middle Eocene planktonic foraminifera specimens present from samples 1411B-21X to 1411B-28X and middle Eocene nannofossils from 1411B-23X through to 1411B-27X (Norris et al., 2014). Sample 1411B-27X-3W, 63 cm included significant reworking with the presence of middle Eocene nannofossils such as *Lophodolithus* spp., *Sphenolithus* *furcatolithoides, Chiasmolithus solitus, Coccolithus mutatus* and *Discoaster distinctus* and has been removed from the dataset.

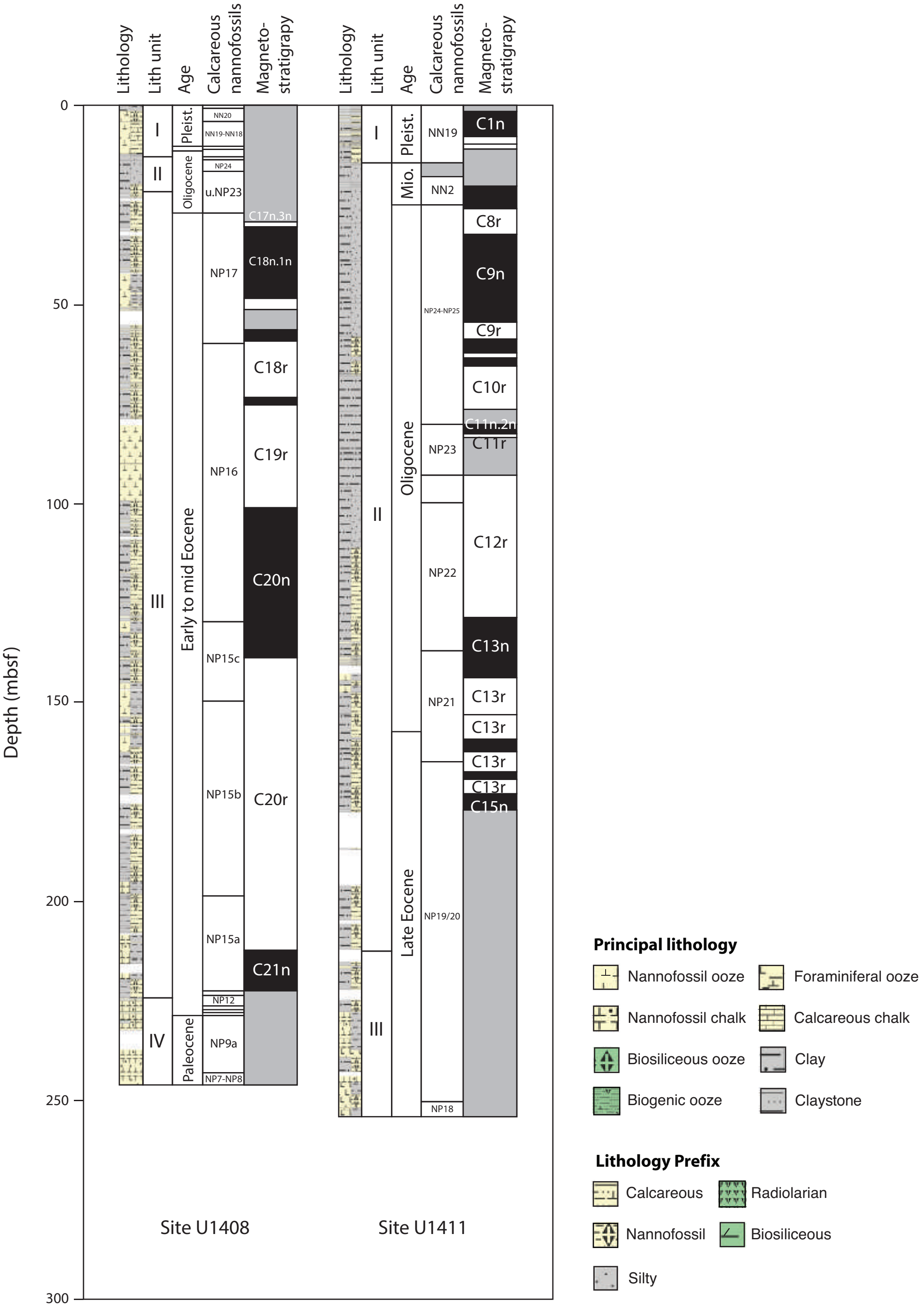

Figure 2.2: Stratigraphic columns for Site U1408 and Site U1411 (modified from Norris et al., 2014).

2.2.2 Age Models

Shipboard biostratigraphy and magnetostratigraphy have been integrated to construct age models for Sites U1408 and U1411 using Geological Time Scale 2012 calibration ages (GTS12; Gradstein et al., 2012; Norris et al., 2014). The nannofossil and planktonic foraminifera datums have been refined during post cruise analysis and are used in this study for more accurate age control. Revised nannofossil datums are taken from this study and planktonic foraminifera datums have been revised by Helen Coxall and Max Holmstrom (pers. comm. 2016, Stockholm University). Sedimentation rates were calculated assuming linear rates between tie points. The average sedimentation rates are 1.95 cm/kyr at Site U1408 and 2.94 cm/kyr at Site U1411 (Tables 2.1a and 2.1b; Figure 2.3). Based on the shipboard age model the study interval spans 45.26 to 38.21 Ma at Site U1408 and 38.20 to 32.50 Ma at Site U1411. Subsequent astronomical tuning has identified a short hiatus at ~107.30 mcd (42 Ma) in the U1408 section, which corresponds to ~4 obliquity cycles (Vahlenkamp, pers. comm. 2015).

2.2.3 Methods

430 smear slides were produced using standard techniques from Bown and Young (1998). Semi-quantitative and quantitative abundance counts were performed using a BX40 Olympus microscope at 1000x magnification under crossed polarized (XPL), phase contrast (PC) and bright field (BF) light. 300 specimens were counted per slide plus extended counts, excluding the dominant taxa and continuing until the total of all other taxa reached a minimum of 300 specimens. Semi-quantitative data were collected by scanning three traverses of each slide. Semi-quantitative abundance classes were: abundant (>10 per field of view (FOV)), common (1-10 per FOV), frequent (<1 per FOV), rare (<1 per 10 FOV) and 3 specimens or less were noted by the number of specimens. 11 samples, at ~1 million year (myr) spacing across the interval, were prepared for scanning electron microscope (SEM) analysis using a JEOL Digital JSM-6480LV SEM. SEM preparations included smear slides on a circular coverslip and raw rock chips which were then mounted onto an aluminium EM stub, secured by colloidal silver cement and gold coated (Bown and Young, 1998). Nannofossils were identified to species level where possible following the taxonomy of Bown (2005a), Bown and Dunkley Jones (2006), Dunkley Jones et al. (2009), Bown and Dunkley Jones (2012) and Nannotax (http://ina.tmsoc.org/Nannotax3/).

Datum tie points	Datum Type	GTS12 Age (Ma)	Midpoint Depth (mcd)	LSR (cm/kyr)
C17n.3n/C17r	Chron boundary	38.33	33.44	
C17r/C18n.1n	Chron boundary	38.62	34.68	0.43
C18n.1n/C18n.1r	Chron boundary	39.63	52.05	1.72
C18n.2n/C18r	Chron boundary	40.14	66.15	2.76
C18r/C19n	Chron boundary	41.15	83.24	1.69
C19n/C19r	Chron boundary	41.39	84.85	0.67
C19r/C20n	Chron boundary	42.3	118.56	3.7
C20n/C20r	Chron boundary	43.43	160.87	3.74
C20r/C21n	Chron boundary	45.72	245.98	3.72

Table 2.1a: Datum tie points used to construct the Site U1408 age model. LSR = linear sedimentation rate.

Datum tie points	Datum Type	GTS12 Age (Ma)	Midpoint Depth (mcd)	LSR (cm/kyr)
Top *Isthmolithus recurvus*	Calcareous nannofossil	32.49	106.84	
C12r/C13n	Chron boundary	33.16	135.34	4.25
C13n/C13r	Chron boundary	33.71	151.7	2.97
Top Hantkeninidae	Planktonic foraminifera	33.89	159.14	4.13
Top *Turborotalia cerroazulensis*	Planktonic foraminifera	34.03	169.85	7.65
C13r/C15n	Chron boundary	35	191.58	2.24
Top *Globigerinatheka semiinvoluta*	Planktonic foraminifera	36.18	228.18	3.1
Top *Chiasmolithus grandis*	Calcareous nannofossil	37.98	268.45	2.24

Table 2.1b: Datum tie points used to construct the Site U1411 age model. Datums given in bold have been revised in post cruise work. LSR = linear sedimentation rate.

a) Site U1408

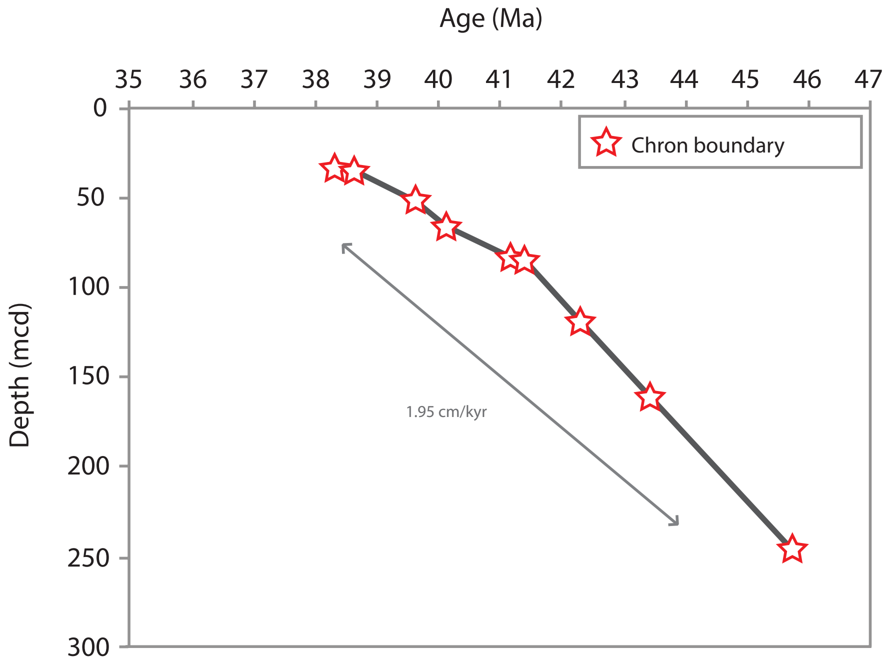

b) Site U1411

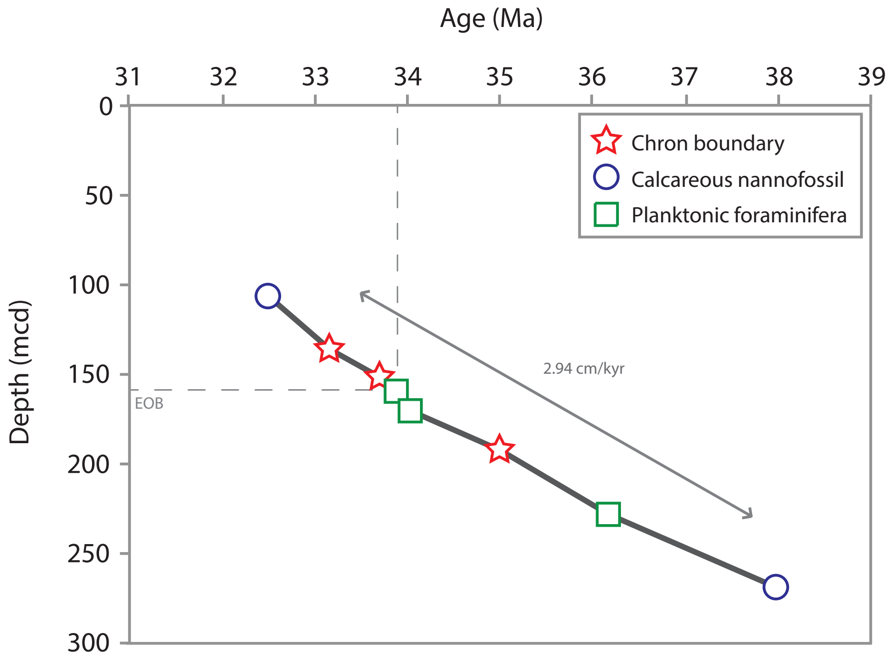

Figure 2.3: Age models for Site U1408 and Site U1411. Average linear sedimentation rates given.

2.3 Results

All study samples yielded abundant calcareous nannofossil assemblages with high diversity, high quality preservation and relatively consistent compositions, dominated by the same groups throughout, despite the wide stratigraphic range. The preservation is good to excellent, with occasional samples moderately preserved, and the diversity is high for this interval, largely reflecting the standard of preservation.

2.3.1 Exceptional preservation

Exceptionally preserved calcareous microfossils, such as those discovered in the Kilwa Group ‘Konservat-Lagerstätten’ of Tanzania (Bown et al., 2008), have highlighted the potential for strengthening our understanding of taphonomy, diversity, ecology, evolution and geochemical proxies (Bown et al., 2008; Pearson et al., 2007, 2001). The nannofossil record described herein from IODP Expedition 342 is comparable in preservation standard to Tanzania and subsequently is virtually unique in providing the first such record from a truly open ocean site.

Exceptional preservation of calcareous nannofossils can be identified by a number of diagnostic features, including high diversity and high abundances of small liths, fragile taxa, fragile structures and holococcoliths (Bown et al., 2008). Diversity is consistently high in the Expedition 342 sediments, comparable to the Tanzania Kilwa Group sediments (113 and 145 species richness in NP15, respectively) and in contrast with values from typical deep sea assemblages (e.g. 48 – Shatsky Rise Site 1209; 45 – Demerara Rise; Bown et al., 2008).

Expedition 342 assemblages are dominated by small reticulofenestrids (<5 microns (µm)), suggesting that the exceptional preservation has conserved a relatively intact assemblage structure. Small coccoliths <3 µm are often rare in deep sea sediments due to the size preservation effect, i.e. increased susceptibility to dissolution due to a higher surface area to volume ratio and smaller, less stable calcite crystals (Bown et al., 2008; Young et al., 2003). This can strongly modify the relative abundance of nannofossil populations due to the loss of these small taxa which are often dominant assemblage components (Young et al., 2005). The extremely high abundance of these small coccoliths within the sediments, often >40 % and the presence of minute liths, such as *Pocillithus spinulifer* - muroliths with narrow spines (Dunkley Jones et al., 2009), revealed under further analysis by SEM, highlight the unusual nature of the Expedition 342 sediments to typical deep sea sediments where assemblages are dominated by larger liths.

High preservation potential is further highlighted by the common and consistent presence of larger, but fragile, taxa with low preservation potential, including species from the genera *Pontosphaera, Helicosphaera* and *Blackites*. The adorned liths of species such as *Helicosphaera papillata* and *Pontosphaera alta* and intricate and delicate bases and spines of *Blackites deflandrei* and *Blackites piriformis* are preserved within the Expedition 342 sediments, shown under LM and SEM in exquisite detail. In particular, the highly diverse *Blackites* group includes many species only previously recorded in the Tanzania Kilwa Group such as *Blackites kilwaensis, Blackites virgatus* and *Blackites furvus* and the presence of *Calciosolenia alternans* and *Syracosphaera tanzanensis* provides a record of extant genera with typically poor fossil records (Bown et al., 2008). A number of new species have also been recorded from these fragile, poor preservational groups in the Expedition 342 sediments; *Pontosphaera wilsonii, Pontosphaera brinkhusii*, *Blackites friedrichii* and *Syracosphaera octiforma* (Bown and Newsam, in review).

Central area grills, bars and crosses in coccolithaceans, such as *Chiasmolithus, Cruciplacolithus* and *Bramletteius* and robust grills and nets in reticulofenestrid species such as *Reticulofenestra reticulata and Reticulofenestra lockeri* are often preserved, but at the Expedition 342 sites these features are consistently recorded and the additional presence of fine imperceptible nets in *Cyclicargolithus floridanus, Reticulofenestra dictyoda* and *Reticulofenestra umbilicus* and a central area cross in *Coccolithus pelagicus* identified in LM and SEM provides further evidence for exceptional preservation.

In additional support the presence of the holococcoliths with relatively high diversities in these Paleogene sediments is a remarkable feature of these deep sea assemblages. In comparison to the robust calcite crystals which form heterococcoliths, the holococcolith group are comprised of minute equi-dimensional calcite crystals which are more prone to dissolution and therefore have a poorer preservation potential. 12 holococcoliths have been recorded in the middle Eocene to early Oligocene Expedition 342 sediments, including *Lanternithus minutus, Holodiscolithus solidus* and *Daktylethra unitatis*.

This standard of preservation is unusual for a deep sea open ocean site, as typically deep sea calcareous nannofossils experience pervasive overgrowth from diagenesis of carbonate rich oozes and/or dissolution from the sites position relative to the calcite compensation depth (CCD). Establishing whether these exceptionally diverse calcareous nannofossil records are due to a taphonomic or ecologic signal is difficult due to the level of overgrowth or dissolution often exhibited in specimens from other deep sea sites (Bown and Newsam, in review). Overall, the exceptionally preserved nannofossils from the Expedition 342 sediments allow us to determine a truer record of diversity through this interval of profound climatic change and to document a history of population dynamics that is less affected by the modifying effects of preservation.

2.3.2 Assemblage composition

In general, the assemblages are dominated by reticulofenestrids (~80 %) and in particular the smaller taxa, *Reticulofenestra minuta, Reticulofenestra dictyoda* (3-5 µm) and *Cyclicargolithus floridanus* (<5 µm), which typically comprise ~60 % of the assemblage. Coccolithaceans, particularly *Coccolithus, Umbilicosphaera* and *Clausicoccus*, are also common components. Notably, the warm water, oligotrophic nannoliths, *Sphenolithus* and *Discoaster,* are frequent to rare. *Helicosphaera* spp., *Pontosphaera* spp., *Blackites* spp. and holococcoliths are consistently present and diverse.

2.3.2.1 Notable absent and infrequent taxa

Notable absences include the Braarudosphaeraceae, which is nevertheless expected as this family is typically restricted to shelf environments, with only rare records of oceanic occurrences (Bown, 2005c). This includes the absence of *Pemma papillatum,* a taxon with an extinction level close to the EOB (Dunkley Jones et al., 2008; Varol, 1998). Fragments of *Pemma papillatum* were identified within a short interval (1411C-16X-1W, 110-111 cm to 1411C-16X-5W, 10-11 cm) but these may have been transported in surface waters or post mortem and do not represent significant in situ occurrences. *Chiasmolithus* is relatively rare with infrequent occurrences in some intervals (e.g. *Chiasmolithus solitus* and *Chiasmolithus oamaruensis*). Haq and Lohmann (1976) suggested that *Chiasmolithus* is associated with southern rather than northern high latitudes, which would explain lower abundances at these sites. As preservation is consistently good in the study samples these absences or rare occurrences are most likely a reflection of primary ecology rather than biases introduced due by taphonomic factors.

2.3.2.2 Origination and extinction levels

The abundance counts and particularly the semi-quantitative data have been used to determine origination and extinction levels. Table 2.2 displays the 34 key bioevents identified: 6 originations (base - B), 20 extinctions (top - T) and 8 other notable events (5 base common - Bc and 3 top common - Tc), 17 of which are used as marker species to define zonal boundaries in the three biozonation schemes used (Agnini et al., 2014; Martini, 1971; Okada and Bukry, 1980) and the 17 others are considered useful secondary markers. Key nannofossil bioevents are shown in Table 2.3 next to GTS12 and Agnini et al. (2014) datums and the shipboard data.

2.4 Calcareous nannofossil biostratigraphy

Biostratigraphic range data has been compiled using records from semi-quantitative data and abundance counts. Due to the high diversity of rare taxa the ranges are given as maximised stratigraphic ranges, interpolating the ranges between known occurrence levels (Figures 2.4a-g, with raw data available in the appendices). All standard zones were recognized across the study section, ranging from Subzone NP15b to Zone NP21 (Martini, 1971 - equivalent to CP Zones 13b-16c (Okada and Bukry, 1980)). The additional bioevents included in Agnini et al. (2014), which compliment the NP and CP zones and further constrain the data, are discussed below. As noted by many authors the base NP16 marker *Blackites gladius* ranges far beyond its initially recorded range and so an alternative marker, top *Nannotetrina fulgens* is used as a proxy for base Zone NP16 (Gradstein et al., 2012; GTS12). Similarly, Zones NP19 and 20 cannot be differentiated due to the unreliability of the marker species *Sphenolithus pseudoradians* (Perch-Nielsen, 1985). As infrequent occurrence and latitudinal diachroneity is recorded in *Chiasmolithus solitus* and *Chiasmolithus oamaruensis*, the CNE zones (Agnini et al., 2014) are considered to provide more accurate biostratigraphic control in the late middle Eocene.

Table 2.2 (following page): Key nannofossil bioevents recorded at Site U1408 and Site U1411. Zonal markers are highlighted in bold. Ages calibrated to GTS12. Depths given in metres composite depth (mcd).

Nannofossil event	Biozonation	Age (Ma) Expedition 342 datums	Age error (+/- Ma)	Midpoint depth (mcd)	Minimum depth (mcd)	Maximum depth (mcd)	Sampling error (+/- mcd)
Top *Coccolithus formosus*	NP21/NP22 CP16b/CP16c CNO1/CNO2	33.14	0.014	134.51	133.90	135.11	0.61
Top *Hayella situliformis*		33.28	0.015	139.16	138.71	139.61	0.41
Top common Clausicoccus subdistichus	CP16a/CP16b	33.50	0.017	145.46	144.96	145.95	0.50
Base common *Clausicoccus subdistichus*	CNE21/CNO1	33.78	0.007	154.84	154.55	155.13	0.29
Top *Umbilicosphaera bramlettei*		33.88	0.007	158.58	158.28	158.88	0.30
Top *Umbilicosphaera protoannula*		33.92	0.004	161.72	161.44	162.00	0.28
Top *Discoaster saipanensis*	NP19/20/NP21 CP15b/CP16a CNE20/CNE21	34.46	0.013	179.60	179.30	179.90	0.30
Top *Discoaster barbadiensis*		34.68	0.012	184.42	184.16	184.68	0.26
Top *Reticulofenestra reticulata*	CNE18/19/CNE20	35.11	0.003	195.16	195.06	195.25	0.09
Top *Neococcolithes dubius*		36.97	0.022	245.80	245.30	246.30	0.50
Top common *Reticulofenestra erbae*	CNE17/CNE18/19	37.46	0.034	256.85	256.10	257.60	0.75
Base common *Isthmolithus recurvus*	NP18/NP19/20 CP15a/CP15b	37.95	0.021	267.70	267.22	268.17	0.48
Base common *Reticulofenestra erbae*	CNE16/CNE17	37.98	0.013	268.45	268.17	268.72	0.27
Top *Chiasmolithus grandis*	CP14b/CP15a	37.98	0.013	268.45	268.17	268.72	0.27
Top *Campylosphaera dela*		38.20	0.005	Between cores	273.25	32.88	Between cores
Top *Sphenolithus obtusus*	CNE15/CNE16	38.20	0.005	Between cores	273.25	32.88	Between cores
Base *Chiasmolithus oamaruensis*	NP17/NP18	38.70	0.017	36.18	35.88	36.48	0.30
Top common *Sphenolithus spiniger*		39.89	0.003	59.16	59.08	59.23	0.07
Base *Sphenolithus obtusus*		40.00	0.006	62.28	62.13	62.43	0.15
Top *Chiasmolithus solitus*	NP16/NP17 CP14a/CP14b	40.19	0.009	66.93	66.78	67.08	0.15
Base *Reticulofenestra stavensis*	CNE14/CNE15	40.44	0.004	71.15	71.07	71.22	0.08
Base *Reticulofenestra bisecta*		40.52	0.009	72.57	72.42	72.72	0.15
Base *Reticulofenestra filewiczii*		40.58	0.009	73.47	73.32	73.62	0.15
Base common *Sphenolithus predistentus*		40.65	0.009	74.67	74.52	74.82	0.15
Top *Umbilicosphaera bramlettei* (>7.5 µm)		40.81	0.009	77.37	77.22	77.52	0.15
Top *Sphenolithus strigosus*		40.88	0.009	78.57	78.42	78.72	0.15
Top *Sphenolithus furcatolithoides*		40.88	0.009	78.57	78.42	78.72	0.15
Base common *Reticulofenestra reticulata*	CNE13/CNE14	42.00	0.008	107.46	107.16	107.76	0.30
Base common *Reticulofenestra umbilicus*	CP13c/CP14a CNE12/CNE13	42.32	0.020	119.11	118.38	119.84	0.73
Top *Lophodolithus*		42.50	0.020	126.13	125.38	126.88	0.75
Top *Discoaster wemmelensis*		42.79	0.020	136.93	136.18	137.68	0.75
Top *Coccolithus mutatus*		42.79	0.020	136.93	136.18	137.68	0.75
Top *Nannotetrina fulgens*	NP15c/NP16	43.27	0.020	156.20	155.67	156.72	0.60
Top *Chiasmolithus gigas*	NP15b/NP15c CP13b/CP13c CNE10/11/CNE12	43.96	0.130	180.34	175.51	185.17	4.83

Table 2.3: Key nannofossil bioevents from this study compared with the GTS12 nannofossil datums, the Agnini et al. (2014) biozonation scheme and the shipboard records. Site U1408 is shown in red and Site U1411 is shown in purple. *recalibrated age given in the shipboard records. **depth given including 'suspect specimens'.

Nannofossil event	GTS12	Agnini et al., 14 (Pälike et al., 2006)	Agnini et al., 14 converted to GTS12	This study age GTS12 (Ma)	Age error (+/- Ma)	This study depth (mcd)	Depth error (+/- mcd)	Shipboard depth (mcd)
T C. formosus	32.92	32.92	32.86	33.14	0.014	134.51	0.61	143.64
Tc C. subdistichus	33.43			33.50	0.017	145.46	0.50	
Bc C. subdistichus		33.88	33.86	33.78	0.007	154.84	0.29	
T D. saipanensis	34.44	34.44	34.37	34.46	0.013	179.60	0.30	184.59
T D. barbadiensis	34.76	34.77	34.67	34.68	0.012	184.42	0.26	196.32
T R. reticulata	35.40	35.24	35.26	35.11	0.003	195.16	0.10	196.00
B/Bc I. recurvus	36.97	36.84	37.13	37.95	0.021	267.70	0.48	270.13
Tc R. erbae		37.46	37.70	37.46	0.034	256.85	0.75	259.09
T C. grandis	37.98	37.77	37.97	37.98	0.013	268.45	0.28	272.67
B C. oamaruensis	38.09	37.84	38.03	38.70	0.018	36.18	0.30	273.98
Bc R. erbae		37.88	38.07	37.98	0.013	268.45	0.28	272.67
T S. obtusus		38.47	38.64	38.20	0.005	Between cores		
T C. solitus	40.40			40.19	0.009	66.93	0.15	67.98
B R. stavensis	40.36*	40.34	40.35	40.44	0.004	71.15	0.08	72.02
T S. furcatolithoides		40.51	40.48	40.88	0.009	78.57	0.15	75.15
Bc R. reticulata		42.37	42.57	42.00	0.008	107.46	0.30	
B R. reticulata	41.66			42.46	0.020	124.63	0.75	113.96
Bc R. umbilicus		43.06	43.32	42.32	0.020	119.11	0.73	
B R. umbilicus	41.94			44.78	0.016	211.11	0.60	213.82**
T N. fulgens	42.87			43.27	0.020	156.20	0.52	154.01
T C. gigas	44.12	43.96	44.15	43.96	0.130	180.34	4.83	176.42

Zone NP15, CP13, CNE10/11 and 12

Chiasmolithus gigas is present in our lowest sample, which can therefore be assigned to Subzone NP15b (=CP13b). *Chiasmolithus gigas* is rare/frequent up to its last occurrence (recorded in sample 1408B-20X-5W, 3-4cm, midpoint depth 180.34 mcd), which defines the base of Subzone NP15c (=CP13c and CNE12). Zone CNE11 cannot be differentiated from Zone CNE10 or CNE12 as the first occurrence of *Sphenolithus cuniculus* (base of CNE11) occurs above the last occurrence of *Chiasmolithus gigas* (base of CNE12).

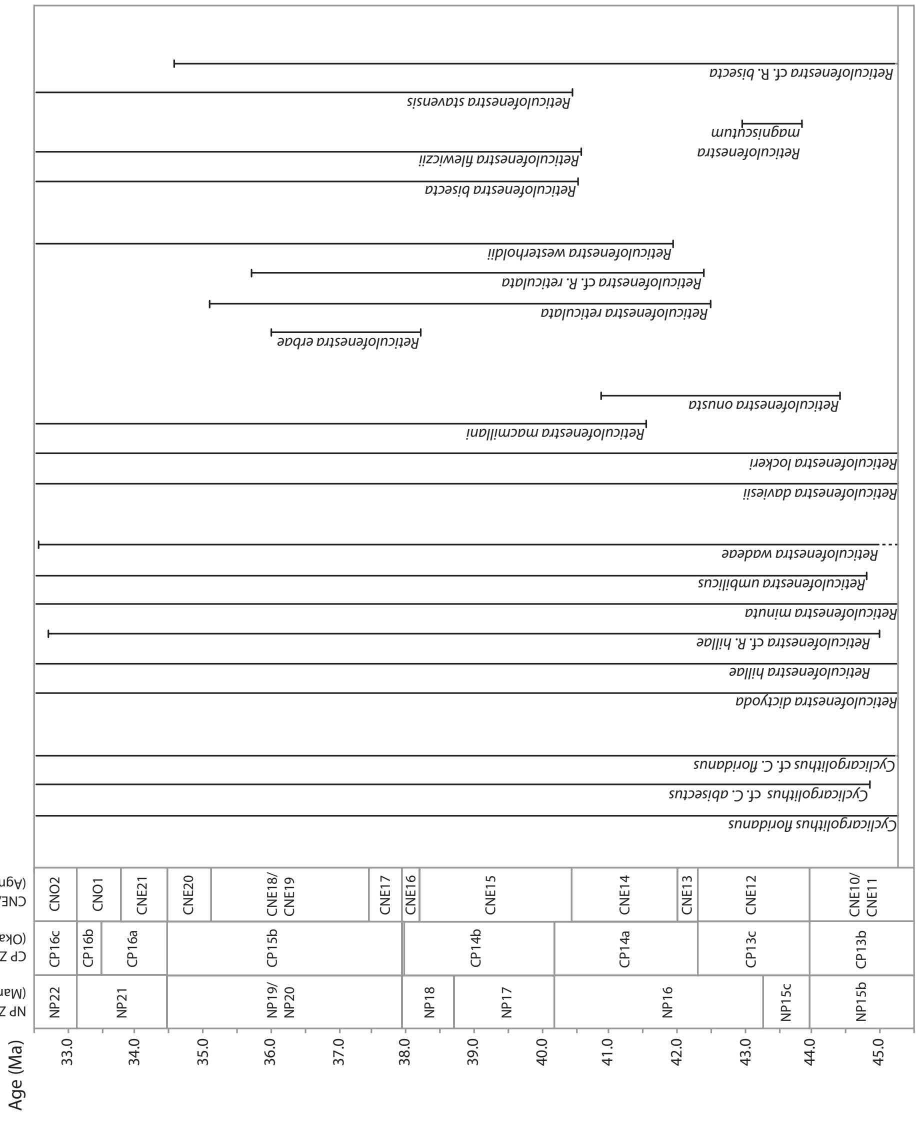

Figure 2.4a: Stratigraphic range chart of the Noelaerhabdaceae.

Figure 2.4b (following page): Stratigraphic range chart of the Calcidiscaceae and Coccolithaceae.

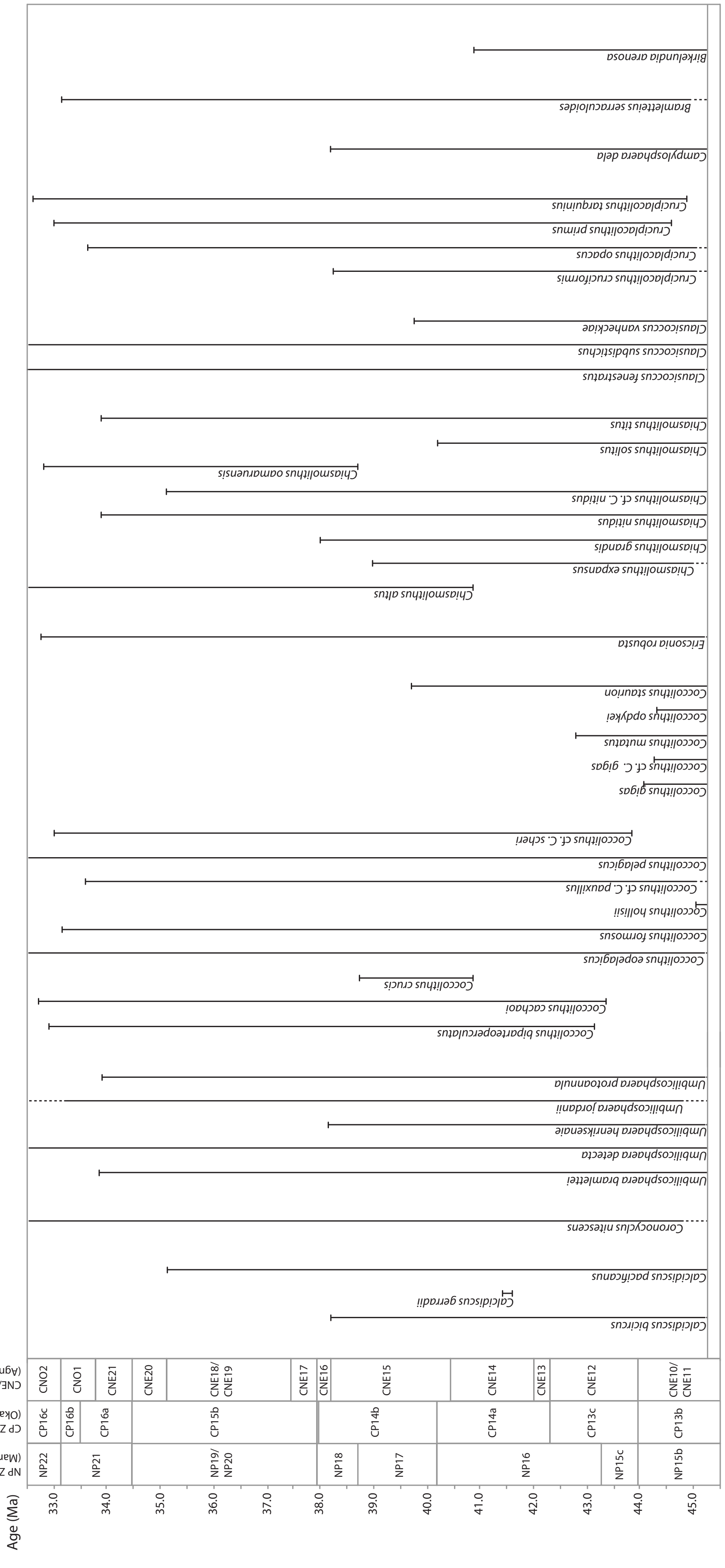
Birkelundia arenosa
Bramletteius serraculoides
Campylosphaera dela
Cruciplacolithus tarquinius
Cruciplacolithus primus
Cruciplacolithus opacus
Cruciplacolithus cruciformis
Clausicoccus vanheckiae
Clausicoccus subdistichus
Clausicoccus fenestratus
Chiasmolithus titus
Chiasmolithus solitus
Chiasmolithus oamaruensis
Chiasmolithus cf. C. nitidus
Chiasmolithus nitidus
Chiasmolithus grandis
Chiasmolithus expansus
Chiasmolithus altus
Ericsonia robusta
Coccolithus staurion
Coccolithus opdykei
Coccolithus mutatus
Coccolithus cf. C. gigas
Coccolithus gigas
Coccolithus cf. C. scheri
Coccolithus pelagicus
Coccolithus cf. C. pauxillus
Coccolithus hollisii
Coccolithus formosus
Coccolithus eopelagicus
Coccolithus crucis
Coccolithus cachaoi
Coccolithus bipartoperculatus
Umbilicosphaera protoannula
Umbilicosphaera jordanii
Umbilicosphaera henriksenaie
Umbilicosphaera detecta
Umbilicosphaera bramlettei
Coronocyclus nitescens
Calcidiscus pacificanus
Calcidiscus gerradii
Calcidiscus bicircus
CNE/O Zones
(Agnini et al, 2014)
CNO2
CNO1
CNE21
CNE20
CNE18/
CNE19
CNE17
CNE16
CNE15
CNE14
CNE13
CNE12
CNE10/
CNE11
CP Zones
(Okada & Bukry, 1980)
CP16c
CP16b
CP16a
CP15b
CP14b
CP14a
CP13c
CP13b
NP Zones
(Martini, 1971)
NP22
NP21
NP19/
NP20
NP18
NP17
NP16
NP15c
NP15b
Age (Ma)
33.0
34.0
35.0
36.0
37.0
38.0
39.0
40.0
41.0
42.0
43.0
44.0
45.0

Zone NP16, CP14a, CNE13 and 14

The base of Zone NP16 is identified here at the last occurrence of *Nannotetrina fulgens* (1408C-17H-4W, 3-4 cm), as was used in the shipboard record (Norris et al., 2014). This replaces the original top *B. gladius* event, which is now known to occur far higher than was originally thought (e.g. Bown, 2005a; NP14b/15a-NP17). This is for the most part because it is a dissolution susceptible taxon and is only rarely and infrequently preserved in typical deep sea sediments. In the Expedition 342 sections it ranges to the base of NP18 (1408B-5H-4W, 93-94 cm).

The base of Subzone CP14a is defined by the first occurrence of *Reticulofenestra umbilicus*, however the Expedition 342 material includes large elliptical reticulofenestrids some way below the level originally identified by Backman and Hermelin (1986) (within Chron 19r) and ~3 myr earlier than the current GTS12 calibration of 41.94 Ma. Agnini et al. (2014) have suggested that the first common occurrence of this taxon may be a more consistent horizon and this has been used to define the base of zone CP14a (=CNE13) (recorded in sample 1408C-13H-6W, 3-4 cm, midpoint age 42.32 Ma).

The base of Zone CNE14 is defined by the base common of *Reticulofenestra reticulata* which we record in sample 1408C-12H-3W, 63-64 cm (midpoint depth 107.46 mcd). From this sample onwards this species is consistently observed with increased abundance until its last occurrence in the uppermost Eocene.

Zone NP17, CP14b, CNE15

Zone NP17 (=CP14b) is defined by the last occurrence of *Chiasmolithus solitus* recorded in 1408B-8H-6W, 63-64 cm (midpoint depth 66.93 mcd). This species has an infrequent occurrence through NP16 and reworked specimens of this species are recorded in the late middle Eocene making the placement of base Zone NP17 difficult.

The base of Zone CNE15 is defined by the first occurrence of *Reticulofenestra stavensis* (*D. bisectus* of Agnini et al. (2014)) (midpoint depth 71.15 mcd). The first specimens occur in sample 1408A-8H-2W, 63-64 cm and closely follows the origination of *Reticulofenestra bisecta* and *Reticulofenestra filewiczii* (the *Reticulofenestra bisecta* group), providing useful additional bioevents.

Zone NP18, CP15a, CNE16

The base of *Chiasmolithus oamaruensis* defines the base of Zone NP18 (midpoint depth

36.18 mcd) with the first specimens identified in sample 1408B-5H-5W, 63-64 cm. Agnini et al. (2014) have noted issues with this taxon as a marker species due to its discontinuous and sporadic occurrences. Significant latitudinal diachroneity is also identified with the first occurrence recorded at high southern latitudes at 38.99 Ma (Villa et al. 2008; converted to GTS12) and high northern latitudes at 39.91 Ma (Firth, pers. comm. 2014; converted to GTS12). The first occurrence in the Expedition 342 sediments at 38.70 Ma is significantly older than the GTS12 calibration age for *C. oamaruensis* rare of 38.09 Ma, but is in keeping with these high latitude records.

Subzone CP15a is defined by the last occurrence of *Chiasmolithus grandis* at 37.98 Ma. Due to the extended range of *Isthmolithus recurvus*, the Zone NP19 (=CP15b) marker (see below), Subzone CP15a is limited to one sample, 1411B-28X-3W, 105 cm.

Zone CNE16 is a short biozone defined by the top of *Sphenolithus obtusus* in sample 1408B-5H-3W, 63-64cm with the extinction occurring within the interval between the cores from Site U1408 and Site U1411 at 38.20 Ma.

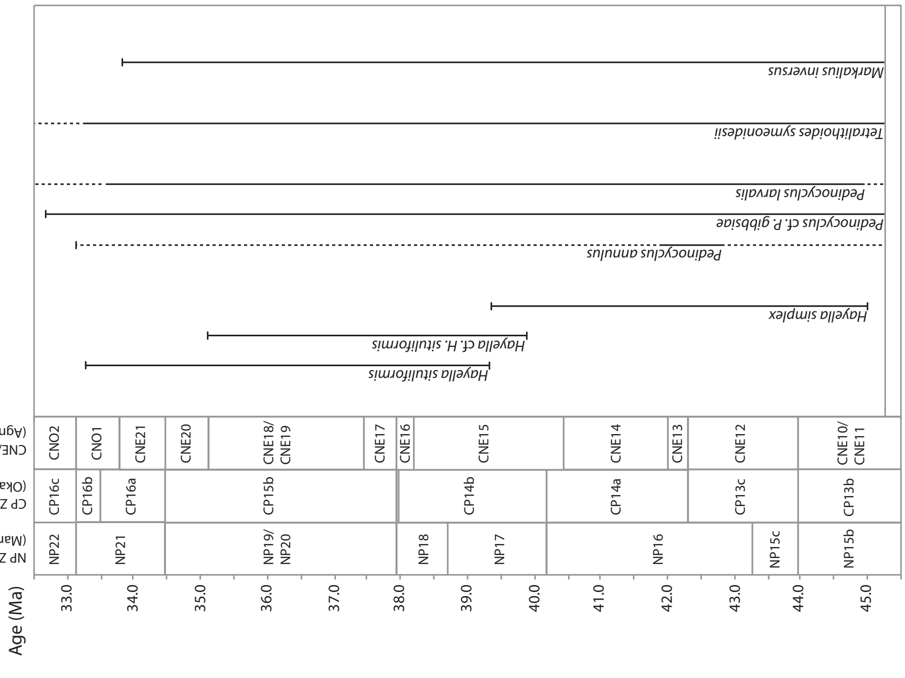

Figure 2c: Stratigraphic range chart of the Placolith coccoliths Incertae Sedis.

Figure 2d (following page): Stratigraphic range chart of the Helicosphaeraceae and Pontosphaeraceae.

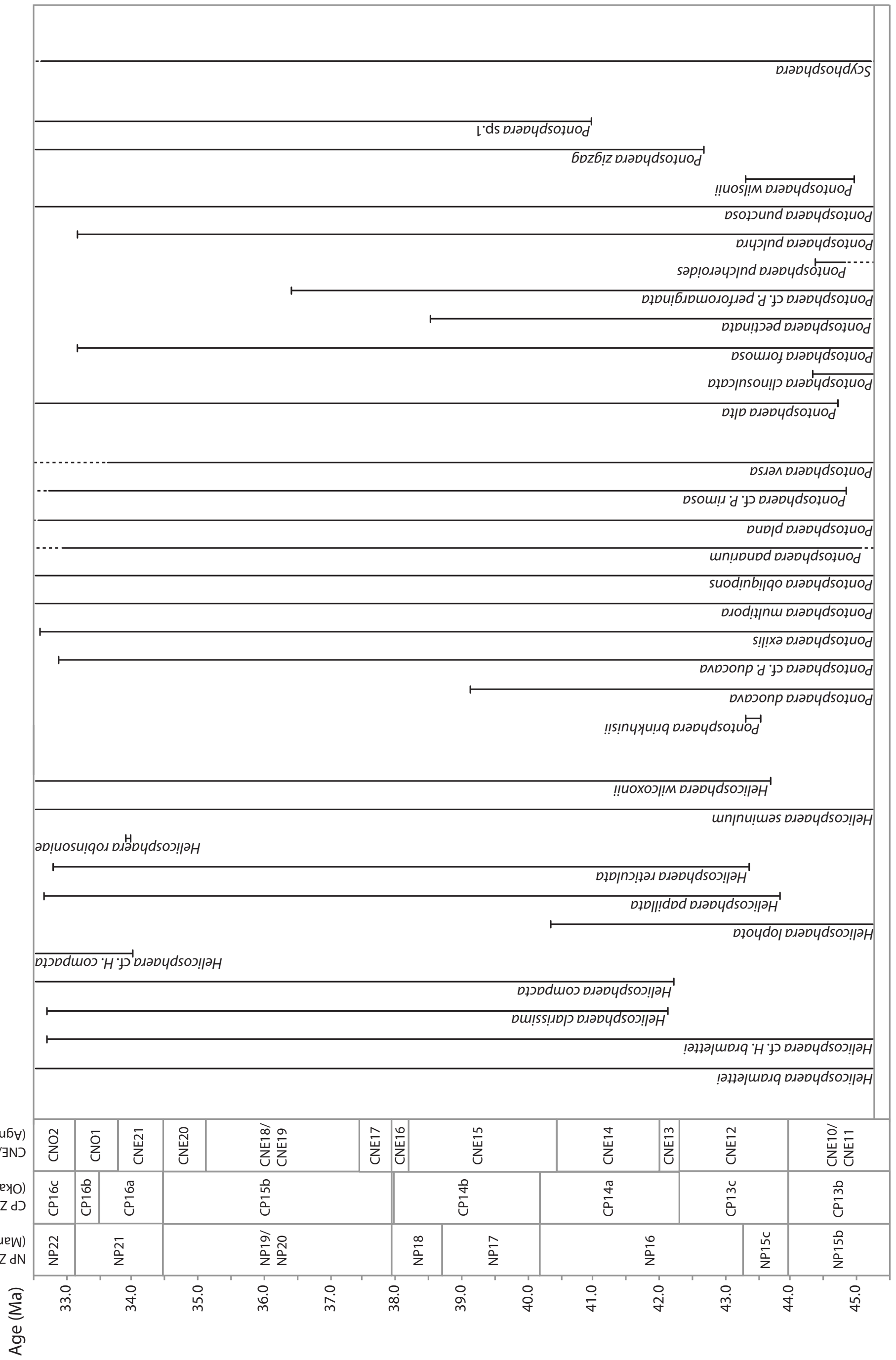

Zone NP19/20, CP15b, CNE 17, 18/19 and 20

Zone NP19 (=CP15b) is defined by the first occurrence of *Isthmolithus recurvus*. Agnini et al. (2014) note significant variability in the first occurrence of *Isthmolithus recurvus* in different studies due to rare occurrence at the base of its range and we have subsequently used the base common of *I. recurvus* to define this zonal boundary. The base common of *Isthmolithus recurvus* at the Expedition 342 sites is still identified earlier than is typically reported (sample 1411B-28X-3W, 10-11 cm, midpoint depth 267.70 mcd at 37.95 Ma) around 980 kyr before the GTS12 calibration age, 36.97 Ma. However, North Atlantic ODP Site 647 also records an earlier first occurrence of *I.*

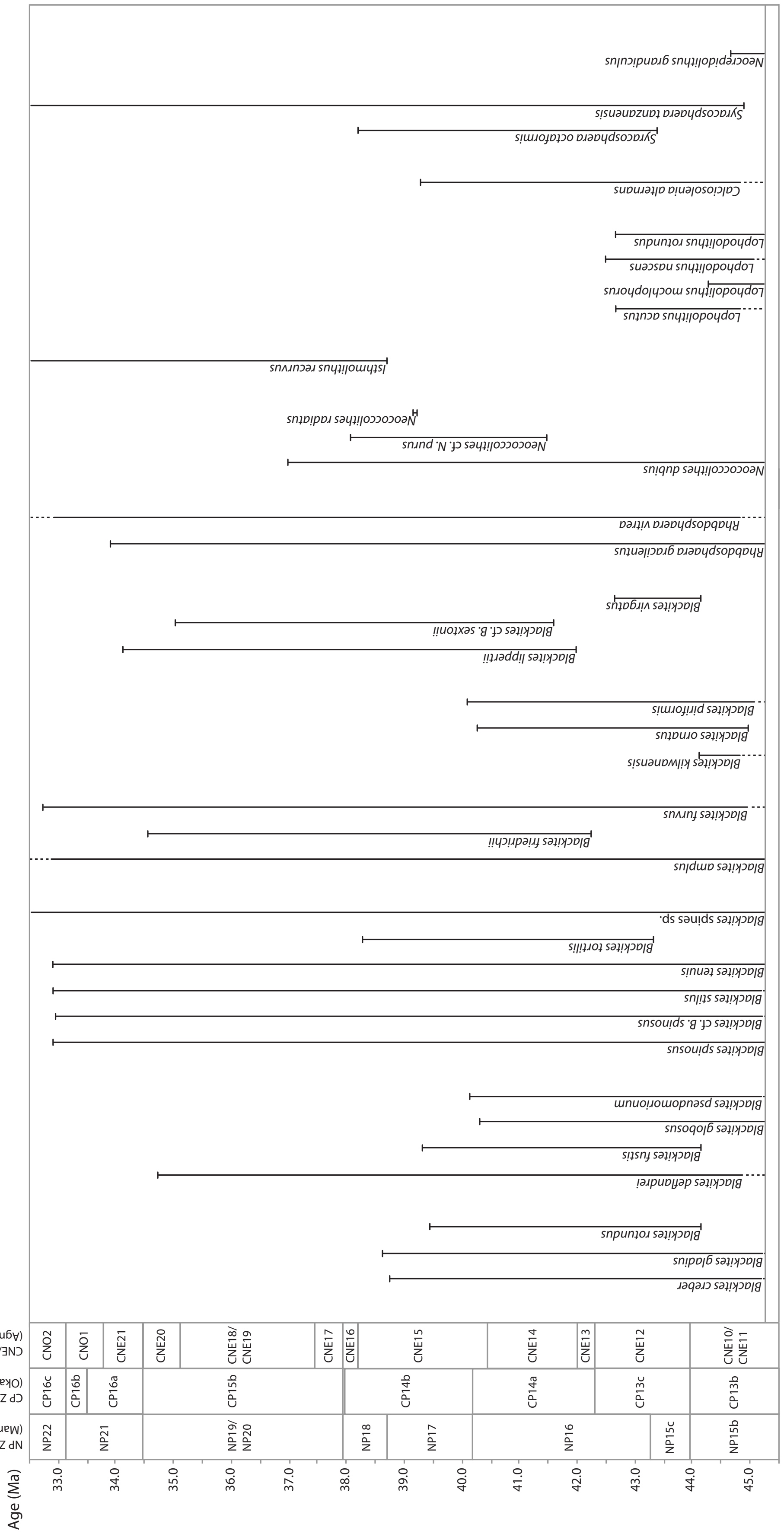

Figure 2e: Stratigraphic range chart of the Rhabdosphaeraceae and Zygodiscaceae.

recurvus at 38.87 Ma (Firth, pers. comm. 2014; converted to GTS12). Zones NP19 and 20 cannot be differentiated due to the unreliability of the *Sphenolithus pseudoradians* biomarker (Perch-Nielsen, 1985).

Agnini et al. (2014) have divided the NP19/20 (=CP15b) interval into three zones (CNE18-20). Zone CNE17 and 18 are defined by the base common and top common of *Reticulofenestra erbae* (1411B-28X-3W, 105 cm and 1411B-27X-3W, 138-139 cm, respectively). CNE19 is defined by base *Reticulofenestra isabellae* (*Cribocentrum isabellae*) which we were unable to identify, as this species is rather poorly defined and difficult to distinguish from *Reticulofenestra reticulata*. CNE20 is defined by the last occurrence of *Reticulofenestra reticulata* identified in sample 1411B-20H-4W, 50 cm with midpoint age of 35.11 Ma.

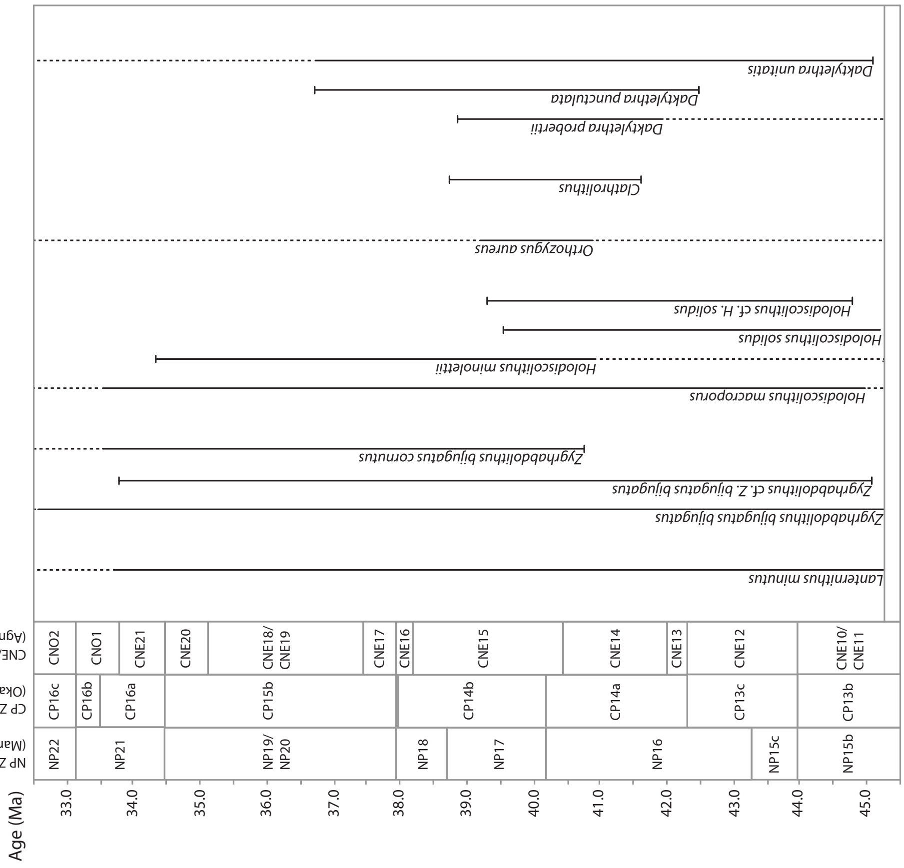

Figure 2f: Stratigraphic range chart of the holococcoliths.

Zone NP21, CP16a and 16b, CNE21 and CNO1

Zone NP21 (=CP16a and CNE21) is defined by the last occurrence of *Discoaster saipanensis* and is just preceded by the last occurrence of *Discoaster barbadiensis.* These events occur in samples 1411B-19H-2W, 120 cm (midpoint age 34.46 Ma) and

1411B-19H-5W, 148 cm (midpoint age 34.68 Ma).

Zone CNO1 is defined by the base acme of *Clausicoccus subdistichus* and subzone CP16b by the top of the acme. The increase and decrease in abundance occur in samples 1411B-17H-3W, 90 cm and 1411C-8H-2W, 30 cm, respectively with midpoint ages for the acme between 33.78 Ma and 33.50 Ma, although the acme top is hard to precisely define.

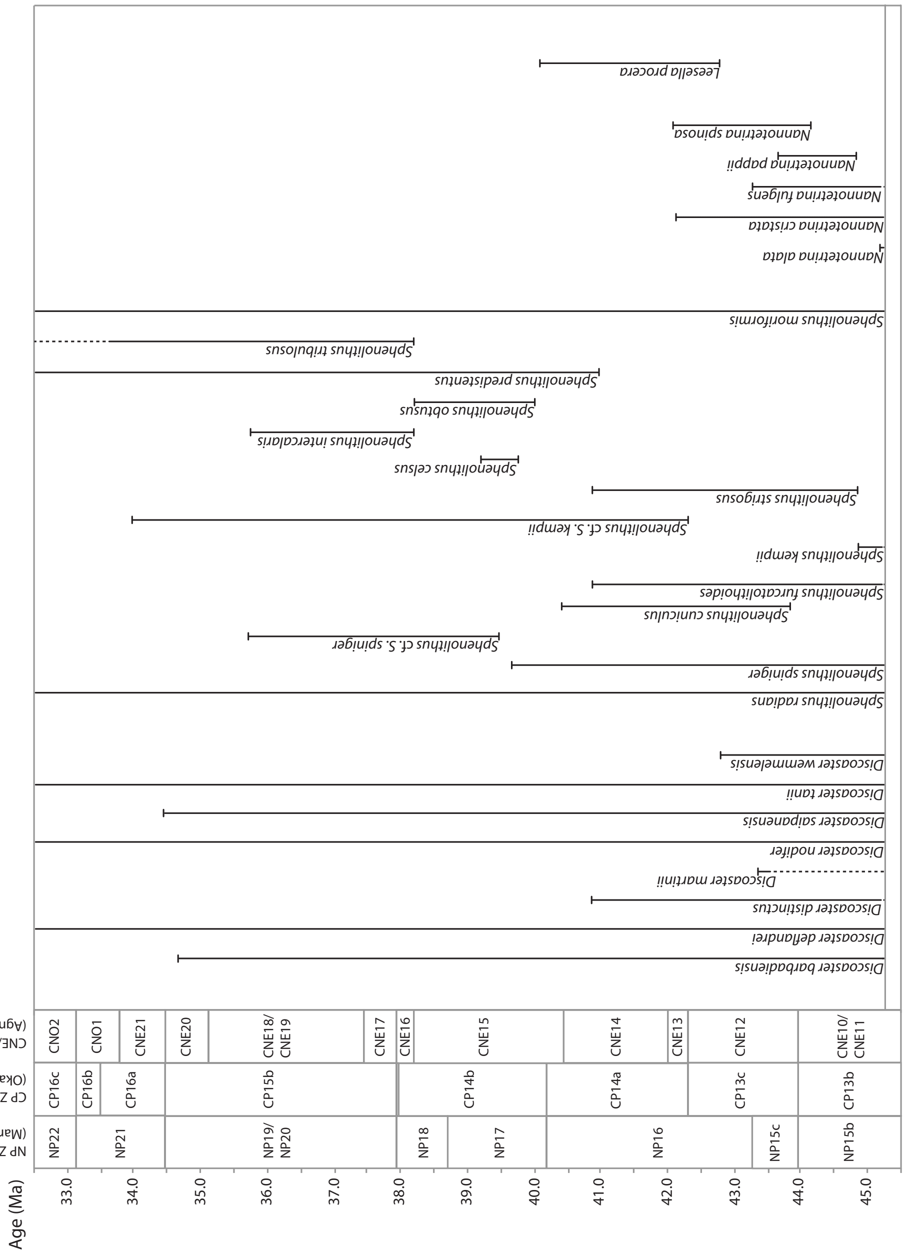

Figure 2g: Stratigraphic range chart of the nannoliths.

Zone NP22, CP16c, CNO2

Zone NP22 (=CP16c and CNO2) is defined by the last occurrence of *Coccolithus formosus* which occurs in sample 1411B-15H-3W, 125.5-126.5 cm (midpoint age 33.14 Ma) and the continued presence of *R. umbilicus* indicates that the overlying zone is not reached in the study section, but was identified in sample 1411B-12H-5W, 30 cm during shipboard biostratigraphy.

2.5 Systematic palaeontology

This section comprises a taxonomic list of all calcareous nannofossils observed during the study of Sites U1408 and U1411. The observed ranges in the Expedition 342 sediments are given using NP zones (Martini, 1971), CP zones (Okada and Bukry, 1980) and CNE/O zones (Agnini et al., 2014). Comments are provided for taxonomically difficult groups and notable taxa. Light microscope images are at the same scale with a 2 µm scale bar beside the first image on each plate. SEM images each have a 1 µm scale bar provided. For certain species multiple images are provided to highlight morphological disparity. Descriptive terminology follows the guidelines of Young et al. (1997). Higher taxonomy follows the scheme for extant taxa (Young et al., 2003) and for extinct taxa the scheme of Young and Bown (1997). Materials and images are stored in the Department of Earth Sciences, University College London. Full references are provided on Nannotax (http://ina.tmsoc.org/Nannotax3/).

2.5.1 Placolith coccoliths

Order **ISOCHRYSIDALES** Pascher, 1910
Family **NOELAERHABDACEAE** Jerkovic, 1970 emend, Young & Bown, 1997
Remarks: The Expedition 342 assemblages are dominated by *Reticulofenestra* and *Cyclicargolithus* which can be divided into groups based on morphological similarities. The sub-generic informal groups are adapted from Bown and Dunkley Jones (2012).

Genus **CYCLICARGOLITHUS** Bukry, 1971
Small to large subcircular reticulofenestrids with a narrow central area, spanned by an imperceptible net.

Cyclicargolithus* cf. *C. abisectus (Muller, 1970) Wise, 1973
Very large specimens of *Cyclicargolithus floridanus* >10 µm. Plate 2.1: Figure 5

Observed range: NP15b-NP22; CP13b-CP16c; CNE10/11-CNO2. Very rare sporadic occurrence.

Cyclicargolithus floridanus (Roth & Hay in Hay et al., 1967) Bukry, 1971

Informally grouped into small (<5 µm), medium (5-8 µm) and large (8-10 µm). Some specimens are so well preserved in the middle Eocene that the central area net is clearly visible. Plate 2.1: Figures 1-3, Plate 2.12: Figures 1-5

Observed range: NP15b-NP22; CP13b-CP16c; CNE10/11-CNO2

Cyclicargolithus* cf. *C. floridanus (Roth & Hay in Hay et al., 1967) Bukry, 1971

Similar to *C. floridanus* but with a closed central area. Plate 2.1: Figure 4

Observed range: NP15b-NP22; CP13b-CP16c; CNE10/11-CNO2. Very rare sporadic occurrence after NP15b.

Genus **RETICULOFENESTRA** Hay et al., 1966

Split into four informal morphological groups: *Reticulofenestra umbilicus* group, *Reticulofenestra lockeri* group, *Reticulofenestra reticulata* group and *Reticulofenestra bisecta* group.

RETICULOFENESTRA UMBILICUS GROUP

Elliptical reticulofenestrids with an open central area spanned by an imperceptible net. This group encompasses a wide range of morphological variability.

Reticulofenestra dictyoda (Deflandre in Deflandre & Fert, 1954) Stradner in Stradner & Edwards, 1968

Informally grouped into small (3-5 µm), medium (5-8 µm), large (8-10 µm) and very large (10-14 µm). Plate 2.1: Figures 7-13, Plate 2.12: Figures 11-12

Observed range: NP15b-NP22; CP13b-CP16c; CNE10/11-CNO2

Reticulofenestra hillae Bukry & Percival, 1971

Elliptical reticulofenestrid with narrow lens shaped central area. Plate 2.1: Figures 16-17, Plate 2.12: Figures 9-10

Observed range: NP15b-NP22; CP13b-CP16c; CNE10/11-CNO2. Rare in occurrence.

Reticulofenestra* cf. *R. hillae Bukry & Percival, 1971

Similar to *R. hillae* but subcircular. Plate 2.1: Figure 14

Observed range: NP15b-NP22; CP13b-CP16c; CNE10/11-CNO2. Rare in occurrence.

Reticulofenestra minuta Roth, 1970

Very small (<3 µm) elliptical reticulofenestrids. Plate 2.1: Figure 6, Plate 2.12: Figures 13-14

Observed range: NP15b-NP22; CP13b-CP16c; CNE10/11-CNO2

Reticulofenestra umbilicus (Levin, 1965) Martini & Ritzkowski, 1968

Very large (>14 µm) elliptical reticulofenestrids. Plate 2.1: Figure 18, Plate 2.12: Figures 6-8

Observed range: NP15b-NP22; CP13b-CP16c; CNE10/11-CNO2. The first appearance of this species is commonly used as a biostratigraphic marker yet the Expedition 342 material records elliptical reticulofenestrids around 3 myr prior to the level of this biohorizon and therefore the use of first common occurrence of this taxon may be a more consistent horizon as suggested by Agnini et al. (2014).

Reticulofenestra wadeae Bown, 2005a

Subcircular reticulofenestrid with wide central area. Included specimens >14 µm which could be referred to as *R.* cf. *R. umbilicus*. Plate 2.1: Figure 19

Observed range: NP15b-NP22; CP13b-CP16c; CNE10/11-CNO2. Very rare in occurrence.

RETICULOFENESTRA LOCKERI GROUP

Elliptical reticulofenestrids with an open central area spanned by a robust visible net.

Reticulofenestra daviesii (Haq, 1968) Haq, 1971

R. daviesii specimens have a cycle of distinct visible pores. Plate 2.1: Figures 20-21, Plate 2.13: Figure 2.

Observed range: NP15b-NP22; CP13b-CP16c; CNE10/11-CNO2. This species is abundant in samples across the Eocene-Oligocene transition but ranges down to the middle Eocene with sporadic rare occurrences.

Reticulofenestra lockeri Muller, 1970

Elliptical reticulofenestrid with the central area spanned by a birefringent net. Plate 2.1, Figures 22-23, Plate 2.13: Figure 1

Observed range: NP15b-NP22; CP13b-CP16c; CNE10/11-CNO2.

Reticulofenestra macmillani Dunkley Jones et al., 2009

Informally grouped into <5 and >5 µm. Plate 2.1: Figure 24, Plate 2.13: Figures 3-4

Observed range: NP16-NP22; CP14a-CP16c; CNE13-CNO2.

Reticulofenestra onusta (Perch-Nielsen, 1971) Wise, 1983

Large elliptical reticulofenestrids with a wide central area spanned by a finely perforate, weakly birefringent net. Plate 2.1: Figure 15

Observed range: NP115b-NP16; CP13b-CP14a; CNE10/11-CNE14

RETICULOFENESTRA RETICULATA GROUP

Typically circular reticulofenestrids with a circular central area spanned by a robust visible net. Some authors classify these taxa in a separate genus *Cribrocentrum.*

Reticulofenestra erbae Fornaciari et al., 2010

Plate 2.1: Figures 25-26, Plate 2.13: Figures 10, 14

Observed range: NP18-NP19/20; CP14b-CP15b; CNE16-CNE18/19

Reticulofenestra reticulata (Gartner & Smith, 1967) Roth & Thierstein, 1972

We include large forms sometimes referred to as *Cribrocentrum isabellae.* Specimens with wide central areas spanned by a visible net have been informally differentiated from *R. reticulata* as *R. reticulata* var.1. Plate 2.1: Figures 27-28, Plate 2.2: Figure 1, Plate 2.13: Figures 5-9, 13, 15

Observed range: NP16-NP19/20; CP13c-CP15b; CNE12-CNE18/19

Reticulofenestra* cf. *R. reticulata (Gartner & Smith, 1967) Roth & Thierstein, 1972

Included specimens of *R.* cf. *R. reticulata* var.1. Plate 2.1; Figure 29, Plate 2.2: Figure 2

Observed range: NP16-NP19/20; CP13c-CP15b; CNE12-CNE18/19

Reticulofenestra westerholdii Bown & Dunkley Jones, 2012

Plate 2.2: Figure 3

Observed range: NP16-NP22; CP14a-CP16c; CNE13-CNO2

RETICULOFENESTRA BISECTA GROUP

Elliptical reticulofenestrids with central area closed by a robust distal plug.

Reticulofenestra bisecta (Hay et al., 1966) Roth, 1970

Used for specimens <10 µm. Plate 2.2: Figure 4-5, Plate 2.13: Figures 11-12

Observed range: NP16-NP22; CP14a-CP16c; CNE14-CNO2

Reticulofenestra filewiczii (Wise & Wiegand, in Wise, 1983) Dunkley Jones et al., 2009

We place *R. filewiczii* in the *Reticulofenestra bisecta* group due to its coeval first occurrence during the MECO interval and similar morphological traits. Plate 2.2: Figures 7-8

Observed range: NP16-NP22; CP14a-CP16c; CNE14-CNO2

Reticulofenestra stavensis (Levin & Joerger, 1967) Varol, 1989

Used for specimens >10 µm. Plate 2.2: Figure 6

Observed range: NP16-NP22; CP14a-CP16c; CNE15-CNO2

Reticulofenestra magniscutum Bown & Newsam, in review

Large elliptical reticulofenestrids with a thickened dome like distal shield and central area closed by a plug. Plate 2.2: Figures 9-10

Observed range: NP15c-NP16; CP13c; CNE12. Rare occurrence over a very short stratigraphic interval. This species extends the range of this group back to lower in the middle Eocene.

OTHER RETICULOFENESTRA SPECIES

Reticulofenestra* cf. *R. bisecta

Specimens with a closed central area but no distinct plug. Plate 2.2: Figure 11, Plate 2.12: Figure 15

Observed range: NP15b-NP19/20; CP13b-CP15b; CNE10/11-CNE20.

Order **COCCOSPHAERALES** Haeckel, 1984 emend. Young & Bown, 1997

Family **CALCIDISCACEAE** Young & Bown, 1997

The classification of Young and Bown (2014) is used here, placing calcidiscids with closed central areas in *Calcidiscus* and open central areas in *Umbilicosphaera*.

Genus **CALCIDISCUS** Kamptner, 1950

Calcidiscus bicircus Bown, 2005a

Plate 2.2: Figure12-13

Observed range: NP15b-NP18; CP13b-CP14b; CNE10/11-CNE15

Calcidiscus gerrardii Bown & Dunkley Jones, 2006

Plate 2.2: Figure 14

Observed range: NP16; CP14a; CNE13. Very short stratigraphic range.

Calcidiscus pacificanus (Bukry, 1971) Varol, 1989

Plate 2.2: Figure 15

Observed range: NP15b-NP19/20; CP13b-CP15b; CNE10/11-CNE18/19

Genus **UMBILICOSPHAERA** Lohmann, 1902

Umbilicosphaera bramlettei (Hay & Towe, 1962) Bown et al., 2007

Informally grouped into small (<7.5 µm) and large (>7.5 µm). Plate 2.2: Figures 16-17, Plate 2.14; Figures 1-2

Observed range: NP15b-NP21; CP13b-CP16a; CNE10/11-CNE21. Larger forms >7.5 µm have a shorter range observed from NP15b-NP16; CP13b-CP14a; CNE10/11-CNE14.

Umbilicosphaera detecta (de Kaenel & Villa, 1996) Young & Bown, 2014

Plate 2.2: Figures 18-19

Observed range: NP15b-NP22; CP13b-CP16c; CNE10/11-CNO2

Umbilicosphaera henrikseniae Bown, 2005a

Plate 2.2: Figures 20-21

Observed range: NP15b-NP18; CP13b-CP14b; CNE10/11-CNE16

Umbilicosphaera jordanii Bown, 2005a

Plate 2.2: Figure 22

Observed range: NP15b-NP21; CP13b-CP16b; CNE10/11-CNO1. There is sporadic occurrence of this species throughout the middle Eocene to early

Oligocene. It is presumed this range extends above and below the observed range, as recorded in Bown et al. (2007).

Umbilicosphaera protoannula (Gartner, 1971) Young and Bown, 2014

Plate 2.2: Figures 23-24, Plate 2.14: Figure 4

Observed range: NP15b-NP21; CP13b-CP16a; CNE10/11-CNE21.

Genus **CORONOCYCLUS** Hay et al., 1966

Coronocyclus nitescens (Kamptner, 1963) Bramlette & Wilcoxon, 1967

Plate 2.2: Figure 25, Plate 2.14: Figure 4

Observed range: NP15b-NP22; CP13b-CP16c; CNE10/11-CNO2.

Family **COCCOLITHACEAE** Poche, 1913 emend. Young and Bown, 1997

Genus **COCCOLITHUS** Schwarz, 1894

Coccolithus biparteoperculatus (Varol, 1991) Bown & Dunkley Jones, 2012

Plate 2.3: Figure 10

Observed range: NP16-NP21; CP13c-CP16; CNE12-CNO1

Coccolithus cachaoi Bown, 2005a

Plate 2.3: Figure 6

Observed range: NP16-NP22; CP13c-CP16c, CNE12-CNO2

Coccolithus crucis Bown, 2005a

Plate 2.3: Figure 8, Plate 2.14: Figure 10

Observed range: NP16-NP17; CP14a-CP14b; CNE14-CNE15. Only two specimens were recorded under LM and one sample in SEM. The true range is likely extended below the observed range as it has previously been recorded to NP14 (Bown, 2005a).

Coccolithus eopelagicus (Bramlette & Riedel, 1954) Bramlette & Sullivan, 1961

Plate 2.3: Figure 9

Observed range: NP15b-NP22; CP13b-CP16c; CNE10/11-CNO2

Coccolithus formosus (Kamptner, 1963) Wise, 1973

Plate 2.3: Figure 1, Plate 2.14: Figure 9

Observed range: NP15b-NP21; CP13b-CP16b; CNE10/11-CNO1

Coccolithus hollisii Bown & Newsam, in review

Elliptical coccolith with a wide central area spanned by a broad traverse bar. Plate 2.3: Figure 3-4
Observed range: NP15b; CP13b; CNE10/11

Coccolithus* cf. *C. pauxillus Bown, 2005a

Circular to subcircular *Coccolithus* <5 µm. Plate 2.3: Figure 2, Plate 2.14: Figure 8
Observed range NP15b-NP21; CP13b-CP16a; CNE10/11-CNO1.

Coccolithus pelagicus (Wallich, 1877) Schiller, 1930

Informally grouped to small (3-5 µm), medium (5-8 µm), large (8-10 µm) and very large (10-14 µm). Plate 2.2: Figures 26-30, Plate 2.14: Figures 5-7, 14
Observed range: NP15b-NP22; CP13b-CP16c; CNE10/11-CNO2

Coccolithus* cf. *C. scheri Bown & Dunkley Jones 2012

Small specimens of *Coccolithus* with a transverse bar across the central area. Plate 2.3: Figure 5
Observed range NP15c-NP22; CP13c-CP16c; CNE12-CNO2

COCCOLITHUS GIGAS GROUP

We assign middle Eocene large to very large *Coccolithus* species with central area cross bars to this group following Bown and Newsam (in review).

Coccolithus gigas (Bramlette & Sullivan, 1961) Bown & Newsam, in review

This species has been re-assigned to the genus *Coccolithus* which is consistent with its morphology and extant species of this genus which produce central area crosses. Plate 2.3: Figure 13, Plate 2.14: Figure 15
Observed range: NP15b; CP13b; CNE10/11.

Coccolithus* cf. *C. gigas (Bramlette & Sullivan, 1961) Bown & Newsam, in review

Differentiated from *C. gigas* by having near-axial to slightly rotated cross bars rather than diagonal or near diagonal and from *C. mutatus* by thicker cross bars. Plate 2.3: Figure 14-15

Observed range: NP15b; CP13b; CNE10/11

Coccolithus mutatus (Perch-Nielsen, 1971) Bown, 2005a

Plate 2.3: Figure 12, Plate 2.14: Figure 13

Observed range: NP15b-NP16; CP13b-CP13c; CNE10/11-CNE12

Coccolithus opdykei Bown & Newsam, in review

Coccolithus with narrow central area spanned by axial to near axial broad cross bars. Plate 2.3: Figure 7

Observed range: NP15b; CP13b; CNE10/11

Coccolithus staurion Bramlette & Sullivan, 1961

Plate 2.3: Figure 11

Observed range: NP15b-NP17; CP13b-CP14b; CNE10/11-CNE15. Rare sporadic occurrence.

Genus **ERICSONIA** Black, 1964

Ericsonia robusta (Bramlette & Sullivan, 1961) Edwards & Perch-Nielsen, 1975

Plate 2.3: Figure 16

Observed range: NP15b-NP22; CP13b-CP16c; CNE10/11-CNO2. Rare in occurrence.

Genus **CHIASMOLITHUS** Hay, Mohler & Wade, 1966

The abundance of chiasmoliths within the Expedition 342 sediments is variable with some intervals sparse relative to others.

Chiasmolithus altus Bukry & Percival, 1971

We include forms sometimes referred to as *Chiasmolithus eoaltus* (Persico and Villa, 2008). Plate 2.4: Figures 8-9, Plate 2.15: Figures 3, 9

Observed range: NP16-NP22; CP14a-CP16c; CNE10/11CNO2

Chiasmolithus expansus (Bramlette & Sullivan, 1961) Gartner, 1970

Plate 2.4: Figure 3

Observed range: NP15b-NP17; CP13b-CP14b; CNE10/11-CNE15

Chiasmolithus grandis (Bramlette & Riedel, 1954) Radomski, 1968

Plate 2.4: Figure 10, Plate 2.15: Figure 4

Observed range: NP15b-NP18; CP13b-CP14b; CNE10/11-CNE16

Chiasmolithus nitidus Perch-Nielsen, 1971

Plate 2.3: Figure 17, Plate 2.15: Figure 2

Observed range: NP15b-NP21; CP13b-CP16a; CNE10/11-CNE21

Chiasmolithus* cf. *C. nitidus Perch-Nielsen, 1971

Plate 2.3: Figures 18-19

Observed range: NP15b-NP19/20; CP13b-CP15b; CNE10/11-CNE18/19

Chiasmolithus oamaruensis (Deflandre, 1954) Hay et al., 1966

Plate 2.4: Figures 2, 6

Observed range: NP18-NP22; CP14b-CP16c; CNE15-CNO2

Chiasmolithus solitus (Bramlette & Sullivan, 1961) Locker, 1968

Plate 2.4: Figures 2, 6, Plate 2.15: Figure 1

Observed range: NP15b-NP16; CP13b-CP14a; CNE10/11-CNE15. Rare reworked specimens through the late Eocene.

Chiasmolithus titus Gartner, 1970

Plate 2.3: Figure 20

Observed range: NP15b-NP21; CP13b-CP16a; CNE10/11-CNE21

Genus **CLAUSICOCCUS** Prins, 1979

Clausicoccus fenestratus (Deflandre & Fert, 1954) Prins, 1979

Plate 2.4: Figures 12-13, Plate 2.15: Figures 5-6

Observed range: NP15b-NP22; CP13b-CP16c; CNE10/11-CNO2

Clausicoccus subdistichus (Roth & Hay in Hay et al., 1967) Prins, 1979

Plate 2.4: Figure 11, Plate 2.15: Figures 7-8

Observed range: NP15b-NP22; CP13b-CP16c; CNE10/11-CNO2

Clausicoccus vanheckiae (Perch-Nielsen, 1986) de Kaenel & Villa, 1996

Plate 2.4: Figures 14-15, Plate 2.15: Figure 10

Observed range: NP15b-NP17; CP13b-CP14b; CNE10/11-CNE15

Genus **CRUCIPLACOLITHUS** Hay & Mohler in Hay et al., 1967

Cruciplacolithus cruciformis (Hay & Towe, 1962) Roth, 1970

Plate 2.4: Figure 16

Observed range: NP15b-NP18; CP13b-CP14b; CNE10/11-CNE15

Cruciplacolithus inseadus Perch-Nielsen, 1969

Plate 2.15: Figure 14

Observed range: NP17; CP14b; CNE15. Only observed under the SEM.

Cruciplacoltihus opacus Shamrock and Watkins, 2012

Plate 2.4: Figures 20-21

Observed range: NP15b-NP21; CP13b-CP16a; CNE10/11-CNO1

Cruciplacolithus* cf. *C. primus Perch-Nielsen, 1977

Plate 2.4: Figure 17-18

Observed range: NP15b-NP22; CP13b-CP16c; CNE10/11-CNO2

Cruciplacolithus tarquinius Roth & Hay in Hay et al., 1967

Plate 2.4: Figure 19, Plate 2.15: Figure 13

Observed range: NP15b-NP22; CP13b-CP16c; CNE10/11-CNO2

Genus **CAMPYLOSPHAERA** Kamptner, 1963

Campylosphaera dela (Bramlette and Sullivan, 1961) Hay & Mohler, 1967

Specimens were found with and without their central area cross. Plate 2.4: Figure 22, Plate 2.15: Figure 15

Observed range: NP15b-NP18; CP13b-CP14b; CNE10/11-CNE15.

Genus **BRAMLETTEIUS** Gartner, 1969

Bramletteius serraculoides Gartner, 1969

We identified both spines and bases of this species. Plate 2.4: Figures 23-24, Plate 2.15: Figure 11

Observed range: NP15b-NP21; CP13b-CP16b; CNE10/11-CNO1. Sporadic occurrence in NP15b. It is presumed this range extends back further, based on previous studies (Perch-Nielsen, 1985).

Genus **BIRKELUNDIA** Perch-Nielsen, 1971

Birkelundia arenosa Perch-Nielsen, 1971

Plate 2.4: Figure 25

Observed range: NP15b-NP16; CP13b-CP14a; CNE10/11-CNE14. Extremely rare occurrence.

PLACOLITH COCCOLITHS INCERTAE SEDIS

Genus **PEDINOCYCLUS** Bukry & Bramlette, 1971

Pedinocyclus annulus Shamrock & Watkins, 2012

Plate 2.5: Figures 6-7

Observed range: NP16; CP13c-CP14a; CNE12-CNE14. Only recorded in two samples. The range is expected to extend above and below the observed occurrences based on previous work.

Pedinocyclus* cf. *P. gibbsiae Bown & Dunkley Jones, 2012

Plate 2.5: Figure 4-5

Observed range: NP15b-NP22; CP13b-CP16c; CNE10/11-CNO2. Extremely rare occurrence.

Pedinocyclus larvalis Bukry & Bramlette, 1971

Plate 2.5: Figure 1-3

Observed range: NP15b-NP21; CP13b-CP16a; CNE10/11-CNO1. Rare sporadic occurrence but it is presumed to extend above and below the observed range, based on previous observations (Nannotax).

Genus **HAYELLA** Gartner, 1969

Hayella situliformis Gartner, 1969

Plate 2.5: Figures 10-11

Observed range: NP17-NP21; CP14b-CP16b; CNE15-CNO1

Hayella* cf. *H. situliformis Gartner, 1969

Morphotype of *H. situliformis* but subcircular not circular. Plate 2.5: Figure 12

Observed range: NP17-NP19/20; CP14b-CP15b; CNE15-CNE18/19

Hayella simplex Bown & Dunkley Jones, 2006

Plate 2.5: Figures 13-14

Observed range: NP15b-NP17; CP13b-CP14b; CNE10/11-CNE15.

Genus **MARKALIUS** Bramlette & Martini, 1964

Markalius inversus (Deflandre in Deflandre & Fert, 1954) Bramlette & Martini, 1964

Plate 2.5: Figure 15

Observed range: NP15b-NP21; CP13b-CP16a; CNE10/11-CNE21

Genus **TETRALITHOIDES (**Theodoridis, 1984) Jordan et al., 1993

Tetralithoides symeonidesii Theodoridis, 1984

Plate 2.5: Figures 8-9

Observed range: NP15b-NP21; CP13b-CP16b; CNE10/11-CNO1

Genus **POCILLITHUS** Dunkley Jones et al., 2009

Pocillithus spinulifer Dunkley Jones et al., 2009

Plate 2.14: Figures 11-12

Observed range: NP15b-NP16; CP13b-CP13c; CNE10/11-CNE12. Only recorded in two samples under the SEM.

2.5.2 Murolith coccoliths

Order **ZYGODISCALES** Young & Bown, 1997

Family **HELICOSPHAERACEAE** Black, 1971

Genus **HELICOSPHAERA** Kamptner, 1954

Helicosphaera bramlettei (Muller, 1970) Jafar & Martini, 1975

Plate 2.6: Figures 12-13, Plate 2.16: Figures 3-4

Observed range: NP15b-NP22; CP13b-CP16c; CNE10/11-CNO2

Helicosphaera* cf. *H. bramlettei Bramlette & Wilcoxon, 1967

Similar to *H. bramlettei* but with a near-longitudinal disjunct bar. Plate 2.6: Figures 14-15

Observed range: NP15b-NP22; CP13b-CP16c; CNE10/11-CNO2

Helicosphaera clarissima Bown, 2005a

Plate 2.6: Figure 1, Plate 2.16: Figure 2

Observed range: NP16-NP22; CP14a-CP16c; CNE13-CNO2

Helicosphaera compacta Bramlette & Wilcoxon, 1967

Plate 2.6, Figures 2-4, Plate 2.16, Figure 1

Observed range: NP16-NP22; CP14a-CP16c; CNE13-CNO2.

Helicosphaera* cf. *H. compacta Haq, 1966 (Jafar & Martini, 1975)

Similar to *H. compacta* but with large central area pores. Plate 2.6: Figure 5

Observed range: NP21-NP22; CP16-CP16c; CNE21-CNO2.

Helicosphaera lophota (Bramlette & Sullivan, 1961) Locker, 1973

Plate 2.6: Figures 9-10

Observed range: NP15b-NP16; CP13b-CP14a; CNE10/11-CNE15

Helicosphaera papillata (Bukry & Bramlette, 1969) Jafar & Martini, 1975

Plate 2.6: Figures 7-8, Plate 2.16: Figure 7-8

Observed range: NP15c-NP22; CP14a-CP16c; CNE12-CNO2

Helicosphaera reticulata Bramlette & Wilcoxon, 1967

Plate 2.6: Figure 6

Observed range: NP15c-NP22; CP13c-CP16c; CNE12-CNO2

Helicosphaera robinsoniae Bown & Dunkley Jones, 2012

Plate 2.6: Figure 11

Observed range: NP19/20; CP16; CNE21. Extremely rare in occurrence, only recorded in two samples.

Helicosphaera seminulum Bramlette & Sullivan, 1961

Plate 2.6: Figures 16-17, Plate 2.16: Figure 6

Observed range: NP15b-NP22; CP13b-CP16c; CNE10/11-CNO2

Helicosphaera wilcoxonii (Gartner, 1971) Jafar & Martini, 1975

Plate 2.6: Figure 18, Plate 2.16: Figure 5

Observed range: NP15c-NP21; CP13c-CP16; CNE12-CNO1. Rare occurrence but it is presumed that the range extends further into the Oligocene than observed.

Family **PONTOSPHAERACEAE** Lemmermann, 1908

Genus **PONTOSPHAERA** Lohmann, 1902

Species of *Pontosphaera* have been divided into two groups, adorned (*Pontosphaera pectinata* group) and unadorned (*Pontosphaera plana* group), based on Bown (2005a).

PONTOSPHAERA PLANA GROUP

Pontosphaerids which are plain and unadorned.

Pontosphaera brinkhuisii Bown & Newsam, in review

Very large elliptical pontosphaerids with thick rim cycle and narrow central area. Plate 2.6: Figure 25, Plate 2.16: Figures 13

Observed range: NP15c-NP16; CP13c; CNE12. Occurs within a short stratigraphic interval.

Pontosphaera duocava (Bramlette & Sullivan, 1961) Romein, 1979

Plate 2.6: Figure 14

Observed range: NP15b-NP17; CP13b-CP14b; CNE10/11-CNE15

Pontosphaera* cf. *P. duocava (Bramlette & Sullivan, 1961) Romein, 1979

Plate 2.7: Figure 1

Observed range: NP15b-NP22; CP13b-CP16c; CNE10/11-CNO2

Pontosphaera exilis (Bramlette & Sullivan, 1961) Romein, 1979

Plate 2.7: Figure 2

Observed range: NP15b-NP22; CP13b-CP16c; CNE10/11-CNO2

Pontosphaera multipora (Kamptner, 1948 ex Deflandre, 1954) Roth, 1970

Plate 2.7: Figures 6, 13, Plate 2.16: Figure 9

Observed range: NP15b-NP22; CP13b-CP16c; CNE10/11-CNO2

Pontosphaera obliquipons (Deflandre in Deflandre & Fert, 1954) Romein, 1979

Plate 2.7: Figures 3-4

Observed range: NP15b-NP22; CP13b-CP16c; CNE10/11-CNO2

Pontosphaera panarium (Deflandre in Deflandre & Fert, 1954) Aubry, 1986

Plate 2.6: Figures 22-23

Observed range: NP15b-NP22; CP13b-CP16c; CNE10/11-CNO2

Pontosphaera plana (Bramlette & Sullivan, 1961) Haq, 1971

Plate 2.6: Figures 19-20

Observed range: NP15b-NP22; CP13b-CP16c; CNE10/11-CNO2

Pontosphaera* cf. *P. rimosa (Bramlette & Sullivan, 1961) Roth & Thierstein, 1972

Plate 2.7: Figure 5

Observed range: NP15b-NP22; CP13b-CP16c; CNE10/11-CNO2

Pontosphaera versa (Bramlette & Sullivan, 1961) Sherwood, 1974

Plate 2.6: Figures 21, 24

Observed range: NP15b-NP21; CP13b-CP16a; CNE10/11-CNO1. It is presumed that the range extends higher into NP22 based on previous studies (Bown, 2005a), but it exhibits a rare sporadic occurrence from NP16.

PONTOSPHAERA PECTINATA GROUP

Pontophaerids which are adorned with depressions, furrows and slits.

Pontosphaera alta Roth, 1970

Plate 2.7: Figure 7, Plate 2.16: Figure 12

Observed range: NP15b-NP22; CP13b-CP16c; CNE10/11-CNO2. Extremely rare in the middle Eocene.

Pontosphaera clinosulcata Bown, 2005a

Plate 2.7: Figure 8

Observed range: NP15b; CP13b; CNE10/11

Pontosphaera formosa (Bukry & Bramlette, 1968) Romein, 1979

Plate 2.7: Figures 11-12
Observed range: NP15b-NP21; CP13b-CP16b; CNE10/11-CNO1

Pontosphaera pectinata (Bramlette & Sullivan, 1961) Sherwood, 1974

Plate 2.7, Figure 9
Observed range: NP15b-NP22; CP13b-CP16c; CNE10/11-CNO2

Pontosphaera* cf. *P. perforomarginata Bown, 2005a

Plate 2.7: Figure 15
Observed range: NP15b-NP19/20; CP13b-CP15b; CNE10/11-CNE18/19

Pontosphaera pulcheroides (Sullivan, 1964) Romein, 1979

Plate 2.7: Figure 16
Observed range: NP15b; CP13b; CNE10/11. Extremely rare, only recorded in two samples.

Pontosphaera pulchra (Deflandre in Deflandre & Fert, 1954) Romein, 1979

Plate 2.7: Figure 10, Plate 2.16: Figure 10
Observed range: NP15b-NP21; CP13b-CP16; CNE10/11-CNO1

Pontosphaera punctosa (Bramlette & Sullivan, 1961) Perch-Nielsen, 1984

Plate 2.7: Figure 19
Observed range: NP15b-NP22; CP13b-CP16c; CNE10/11-CNO2

Pontosphaera wilsonii Bown & Newsam, in review

Elliptical pontosphaerid with central area plate crossed by prominent oblique ridges that are bright in XPL. Plate 2.7: Figure 20
Observed range: NP15b-NP16; CP13b-CP13c; CNE10/11-CNE12

Pontosphaera zigzag (Roth & Hay, 1967 in Hay et al. 1967) Bown & Newsam, in review

Plate 2.7: Figure 21, Plate 2.16: Figure 11
Observed range: NP16-NP22; CP13c-CP16c; CNE12-CNO2. Extremely rare until NP19/20.

***Pontosphaera* sp. 1 sp. nov.**

Small pontosphaerids with two large holes separated by a traverse bar and a bright longitudinal bar. Plate 2.7: Figure 22

Observed range: NP16-NP22; CP14a-CP16c; CNE13-CNO2

Genus **SCYPHOSPHAERA** Lohmann, 1902

Due to the rare and infrequent observance of this genus, species names were not applied.

Plate 2.7: Figures 17-18, 23-24, Plate 2.16: Figures 14-15

Observed range: NP15b-NP22; CP13b-CP16c; CNE10/11-CNO2

Family **ZYGODISCACEAE** Hay & Mohler, 1967

Genus **NEOCOCCOLITHES** Sujkowski, 1931

Neococcolithes dubius (Deflandre in Deflandre & Fert, 1954) Black 1967

Plate 2.5: Figures 16-17, Plate 2.17: Figure 1

Observed range: NP15b-NP19/20; CP13b-CP15b; CNE10/11-CNE18/19

Neococcolithes* cf. *N. purus Bown & Newsam, in review

Narrowly elongate murolith with a wide vacant central area. Differs from *N. purus* by its thicker rim. Plate 2.5: Figure 18

Observed range: NP16-NP18; CP14a-CP14b; CNE13-CNE16

Neococcolithes radiatus Bown & Newsam, in review

Narrowly elongate murolith with a wide central area with numerous radiating bars. Plate 2.5: Figures 19-20

Observed range: NP17; CP14b, CNE15. Extremely rare occurrence.

Genus **ISTHMOLITHUS** Deflandre in Deflandre & Fert, 1954

Isthmolithus recurvus Deflandre in Deflandre & Fert, 1954

Plate 2.5: Figure 21, Plate 2.17: Figure 2

Observed range: NP19/20-NP22; CP15b-CP16c; CNE17-CNO2. Due to the variability in the first occurrence of this species, the base common occurrence has been used to define zone NP19/20 which occurs at 37.95 Ma.

Genus **LOPHODOLITHUS** Deflandre in Deflandre & Fert, 1954

Lophodolithus acutus Bukry & Percival, 1971

Plate 2.5: Figure 22

Observed range: NP15b-NP16; CP13b-CP13c; CNE10/11-CNE12

Lophodolithus mochlophorus Deflandre in Deflandre & Fert, 1954

Plate 2.5: Figure 23

Observed range: NP15b; CP13b; CNE10/11

Lophodolithus nascens Bramlette & Sullivan, 1961

Plate 2.5: Figure 24, Plate 2.16: Figure 16

Observed range: NP15b-NP16; CP13b-CP13c; CNE10/11-CNE12

Lophodolithus rotundus Bukry & Percival, 1971

Plate 2.5: Figure 25

Observed range: NP15b-NP16; CP13b-CP13c; CNE10/11-CNE12

Order **SYRACOSPHAERALES** Hay, 1977 emend. Young et al., 2003

Family **CALCIOSOLENIACEAE** Kamptner, 1927

Genus **CALCIOSOLENIA** Gran, 1912

Calciosolenia alternans Bown & Dunkley Jones, 2006

Plate 2.5: Figure 26

Observed range: NP15b-NP17; CP13b-CP14b; CNE10/11-CNE15

Family **SYRACOSPHAERACEAE** Lemmermann, 1908

Genus **SYRACOSPHAERA** Lohmann, 1902

Syracosphaera? octiforma Bown & Newsam, in review

Narrow rimmed coccolith with figure of eight outline. Plate 2.5: Figures 28-29

Observed range: NP15c-NP18; CP13c-CP14b; CNE12-CNE15. Extremely rare until NP17.

Syracosphaera tanzanensis Bown, 2005a

Plate 2.5: Figure 27

Observed range: NP15b-NP22; CP13b-CP16c; CNE10/11-CNO2

Family **RHABDOSPHAERACEAE** Haeckel, 1894

Genus **BLACKITES** Hay & Towe, 1962

Species within *Blackites* have been split into informal groups following Bown (2005a) and Nannotax.

BLACKITES GLADIUS GROUP

Moderately tall spines with a distinct rim structure with the outer cycle lying distally over the inner cycle.

Blackites creber (Deflandre in Deflandre & Fert, 1954) Sherwood, 1974

Plate 2.8: Figure 1

Observed range: NP15b-NP17; CP13b-CP14b; CNE10/11-CNE15

Blackites gladius (Locker, 1967) Varol, 1989

Plate 2.8: Figure 2, Plate 2.17: Figures 3-4

Observed range: NP15b-NP18; CP13b-14b; CNE10/11-CNE15. The range of this species is seen higher than previously documented, as recognised in the Tanzania sediments. This most likely reflects its rare and inconsistent record in most deep sea sediments, contrasting with more consistent records in well preserved sections such as Expedition 342 and Tanzania. This species is therefore not an appropriate marker species for the Martini (1971) Zone NP16 and *Nannotetrina fulgens* is used.

Blackites rotundus Bown, 2005a

Plate 2.8: Figure 3

Observed range: NP15b-NP17; CP13b-CP14b; CNE10/11-CNE15.

BLACKITES MORIONUM GROUP

Short to moderately tall wide spines with typical rim structure with two cycles (the outer cycle smaller) lying side by side.

Blackites deflandrei (Perch-Nielsen, 1968) Bown, 2005a

Plate 2.8: Figure 3

Observed range: NP15b-NP19/20; CP13b-CP15b; CNE10/11-CNE20

Blackites fustis Bown, 2005a

Observed range: NP15b-NP17; CP13b-CP14b; CNE10/11-CNE15. Only observed in two samples.

Blackites globosus Bown, 2005a

Plate 2.8: Figure 6

Observed range: NP15b-NP16; CP13b-CP14a; CNE10/11-CNE15

Blackites pseudomorionum (Locker, 1967) Aubry, 1999

Plate 2.8: Figure 7

Observed range: NP15b-NP17; CP13b-CP14b; CNE10/11-CNE15

BLACKITES SPINOSUS GROUP

Tall narrow spines and typical rim structure.

***Blackites* spines sp.**

Fragments of *Blackites* spines are observed throughout the studied section.

Observed range: NP15b-NP22; CP13b-CP16c; CNE10/11-CNO2

Blackites spinosus (Deflandre & Fert, 1954) Hay & Towe, 1962

Plate 2.8: Figure 13, Plate 2.17: Figure 14

Observed range: NP15b-NP22; CP13b-CP16c; CNE10/11-CNO2

Blackites* cf. *B. spinosus (Deflandre & Fert, 1954) Hay & Towe, 1962

Similar to *B. spinosus* but with a shorter spine which rapidly tapers. Plate 2.8: Figure 12

Observed range: NP15b-NP22; CP13b-CP16c; CNE10/11-CNO2

Blackites stilus Bown, 2005a

Plate 2.8: Figure 15

Observed range: NP15b-NP22; CP13b-CP16c; CNE10/11-CNO2

Blackites tenuis Bramlette & Sullivan, 1961

Plate 2.8: Figure 11, Plate 2.17: Figure 13

Observed range: NP15b-NP22; CP13b-CP16c; CNE10/11-CNO2

Blackites tortilis Bown & Dunkley Jones, 2006

Plate 2.8: Figure 14, Plate 2.17: Figure 9

Observed range: NP16-NP18; CP13c-CP14b; CNE12-CNE15

BLACKITES AMPLUS GROUP

Blackites bases, spine absent or very small.

Blackites amplus Roth & Hay, 1967

Plate 2.8: Figure 8

Observed range: NP15b-NP22; CP13b-CP16c; CNE10/11-CNO2

Blackites friedrichii Bown & Newsam, in review.

Blackites base which is broad and circular with a low thin walled globular spine with a distinct image in XPL; crenulate edge and strong extinction cross. Plate 2.8: Figure 9

Observed range: NP16-NP19/20; CP14a-CP15b; CNE13-CNE20

Blackites furvus Bown & Dunkley Jones, 2006

Plate 2.8: Figure 10

Observed range: NP15b-NP22; CP13b-CP16c; CNE10/11-CNO2

BLACKITES INFLATUS GROUP

Inflated spine with maximum width above the base

Blackites kilwaensis Bown, 2005a

Plate 2.8: Figure 20

Observed range: NP15b; CP13b; CNE10/11

Blackites ornatus Bown & Dunkley Jones, 2006

Plate 2.8: Figure 21, Plate 2.17: Figure 10

Observed range: NP15b-NP16; CP13b-CP14a; CNE10/11-CNE14

Blackites piriformis (Pavsic in Khan et al., 1975) Aubry, 1999

Plate 2.8: Figure 17

Observed range: NP15b-NP17; CP13b-CP14b; CNE10/11-CNE18/19

OTHER BLACKITES SPECIES

Blackites lippertii Bown & Newsam, in review.

Broad base and broad thin walled moderately tall bullet shaped spine which tapers to a point. Plate 2.8: Figure 18

Observed range: NP16-NP21; CP14a-CP16a; CNE13-CNE21

Blackites* cf. *B. sextonii Bown & Newsam, in review

Broad base and broad thin walled spine which tapers sharply to a point. Differentiated from *B. sextonii* by the shorter length of spine. Plate 2.8: Figure 19

Observed range: NP16-NP19/20; CP14a-CP15b; CNE14-CNE20

Blackites virgatus Bown, 2005a

Plate 2.8: Figure 22

Observed range: NP15b-NP16; CP13b-CP13c; CNE10/11-CNE12

GENUS **RHABDOSPHAERA**

Rhabdosphaera gracilentus Bown & Dunkley Jones, 2006

Plate 2.8: Figure 16

Observed range: NP15b-NP21; CP13b-CP16a; CNE10/11-CNE21

Rhabdosphaera vitrea (Deflandre in Deflandre & Fert, 1954) Shafik, 1981

Included within this species are bases which previously were described as *Holodiscolithus geisenii* (Bown, 2005a). Plate 2.8: Figures 23-24

Observed range: NP15b-NP22; CP13b-CP16c; CNE10/11-CNO2

Order **EIFFELLITHALES** Rood et al., 1971
Family **CHIASTOZYGACEAE** Rood et al., 1973
Genus **NEOCREPIDOLITHUS** Romein, 1979

Neocrepidolithus grandiculus Bown, 2005a

Plate 2.5: Figure 25

Observed range: NP15b; CP13b; CNE10/11.

2.5.3 Holococcoliths

Rare in occurrence apart from *Zyghrablithus bijugatus* and *Daktylethra.*

Family **CALYPTROSPHAERACEAE** Boudreaux & Hay, 1967
Genus **HOLODISCOLITHUS** Roth, 1970

Holodiscolithus macroporus (Deflandre in Deflandre & Fert, 1954) Roth, 1970

We have included the new species *Holodiscolithus scullyae* (Bown & Newsam, in review) within *H. macroporus.* Plate 2.9, Figures 1-3

Observed range: NP15b-NP21; CP13b-CP16a; CNE10/11-CNO1. Very rare occurrence.

Holodiscolithus minolettii Bown, 2005a

Observed range: NP16-NP21; CP14a-CP16a; CNE13-CNE21

Holodiscolithus solidus (Deflandre in Deflandrei & Fert, 1954) Roth, 1970

Plate 2.9: Figure 4

Observed range: NP15b-NP17; CP13b-CP14b; CNE10/11-CNE15

Holodiscolithus* cf. *H. solidus (Deflandre in Deflandrei & Fert, 1954) Roth, 1970

Plate 2.9: Figure 5

Observed range: NP15b-NP17; CP13b-CP14b; CNE10/11-CNE15

Genus **ZYGRHABLITHUS** Deflandre, 1959

Zygrhablithus bijugatus bijugatus (Deflandre in Deflandre & Fert, 1954) Deflandre, 1959

Plate 2.9: Figures 6-7, Plate 2.18: Figures 1-2

Observed range: NP15b-NP22; CP13b-CP16c; CNE10/11-CNO2

Zygrhablithus* cf. *Z. bijugatus bijugatus (Deflandre in Deflandre & Fert, 1954) Deflandre, 1959

Plate 2.9: Figure 10

Observed range: NP15b-NP21; CP13b-CP16a; CNE10/11-CNO1

Zygrhablithus bijugatus (Deflandre in Deflandre & Fert, 1954) Deflandre, 1959 ***cornutus*** Bown, 2005a

Plate 2.9: Figures 8-9, Plate 2.18: Figures 3-4

Observed range: NP16-NP21; CP14a-CP16a; CNE14-CNO1

Genus **LANTERNITHUS** Stradner, 1962

Lanternithus minutus Stradner, 1962

Plate 2.9: Figures 13-15, Plate 2.18: Figures 5, 9

Observed range: NP15b-NP21; CP13b-CP16a; CNE10/11-CNO1

Genus **DAKTYLETHRA** Gartner in Gartner & Bukry, 1969

Daktylethra probertii Bown & Dunkley Jones, 2006

Plate 2.9: Figure 18

Observed range: NP16-NP17; CP14a-CP14b; CNE13-CNE15. Extremely rare.

Daktylethra punctulata Gartner in Gartner & Bukry, 1969

Plate 2.9: Figures 16-17, Plate 2.18: Figure 8

Observed range: NP16-NP19/20; CP13c-CP15b; CNE12-CNE18/19

Daktylethra unitatis Bown & Dunkley Jones, 2006

Plate 2.9: Figures 19-23, Plate 2.18: Figure 7

Observed range: NP15b-NP17; CP13b-CP14b; CNE10/11-CNE15

Genus **ORTHOZYGUS** Bramlette & Wilcoxon, 1967

Orthozygus aureus (Stradner, 1962) Bramlette & Wilcoxon, 1967

Plate 2.9: Figures 26-27

Observed range: NP16-NP17; CP14a-CP14b; CNE14-CNE15

Genus **CLATHROLITHUS** Deflandre in Deflandre & Fert, 1954

Due to the rare and infrequent observance of this genus species names were not applied.

Plate 2.9: Figures 28-30, Plate 2.18: Figure 10

Observed range: NP16-NP17; CP14a-CP14b; CNE13-CNE15

2.5.4 Nannoliths

Family **DISCOASTERACEAE** Tan, 1927

Genus **DISCOASTER** Tan, 1927

Discoaster barbadiensis Tan, 1927

Plate 2.10: Figures 1-2, Plate 2.19: Figure 1

Observed range: NP15b-NP19/20; CP13b-CP15b; CNE10/11-CNE20

Discoaster deflandrei Bramlette & Riedel, 1954

Plate 2.10: Figures 7-8, Plate 2.19: Figure 6

Observed range: NP15b-NP22; CP13b-CP16c; CNE10/11-CNO2

Discoaster distinctus Martini, 1958

Plate 2.10: Figures 16-17, Plate 2.19: Figure 5

Observed range: NP15b-NP16; CP13b-CP14a; CNE10/11-CNE14

Discoaster martinii Stradner, 1959

Plate 2.10: Figures 22-23

Observed range: NP15c; CP13c; CNE12. Only recorded in a couple of samples, but it is presumed the range extends further back into the middle Eocene based on previous observations (Nannotax).

Discoaster nodifer (Bramlette & Riedel, 1954) Bukry, 1973

Plate 2.10: Figures 9-10, Plate 2.19: Figures 4, 7-8

Observed range: NP15b-NP22; CP13b-CP16c; CNE10/11-CNO2

Discoaster saipanensis Bramlette & Riedel, 1954

Plate 2.10: Figures 3-4, Plate 2.19: Figure 2

Observed range: NP15b-NP19/20; CP13b-CP15b; CNE10/11-CNE20

Discoaster tanii Bramlette & Riedel, 1954

Plate 2.10: Figures 5-6, Plate 2.19: Figure 3

Observed range: NP15b-NP22; CP13b-CP16c; CNE10/11-CNO2

Discoaster wemmelensis Achuthan & Stradner, 1969

Plate 2.10: Figures 11-12

Observed range: NP15b-NP16; CP13b-CP13c; CNE10/11-CNE12

Family **SPHENOLITHACEAE** Deflandre, 1952

Genus **SPHENOLITHUS** Deflandre in Grasse, 1952

Sphenoliths were split into informal groups following Bown and Dunkley Jones (2012) and Nannotax; *Sphenolithus radians* group, *Sphenolithus furcatolithoides* group, *Sphenolithus predistentus* group and *Sphenolithus moriformis* group.

SPHENOLITHUS RADIANS GROUP

Sphenolith base with four distinct quadrants, spines can be compound, duo or monocrystalline.

Sphenolithus radians Deflandre in Grasse, 1952

Plate 2.10: Figure 13
Observed range: NP15b-NP22; CP13b-CP16c; CNE10/11-CNO2

Sphenolithus spiniger Bukry, 1971

Plate 2.10: Figure 14, Plate 2.19: Figures 9, 12
Observed range: NP15b-NP17; CP13b-CP14b; CNE10/11-CNE15. Top common recorded ~200 kyr before the last occurrence.

Sphenolithus* cf. *S. spiniger Bukry, 1971

Plate 2.10: Figure 15
Observed range: NP17-NP19/20; CP14b-CP15b; CNE15-CNE18/19.

SPHENOLITHUS FURCATOLITHOIDES GROUP

A subgroup of *Sphenolithus radians* group. Divided into species using spine size and degree of taper as well as height and shape.

Sphenolithus cuniculus Bown, 2005a

Plate 2.10: Figure 24
Observed range: NP15c-NP16; CP13c-CP14a; CNE12-CNE14

Sphenolithus furcatolithoides Locker, 1967

Plate 2.10: Figures 18-19
Observed range: NP15b-NP16; CP13b-CP14a; CNE10/11-CNE13

Sphenolithus kempii Bown & Dunkley Jones, 2012

Plate 2.11: Figure 1
Observed range: NP15b; CP13b; CNE10/11. Only two specimens recorded.

Sphenolithus* cf. *S. kempii Bown & Dunkley Jones, 2012

Plate 2.11: Figure 2
Observed range: NP16-NP21; CP14a-CP16a; CNE13-CNE21

Sphenolithus strigosus Bown & Dunkley Jones, 2006

Plate 2.10: Figures 20-21, Plate 2.11: Figure 11, Plate 2.19: Figure 11

Observed range: NP15b-NP16; CP13b-CP14a; CNE10/11-CNE14

SPHENOLITHUS PREDISTENTUS GROUP

A moncyclic base with two low quadrants and tall spines that are duo or monocrystalline and can taper in bifurcations.

Sphenolithus celsus Haq, 1971

Plate 2.11: Figure 3

Observed range: NP17; CP14b; CNE15

Sphenolithus intercalaris Martini, 1976

Plate 2.11: Figure 4

Observed range: NP18-NP19/20; CP14b-CP15b; CNE16-CNE18/19

Sphenolithus obtusus Bukry, 1971

Plate 2.11: Figure 5, Plate 2.19: Figures 13-14

Observed range: NP17-NP18; CP14b; CNE15

Sphenolithus predistentus Bramlette & Wilcoxon, 1967

Plate 2.11: Figure 6

Observed range: NP16-NP22; CP14a-CP16c; CNE13-CNO2. Rare occurrence in first ~300 kyr with an increase in abundance (base common) in CNE14.

Sphenolithus tribulosus Roth, 1970

Plate 2.11: Figure 7

Observed range: NP18-NP21; CP14b-NP16a; CNE16-CNO1. This species is known to range higher into the Oligocene based on previous studies (Bown and Dunkley Jones, 2006) but this is not observed in this study, presumably due to its rare occurrence.

SPHENOLITHUS MORIFORMIS GROUP

Sphenoliths without apical spines.

Sphenolithus moriformis (Bronniman & Stradner, 1960) Bramlette & Wilcoxon, 1967

Plate 2.11: Figure 8, Plate 2.19: Figure 10

Observed range: NP15b-NP22; CP13b-CP16c; CNE10/11-CNO2

Genus **PEMMA** Klumpp, 1953

These are extremely rare due to the open ocean location and only a few specimens were identified.

Pemma papillatum Martini, 1959

Plate 2.11: Figure 9

Observed range: NP19/20; CP15b; CNE18/19. Between 36.22 and 36.05 Ma four samples recorded a one specimen observation of a *Pemma papillatum* segment and the sample at 36.22 Ma records rare observations of *Pemma papillatum* segments (<1 per 1-10 FOV). These observations do not represent the true range of this species.

Pemma triqueta Bown & Dunkley Jones, 2006

Plate 2.11: Figure 10

Observed range: NP19/20; CP15b; CNE18/19. There are three samples where one specimen of *Pemma triqueta* is observed.

INCERTAE SEDIS NANNOLITHS

Genus **NANNOTETRINA** Achuthan & Stradner, 1969

Nannotetrina alata (Martini, 1960) Haq and Lohmann, 1976

Observed range: NP15b; CP13b; CNE10/11. Only recorded in two samples.

Nannotetrina cristata (Martini, 1958) Perch-Nielsen, 1971

Plate 2.11: Figures 12, 17-18

Observed range: NP15b-NP16; CP13b-CP14a; CNE10/11-CNE13

Nannotetrina fulgens (Stradner in Martini & Stradner, 1960) Achuthan & Stradner, 1969

Plate 2.11: Figures 13, 16

Observed range: NP15b-NP15c; CP13b-CP14a; CNE10/11-CNE12. Very rare occurrence.

Nannotetrina pappii (Stradner, 1959) Perch-Nielsen, 1971

Plate 2.11: Figure 15

Observed range: NP15b-NP15c; CP13b-CP14a; CNE10/11-CNE12

Nannotetrina spinosa (Stradner in Martini & Stradner, 1960) Bukry, 1973

Plate 2.11: Figures 14, 19

Observed range: NP15b-NP16; CP13b-CP14a; CNE10/11-CNE13

Genus **LEESELLA** Bown & Dunkley Jones, 2006

Leesella procera Bown & Dunkley Jones, 2006

Plate 2.11: Figures 20-21

Observed range: NP16-NP17; CP13c-CP14b; CNE12-CNE15. Rare occurrence.

PLATE 2.1
Noelaerhabdaceae: *Cyclicargolithus; Reticulofenestra*

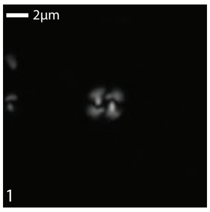

1
Cyclicargolithus floridanus
1408B-14H-3W, 123-124cm

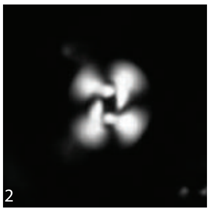
2
Cyclicargolithus floridanus
1408C-10H-2W, 123-124cm

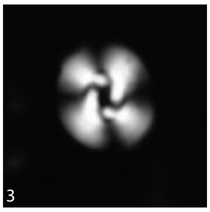
3
Cyclicargolithus floridanus
1411B-27X-5W, 72cm

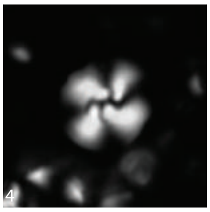
4
C. cf. *C. floridanus*
1408B-24X-5W, 3-4cm

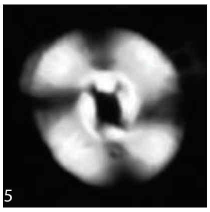
5
C. cf. *C. abisectus*
1408B-22X-2W, 123-124cm

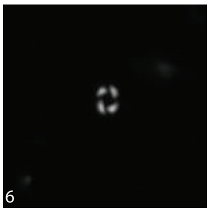
6
Reticulofenestra minuta
1408B-14H-3W, 123-124cm


7
Reticulofenestra dictyoda
1408B-14H-3W, 123-124cm

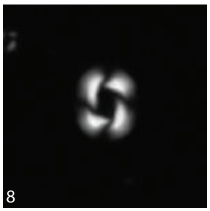
8
Reticulofenestra dictyoda
1408B-14H-3W, 123-124cm

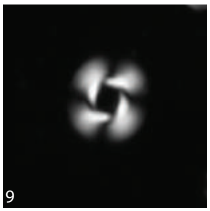
9
Reticulofenestra dictyoda
1408B-14H-3W, 123-124cm

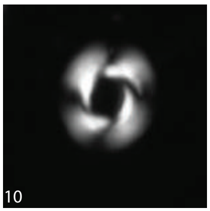
10
Reticulofenestra dictyoda
1408B-14H-3W, 123-124cm

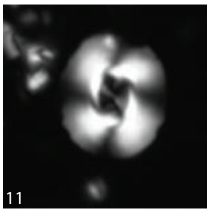
11
Reticulofenestra dictyoda
1408A-21X-4W, 3-4cm

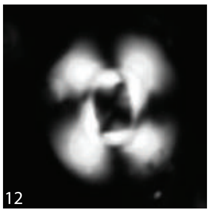
12
Reticulofenestra dictyoda
1408A-21X-4W, 3-4cm

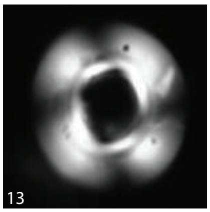
13
Reticulofenestra dictyoda
1408B-14H-3W, 123-124cm

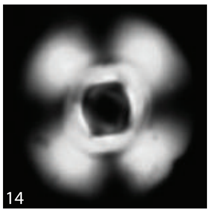
14
Reticulofenestra cf. *R. hillae*
1408A-14H-4W, 63-64cm

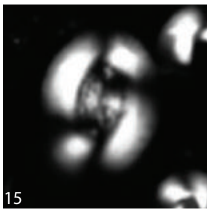
15
Reticulofenestra onusta
1408B-21X-6H, 63-64cm

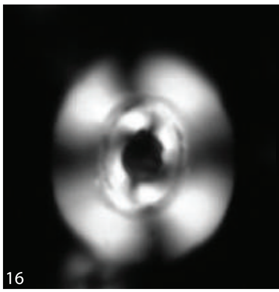
16
Reticulofenestra hillae
1411B-18H-2W, 90cm

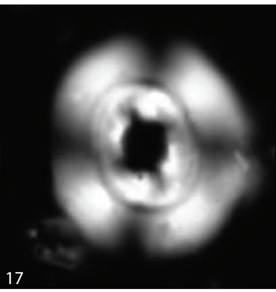
17
Reticulofenestra hillae
1411B-18H-2W, 90cm

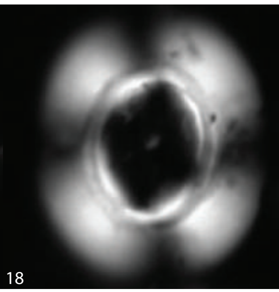
18
Reticulofenestra umbilicus
1411B-18H-2W, 90cm

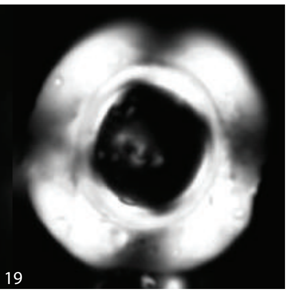
19
Reticulofenestra wadeae
1411B-28X-7H, 22cm

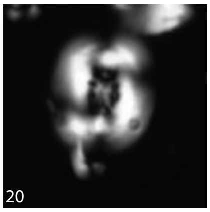
20
Reticulofenestra daviesii
1411B-18H-2W, 90cm

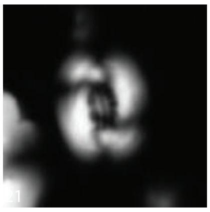
21
Reticulofenestra daviesii
1411B-18H-2W, 90cm

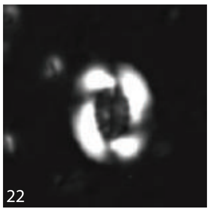
22
Reticulofenestra lockeri
1411B-18H-7W, 60cm

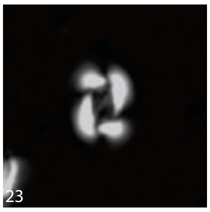
23
Reticulofenestra lockeri
1411B-18H-7W, 60cm

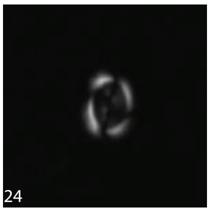
24
Reticulofenestra macmillani
1411B-18H-2W, 90cm

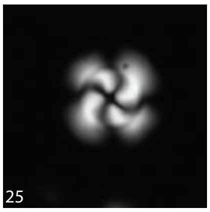
25
Reticulofenestra erbae
1411B-27X-5W, 72cm

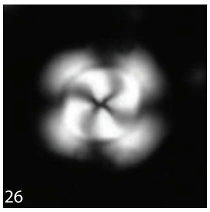
26
Reticulofenestra erbae
1411B-27X-5W, 72cm

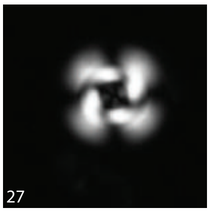
27
Reticulofenestra reticulata
1408C-6H-3W, 123-124cm

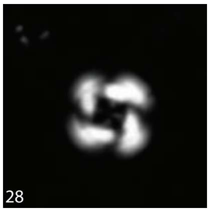
28
Reticulofenestra reticulata
1408C-10H-2W, 123-124cm

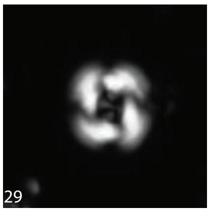
29
R. cf. *R. reticulata*
1408B-14H-3W, 123-124cm

PLATE 2.2

Noelaerhabdaceae: *Reticulofenestra*; Calcidiscaceae: *Calcidiscus, Umbilicosphaera, Coronocyclus*; Coccolithaceae: *Coccolithus*

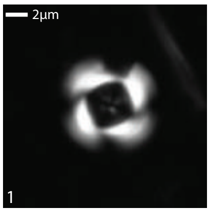

1
R. reticulata var. 1
1408C-6H-3W, 123-124cm

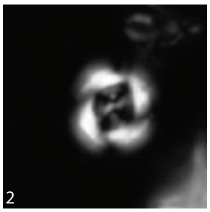
2
R. cf. *R. reticulata* var. 1
1408B-14H-3W, 123-124cm

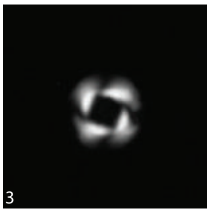
3
Reticulofenestra westerholdii
1411B-27X-5W, 72cm

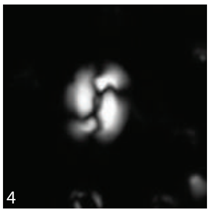
4
Reticulofenestra bisecta
1411B-27X-5W, 72cm

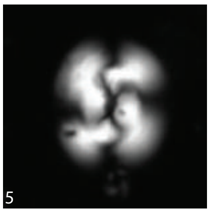
5
Reticulofenestra bisecta
1411B-18H-2W, 90cm

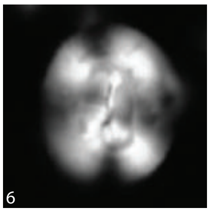
6
Reticulofenestra stavensis
1411B-18H-2W, 90cm

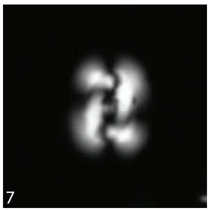
7
Reticulofenestra filewiczii
1411B-18H-2W, 90cm

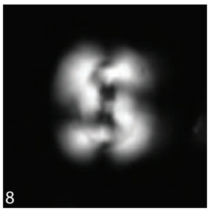
8
Reticulofenestra filewiczii
1411B-18H-2W, 90cm

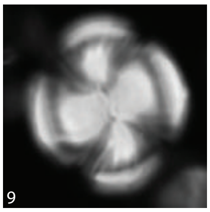
9
R. magniscutum
1408C-15H-6W, 3-4cm

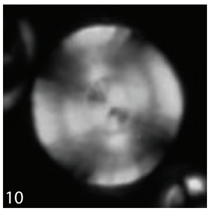
10
R. magniscutum
1408C-15H-6W, 3-4cm

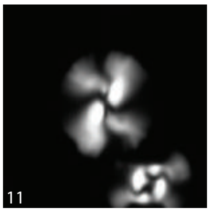
11
R. cf. *R. bisecta*
1408B-24X-5W, 123-124cm

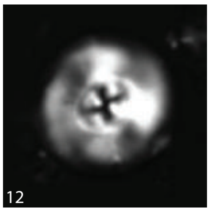
12
Calcidsicus bicircus
1408A-8H-3W, 48-49cm

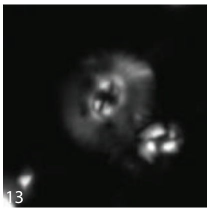
13
Calcidiscus bicircus
1408B-14H-3W, 123-124cm

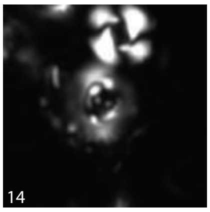
14
Calcidiscus gerrardii
1408C-10H-2W, 63-64cm

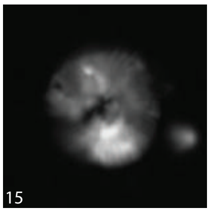
15
Calcidiscus pacificanus
1408B-14H-3W, 123-124

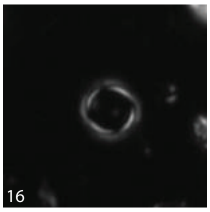
16
Umbilicosphaera bramlettei
1408B-14H-3W, 123-124cm

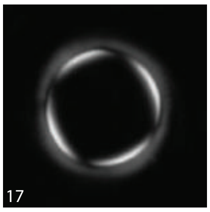
17
Umbilicosphaera bramlettei
1408B-14H-3W, 123-124cm

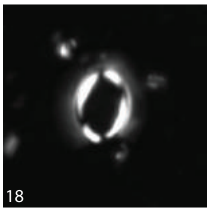
18
Umbilicosphaera detecta
1411B-18H-7W, 60cm

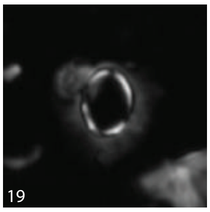
19
Umbilicosphaera detecta
1408B-14H-3W, 123-124cm

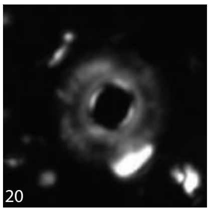
20
U. henrikseniae
1408C-10H-2W, 123-124cm

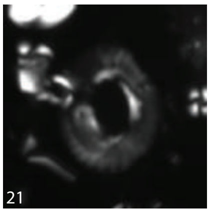
21
U. henrikseniae
1411B-28X-6W, 67cm

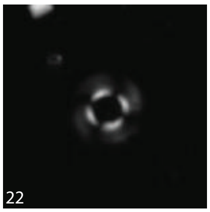
22
Umbilicosphaera jordanii
1408B-14H-3W, 123-124cm

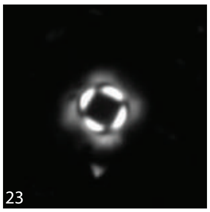
23
U. protoannula
1408C-10H-2W, 123-124cm

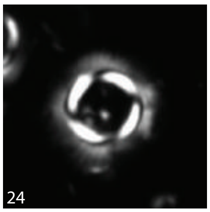
24
U. protoannula
1411B-26X-5W, 10-11cm

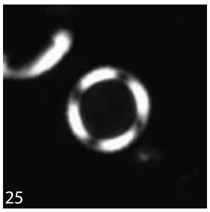
25
Coronocyclus nitescens
1411B-18H-7W, 60cm

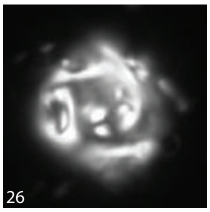
26
Coccolithus pelagicus
1408B-15H-6W, 3-4cm

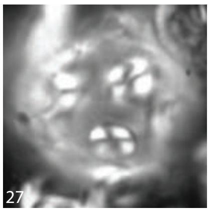
27
Coccolithus pelagicus
1411B-28X-3W, 105cm


28
Coccolithus pelagicus
1408B-14H-3W, 123-124cm

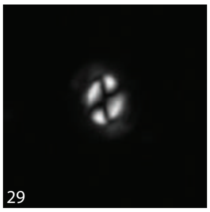
29
Coccolithus pelagicus
1408B-14H-3W, 123-124cm

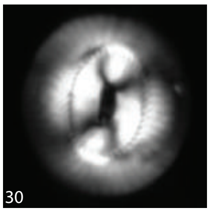
30
Coccolithus pelagicus
1408B-14H-3W, 123-124cm

PLATE 2.3
Coccolithaceae: *Coccolithus, Ericosonia, Chiasmolithus*

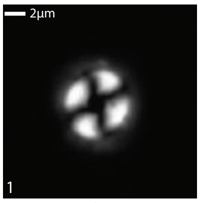

1
Coccolithus formosus
1408B-14H-3W, 123-124cm

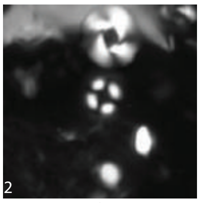
2
Coccolithus cf. *C. pauxillus*
1408A-21X-4W, 3-4cm

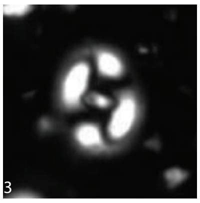
3
Coccolithus hollisii
1408B-24X-5W, 3-4cm

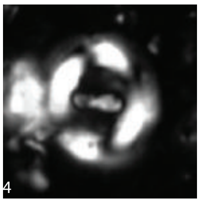
4
Coccolithus hollisii
1408B-24X-5W, 3-4cm

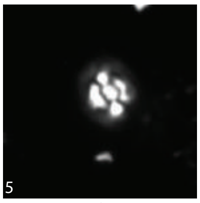
5
Coccolithus cf. *C. scheri*
1411B-28X-6W, 67cm

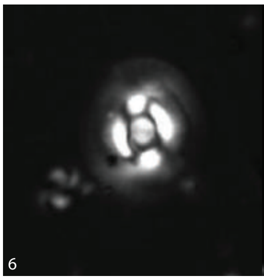
6
Coccolithus cachaoi
1408C-9H-4W, 78-79cm

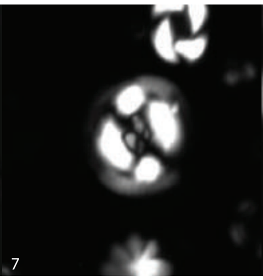
7
Coccolithus opdykei
1408A-22X-3W, 3-4cm

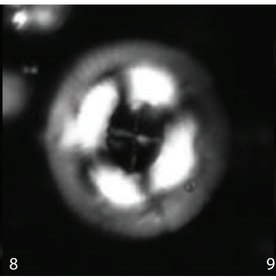
8
Coccolithus crucis
1408A-21X-4W, 3-4cm

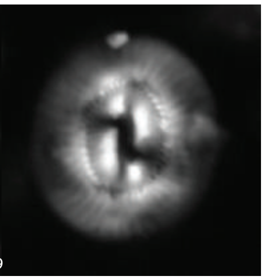
9
Coccolithus eopelagicus
1408B-14H-3W, 123-124cm

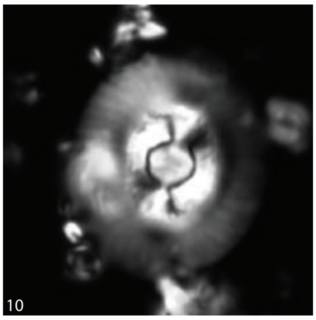
10
Coccolithus biparteoperculatus
1408A-14H-4W, 63-64cm

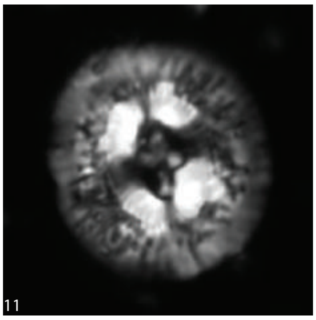
11
Coccolithus staurion
1408B-24X-5W, 3-4cm

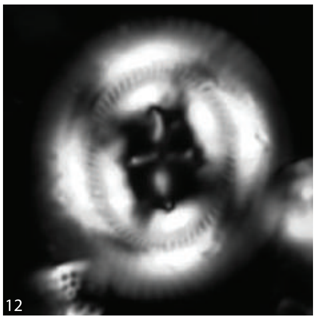
12
Coccolithus mutatus
1408C-15H-6W, 3-4cm

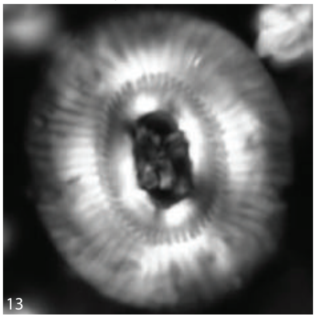
13
Coccolithus gigas
1408A-14H-4W, 63-64cm

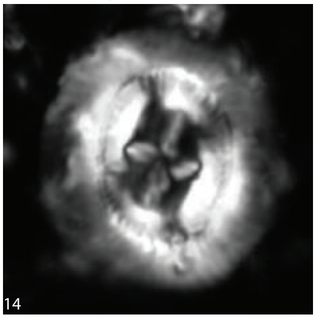
14
Coccolithus cf. *C. gigas*
1408B-24X-5W, 3-4cm

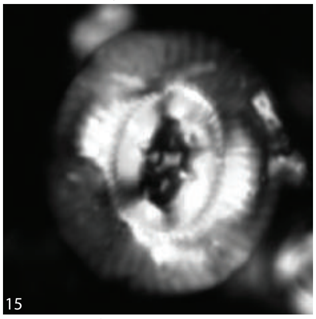
15
Coccolithus cf. *C. gigas*
1408C-15H-6W, 3-4cm

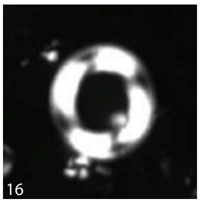
16
Ericsonia robusta
1408A-14H-4W, 63-64cm

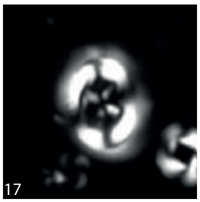
17
Chiasmolithus nitidus
1408B-22X-2W, 123-124cm

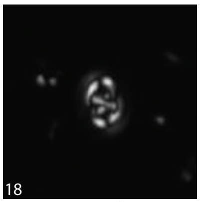
18
Chiasmolithus cf. *C. nitidus*
1408B-14H-3W, 123-124cm

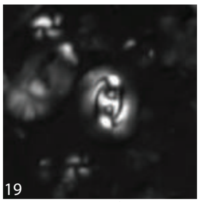
19
Chiasmolithus cf. *C. nitidus*
1408C-20X-3W, 3-4cm

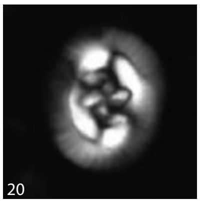
20
Chiasmolithus titus
1408B-14H-3W, 123-124cm

PLATE 2.4
Coccolithaceae: *Chiasmolithus, Clausicoccus, Cruciplacolithus, Campylosphaera, Bramletteius, Birkelundia*

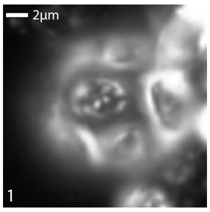

1
Chiasmolithus nitidus
1408B-14H-3W, 123-124cm

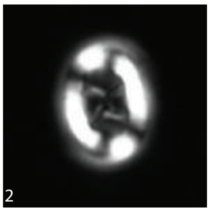
2
Chiasmolithus solitus
1408C-10H-2W, 123-124cm

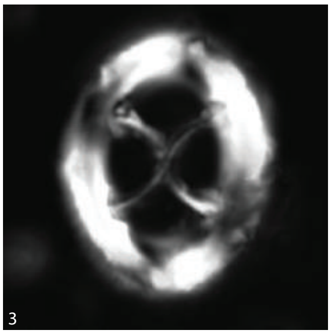
3
Chiasmolithus expansus
1408B-19X-4W, 3-4cm

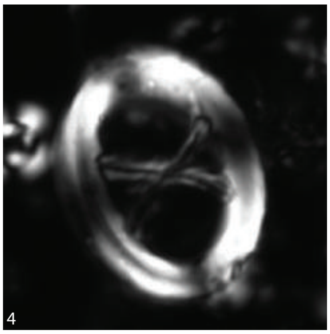
4
Chiasmolithus oamaruensis
1411B-18H-2W, 90cm

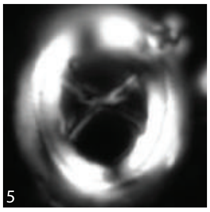
5
Chiasmolithus oamaruensis
1408B-14H-3W, 123-124cm

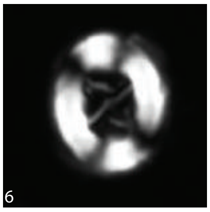
6
Chiasmolithus solitus
1408B-24X-5W, 123-124cm

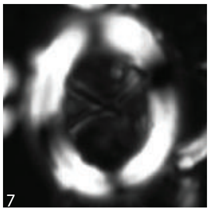
7
Chiasmolithus oamaruensis
1411C-9H-5W, 90cm

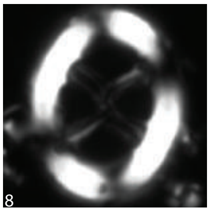
8
Chiasmolithus altus
1408C-6H-4W, 123-124cm

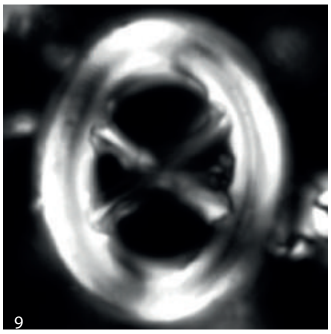
9
Chiasmolithus altus
1411C-16X-5W, 10-11cm

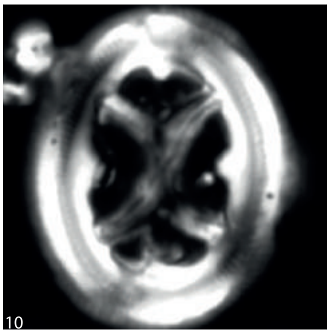
10
Chiasmolithus grandis
1408B-22X-2W, 123-124cm

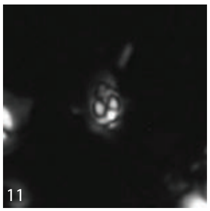
11
Clausicoccus subdistichus
1408A-21X-4W, 3-4cm

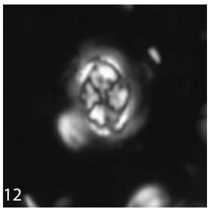
12
Clausicoccus fenestratus
1408A-21X-4W, 3-4cm

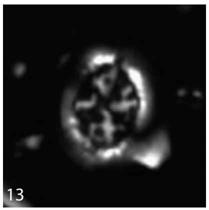
13
Clausicoccus fenestratus
1408C-10H-2W, 123-124cm

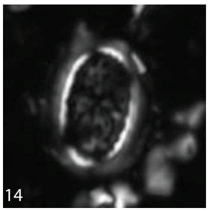
14
Clausicoccus vanheckiae
1408B-23X-4W, 63-64cm

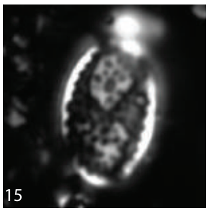
15
Clausicoccus vanheckiae
1408B-24X-5W, 3-4cm

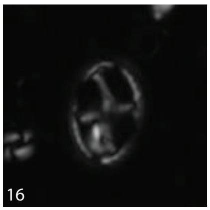
16
Cruciplacolithus cruciformis
1408B-14H-3W, 123-124cm

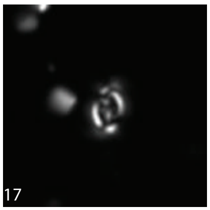
17
Cruciplacolithus cf. *C. primus*
1408C-10H-2W, 123-124cm

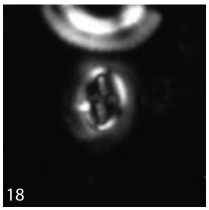
18
Cruciplacolithus cf. *C. primus*
1408B-19X-4W, 3-4cm

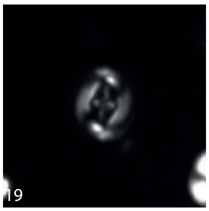
19
Cruciplacolithus tarquinius
1411B-18H-2W, 90cm

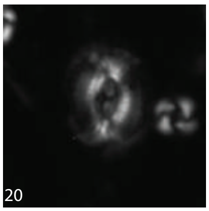
20
Cruciplacolithus opacus
1411B-18H-2W, 90cm

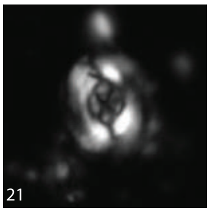
21
Cruciplacolithus opacus
1408A-21X-4W, 3-4cm

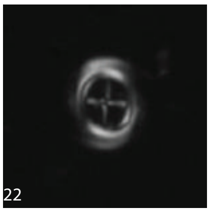
22
Campylosphaera dela
1408B-14H-3W, 123-124cm


23
Bramletteius serraculoides
1411B-27X-5W, 72cm

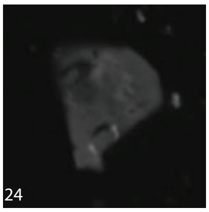
24
Bramletteius serraculoides
1408B-14H-3W, 123-124cm

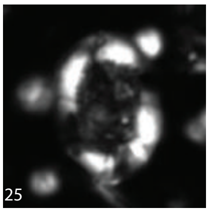
25
Birkelundia arenosa
1408C-10H-2W, 123-124cm

PLATE 2.5

Placolith coccoliths Incertae Sedis: *Pedinocyclus, Tetralithoides, Hayella, Markalius*; Zygodiscaceae: *Neococcolithes, Isthmolithus, Lophodolithus*; Calciosoleniaceae: *Calciosolenia*; Syracosphaeraceae: *Syracosphaera*; Chiastozygaceae: *Neocrepidolithus*

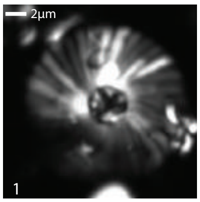

1
Pedinocyclus larvalis
1408C-10H-2W, 123-124cm

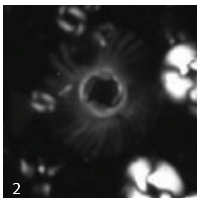

2
Pedinocyclus larvalis
1411B-28X-3W, 105cm

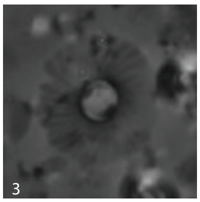

3
Pedinocyclus larvalis
1411B-28X-3W, 105cm

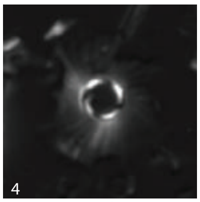

4
Pedinocyclus cf. *P. gibbsiae*
1408C-20X-3W, 3-4cm

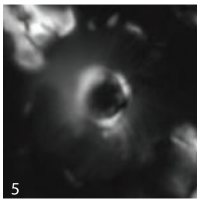

5
Pedinocyclus cf. *P. gibbsiae*
1408B-14H-3W, 123-124cm

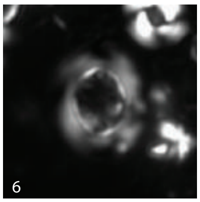

6
Pedinocyclus annulus
1408C-15H-6W, 3-4cm

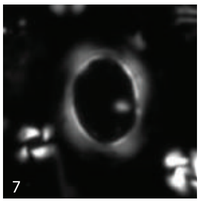

7
Pedinocyclus annulus
1408B-12H-5W, 123-124cm

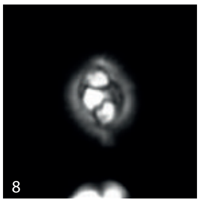

8
Tetralithoides symeonidesii
1408A-21X-4W, 3-4cm

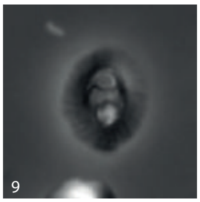

9
Tetralithoides symeonidesii
1408A-21X-4W, 3-4cm

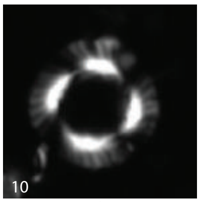

10
Hayella situliformis
1411B-28X-3W, 105cm

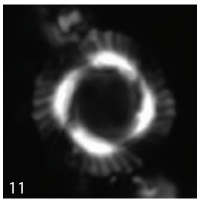

11
Hayella situliformis
1411B-28X-3W, 105cm

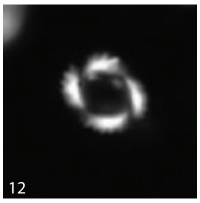

12
Hayella cf. *H. situliformis*
1408C-6H-3W, 123-124cm

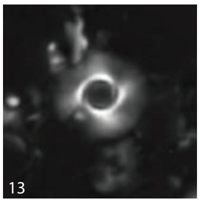

13
Hayella simplex
1408C-6H-3W, 123-124cm

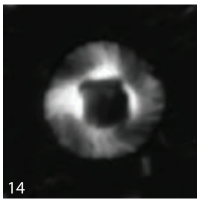

14
Hayella simplex
1408C-20X-3W, 3-4cm

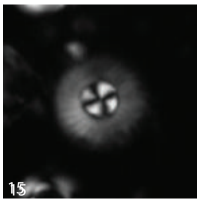

15
Markalius inversus
1408B-14H-3W, 123-124cm

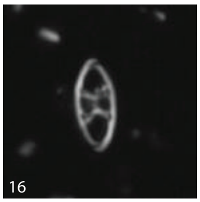

16
Neococcolithes dubius
1408B-14H-3W, 123-124cm

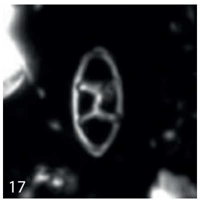

17
Neococcolithes dubius
1408B-22X-2W, 123-124cm

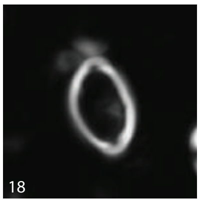

18
Neococcolithes cf. *N. purus*
1408C-6H-3W, 123-124cm

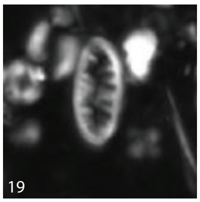

19
Neococcolithes radiatus
1408C-6H-3W, 123-124cm

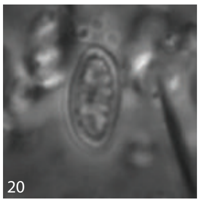

20
Neococcolithes radiatus
1408C-6H-3W, 123-124cm

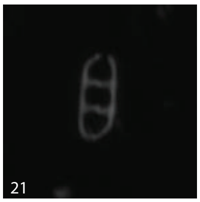

21
Isthmolithus recurvus
1411B-18H-2W, 90cm

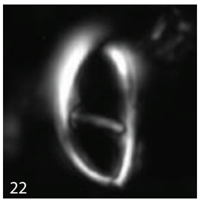

22
Lophodolithus acutus
1408B-19X-4W, 3-4cm

23
L. mochlophorus
1408C-20X-3W, 3-4cm

24
Lophodolithus nascens
1408B-19X-4W, 3-4cm

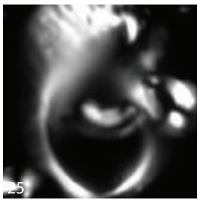

25
Lophodolithus rotundus
1408B-22X-3W, 3-4cm

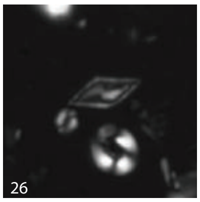

26
Calciosolenia alternans
1408A-21X-4W, 3-4cm

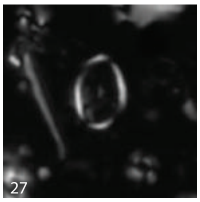

27
Syracosphaera tanzanensis
1408C-6H-3W, 123-124cm

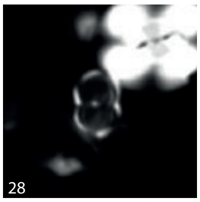

28
Syracosphaera? octiforma
1408C-7H-6W, 3-4cm

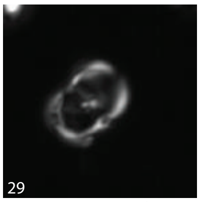

29
Syracosphaera? octiforma
1408B-6H-3W, 123-124cm

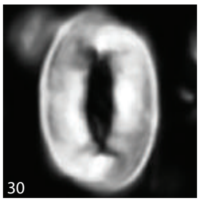

30
Neocrepidolithus grandiculus
1408B-24X-5W, 3-4cm

PLATE 2.6

Helicosphaeraceae: *Helicosphaera*; Pontosphaeraceae: *Pontosphaera*

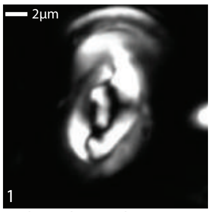

1
Helicosphaera clarissima
1408C-10H-2W, 123-124cm

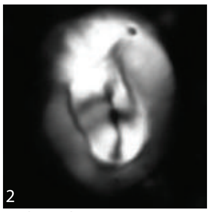
2
Helicosphaera compacta
1411C-11X-2W, 90cm

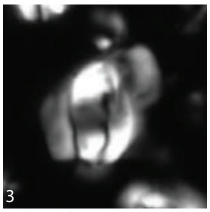
3
Helicosphaera compacta
1411B-18H-2W, 90cm

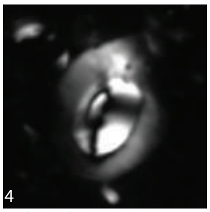
4
Helicosphaera compacta
1411C-5H-3W, 75-76cm

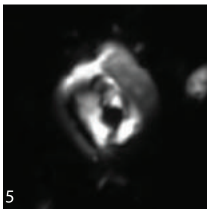
5
H. cf. *H. compacta*
1411C-5H-3W, 75-76cm

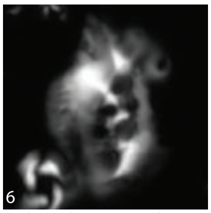
6
Helicosphaera reticulata
1411C 11X 2W 90cm

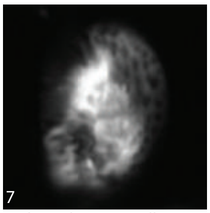
7
Helicosphaera papillata
1408B 14H 3W 123-124cm

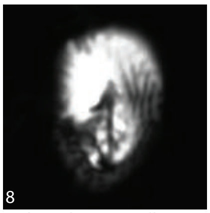
8
Helicosphaera papillata
1408C 15H 6W 3-4cm

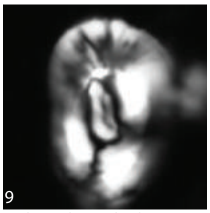
9
Helicosphaera lophota
1408B 19X 4W 3-4cm

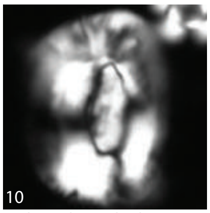
10
Helicosphaera lophota
1408B-23X-4W, 63-64cm

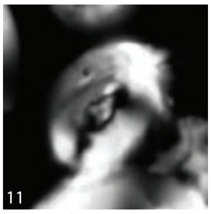
11
Helicosphaera robinsoniae
1411C-9H-4W, 90cm

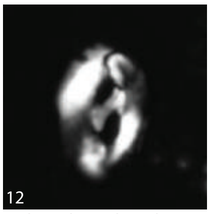
12
Helicosphaera bramlettei
1408B-14H-3W, 123-124cm

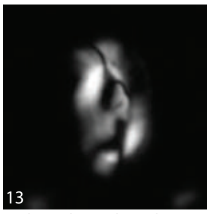
13
Helicosphaera bramlettei
1411B-27X-5W, 72cm

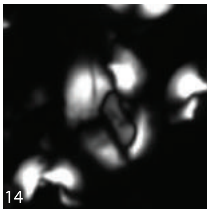
14
H. cf. *H. bramlettei*
1408B-24X-5W, 3-4cm

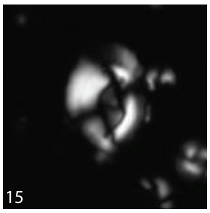
15
H. cf. *H. bramlettei*
1408B-19X-4W, 3-4cm

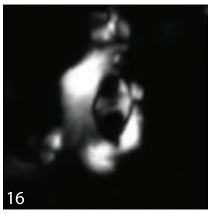
16
Helicosphaera seminulum
1411B-18H-2W, 90cm

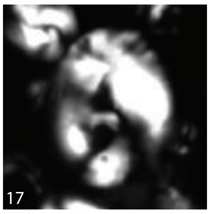
17
Helicosphaera seminulum
1408C-10H-2W, 123-124cm

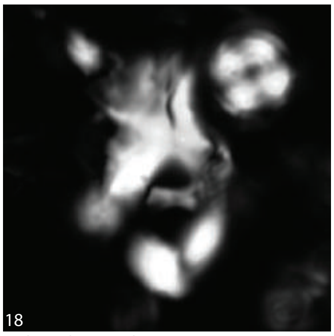
18
Helicosphaera wilcoxonii
1408A-8H-3W, 48-49cm

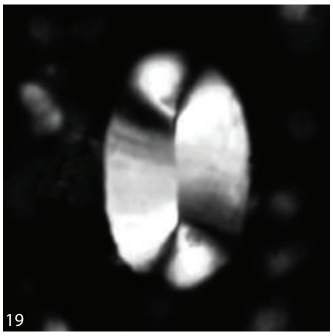
19
Pontopshaera plana
1408B-24X-5W, 3-4cm

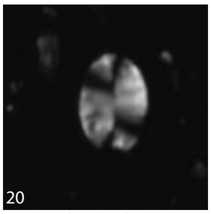
20
Pontosphaera plana
1408A-21X-4W, 3-4cm

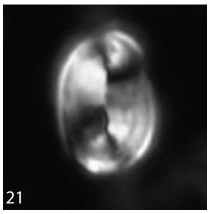
21
Pontosphaera versa
1408B-14H-3W, 123-124cm

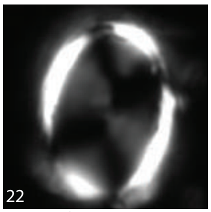
22
Pontosphaera panarium
1408A-8H-4W, 108-109cm

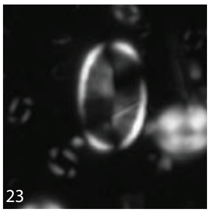
23
Pontosphaera panarium
1408C-6H-3W, 123-124cm

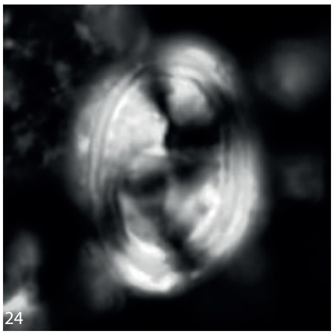
24
Pontosphaera versa
1408B-22X-2W, 123-124cm

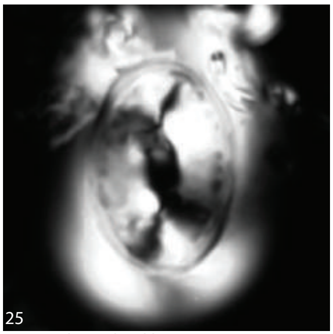
25
Pontopshaera brinkhuisii
1408A-18H-3W, 123-124cm

PLATE 2.7
Pontosphaeraceae: *Pontosphaera; Scyphosphaera*

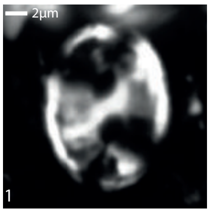

1
Pontosphaera cf. *P. duocava*
1408C-7H-5W, 3-4cm

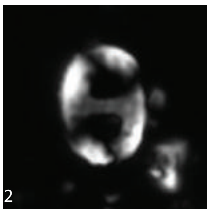
2
Pontosphaera exilis
1408B-23X-4W, 63-64cm

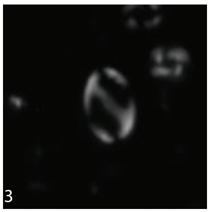
3
Pontopshaera obliquipons
1411B-18H-2W, 90cm

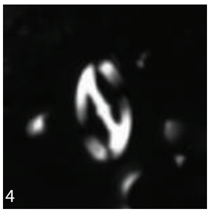
4
Pontopshaera obliquipons
1408C-20X-3W, 3-4cm

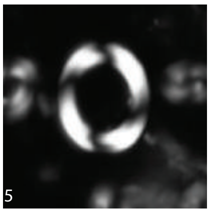
5
Pontosphaera cf. *P. rimosa*
1411B-18H-2W, 90cm

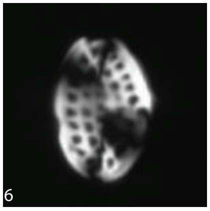
6
Pontosphaera multipora
1408B-14H-3W, 123-124cm

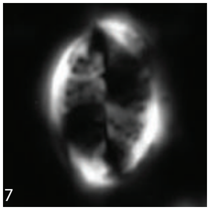
7
Pontosphaera alta
1411B-27X-5W, 72cm

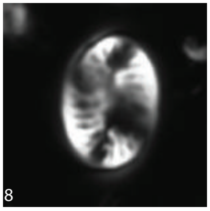
8
Pontosphaera clinosulcata
1408C-20X-3W, 3-4cm

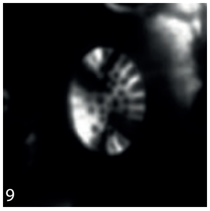
9
Pontosphaera pectinata
1408C-7H-5W, 3-4cm


10
Pontosphaera pulchra
1408B-12H-5W, 123-124cm

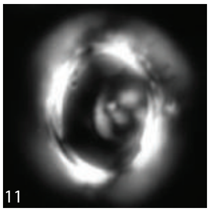
11
Pontosphaera formosa
1411B-27X-5W, 72cm

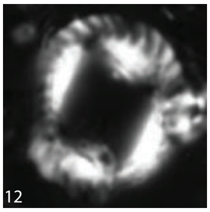
12
Pontosphaera formosa
1408C-20X-3W, 3-4cm

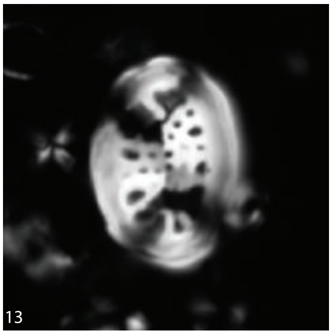
13
P cf. *P. multipora* 1408A-22X-3W, 3-4cm

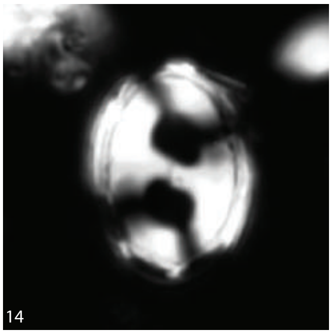
14
P. duocava 1408A-8H-3W, 48-49cm

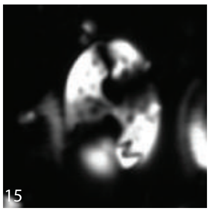
15
P. cf. *P. perforomarginata*
1408A-8H-3W, 48-49cm

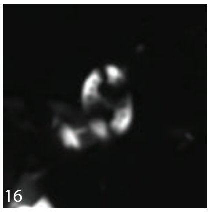
16
Pontosphaera pulcheroides
1408A-8H-3W, 48-49cm

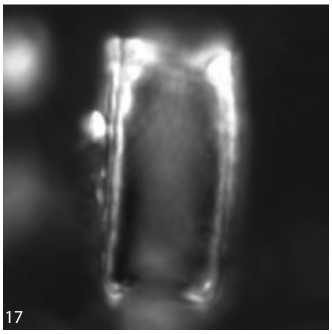
17
Scyphosphaera sp. 1408C-20X-3W, 3-4cm

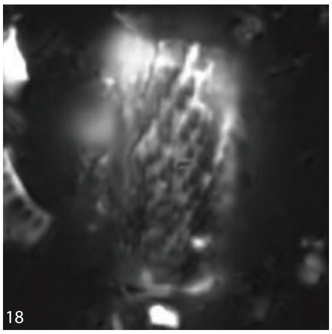
18
Scyphosphaera sp. 1408C-20X-3W, 3-4cm

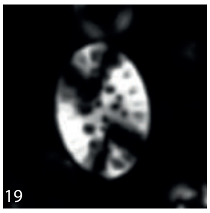
19
Pontosphaera punctosa
1408C-7H-5W, 3-4cm

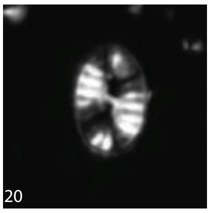
20
Pontosphaera wilsonii
1408C-6H-3W, 123-124cm

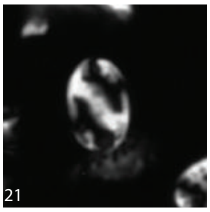
21
Pontosphaera zigzag
1411B-18H-2W, 90cm

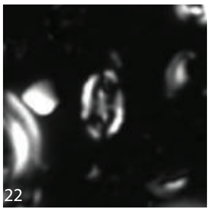
22
Pontosphaera sp. 1
1408A-8H-3W, 48-49cm

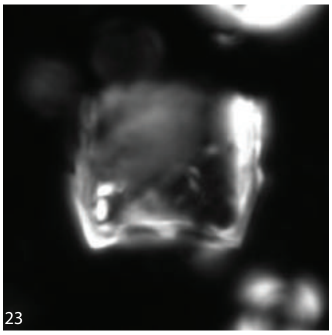
23
Scyphosphaera sp.
1408A-8H-4W, 108-109cm

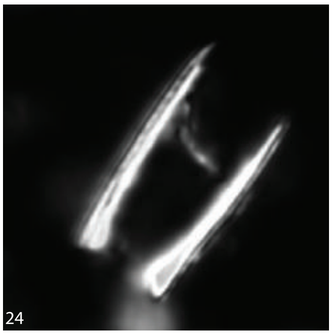
24
Scyphosphaera sp.
1408B-24X-5W, 3-4cm

PLATE 2.8
Rhabdosphaeraceae: *Blackites, Rhabdosphaera*

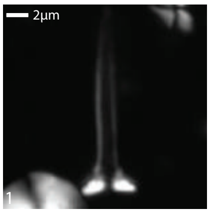

1
Blackites creber
1408B-14H-3W, 123-124cm

2
Blackites gladius
1408B-14H-3W, 123-124cm

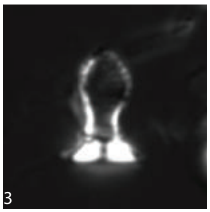

3
Blackites rotundus
1408C-20X-3W, 3-4cm

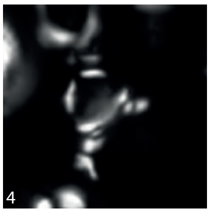

4
Blackites deflandrei
1408C-7H-5W, 3-4cm

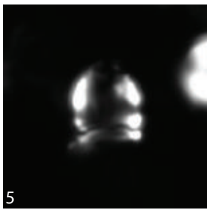

5
Blackites deflandrei
1408C-7H-5W, 3-4cm

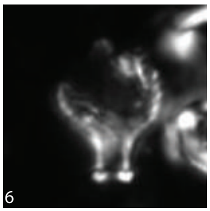

6
Blackites globosus
1408B-24X-5W, 3-4cm

7
Blackites pseudomorionum
1408C-20X-3W, 3-4cm

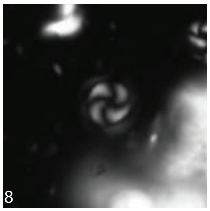

8
Blackites amplus
1408A-21X-4W, 3-4cm

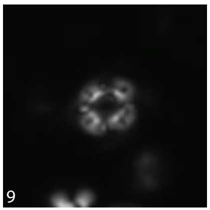

9
Blackites friedrichii
1408C-6H-3W, 123-124cm

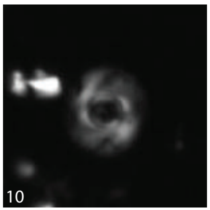

10
Blackites furvus
1408B-14H-3W, 123-124cm

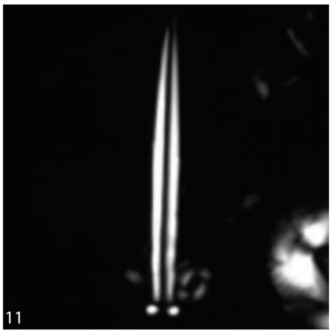

11
Blackites tenuis
1408C-10H-2W, 123-124cm

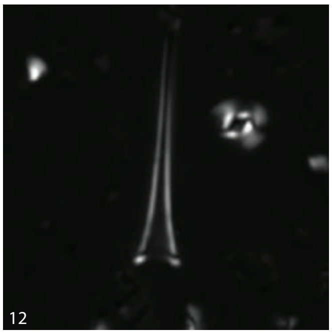

12
Blackites cf. *B. spinosus*
1408C-20X-3W, 3-4cm

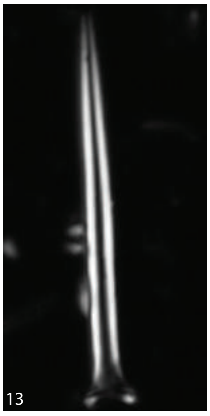

13
Blackites spinosus
1411C-11X-2W, 90cm

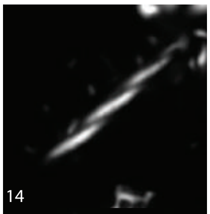

14

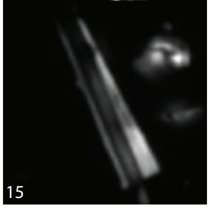

15
Blackites tortilis (14)
1408C-10H-2W, 123-124cm
Blackites stilus (15)
1408C-20X-3W, 3-4cm

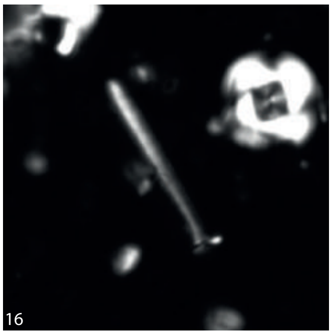

16
Rhabdosphaera gracilentus
1408C-7H-5W, 3-4

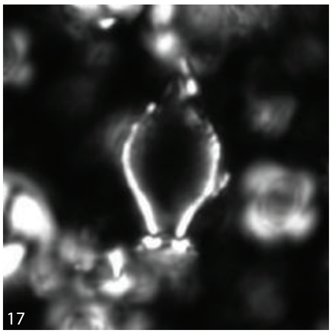

17
Blackites piriformis
1408A-21X-4W, 3-4cm

18
Blackites lippertii
1411B-28X-3W, 105cm

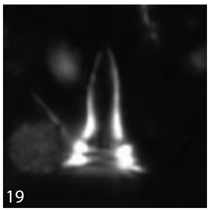

19
Blackites cf. *B. sextonii*
1408A-8H-3W, 48-49cm

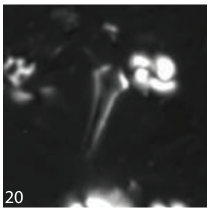

20
Blackites kilwaensis
1408C-20X-3W, 3-4cm

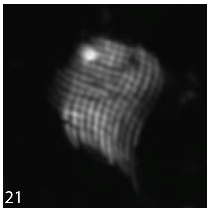

21
Blackites ornatus
1408B-14H-3W, 123-124cm

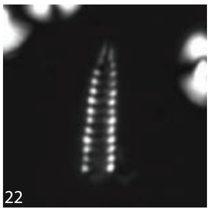

22
Blackites virgatus
1408C-20X-3W, 3-4cm

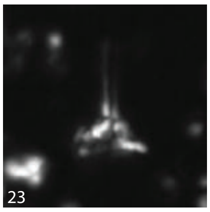

23
Rhabdosphaera vitrea
1408C-20X-3W, 3-4cm

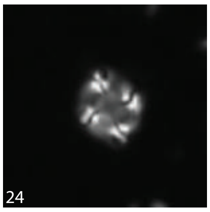

24
Rhabdosphaera vitrea
1411B-27X-5W, 72cm

PLATE 2.9
Holococcoliths: *Holodiscolithus, Zygrhabdolithus, Lanternithus, Daktylethra, Orthozygus, Clathrolithus*

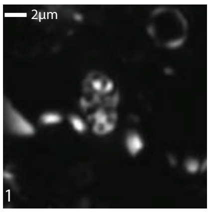

1
Holodiscoithus macroporus
1411B-17H-2W, 90cm

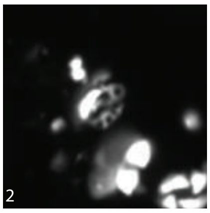
2
Holodiscolithus macroporus
1411B-17H-2W, 90cm

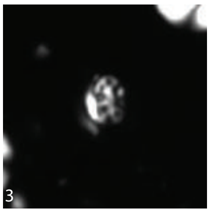
3
Holodiscolithus macroporus
1411B-17H-2W, 90cm

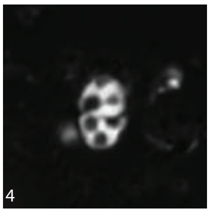
4
Holodiscolithus solidus
1408C-6H-3W, 123-124cm

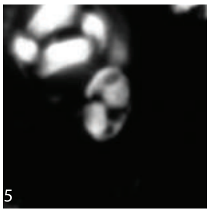
5
Holodiscolithus solidus
1408C-20X-3W, 3-4cm

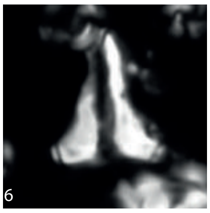
6
Zygrhabdolithus bijugatus
1408B-22X-2W, 123-124cm

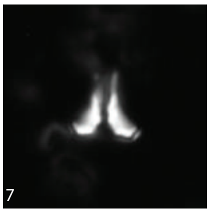
7
Zygrhabdolithus bijugatus
1408C-20X-3W, 3-4cm


8
Z. bijugatus ssp. *cornutus*
1408B-24X-5W, 3-4cm

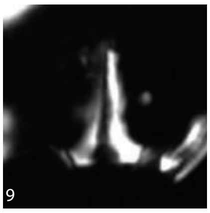
9
Z. bijugatus ssp. *cornutus*
1408A-21X-4W, 3-4cm

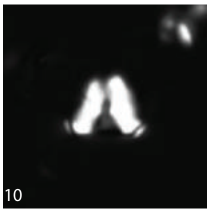
10
Z. cf. *Z. bijugatus bijugatus*
1408C-6H-3W, 123-124cm

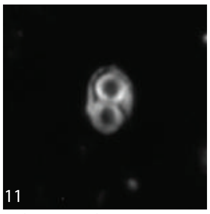
11
Z. bijugatus base
1408B-24X-5W, 3-4cm

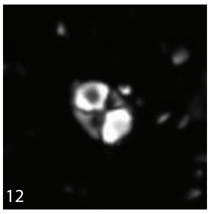
12
Z. bijugatus base
1408C-10H-2W, 123-124cm

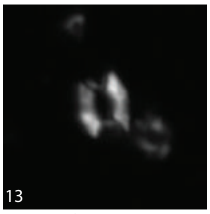
13
Lanternithus minutus
1408A-21X-4W, 3-4cm

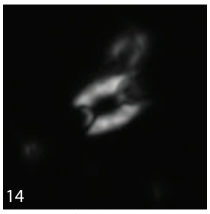
14
Lanternithus minutus
1408C-6H-3W, 123-124cm

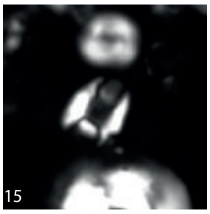
15
Lanterithus minutus
1408C-7H-5W, 3-4cm

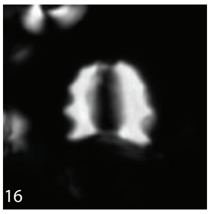
16
Daktylethra punctulata
1408B-24X-5W, 3-4cm

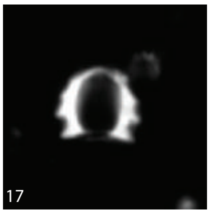
17
Daktylethra punctulata
1408C-20X-3W, 3-4cm

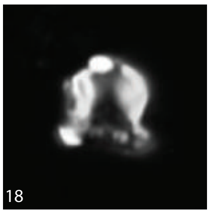
18
Daktylethra probertii
1408A-21X-4W, 3-4cm

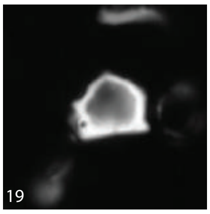
19
Daktylethra unitatis
1408C-6H-3W, 123-124cm

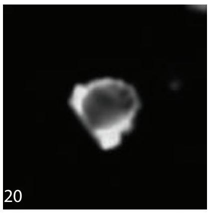
20
Daktylethra unitatis
1408B-21X-6W, 63-64cm

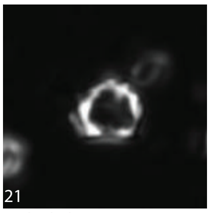
21
Daktylethra unitatis
1408B-24X-5W, 3-4cm

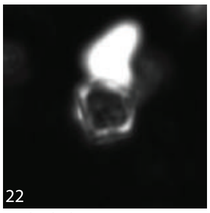
22
Daktylethra unitatis
1408C-20X-3W, 3-4cm

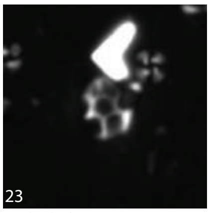
23
Daktylethra unitatis
1408A-21X-4W, 3-4cm

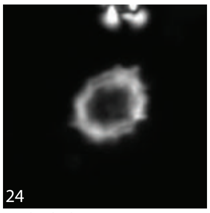
24
Daktylethra top view
1408C-6H-3W, 123-124cm

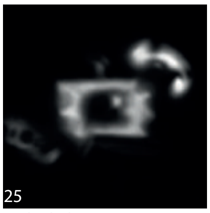
25
Daktylethra top view
1408C-7H-5W, 3-4cm

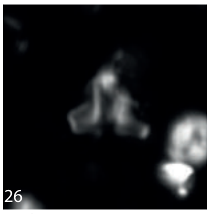
26
Orthozygus aureus
1411C-16X-5W, 10-11cm

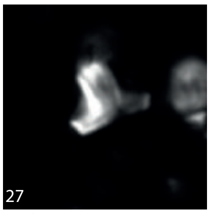
27
Orthozygus aureus
1411C-16X-5W, 10-11cm

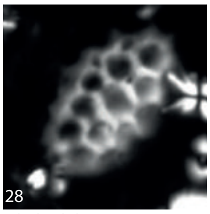
28
Clathrolithus sp.
1408B-7H-2W, 108-109cm

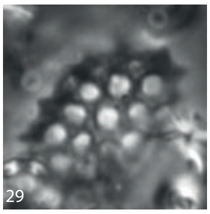
29
Clathrolithus sp.
1408B-7H-2W, 108-109cm

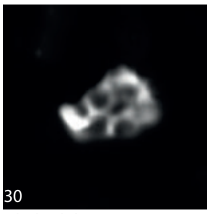
30
Clathrolithus sp.
1408C-7H-5W, 3-4cm

PLATE 2.10
Discoasteraceae: *Discoaster*; Sphenolithaceae: *Sphenolithus*

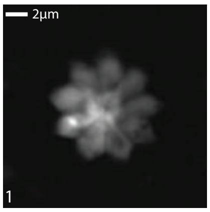

1
Discoaster barbadiensis
1408B-14H-3W, 123-124cm

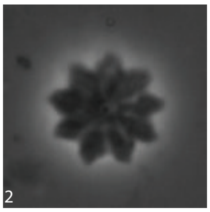
2
Discoaster barbadiensis
1408B-14H-3W, 123-124cm

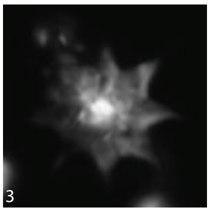
3
Discoaster saipanensis
1408B-14H-3W, 123-124cm

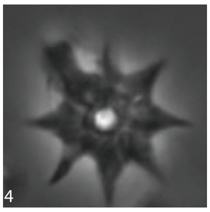
4
Discoaster saipanensis
1408B-14H-3W, 123-124cm

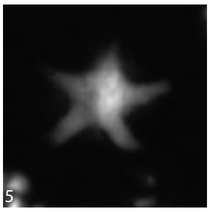
5
Discoaster tanii
1411B-18H-2W, 90cm

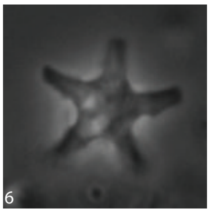
6
Discoaster tanii
1411B-18H-2W, 90cm

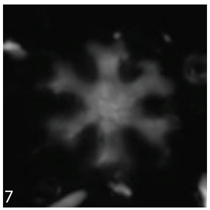
7
Discoaster deflandrei
1408B-14H-3W, 123-124cm

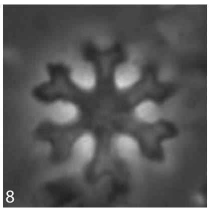
8
Discoaster deflandrei
1408B-14H-3W, 123-124cm

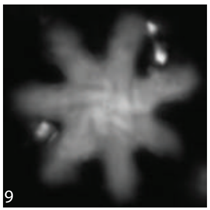
9
Discoaster nodifer
1408B-14H-3W, 123-124cm

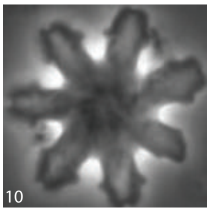
10
Discoaster nodifer
1408B-14H-3W, 123-124cm

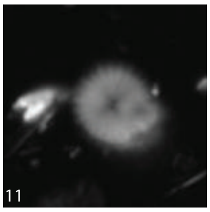
11
Discoaster wemmelensis
1408B-21X-4W, 3-4cm

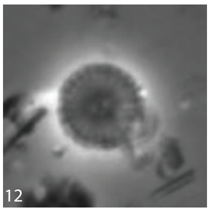
12
Discoaster wemmelensis
1408C-21X-4W, 3-4cm

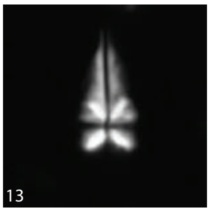
13
Sphenolithus radians
1408B-14H-3W, 123-124cm

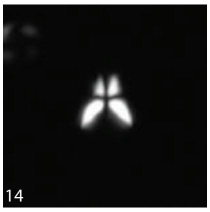
14
Sphenolithus spiniger
1408B-14H-3W, 123-124cm

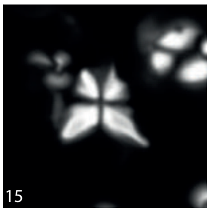
15
Sphenolithus cf. *S. spiniger*
1411C-16X-5W, 10-11cm

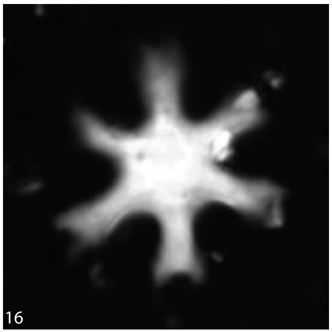
16
Discoaster distinctus
1408C 10H 2W 123-124cm

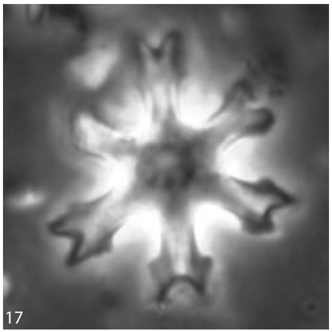
17
Discoaster distinctus
1408C 10H 2W 123-124cm

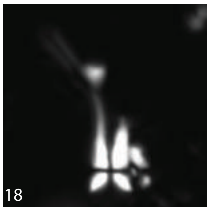
18
Sphenolithus furcatolithoides
1408C-20X-3W, 3-4cm

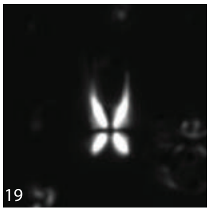
19
S. furcatolithoides
1408C-20X-3W, 3-4cm

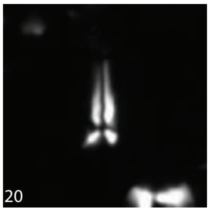
20
Sphenolithus strigosus
1408C-15H-6W, 3-4cm

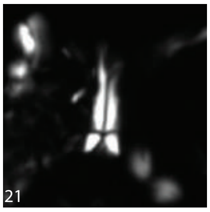
21
Sphenolithus strigosus
1408C-10H-2W, 123-124cm

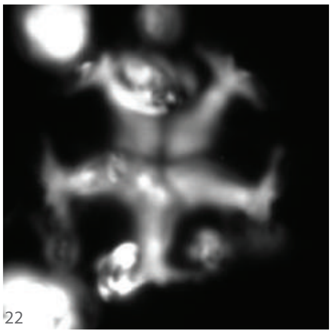
22
Discoaster martinii
1408A-16H-5W, 123-124cm

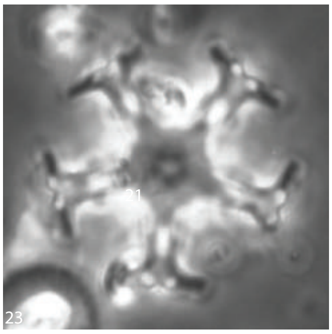
23
Discoaster martinii
1408A-16H-5W, 123-124cm

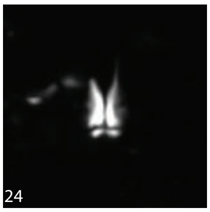
24
Sphenolithus cuniculus
1408A-8H-3W, 48-49cm


25
Sphenolithus cuniculus
1408B-19X-4W, 3-4cm

PLATE 2.11
Sphenolithaceae: *Sphenolithus*; Braarudosphaeraceae: *Pemma*; Incertae Sedis Nannoliths: *Nannotetrina, Leesella*

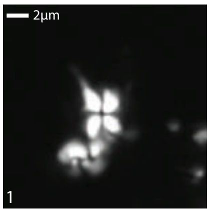

1
Sphenolithus kempii
1408A-21X-4W, 3-4cm

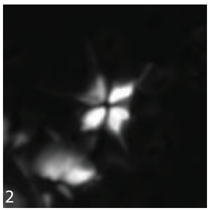

2
Sphenolithus cf. *S. kempii*
1408A-22X-3W, 3-4cm

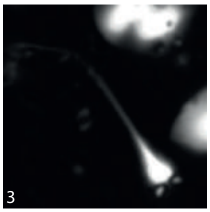

3
Sphenolithus celsus
1408B-7H-2W, 108-109cm

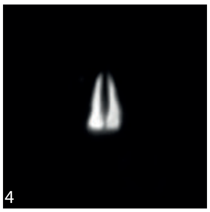

4
Sphenolithus intercalaris
1411B-28X-7W, 22cm

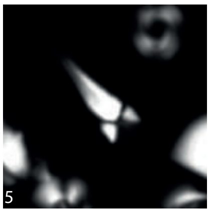

5
Sphenolithus obtusus
1408B-7H-2W, 108-109cm

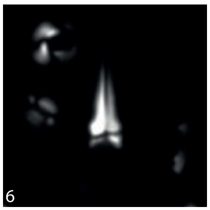

6
Sphenolithus predistentus
1408C-7H-5W, 3-4cm

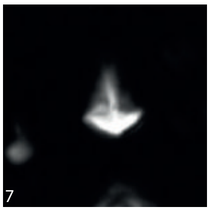

7
Sphenolithus tribulosus
1411B-28X-7W, 22cm

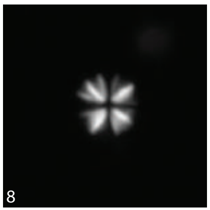

8
Sphenolithus moriformis
1408B-14H-3W, 123-124cm

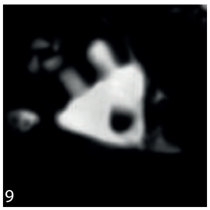

9
Pemma papillatum
1411C-16X-5W, 10-11cm

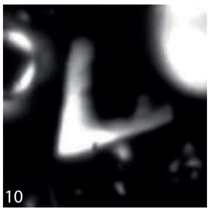

10
Pemma triquetra
1411C-16X-5W, 10-11cm

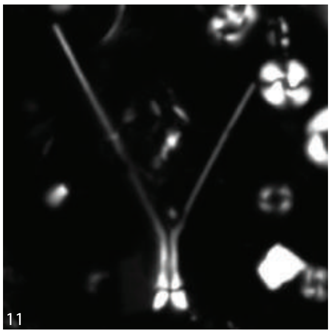

11
Sphenolithus strigosus
1408C-10H-2W, 123-124cm

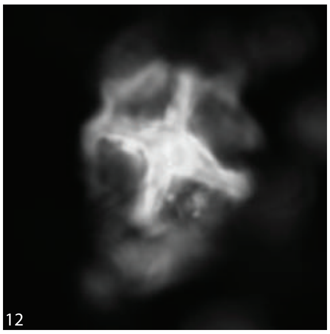

12
Nannotetrina cristata
1408A-16H-5W, 123-124cm

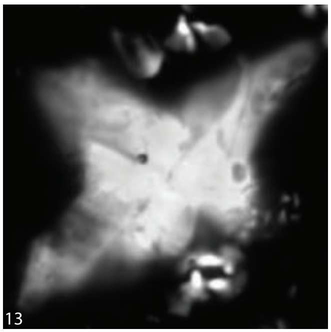

13
Nannotetrina fulgens
1408B-24X-5W, 3-4cm

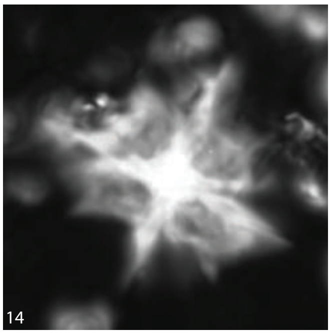

14
Nannotetrina spinosa
1408C-20X-3W, 3-4cm

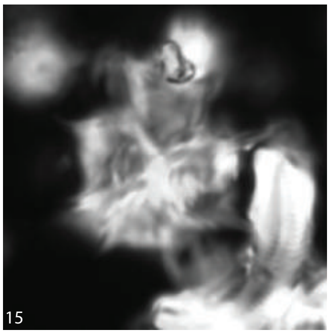

15
Nannotetrina pappii
1408C-20X-3W, 3-4cm

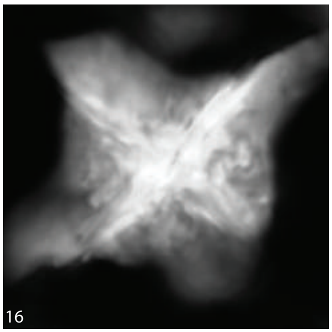

16
Nannotetrina fulgens
1408B-24X-5W, 3-4cm

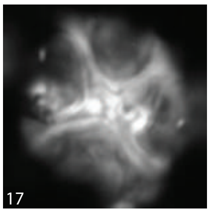

17
Nannotetrina cristata
1408B-19X-4W, 3-4cm

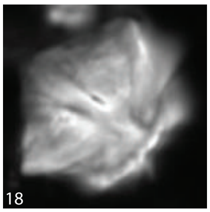

18
Nannotetrina cristata
1408B-19X-4W, 3-4cm

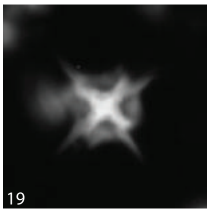

19
Nannotetrina spinosa
1408B-19X-4W, 3-4cm

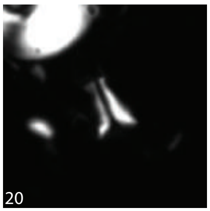

20
Leesella procera
1408C-10H-2W, 123-124cm

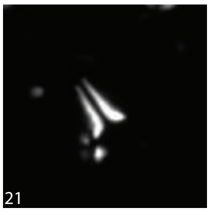

21
Leesella procera
1408C-10H-2W, 123-124cm

PLATE 2.12
Cyclicargolithus, Reticulofenestra

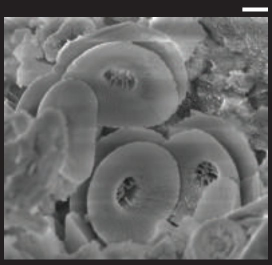

1. *Cyclicargolithus floridanus*
1411C-12X-3W, 125.5-126.5cm

2. *Cyclicargolithus floridanus*
1408A-14H-5W, 63-64cm

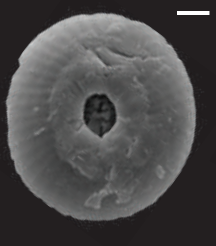

3. *Cyclicargolithus floridanus*
1411B-28X-3W, 105cm

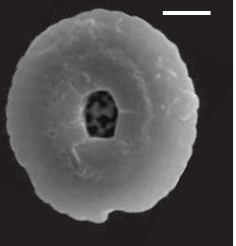

4. *Cyclicargolithus floridanus*
1411B-28X-3W, 105cm

5. *Cyclicargolithus floridanus*
1408A-14H-5W, 63-64cm

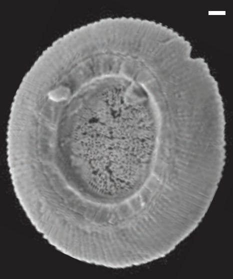

6. *Reticulofenestra umbilicus*
1408C-10H-3W, 63-64cm

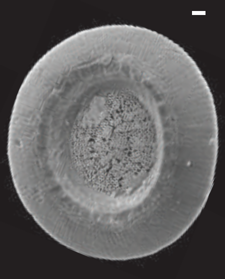

7. *Reticulofenestra umbilicus*
1408C-10H-3W, 63-64cm

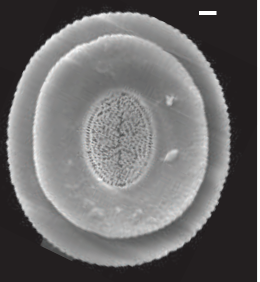

8. *Reticulofenestra umbilicus*
1408C-10H-3W, 63-64cm

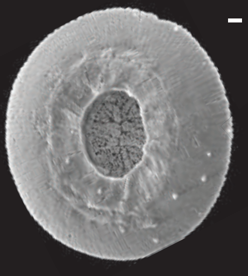

9. *Reticulofenestra hillae*
1408C-10H-3W, 63-64cm

10. *Reticulofenestra hillae*
1408A-14H-5W, 63-64cm

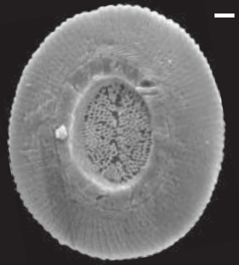

11. *Reticulofenestra dictyoda*
1408C-10H-3W, 63-64cm

12. *Reticulofenestra dictyoda*
1408C-7H-4W, 93-94cm

13. *Reticulofenestra minuta*
1411B-28X-3W, 105cm

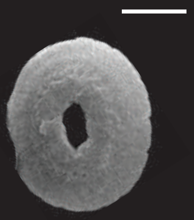

14. *Reticulofenestra minuta*
1408A-14H-5W, 63-64cm

15. *Reticulofenestra* cf. *R. bisecta*
1408A-14H-5W, 63-64cm

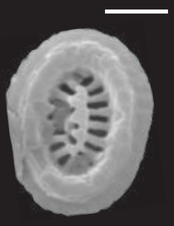

16. *Reticulofenestra* sp.
1408A-14H-5W, 63-64cm

PLATE 2.13
Reticulofenestra

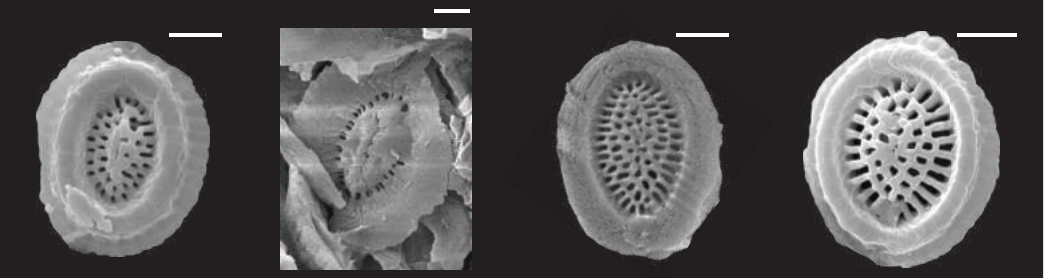

1. *Reticulofenestra lockeri*
1408A-14H-5W, 63-64cm

2. *Reticulofenestra daviesii*
1408A-22X-2W, 63-64cm

3. *Reticulofenestra macmillani*
1408C-7H-4W, 93-94cm

4. *Reticulofenestra macmillani?*
1408A-14H-5W, 63-64cm

5. *Reticulofenestra reticulata*
1408C-10H-3W, 63-64cm

6. *Reticulofenestra reticulata*
1408B-5H-5W, 63-64cm

7. *Reticulofenestra reticulata*
1411B-28X-3W, 105cm

8. *Reticulofenestra reticulata*
1411B-28X-3W, 105cm

9. *Reticulofenestra reticulata*
1408B-5H-5W, 63-64cm

10. *Reticulofenestra erbae*
1411B-28X-3W, 105cm

11. *Reticulofenestra bisecta*
1411B-18H-2W, 30cm

12. *Reticulofenestra bisecta*
1411B-18H-2W, 30cm

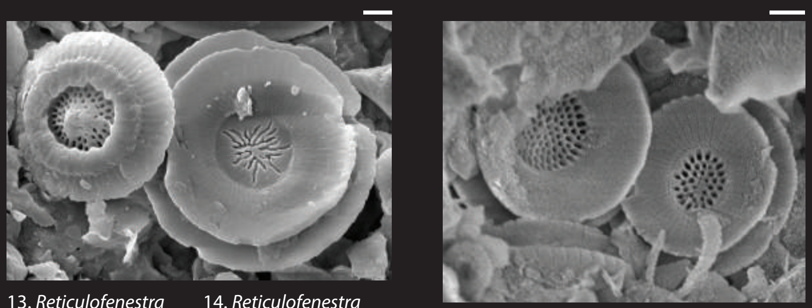

13. *Reticulofenestra reticulata*
1411B-28X-3W, 105cm

14. *Reticulofenestra erbae?*

15. *Reticulofenestra reticulata*
1408C-7H-4W, 93-94cm

PLATE 2.14
Umbilicosphaera, Coronocyclus, Coccolithus, Pocillithus


1. *Umbilicosphaera bramlettei*
1408A-14H-5W, 63-64cm


2. *Umbilicosphaera bramlettei*
1408A-14H-5W, 63-64cm

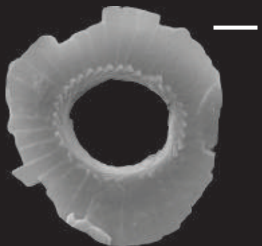
3. *Umbilicosphaera protoannula*
1408A-14H-5W, 63-64cm


4. *Coronocyclus nitescens*
1408A-14H-5W, 63-64cm


5. *Coccolithus pelagicus*
1408A-22X-2W, 63-64cm


6. *Coccolithus pelagicus*
1408C-10H-3W, 63-64cm


7. *Coccolithus pelagicus*
1408A-14H-5W, 63-64cm


8. *Coccolithus* cf. *C. pauxillus*
1408A-14H-5W, 63-64cm

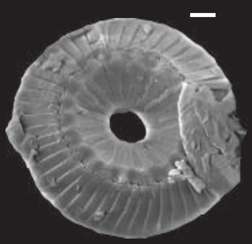
9. *Coccolithus formosus*
1411C-12X-3W, 125.5-126.5cm


10. *Coccolithus crucis*
1408A-14H-5W, 63-64cm


11. *Pocillithus spinulifer*
1408A-22X-2W, 63-64cm

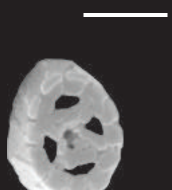
12. *Pocillithus spinulifer*
1408A-14H-5W, 63-64cm

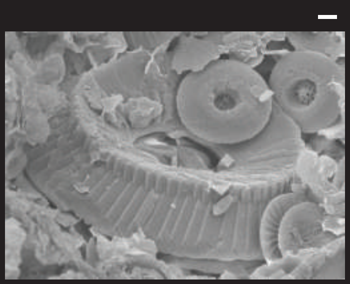
13. *Coccolithus mutatus*
1408A-22X-2W, 63-64cm

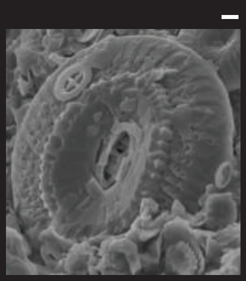
14. *Coccolithus pelagicus*
1408A-14H-5W, 63-64cm

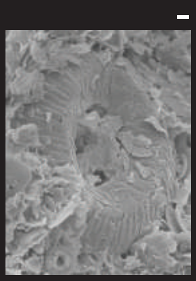
15. *Coccolithus gigas*
1408A-14H-5W, 63-64cm

PLATE 2.15
Chiasmolithus, Clausicoccus, Cruciplacolithus, Campylosphaera, Bramletteius

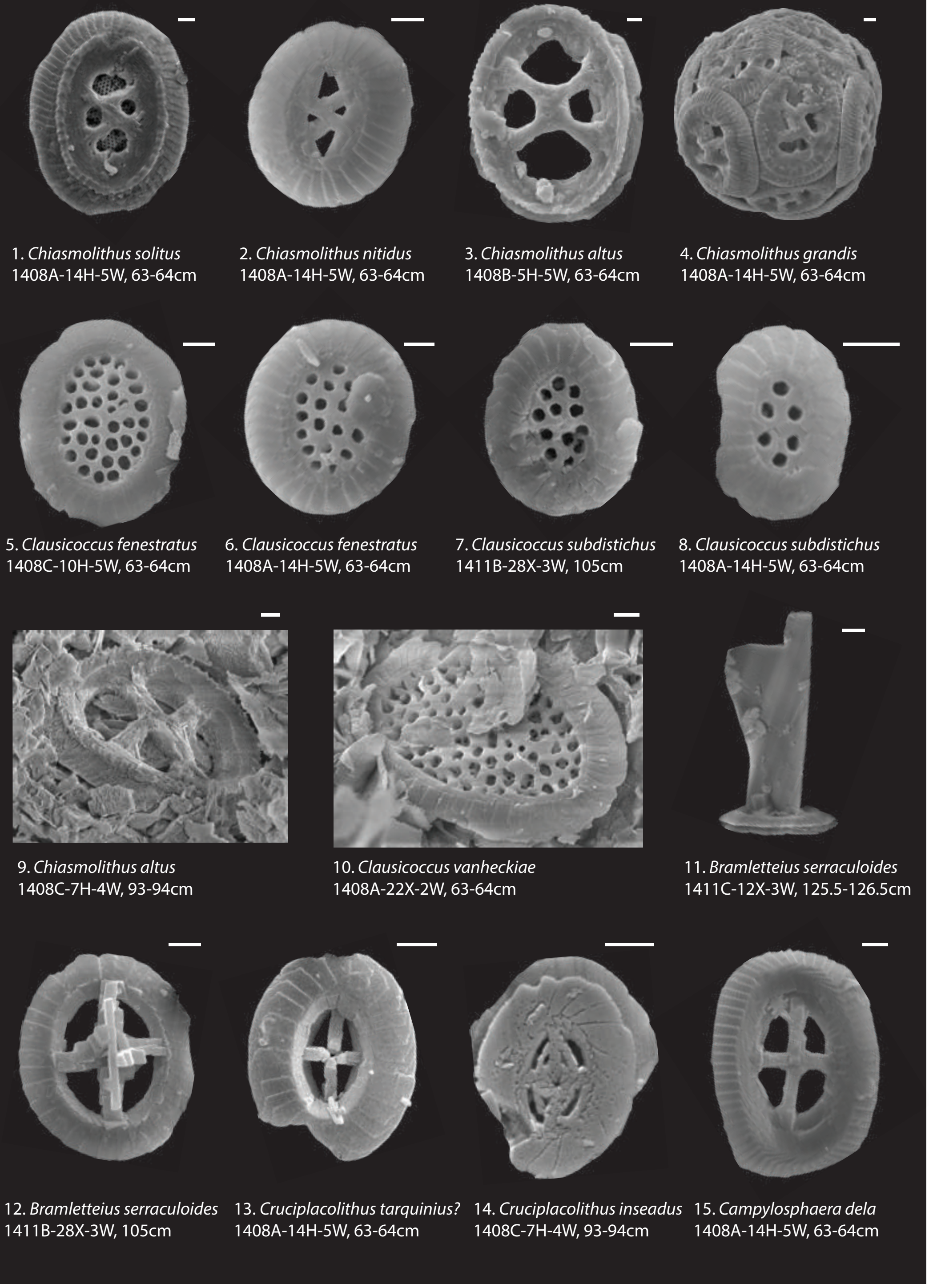

1. *Chiasmolithus solitus*
1408A-14H-5W, 63-64cm

2. *Chiasmolithus nitidus*
1408A-14H-5W, 63-64cm

3. *Chiasmolithus altus*
1408B-5H-5W, 63-64cm

4. *Chiasmolithus grandis*
1408A-14H-5W, 63-64cm

5. *Clausicoccus fenestratus*
1408C-10H-5W, 63-64cm

6. *Clausicoccus fenestratus*
1408A-14H-5W, 63-64cm

7. *Clausicoccus subdistichus*
1411B-28X-3W, 105cm

8. *Clausicoccus subdistichus*
1408A-14H-5W, 63-64cm

9. *Chiasmolithus altus*
1408C-7H-4W, 93-94cm

10. *Clausicoccus vanheckiae*
1408A-22X-2W, 63-64cm

11. *Bramletteius serraculoides*
1411C-12X-3W, 125.5-126.5cm

12. *Bramletteius serraculoides*
1411B-28X-3W, 105cm

13. *Cruciplacolithus tarquinius?*
1408A-14H-5W, 63-64cm

14. *Cruciplacolithus inseadus*
1408C-7H-4W, 93-94cm

15. *Campylosphaera dela*
1408A-14H-5W, 63-64cm

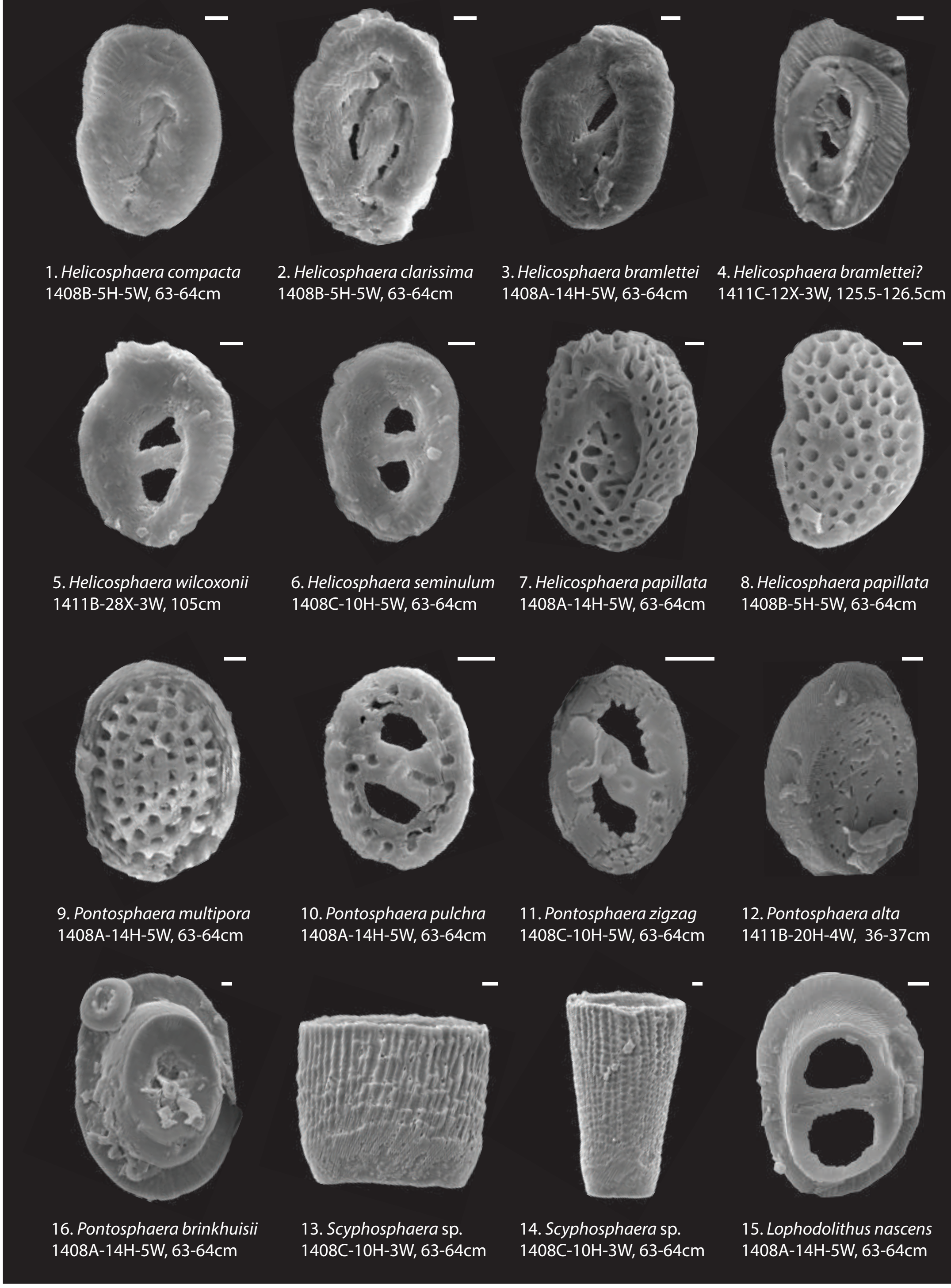

PLATE 2.16
Helicosphaera, Pontosphaera, Scyphosphaera, Lophodolithus

1. *Helicosphaera compacta* 1408B-5H-5W, 63-64cm

2. *Helicosphaera clarissima* 1408B-5H-5W, 63-64cm

3. *Helicosphaera bramlettei* 1408A-14H-5W, 63-64cm

4. *Helicosphaera bramlettei?* 1411C-12X-3W, 125.5-126.5cm

5. *Helicosphaera wilcoxonii* 1411B-28X-3W, 105cm

6. *Helicosphaera seminulum* 1408C-10H-5W, 63-64cm

7. *Helicosphaera papillata* 1408A-14H-5W, 63-64cm

8. *Helicosphaera papillata* 1408B-5H-5W, 63-64cm

9. *Pontosphaera multipora* 1408A-14H-5W, 63-64cm

10. *Pontosphaera pulchra* 1408A-14H-5W, 63-64cm

11. *Pontosphaera zigzag* 1408C-10H-5W, 63-64cm

12. *Pontosphaera alta* 1411B-20H-4W, 36-37cm

16. *Pontosphaera brinkhuisii* 1408A-14H-5W, 63-64cm

13. *Scyphosphaera* sp. 1408C-10H-3W, 63-64cm

14. *Scyphosphaera* sp. 1408C-10H-3W, 63-64cm

15. *Lophodolithus nascens* 1408A-14H-5W, 63-64cm

PLATE 2.17
Neoccolithes, Isthmolithus, Blackites

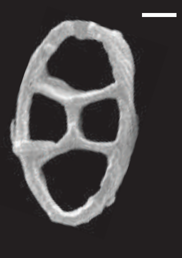

1. *Neococcolithes dubius*
1408A-14H-5W, 63-64cm

2. *Isthmolithus recurvus*
1411C-17X-2W, 110-111cm

3. *Blackites gladius*
1408A-14H-5W, 63-64cm

4. *Blackites gladius*
1408C-10H-5W, 63-64cm

5. *Blackites deflandrei*
1408B-5H-5W, 63-64cm

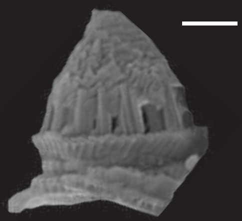

6. *Blackites deflandrei*
1408C-7H-4W, 93-94cm

7. *Blackites base*
1408A-14H-5W, 63-64cm

8. *Blackites base*
1408A-14H-5W, 63-64cm

9. *Blackites tortilis*
1408A-14H-5W, 63-64cm

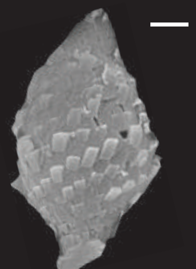

10. *Blackites ornatus*
1408A-22X-2W, 63-64cm

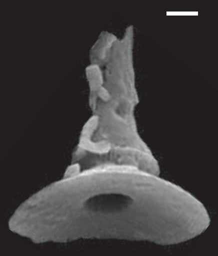

11. *Blackites gladius group base*
1408C-10H-5W, 63-64cm

12. *Blackites deflandrei group base*
1408B-5H-5W, 63-64cm

13. *Blackites tenuis*
1408A-14H-5W, 63-64cm

14. *Blackites spinosus*
1408A-22X-2W, 63-64cm

PLATE 2.18
Zygrhablithus, Lanternithus, Holodiscolithus, Daktylethra

1. *Z. bijugatus* ssp. *bijugatus*
1408A-14H-5W, 63-64cm

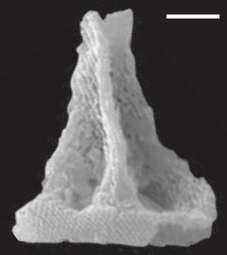

2. *Z. bijugatus* ssp. *bijugatus*
1408C-10H-5W, 63-64cm

3. *Z. bijugatus* ssp. *cornutus*
1408A-14H-5W, 63-64cm

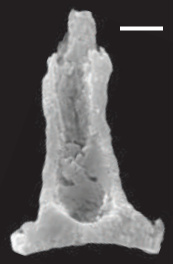

4. *Z. bijugatus* ssp. *cornutus*
1411B-18H-2W, 30cm

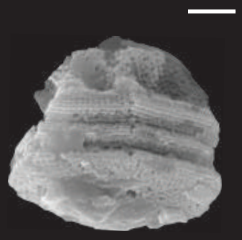

5. *Lanternithus minutus*
1408C-10H-5W, 63-64cm

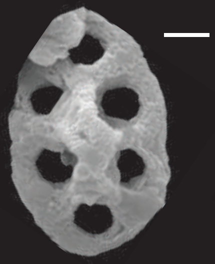

6. *Holodiscolithus solidus*
1408C-10H-5W, 63-64cm

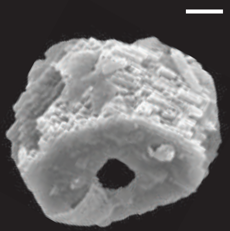

7. *Daktylethra unitatis*
1408B-5H-5W, 63-64cm

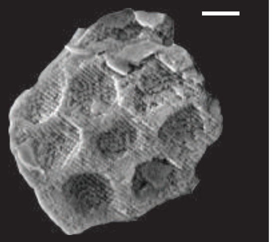

8. *Daktylethra punctulata?*
1408C-7H-4W, 93-94cm

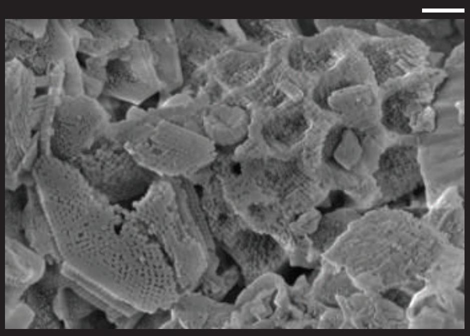

9. *Lanternithus minutus*
1408C-7H-4W, 93-94cm

10. *Clathrolithus* sp.?

PLATE 2.19
Discoaster, Sphenolithus

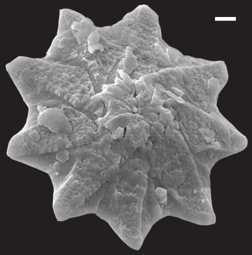
1. *Discoaster barbadiensis*
1411B-20H-4W, 36-37cm

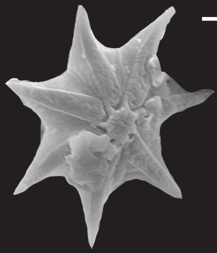
2. *Discoaster saipanensis*
1408B-5H-5W, 63-64cm

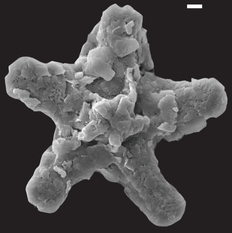
3. *Discoaster tanii*
1411B-18H-2Wl 30cm

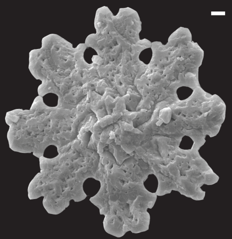
4. *Discoaster nodifer*
1408A-14H-5W, 63-64cm

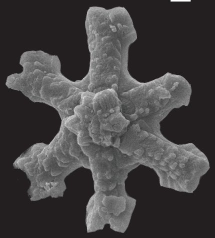
5. *Discoaster distinctus*
1408C-10H-5W, 63-64cm

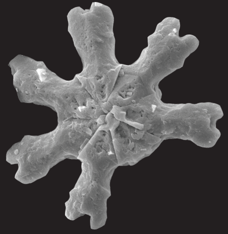
6. *Discoaster deflandrei*
1411C-17X-2W, 110-111cm

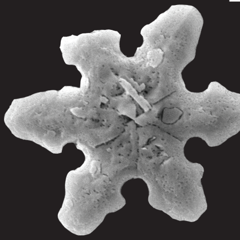
7. *Discoaster nodifer*
1408B-5H-5W, 63-64cm


8. *Discoaster nodifer*
1408B-5H-5W, 63-64cm

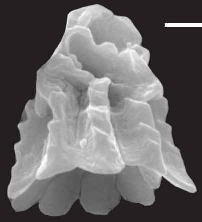
9. *Sphenolithus spiniger*
1408A-14H-5W, 63-64cm

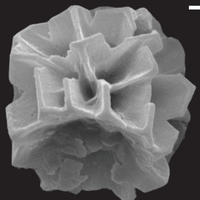
10. *Sphenolithus moriformis*
1408B-5H-5W, 63-64cm


11. *Sphenolithus strigosus*
1408A-14H-5W, 63-64cm

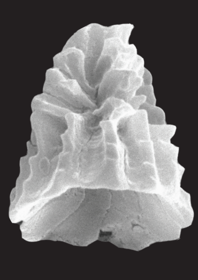
12. *Sphenolithus spiniger*
1408C-10H-5W, 63-64cm

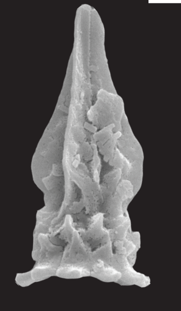
13. *Sphenolithus obtusus?*
1408B-5H-5W, 63-64cm

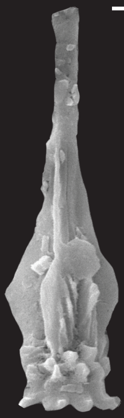
14. *Sphenolithus obtusus*
1408A-14H-5W, 63-64cm

Chapter 3

Calcareous nannoplankton population dynamics and evolution during the Middle Eocene Climatic Optimum in the North Atlantic (IODP Site U1408)

3.1 Introduction

The Eocene epoch was an interval of profound global climatic change, seeing peak greenhouse conditions at its start and terminating at the major switch into icehouse climates. The early Eocene was the core of the greenhouse world, with a series of transient warming events, hyperthermals, punctuating the background warming climatic trend. The principal hyperthermal, the Paleocene-Eocene Thermal Maximum (PETM) at ~56 million years ago (Ma), was followed by a series of smaller events (ETM2, H2, I1, I2 and ETM3) and sustained peak global temperatures that characterized the Early Eocene Climatic Optimum (EECO; 53-50 Ma). The EECO was followed by a 17 million year (myr) cooling trend, through the middle and late Eocene and into the early Oligocene icehouse world (e.g., Inglis et al., 2015; Zachos et al., 2001). At ~40 Ma this background cooling trend was punctuated by another transient warming event, the Middle Eocene Climatic Optimum (MECO), sustained over 500-800 kyr, with a gradual onset, peak warming in less than 100 thousand years (kyr) and rapid cooling to background levels (Bijl et al., 2010; Bohaty et al., 2009; Edgar et al., 2013). A negative shift in oxygen isotopes indicates a 4-6°C warming in surface and deep waters and this was accompanied by a temporary shoaling of the calcite compensation depth (CCD) (Pälike et al., 2012). The MECO differs from the earlier Eocene hyperthermals however, lacking an initial negative carbon isotope excursion and having a more gradual onset of warming (~4 kyr at the PETM (Zeebe et al., 2016) vs. ~500-800 kyr at the MECO (Bohaty et al., 2009)). Nevertheless, the MECO warming has been linked to an increase in CO_2 (Bohaty et al., 2009) possibly due to increases in ridge or arc volcanism or metamorphic decarbonation (Bohaty and Zachos, 2003), but uncertainties in these sources of carbon highlight the lack of current understanding on carbon cycle dynamics at this time (Bijl et al., 2010; Sexton et al., 2006; Sluijs et al., 2013). A greater insight into the MECO interval is required to enhance our understanding of Paleogene climatic change on these intermediate timescales (Sluijs et al., 2013).

Calcareous nannoplankton (marine coccolithophorid algae), are an important phytoplankton group with a long and complete fossil record, enabled by the preservation of their calcitic exoskeletons within the sedimentary record. Individual species are responsive to changes in environmental parameters, particularly temperature and nutrients and using quantitative assemblage data we are able to reconstruct past palaeoceanographic conditions. Nannoplankton were the dominant phytoplankton group of the early Paleogene but suffered long term loss of diversity through the Eocene greenhouse to icehouse transition, most likely in response to the palaeoclimatic and biotic changes through this interval. The MECO is a key interval of environmental change lying within this transition, and it marks one of the last intervals of high diversity in this group (Shamrock and Watkins, 2012), but as yet there are relatively few high resolution studies of calcareous nannoplankton assemblages across this event (O'Dea, 2013; Toffanin et al., 2011; Villa et al., 2014). Here we present calcareous nannoplankton data from Integrated Ocean Drilling Program (IODP) Site U1408, a stratigraphically expanded MECO section, recovered from the Northwest Atlantic Ocean. The site yields exceptionally well preserved calcareous nannofossils, which allows us to precisely determine origination and extinction events, document high-fidelity diversity trends, identify major shifts in population abundance and interpret the calcareous nannoplankton response to this rapid warming event.

3.2 Materials and Methods

3.2.1 Site description

IODP Site U1408 is located on the Southeast Newfoundland Ridge, in the Northwest Atlantic (41°26'N 49°47'W) (Figure 3.1). The site is currently at 3022 metres below sea level (mbsl) and was at 2575 mbsl in the middle Eocene (50 Ma), high above the CCD during the MECO (CCD 4-5 km; Norris et al., 2014). Three holes achieved 99 % recovery and form a 280.62 m thick splice (post cruise working version splice). The studied section is located between 41.38 and 87.47 metres composite depth (mcd) and comprises greenish grey nannofossil clays with interbedded white to light grey nannofossil ooze. The sediments contain moderate bioturbation, sand sized lithics and post-depositional glauconite bands and show well defined cyclicity (greenish grey/dark green to very light grey) at a decimetre scale, considered to be orbital cycles (Norris et al., 2014). Carbonate content increases across the MECO interval (~34 to 44 %) and clay content varies from 1-10 % to 25-50 %. The clays were sourced from contourite currents which formed the expanded Paleogene drift sediments on the ridge, with relatively high sedimentation rates across the MECO interval of 1.39-3.03 cm/kyr. The clay-rich nature of these deep sea sediments has facilitated the exceptional preservation of calcareous microfossils, with calcareous nannofossils, planktonic foraminifera and benthic foraminifera recording good to exceptional preservation across the interval, with the occasional sample with moderate preservation. Microfossil reworking is rare within the sediments. The high sedimentation rates, exceptionally well preserved calcareous microfossils and stratigraphically continuous succession result in this being one of the best middle Eocene successions ever recovered, providing an exceptionally high quality MECO section.

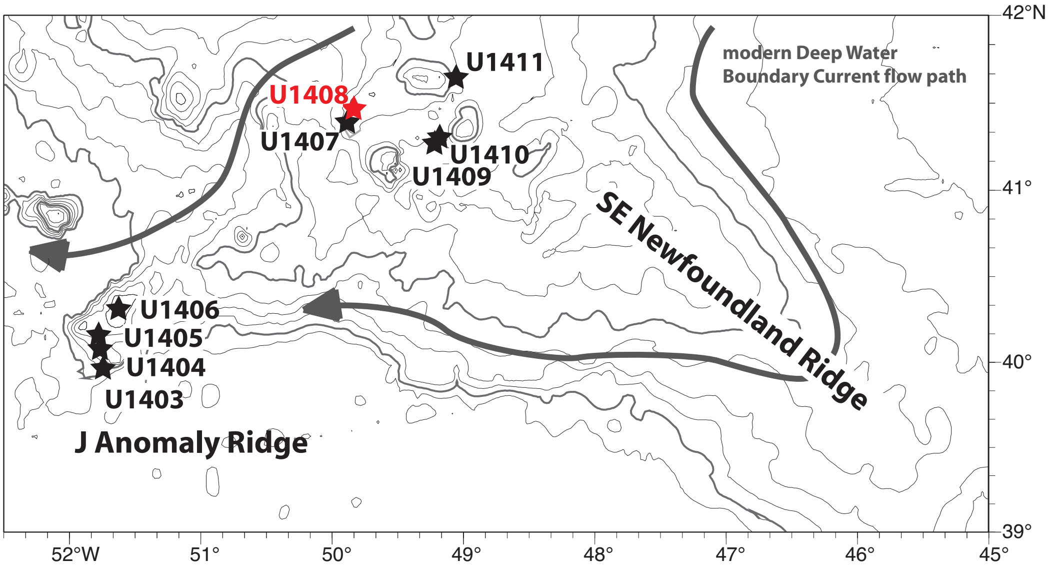

Figure 3.1: Location map for Site U1408, IODP Expedition 342 in the North Atlantic. Modified from Norris et al. (2014).

3.2.2 Age Model

The age model is based on integrated shipboard bio- and magnetostratigraphic data using the Geological Time Scale 2012 (GTS12) calibration ages (Gradstein et al., 2012; Norris et al., 2014) (Figure 3.2). Palaeomagnetic datums, which form the principal tie points, and revised principal calcareous nannofossil bioevents, are shown in Table 3.1. Ages for the base of *Reticulofenestra stavensis* and the top of *Chiasmolithus solitus* are within 80 kyr and 210 kyr, respectively, of the GTS12 calibration, which may represent slight error within the current age model. The top of *Chiasmolithus solitus* is, in any case, poorly constrained due to its sporadic occurrence towards the top of its range and it varies latitudinally, which may also account for the discrepancy from the GTS12 calibration age, as seen here (Agnini et al., 2014; Gradstein et al., 2012). The low resolution oxygen isotope record generated at the University of California (Don Penman, pers. comm. 2016, documented in Baba, 2014) is consistent with the age model, indicating the onset of MECO warming within C18r (40.74 Ma) and the peak warmth at the base of C18n.2n (40.19-40.09 Ma). The shipboard record of the *Orbulinoides beckmanni* range, 39.57-39.98 Ma (specimens only recorded in two samples), does not coincide with MECO warming which has been previously shown as concurrent (Edgar et al., 2010). However, this species shows latitudinal diachroneity between low and mid latitude sites (Edgar et al., 2010) and the later appearance of this species at Site U1408 may represent the delayed expansion of this tropical species range to the mid to high latitudes.

Datum tie points	**Datum type (Zones)**	**GTS12 age (Ma)**	**Revised calibrated age (this study) (Ma)**	**Shipboard midpoint depth (mcd)**	**Revised midpoint depth (mcd)**	**LSR (cm/kyr)**
C17r/C18n.1n	Chron boundary	38.62		34.68		
C18n.1n/C18n.1r	Chron boundary	39.63		52.05		1.72
Top common Sphenolithus spiniger	Nannofossil (Within NP17) (Within CNE15)		39.72	60.41	54.66	
Base Sphenolithus obtusus	Nannofossil (Within NP17) (Within CNE15)		40	60.41	62.28	
C18n.2n/C18r	Chron boundary	40.14		66.15		2.76
Top *Chiasmolithus solitus*	Nannofossil (NP16/17)	40.4	40.19	67.98	66.93	
Base *Reticulofenestra stavensis*	Nannofossil (CNE14/CNE15)	40.36	40.44	70.71	71.15	
Base common Sphenolithus predistentus*	Nannofossil (Within NP16) (Within CNE14)		40.65	70.71	74.67	
Top *Sphenolithus furcatolithoides*	Nannofossil (Within NP16) (Within CNE14)		40.88	75.15	78.57	
C18r/C19n	Chron boundary	41.15		83.24		1.69
C19n/C19r	Chron boundary	41.39		84.85		0.67
C19r/C20n	Chron boundary	42.3		118.56		3.7

Table 3.1: Datum tie points for the age model at Site U1408 shown in bold. Principal calcareous nannofossil bioevents with shipboard and revised depths are also shown. *Base common rather than base is given for the revised depth and age as this appears to be a more reliable event. LSR = linear sedimentation rate. NP Zones (Martini, 1971) and CNE/O Zones (Agnini et al., 2014).

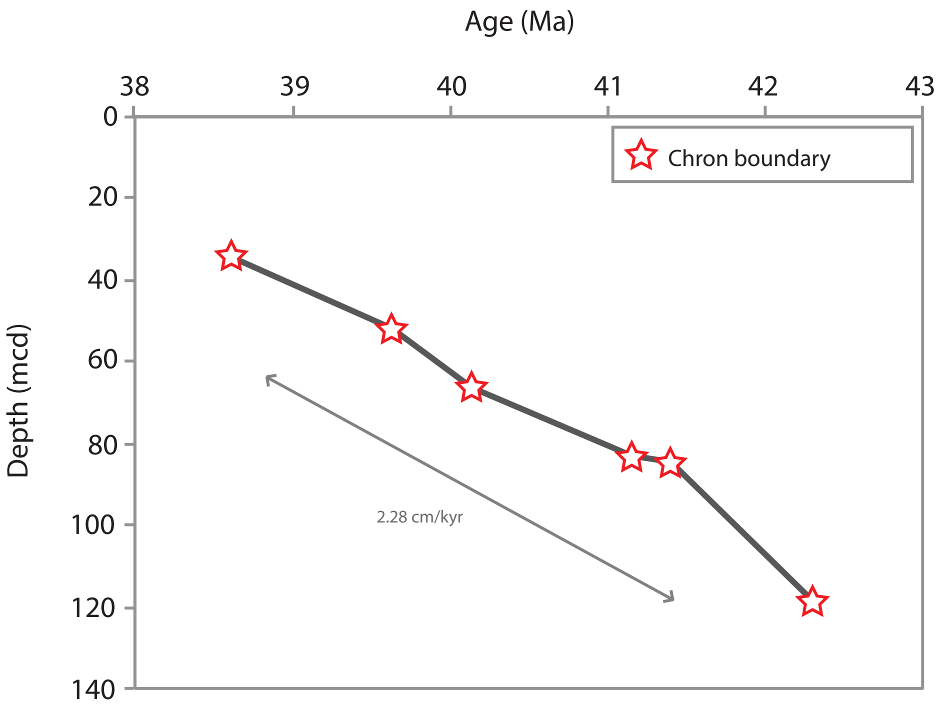

Figure 3.2: Age model for Site U1408 across the MECO interval, datums taken from Table 3.1. Average linear sedimentation rate shown.

3.2.3 Data collection techniques

138 samples were studied across the MECO interval at ~17 kyr resolution (every ~33 cm). Smear slides were produced using standard methods (Bown and Young, 1998) and analysed using transmitted light microscopy at x1000 magnification on an Olympus BX40 under cross polarized, bright field and phase contrast light. The first 300 nannofossil specimens were identified to species level per smear slide, and extended counts were then performed, excluding the dominant taxa (small placoliths of reticulofenestrids <5 µm and *Coccolithus pelagicus* <5 µm, which comprise ~60 % of the assemblages), until all other taxa totalled at least 300. Semi-quantitative analysis was also performed (three traverses per slide) to enable identification of the diverse but rare assemblage components.

3.2.4 Analytical techniques

3.2.4.1 Diversity

Diversity is documented using raw species richness from the quantitative count data, maximised species richness from the semi-quantitative and quantitative data, the Shannon H index and Evenness. Maximised species richness is calculated by interpolating taxon ranges between first and last occurrences, reducing the noise introduced by relatively large numbers of rare taxa (<1 %). Shannon H and Evenness incorporate both abundance and species richness from the quantitative records.

3.2.4.2 Palaeoecological classifications

Many nannofossil species display preferences for different environmental conditions and can be used as proxies for parameters such as temperature and productivity. Here we apply palaeoecological groupings to key MECO calcareous nannofossil taxa for which preferences are relatively well known from previous work, supplemented by observations from this study.

Warm water and/or oligotrophic favouring taxa

Discoaster spp. and *Coccolithus formosus* are considered warm water oligotrophs due to their preference for low latitude open ocean environments (Schneider et al., 2013; Villa et al., 2008; Wei and Wise, 1990). *Coccolithus pelagicus* is a common component of Eocene assemblages at all latitudes but displays a preference for low and mid latitudes during the early Paleogene indicating a warm temperate preference (Gibbs et al., 2006; Haq and Lohmann, 1976). *Zygrhablithus bijugatus* has enigmatic distribution and may be affected by preservational bias, but has been interpreted as both a warm temperate water oligotroph (Bralower, 2002; Gibbs et al., 2006; Pea, 2010; Shamrock and Watkins, 2012) and cool temperate eutroph (Tremolada and Bralower, 2004; Villa et al., 2008). Here it displays abundance trends that are similar to *Discoaster* spp. and so we tentatively consider it a warm water oligotroph.

Cold water and/or meso/eutrophic favouring taxa

Chiasmolithus spp., *Reticulofenestra daviesii* and *Reticulofenestra lockeri* are distinctly cold water taxa with highest abundances at high latitudes and with a preference for mesotrophic or eutrophic surface water conditions (Bralower, 2002; Fioroni et al., 2015; Schneider et al., 2013; Villa et al., 2014; Wei and Wise, 1990). *Clausicoccus subdistichus* is a mid to high latitude taxon (Wei and Wise, 1990) and therefore considered cold water favouring and its striking acme at the Eocene-Oligocene boundary has long been considered strong support for this interpretation. *Reticulofenestra dictyoda* is abundant and widely distributed during the Eocene but is considered to have a cool temperate meso/eutrophic preference (Pea, 2010; Villa et al., 2014).

Warm oligotrophic species	**Cold meso/eutrophic species**
Discoaster spp.	*Reticulofenestra dictyoda*
Coccolithus formosus	*Reticulofenestra daviesii*
Coccolithus pelagicus	*Reticulofenestra lockeri*
Zygrhablithus bijugatus	*Clausicoccus subdistichus*
	Chiasmolithus spp.

Table 3.2: A summary of the palaeoecological groupings assigned in this study and used in the PEI based on previous work as summarized in the text.

To provide a synthesis of these abundance records we have formulated an index that incorporates these two contrasting palaeoecological groups of taxa (Table 3.2), as follows:

$$Palaeoenvironmental\ Index\ (PEI) = \frac{(cold\ meso/eutrophs)}{(cold\ meso/eutrophs + warm\ oligotrophs)}$$

3.3 Results

3.3.1 Diversity and species turnover

Calcareous nannofossils are abundant in all samples and there is relatively high, raw species richness of ~40 pre-MECO, decreasing to ~34 species across the peak-MECO and rapidly increasing to ~46 species during the post-MECO (Figure 3.6). Maximised species richness records show ~122 species pre-MECO, peaking at 125 species at 40.96 Ma, followed by a decline in diversity from 40.89 Ma to 118 at the peak-MECO decreasing further in the post-MECO to 112 (Figure 3.6), highlighting the number of rare taxa within the assemblages. Shannon H and Evenness show an overall increase through the interval, ~1.75 to 2.23 and ~0.15 to 0.25, respectively (Figure 3.6).

Two significant evolutionary events fall within the MECO interval at Site U1408: the origination of the *Reticulofenestra bisecta* group during the onset (*Reticulofenestra*

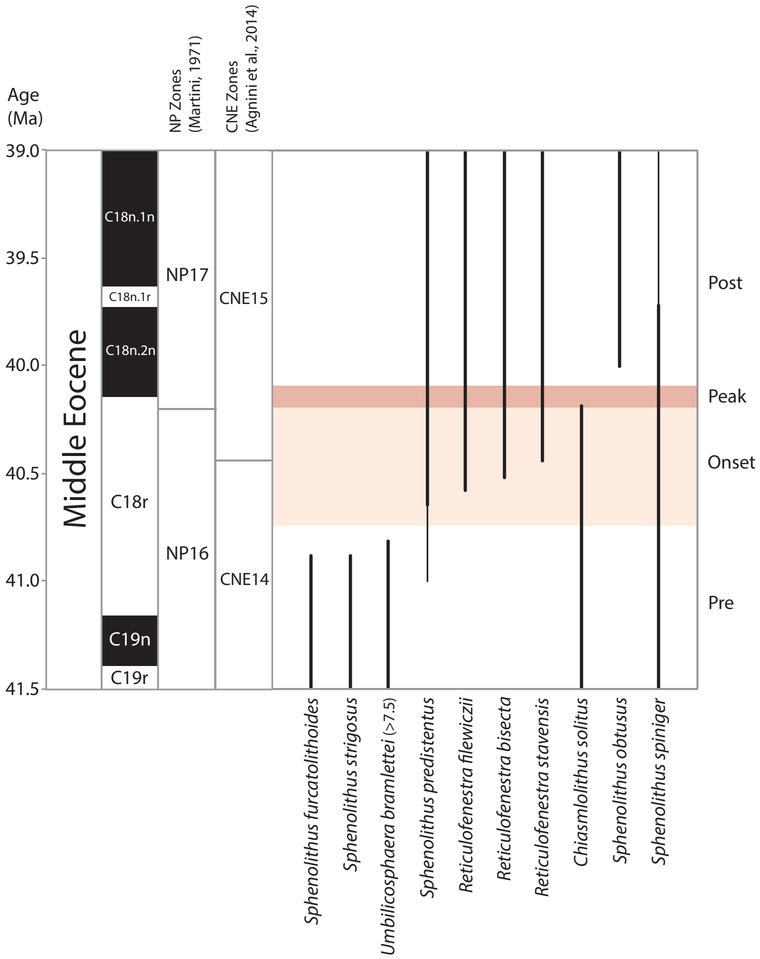

Figure 3.3: Biostratigraphic range chart of principal calcareous nannofossil events through the MECO interval. The thin line represents rare occurrence. The onset and peak-MECO are defined using the oxygen isotope record. Magnetostratigraphy is taken from the Expedition 342 shipboard records.

bisecta at 40.52 Ma, *Reticulofenestra stavensis* at 40.44 Ma and *Reticulofenestra filewiczii* at 40.58 Ma) and a turnover within the sphenolith taxa immediately preceding, during and immediately after the MECO event. In total there are eleven key bioevents (Figure 3.3) including the origination of five species (the *Reticulofenestra bisecta* group, *Sphenolithus predistentus* at 41.00 Ma and *Sphenolithus obtusus* at 40.00 Ma), extinction of four species (*Sphenolithus strigosus* and *Sphenolithus furcatolithoides* at 40.88 Ma, large *Umbilicosphaera bramlettei* >7.5 µm at 40.81 Ma and *Chiasmolithus solitus* at 40.19 Ma) and the top common occurrence of *Sphenolithus spiniger* (39.89 Ma) (Figure 3.3). The extinctions of *Sphenolithus furcatolithoides, Sphenolithus strigosus* and large *Umbilicosphaera bramlettei,* which occur within ~60 kyr, and the first very rare occurrences of *Sphenolithus predistentus* all occur in the pre-MECO interval, 80-260 kyr before the onset of the MECO. Within the onset interval there is the base common of *Sphenolithus predistentus* at 40.65 Ma, followed by the origination of the *Reticulofenestra bisecta* group, within 130 kyr and 250 kyr prior to the peak-MECO. *Chiasmolithus solitus* becomes extinct at the beginning of peak-MECO conditions and *Sphenolithus obtusus* originates shortly after the peak (90 kyr). The last common occurrence of *Sphenolithus spiniger* occurs 370 kyr after the peak.

3.3.2 Nannofossil abundance records

Out of the total 125 species identified, 12 have a relative abundance of >1 % accounting for the majority of the assemblages. This reflects the dominance of the small placoliths (~60 %) (Figure 3.4) which reduces the relative abundance of other taxa. Relative abundances for each taxon described herein were calculated excluding the dominant small placoliths (reticulofenestrids <5 µm and *Coccolithus pelagicus* <5 µm), which strengthens the signals in these non-dominant taxa.

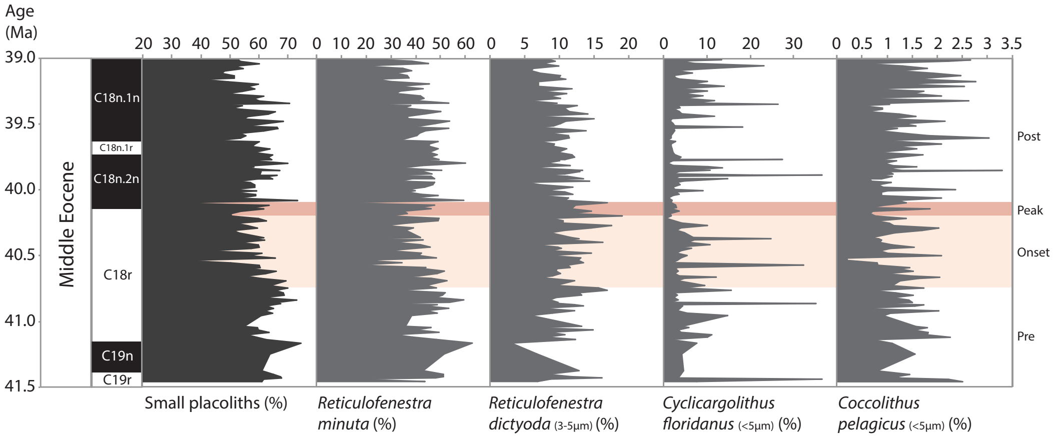

Figure 3.4: Small placoliths relative abundance data. The onset and peak-MECO are defined using the oxygen isotope record. Magnetostratigraphy is taken from the Expedition 342 shipboard records.

The Site U1408 middle Eocene nannofossil assemblages are dominated by reticulofenestrids, which contribute on average 50 % (Figure 3.5). Most taxa have large fluctuations in their abundance records. *Reticulofenestra dictyoda* (5-8 µm) is a common component of the assemblages ~18 % and larger specimens (8-14 µm) decrease in abundance post-MECO from ~3 to 1 %. Other common reticulofenestrids include *Cyclicargolithus floridanus,* the *Reticulofenestra reticulata* group (*Reticulofenestra reticulata* and *Reticulofenestra westerholdii*) and *Reticulofenestra lockeri*, which all increase in abundance from ~5 to 20 %, ~2 to 20 % and ~4 to 13 %, respectively.

Cyclicargolithus floridanus and the *Reticulofenestra reticulata* group have peaks in abundance at 22 and 15 %, respectively, immediately following the peak-MECO before decreasing and peaking again at the top of the study interval (22 and 23 %). Following their origination, *Reticulofenestra bisecta* and *Reticulofenestra stavensis* have average abundances of ~4 and 1 %, whereas *Reticulofenestra filewiczii* initially peaks at ~4 % abundance, declining to an average of ~1 % from ~40 Ma.

The Coccolithaceae account for ~30 % of the assemblages (Figure 3.5) with *Coccolithus pelagicus* most abundant (~13 % on average) and *Coccolithus formosus* accounting for ~2.7 %. Both species show overall abundance decreases from 40.73 Ma across the peak-MECO. *Clausicoccus* spp. decrease slightly prior to the MECO and during the onset but then stabilize (~4 %) from ~40.6 Ma. Rare species include *Bramletteius serraculoides* (increases in abundance from ~0.3 % to 3.5 %) and small specimens of *Umbilicosphaera bramlettei* <7.5 µm (decreases in abundance to 1 % at 40.10 Ma then increases to an average of 4 % post-MECO). Chiasmoliths are consistently rare, decreasing to <1 %.

Blackites spp. are highly diverse in the middle Eocene and account for ~10 % of the assemblages at the base of the study interval, decreasing to ~4 % at the peak-MECO before recovering to pre-event values post-MECO. *Pontosphaera* spp. and *Helicosphaera* spp. are consistently rare (both ~2 %) and show large fluctuations (Figure 3.5).

Discoaster spp. is rare (overall an average of 2 %), peaking at 6.5 % in the MECO onset before overall decreasing in abundance to ~1 %, but with a second spike in abundance at the peak-MECO (4 %), returning to 2 % post-MECO. *Zygrhablithus bijugatus* is rare and declines from ~5 % in the pre-MECO interval to 0 % across the peak-MECO, returning at 40.05 Ma to 2.7 % (Figure 3.5).

Sphenoliths are relatively rare comprising ~4 % of the assemblages (Figure 3.5). The last occurrences of *Sphenolithus strigosus* and *Sphenolithus furcatolithoides* occur at 40.88 Ma following low final abundances of 1-2.5 %. A sudden decrease of *Sphenolithus spiniger* occurs at ~40 Ma (~3 to 0.6 %) with the top common (Tc) occurrence identified at 39.89 Ma, where the abundance becomes rare and discontinuous. *Sphenolithus predistentus* originates at 41.00 Ma, with base common occurrence at 40.65 Ma, increasing to ~3 % by 39.5 Ma. Both *Sphenolithus obtusus* and *Sphenolithus moriformis* are rare (~0.6 % and 2 %).

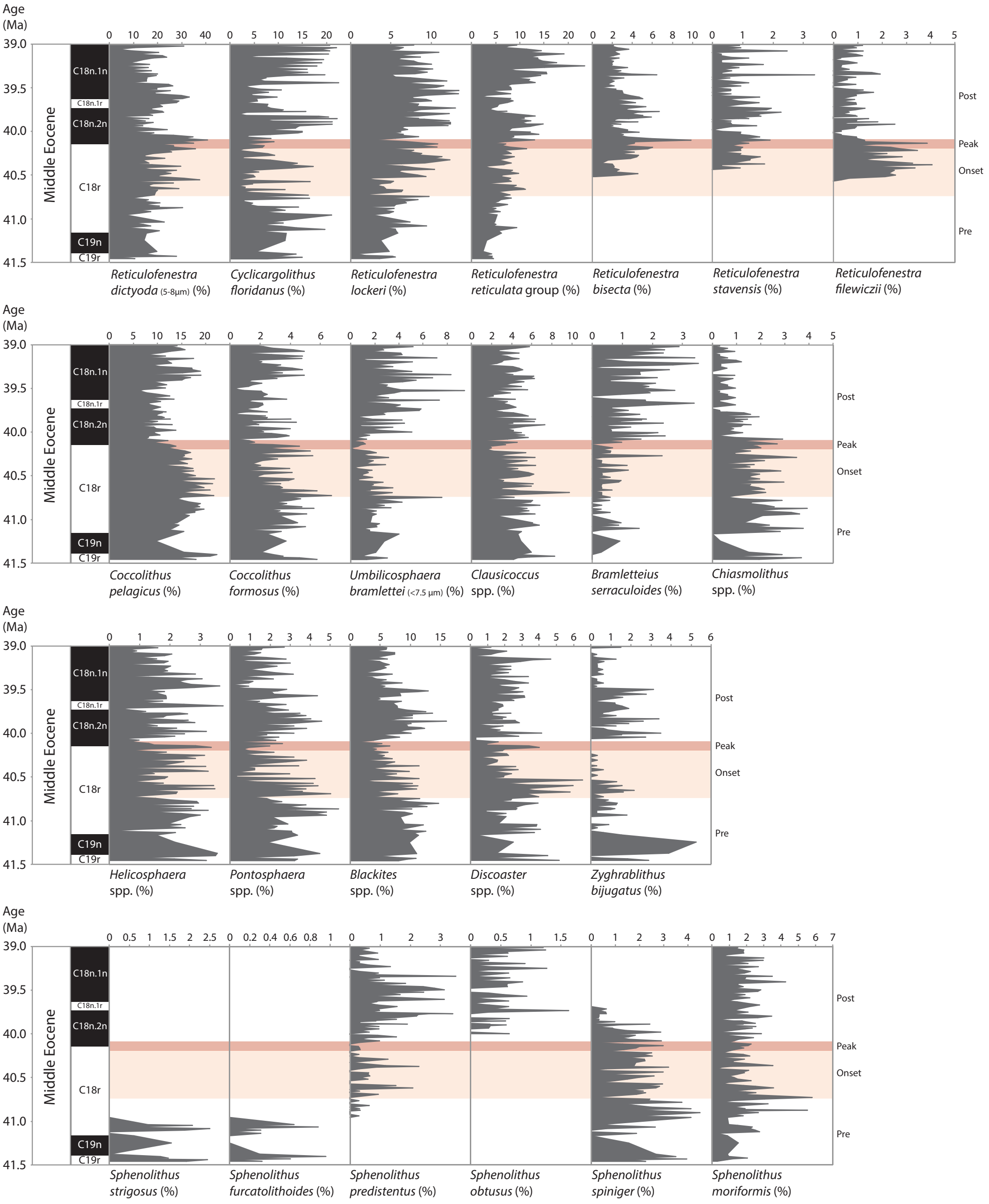

Figure 3.5: Key calcareous nannofossil taxa relative abundance data. The onset and peak-MECO are defined using the oxygen isotope record. Magnetostratigraphy is taken from the Expedition 342 shipboard records.

3.3.3 Palaeoecological results

The pre-MECO nannofossil assemblages comprised a mix of warm water oligotrophs and cold water eutrophs dominated by *Reticulofenestra dictyoda, Cyclicargolithus floridanus* and *Coccolithus pelagicus* with other common components including

Reticulofenestra lockeri, Reticulofenestra reticulata, Clausicoccus and *Blackites*. Early in the MECO onset there are increases and peaks within taxa known to have warm water oligotrophic preferences (*Discoaster, Coccolithus formosus* and *Umbilicosphaera bramlettei* <7.5 µm) and the warm temperate species *Coccolithus pelagicus* but these taxa subsequently go into decline. A second minor peak in *Discoaster* and *Coccolithus formosus* coincides with the onset of the peak-MECO (4 % and 4.6 %, respectively). *Zygrhablithus bijugatus* also declines through the MECO interval, disappearing completely across the peak.

The PEI increases from 40.59 Ma through the onset (0.57 to 0.71) and peak-MECO (0.71 to 0.83) reflecting the increasing dominance of cold water meso/eutrophs (Figure 3.6). Following the peak-MECO there is a sudden shift at 40.05 Ma to pre-peak-MECO values of 0.6. During the post-MECO interval the PEI values gradually increase to another peak of 0.74 at 39.6 Ma before decreasing at the top of the interval. These PEI results highlight that across the onset and peak-MECO the assemblages are predominantly made up of cold water favouring meso/eutrophs but significant shifts in the index during the post-MECO interval suggest unstable palaeoceanographic conditions in the immediate aftermath before returning to pre-MECO compositions at the top of the study interval.

3.4 Discussion

3.4.1 Calcareous nannoplankton response during the MECO at Site U1408

Calcareous nannoplankton assemblage data from Site U1408 reveal significant evolutionary bioevents, species abundance increases and declines, and minor shifts in diversity. An initial minor response to the onset of warming is recorded in warm water oligotrophs but despite continued warming, indicated by the $\delta^{18}O$ records, the declining abundances in these warm water taxa through the interval suggest another factor is dominating the nannoplankton distributions, most likely increasing eutrophy which explains the decline in oligotrophs and increases and peaks within the meso/eutrophic species, such as *Reticulofenestra dictyoda*. Following peak-MECO warmth a distinct shift in the PEI (0.8-0.6) coincides with the interval of rapid cooling. The increasing Shannon H values indicate subtle changes in assemblage structure, mainly due to the declining abundance of small placoliths. These minor abundance and diversity shifts

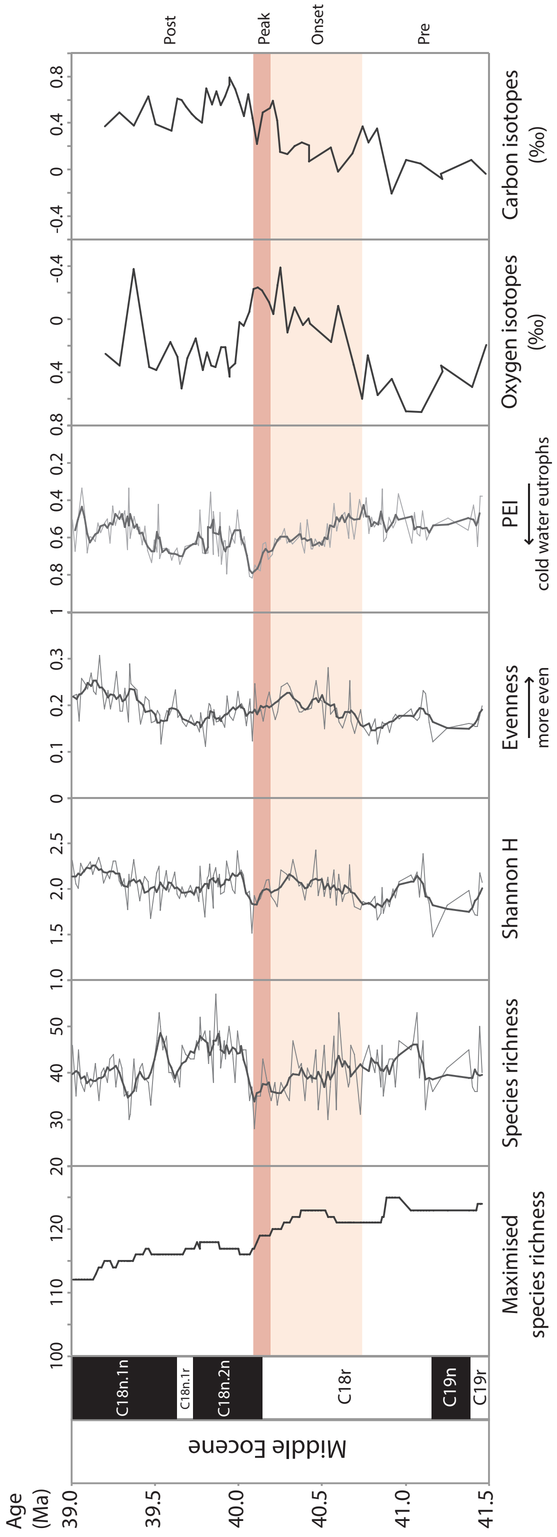

Figure 3.6: Calcareous nannofossil diversity indices and the palaeoenvironmental index (PEI) plotted against oxygen and carbon isotope data (Don Penman, pers. comm. 2016). Quantitative diversity indices and the PEI are shown with a 3 point moving average. The onset and peak-MECO are defined using the oxygen isotope record. Magnetostratigraphy is taken from the Expedition 342 shipboard records.

represent a relatively muted response to changing environmental conditions through the MECO at Site U1408 but two significant evolutionary events, the origination of the *Reticulofenestra bisecta* group and turnover within the sphenoliths, indicate a more significant influence on the nannoplankton at this time.

3.4.1.1 Origination of the *Reticulofenestra bisecta* group

At Site U1408 the origination of the *Reticulofenestra bisecta* group is a distinct and conspicuous event during the MECO interval and these taxa rapidly become established as significant components of late Paleogene nannoplankton assemblages. Unfortunately, the confusing taxonomy of this group has hindered its stratigraphic and palaeoecological application, as a range of different species and genus names appear in the literature (e.g. two different genus names are applied, *Reticulofenestra* and *Dictyococcites*, and multiple species names including *bisecta*, *hesslandii, scrippsae* and *stavensis* are used in different senses by different authors). Here we use *Reticulofenestra bisecta* and *Reticulofenestra stavensis* for forms with a distinct central area plug (<10 µm and >10 µm, respectively) and use *Reticulofenestra filewiczii* for similar forms with a small central pore spanned by a birefringent net. The fact that all three morphotypes appear within 0.13 myr of each other suggests that they are closely related if not the same species or species plexus. The group had a warm temperate preference (Monechi et al., 2000; Villa et al., 2008; Wei and Wise, 1990), which is consistent with its first occurrence during the onset of MECO warming. This also appears to be the case at other sites, with Agnini et al. (2014) recording the first occurrence of *Dictyococcites bisectus* (= *Reticulofenestra stavensis* herein) within Chron 18r (at 40.34 Ma Pälike et al. (2006) ≈ 40.35 Ma GTS12) from Blake Nose ODP Site 1051. The warm water preference of *Reticulofenestra bisecta* is further reinforced through records of its decline during the cool conditions of the early Oligocene (Bordiga et al., 2015; Dunkley Jones, pers. comm. 2014; Monechi et al., 2000) and low abundances and often sporadic occurrence through the Oligocene until its extinction at ~23.13 Ma (GTS12).

3.4.1.2 Sphenolith turnover

Sphenoliths exhibit a high level of species turnover across the MECO at Site U1408. Although the genus is typically considered to have a warm water oligotrophic preference (Bralower, 2002; Gibbs et al., 2006; Schneider et al., 2011), it is clear from MECO records that there was a range of species-specific adaptations, resulting in the decline, extinction, success and origination of different species across this interval of environmental change. This turnover has been noted at other MECO sections (e.g. Alano section, Italy; Toffanin et al. (2011); ODP Site 1051, Blake Nose; O'Dea (2013)) and although only an intra-genus shift, it is suggestive of a global response to palaeoceanographic change at this time. At Site U1408 the extinctions of *Sphenolithus strigosus* and *Sphenolithus furcatolithoides* (40.88 Ma) suggest a response to changing trophic conditions or to the pre-MECO cooling, prior to the onset of warming (Bohaty et al., 2009). Both species are short ranging (~4 to ~5 myr, respectively) middle Eocene taxa and may have had relatively specific ecological preferences making them vulnerable to the rapidly shifting environmental change that characterised the later middle Eocene and onset of the MECO. The origination of *Sphenolithus predistentus* occurred just prior to the MECO with very rare occurrences, increasing in abundance during the MECO-onset (40.65 Ma). This was followed by the origination of *Sphenolithus obtusus* 90 kyr after the peak-MECO (40.00 Ma). *Sphenolithus predistentus* is a relatively long-ranging species that is highly characteristic of the Eocene-Oligocene transition (EOT) and Oligocene assemblages. Its increasing abundance during the EOT has been considered strong evidence for eutrophic adaptation, a notably unusual ecology amongst this group (Dunkley Jones et al., 2008; Fioroni et al., 2015). Its significant increase during the MECO at Site U1408, during an interval when temperature and nutrient availability (shown by the PEI) appear to have been increasing, suggests both these factors may have contributed to its evolutionary appearance. It is notable that *Sphenolithus predistentus* decreases in abundance following the MECO and has sporadic occurrence through the remainder of the late Eocene, suggesting its optimum conditions were not re-established until the further environmental change that accompanied the EOT. Following this, *S. predistentus* was a common and characteristic component of Oligocene assemblages, giving rise to several new species before extinction in the late Oligocene. The final MECO-related sphenolith event is the top common occurrence of *Sphenolithus spiniger* (370 kyr post-MECO), which followed an abundance decline from 40.91 Ma. This conspicuous middle Eocene species decreased to low abundances following the rapid post-MECO cooling, suggesting tolerance of the transient warming at the MECO but an inability to maintain high abundances during the subsequent cooling prior to extinction soon after at 39.67 Ma. A similar trend is observed in the planktonic foraminifera species *Orbulinoides beckmanni* which persisted 600 kyr after the MECO event with decreasing abundance leading to extinction (Edgar et al., 2010).

3.4.2 Palaeoenvironmental controls on the calcareous plankton assemblages

Calcareous nannoplankton records at Site U1408 reveal a series of taxic changes across the MECO interval, which suggest a link between plankton evolution and the significant environmental change that characterized the MECO. More broadly, the turnover within sphenoliths, increase in reticulofenestrid mesotrophs (*Reticulofenestra dictyoda*), decrease of oligotrophs (*Discoaster* spp.) and increase in PEI all indicate increasingly eutrophic conditions, with assemblage shifts principally controlled by productivity rather than temperature. This shift towards more eutrophic assemblages appears to be a relatively widespread feature of MECO sections, with low/mid latitude marginal and slope sites indicating increasingly eutrophic conditions (Italy - Toffanin et al. (2011); North Atlantic - O'Dea (2013)) and high latitude Southern Ocean sites (ODP Sites 702 and 748) indicating consistently highly eutrophic conditions (South Atlantic - Pea (2010); Southern Ocean - Villa et al. (2014)). Temperature is typically considered an important forcing factor in plankton groups, but during the MECO at Site U1408 there is little evidence of its influence on nannoplankton assemblage compositions, despite this being an interval of significant warming. Warm water oligotrophs such as *Discoaster* are relatively rare components, as a consequence of the overriding influence of the relatively high productivity regime at this location and reflected in the dominance of reticulofenestrids at Site U1408 throughout the Eocene. Peaks in warm water taxa during the MECO onset and peak-MECO suggest a muted response to increasing temperatures, but these abundances are low and overall these taxa actually decline across the MECO interval. An increase in *Discoaster* at the onset of the MECO is also recorded in the Southern Ocean (ODP Sites 738 and 748) but this is similarly followed by decreasing abundance through the peak of the event (Villa et al., 2014). A stronger temperature response has been reported in the planktonic foraminifera with increased abundance in the thermophyllic group *Morozovelloides* at the onset of the MECO followed by rapid decline coincident with post event cooling (Witkowski et al., 2014) and range expansions occur in tropical taxa, including incursions of *Hantkenina alabamensis* and *Acarinina spinuloinflata* into the South Atlantic (ODP Site 1090; (Galeotti et al., 2002) and *Orbulinoides beckmanni* from low to mid latitudes (Edgar et al., 2013). However, this zooplankton group also provide evidence for productivity influence on the assemblages during the MECO with decreasing abundances in *Acarinina* and increasing abundances in *Globigerinatheka* suggesting increased eutrophy (Edgar et al., 2010; Witkowski et al., 2014).

The absence of a significant temperature response in calcareous nannoplankton across the peak-MECO is in stark contrast to the earlier Eocene hyperthermals where widespread and striking assemblage shifts are seen and which scale to the magnitude of carbon cycle perturbation (Bralower, 2002; Gibbs et al., 2012, 2006). This contrast may reflect the gradual onset of the MECO warming, compared to the rapid onsets of the early Eocene hyperthermals. Nannoplankton species had time to adapt to the gradually warming hyperthermal conditions, and a similar explanation has been proposed for the muted population response seen in benthic foraminifera in the Atlantic Ocean (Blake Nose - Moebius et al. (2015)). In addition, the transient nature of this event may have been relatively insignificant to the calcareous nannoplankton assemblages relative to the long term Eocene cooling first initiated following the EECO. Despite the relatively minor assemblage shifts, there are nevertheless a series of significant evolutionary events which suggest a broader role for temperature, with the originations restricted to warm water favouring groups (*Reticulofenestra bisecta* group and sphenoliths).

3.4.3 Palaeoceanography during the MECO from geochemical and micropalaeontological evidence

The warming during the MECO was a global phenomenon reflected in $\delta^{18}O$ records (Bohaty et al., 2009), poleward migrations in warm water planktonic foraminifera taxa (Edgar et al., 2013), and an increase in low latitude dinoflagellate cysts (Bijl et al., 2010). Increasing abundances and peaks in warm water nannoplankton (*Discoaster, Coccolithus formosus*, *Umbilicosphaera bramlettei* (<7.5 µm)) as recorded in this study and in planktonic foraminifera (*Morozovelloides*) from the North Atlantic Blake Nose site indicate a temperature control on the plankton assemblages at the onset of the MECO, although during the body and peak of the event, warming seems to have had a negligible effect on the plankton groups.

In addition to these MECO temperature effects, a range of biotic and geochemical proxies indicate elevated surface and bottom water productivity across a wide range of sites and settings (carbon isotopes – Witkowski et al. (2014); benthic foraminifera - Boscolo Galazzo et al. (2013); Moebius et al. (2014); Moebius et al. (2015); planktonic foraminifera - Luciani et al. (2010); calcareous nannoplankton - Toffanin et al. (2011); O'Dea (2013); this study; diatoms - Witkowski et al. (2014); Witkowski et al. (2012)). The timing and intensity of eutrophication varies dependent on latitude and location, with Southern Ocean and southern Atlantic sites indicating increases during the MECO onset, and subtropical sites showing later increases during the peak of the event (Moebius et al., 2015), indicating global increases in productivity yet site-specific differences are apparent, dependent on latitudinal positioning and regional influences (Moebius et al., 2015; Witkowski et al., 2014). However, a number of open ocean sites (IODP U1333, ODP 1218 - Pacific, ODP 702 – Southern Ocean and 1263 – South Atlantic) and a southern latitude shelf site (Site 1172) show decreased or unchanged productivity levels at the MECO (Bijl et al., 2010; Boscolo Galazzo et al., 2014), with some sites recording a 'doubtful' carbon isotope excursion (ODP Sites 1263, 702, 689 and the Contessa Highway and Monte Cagnero sections; Boscolo Galazzo et al. (2014)). This contrasts to PETM records where a distinct shelf to offshore trophic gradient is highlighted across the onset and peak of the event (Gibbs et al., 2006).

High or increased productivity at the MECO has been attributed to changes in upwelling regimes, increased continental runoff and/or changes to ocean currents or water masses (Moebius et al., 2015; O'Dea, 2013), with continental runoff and/or upwelling enhanced by the intensification of the hydrological cycle caused by the global warming (Moebius et al., 2015). Site U1408 is an open ocean site, only minimally affected by changing continental factors, with primary changes at this site therefore likely to reflect changing ocean current patterns. In particular the Gulf Stream, which currently transports nutrients sourced upstream from the tropics and possibly the southern hemisphere (Palter and Lozier, 2008) to the North Atlantic via the 'Nutrient Stream' (Pelegrí et al., 1996), would have had a strong influence on Site U1408 and it is considered to have flown along a similar trajectory to today in the Eocene (Norris et al., 2014). Highly trophic MECO surface waters from the mid Atlantic Blake Nose area, identified from microfossil evidence and the carbon isotope records (Edgar et al., 2010; Moebius et al., 2015; O'Dea, 2013; Witkowski et al., 2014), would have propagated downstream to Site U1408 via the Gulf Stream, supporting the strong nutrient signal shown in the calcareous nannoplankton across the peak-MECO at Site U1408.

3.5 Summary

The work in this chapter has documented the evolution and ecological response of calcareous nannoplankton across the MECO, providing greater insight to this relatively understudied transient warming event. We highlight a series of taxic changes which all indicate increasingly eutrophic conditions through the onset and peak-MECO, particularly reflected in increased abundance of meso/eutrophic reticulofenestrids and the PEI, with only minor evidence for warming, with peaks in the low abundance warm water taxa at the onset of the event. However, a series of significant evolutionary events are recorded in warmer water taxa, the origination of the *Reticulofenestra bisecta* group and turnover within the sphenoliths, suggesting a broad temperature influence across the MECO. Increasing eutrophy through the MECO appears to be relatively widespread and at Site U1408 increasing nutrient availability likely reflects changing ocean current patterns, most probably transported from the Gulf Stream. The muted response in calcareous nannoplankton across this transient warming event is in contrast to the early Eocene hyperthermals but may be explained by the relatively gradual onset of the MECO or reflect the insignificance of the event on the calcareous nannoplankton as it lies within the long term cooling trend.

Chapter 4

Calcareous nannoplankton response and population restructuring across the Eocene-Oligocene transition in the North Atlantic (IODP Site U1411)

4.1 Introduction

The Eocene-Oligocene transition (EOT) was a profound interval of palaeoenvironmental change, marking the culmination of the long term Paleogene climatic shift from a greenhouse into an icehouse world. Two prominent positive shifts in the oxygen isotope record (1.2-1.5 ‰) characterize this interval (Coxall et al., 2005; Miller et al., 2009), representing global cooling and the initiation and expansion of permanent Antarctic ice sheets (Coxall et al., 2005; Lear et al., 2008; Zachos et al., 1996), coincident with global sea level fall of approximately 80 m (Miller et al., 2009). Further perturbations to the palaeoceanographic record include >1 km deepening of the calcite compensation depth (CCD) (Coxall et al., 2005; Pälike et al., 2012; Zachos et al., 1996), restructuring of circulation patterns with increased thermohaline circulation causing ‘spinning up’ of the oceans (Miller et al., 2009), major increases in global productivity (Diester-Haass and Zachos, 2003) and enhanced levels of marine biotic disturbance (Coxall and Pearson, 2007; Dunkley Jones et al., 2008; Wade and Pearson, 2008). The primary forcing of the global cooling and Antarctic glaciation is considered to be declining CO_2 (Pearson et al., 2009), although orbital forcing and the opening of the Southern Ocean gateways and initiation of the Antarctic Circumpolar Current may have also played a significant role (DeConto and Pollard, 2003a; Pagani et al., 2011).

Calcareous nannoplankton dominate the phytoplankton record of the early Paleogene and were highly diverse. Throughout the Paleogene greenhouse to icehouse transition nannoplankton underwent significant diversity loss in the middle Eocene to the early Oligocene, with accelerated loss across the EOT (Aubry, 1992; Bown et al., 2004; see Chapter 6). The group has arguably never fully recovered from this diversity loss, with relatively low species richness recorded throughout the rest of the Cenozoic. Previous work across the EOT has documented changes in calcareous nannoplankton diversity and also identified significant shifts in assemblage structure (Dunkley Jones et al., 2008; Pea, 2010; Persico and Villa, 2004; Villa et al., 2014, 2008), which likely resulted from the dynamic changes in climatic and oceanographic parameters at this time. Here we investigate the relationship between calcareous nannoplankton diversity, assemblage shifts and the palaeoclimatic/oceanographic change that occurred across the EOT in the Northwest Atlantic. Integrated Ocean Drilling Program (IODP) Expedition 342 targeted sites with high sedimentation rates and clay-rich facies which would yield good microfossil preservation. Site U1411 is therefore ideal for this investigation as it is stratigraphically complete and expanded and contains exceptionally well preserved nannofossils, which are crucial prerequisites for the acquisition of high quality diversity and population data. The standard of preservation and completeness of the section presents significantly enhanced records than previously studied deep sea (ODP and DSDP) EOT sections, comparable to high resolution data from Tanzania (Dunkley Jones et al., 2008), documenting full assemblage records of living diversity from these deep sea sediments. There are currently no known high northern latitude nannofossil assemblage records across the EOT and Site U1411, a mid to high latitude oceanic location, is ideally situated to record climate-ocean change of this kind and to identify the effects Southern Ocean cooling and Antarctic glaciation have on northern sub-polar oceans.

4.2 Materials and methods

4.2.1 Site description

Site U1411 is located in the Northwest Atlantic on the Southeast Newfoundland Ridge (41^o 37'N 48^o 6'W) and lies in the flow path of the Deep West Boundary Current and the Gulf Stream (Figure 4.1). The site depth is 3300 metres below sea level (mbsl) and was approximately 2850 mbsl at 50 Ma, therefore a mid-depth site above the CCD in the late Eocene and early Oligocene. The site has a continuous sequence through the EOT with high sedimentation rates, on average 2.74 cm/kyr. Two holes, B and C, form a splice of 274.02 m thickness, with overall recovery of 91.3 % (Hole A was abandoned after one core). The splice interval of interest from 128.61 to 191.56 metres composite depth (mcd) spans the EOT (with the Eocene-Oligocene boundary (EOB) defined by the last occurrence of *Hantkenina* at 159.14 mcd) and nannoplankton NP Zones 19/20 to 22 (Martini, 1971).

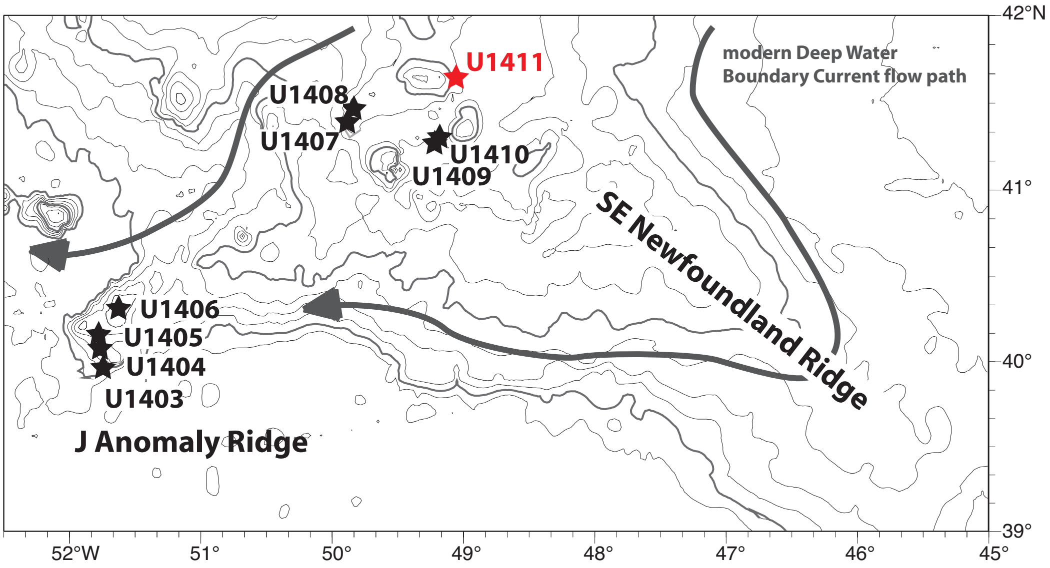

Figure 4.1: Location map of Site U1411 (IODP Expedition 342) in the North Atlantic. Modified from Norris et al. (2014).

The EOT pelagic deep sea sediments from Site U1411 are from lithological Unit II (107.87 to 233.63 mcd) and comprise silty clay, clay with nannofossils and silt, nannofossil clay, and clayey nannofossil ooze varying in colour from grey, dark grey, greenish grey and dark greenish grey. The sediments have prominent mottling from moderate bioturbation, including *Zoophycos, Planolites* and *Chondrites* burrows. The EOT section is predominantly clayey nannofossil ooze bedded on a decimetre scale with increased carbonate content in the early Oligocene (Norris et al., 2014). The high clay content within the sediments (~25-50 %) is due to drift sedimentation forming expanded successions through the Paleogene and is an unusual phenomenon in deep sea settings. The onset of drift sedimentation occurred in the early middle Eocene, which is comparable to other known drifts deposited by contourite currents in the North Atlantic (Hohbein et al., 2012).

The clay-rich nature of the sediments and site location significantly high above the CCD (~4 km in the Eocene) has resulted in exceptional preservation of calcareous microfossils. The standard of preservation is higher than seen in typical deep sea sediments and is comparable with clay-rich shelf/slope sediments (Bown et al., 2008). This quality is demonstrated by the presence of ‘glassy’ foraminifera with surface ornamentation and unfilled tests (including preserved hantkeninids) and highly diverse calcareous nannofossils containing a large proportion of minute coccoliths (<3 μm), fragile taxa such as *Blackites*, *Pontosphaera* and holococcoliths, the preservation of minute scale structures such as micron sized central area nets, the preservation of taxa with poor fossil records (*Calciosolenia* and *Syracosphaera*) and no evidence of etching or overgrowth (see Chapter 2). There is very minor reworking of middle and late Eocene calcareous nannofossils in the sediments through the EOT section of Unit II.

The expanded, complete stratigraphy, excellent microfossil preservation, good magnetostratigraphy and location at the boundary between the mid and high latitudes at the intersection of both high and low latitude currents make this one of the most important EOT sections yet recovered.

4.2.2 Age Model

Shipboard magnetostratigraphic and biostratigraphic data (calcareous nannofossils and planktonic foraminifera bioevents) have been integrated to construct an age model for Site U1411 using the Geological Time Scale 2012 calibration ages (GTS12; Gradstein et al., 2012; Norris et al., 2014). Palaeomagnetic datums provided the primary tie points across the EOT with the addition of refined planktonic foraminifera datums, the top of *Turoborotalia cerroazulensis* and top of Hantkeninidae which marks the EOB (Helen Coxall and Max Holmstrom, pers. comm. 2016, Stockholm University) and calcareous nannofossil *Isthmolithus recurvus* datum (Table 4.1; Figure 4.2). Sedimentation rates were assumed to remain consistent between tie points, with an average linear sedimentation rate of 3.38 cm/kyr through the late Eocene and early Oligocene. Throughout the rest of this chapter all depths are given in metres composite depth (mcd) and ages are based on the calibration from this age model.

We have refined the position of principal nannofossil biostratigraphic events using our high resolution semi-quantitative and quantitative data (shown in Table 4.1). The GTS12 timescale and the recent Agnini et al. (2014) Paleogene nannofossil biozonation scheme both use the astronomically calibrated ages from ODP Site 1218 (Blaj et al., 2009) for the top occurrences of the rosette discoasters (*Discoaster barbadiensis* and *Discoaster saipanensis*) and *Coccolithus formosus*. The age for the top of the rosette discoasters at Site U1411 is very close to the ages given in Agnini et al. (2014) (within ~10-90 kyr) and the last occurrence of *Coccolithus formosus* is ~280 kyr younger than the Agnini et al. (2014) calibration.

Oxygen and carbon isotopes through the EOT interval (Steve Bohaty and Paul Wilson, pers. comm. 2016, generated at the National Oceanography Centre Southampton) are consistent with the age model. A significant positive step in the oxygen isotope ($\delta^{18}O$) record is recorded from 33.72 Ma leading into maximum sustained values between 33.66 and 33.20 Ma, the Eocene-Oligocene Glacial Maximum (EOGM). There is no apparent 'first step' in the oxygen isotope records, as noted at other sites (e.g. Site 1218, St. Stephens Quarry) however a large positive shift in the carbon isotopes at 33.96 Ma is considered to highlight significant environmental change and represent the first step.

Datum tie points	**Datum type (Zones)**	**GTS12 age (Ma)**	**Revised calibrated age (this study) (Ma)**	**Shipboard midpoint depth (mcd)**	**Revised midpoint depth (mcd)**	**LSR (cm/kyr)**
Top *Isthmolithus recurvus*	Nannofossil (Within NP22) (Within CNO2)	32.49		107.34	106.84	
Top *Coccolithus formosus*	Nannofossil (NP21/NP22) (CNO1/CNO2)	32.92	33.14	143.64	134.51	
Base common *Clausicoccus subdistichus*	Nannofossil (CNE21/CNO1)		33.78		154.84	
C12r/13n	Chron boundary	33.16		135.34		4.25
C13n/13r	Chron boundary	33.71		151.7		2.97
Top *Hantkenina albamensis*	Planktonic foraminifera (E16/O1)	33.89		166.56	159.14	4.13
Top *Turborotalia cerroazulensis*	Planktonic foraminifera (Within E16)	34.03		169.56	*160.95 169.85	7.65
Top *Discoaster saipanensis*	Nannofossil (NP19/20/NP21) (CNE20/CNE21)	34.44	34.46	184.59	179.6	
Top *Discoaster barbadiensis*	Nannofossil (Within NP19/20) (Within CNE20)	34.77	34.68	196.32	184.68	
C13r/15n	Chron boundary	35		191.58		2.24

Table 4.1: Datum tie points for the age model at Site U1411 shown in bold. *Optional depth for this bioevent. Principal calcareous nannofossil bioevents with shipboard and revised depths are also shown. LSR = linear sedimentation rate. NP Zones (Martini, 1971) and CNE/O Zones (Agnini et al., 2014).

4.2.3 Data collection techniques

Samples were taken every ~30 kyr (~60-90 cm) spanning the interval from 33 to 35 Ma and at higher resolution, every ~10 kyr (~40 cm), across the EOB and the EOGM $\delta^{18}O$ shift (34-33.5 Ma). 111 smear slides were produced using the method from Bown and Young (1998) and viewed using transmitted light microscopy at x1000 magnification on an Olympus BX40 microscope under cross polarized, bright field and phase contrast light. Quantitative and semi-quantitative data were collected to produce biostratigraphic and relative abundance data. Simple abundance counts of 300 nannofossil specimens per

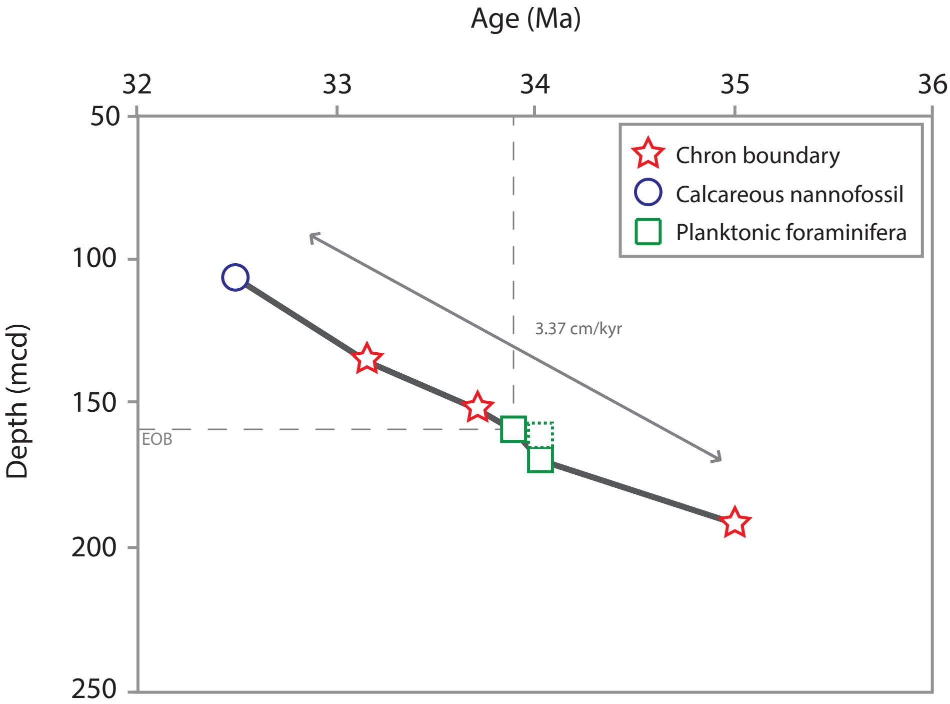

Figure 4.2: Site U1411 age model across the EOT interval, datums taken from Table 4.1. Dashed square indicates an optional datum point due to uncertainty in the planktonic foraminifera *T. cerroazulensis* event. Average linear sedimentation rate shown. EOB = Eocene-Oligocene boundary.

sample were performed across a random traverse (between 3-10 fields of view (FOV)). Extended counts were then performed, excluding the dominant taxa (*Reticulofenestra minuta* which accounts for ~40 % of the assemblages) continuing until the total of all other taxa equalled a minimum of 300 specimens (between 1-11 further FOV), improving the reliability for abundance estimates in rarer taxa, similar to the technique of Bralower (2002). Semi-quantitative counts were also performed to improve the documentation of rare species, which often includes biostratigraphically significant taxa. This was achieved by scanning three full traverses of the slide (~300 FOV). The semi-quantitative abundance classes were abundant (>10 per FOV), common (1-10 per FOV), frequent (<1 per FOV), rare (<1 per 10 FOV) and 3 specimens or less were noted by the number of specimens. Nannofossils were identified to species level following the taxonomy of Bown (2005a), Bown and Dunkley Jones (2006), Dunkley Jones et al. (2009), Bown and Dunkley Jones (2012) and Nannotax (http://ina.tmsoc.org/Nannotax3/).

4.2.4 Analytical techniques

We have calculated relative abundances for each taxon removing *Reticulofenestra minuta* from the dataset in order to remove the effect of this dominant taxon, strengthening the signal in non-dominant taxa. Several diversity metrics were applied to the data including raw and maximised species richness from semi-quantitative data, and the Shannon H index and Evenness from the quantitative data (Magurran, 2004). Species richness provides a standard measure of diversity using the presence and absence of species. The noise in this record that results from large numbers of rare species (<5 %) is removed by maximising species ranges between their first and last occurrence levels. This assumes that most absences in recorded taxa are due to rarity rather than populations constantly shifting in or out of the area. Shannon H and Evenness account for changes in assemblage structure by incorporating both species richness (occurrence data) and relative abundance and is a common approach when studying ecological diversity.

4.3 Results

All samples contain well preserved, abundant and highly diverse calcareous nannofossil assemblages. The assemblages are dominated by reticulofenestrids, which comprise ~80 % (including *R. minuta*) of the taxa on average. Relative abundances for each taxon described herein were calculated excluding *R. minuta* which comprised ~40 % of the assemblages (Figure 4.3).

Seven significant evolutionary bioevents are identified across the two million year study interval (Figure 4.4): the last occurrences of *Discoaster barbadiensis, Discoaster saipanensis, Umbilicosphaera bramlettei, Umbilicosphaera protoannula, Hayella situliformis* and *Coccolithus formosus* together with the acme of *Clausicoccus subdistichus*. The rosette discoaster extinctions (*D. barbadiensis* and *D. saipanensis*) in the late Eocene (34.68 and 34.46 Ma) are ~600 kyr prior to the EOB, and have previously been identified as defining the start of the ecological disturbance at the EOT (Pearson et al., 2008). The last occurrence levels likely represent the true extinction levels for these taxa, as they are close to their globally calibrated ages. The extinctions of *Umbilicosphaera protoannula* at 33.92 Ma and *Umbilicosphaera bramlettei* at 33.88 Ma lie very close to the EOB and the acme of *Clausicoccus subdistichus* (33.78 Ma) and extinction of *Hayella situliformis* (33.28 Ma) occur very close to the isotopic shift and within the EOGM, respectively. *Coccolithus formosus* persists through the EOT but has an extinction level in the early Oligocene at 33.14 Ma.

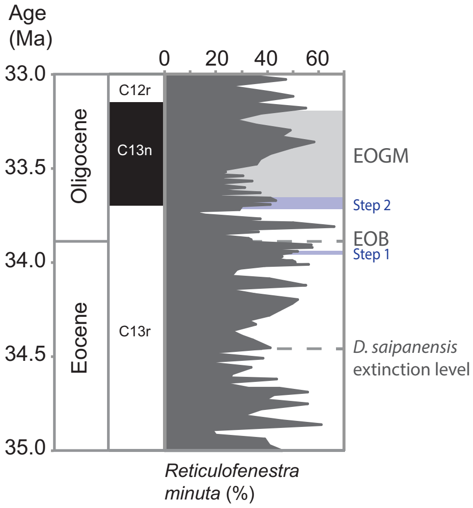

Figure 4.3: Relative abundance of the dominant taxon *Reticulofenestra minuta.* EOB = Eocene-Oligocene boundary, defined by the extinction of Hantkeninidae. Step 1, 2 and the EOGM = Eocene-Oligocene Glacial Maximum, are defined by the isotope records. Magnetostratigraphy is taken from the Expedition 342 shipboard records.

Species richness is high throughout (Figure 4.4) reflecting the exceptional quality of nannofossil preservation. Maximised species richness shows a gradual diversity decline through the late Eocene with accelerated loss from the EOB into the early Oligocene, with species richness 92 pre-EOT to 73 by 33 Ma. Individual sample diversities are lower than maximised species richness due to the number of rare taxa in the assemblages, but clearly track the overall trends showing relatively stable species richness through the late Eocene (~27), followed by significant diversity loss across the EOB (~20) maintained through the initiation of the EOGM and early Oligocene (Figure 4.4). There is muted response in Shannon H and Evenness, yet subtle changes are recorded across the EOB, with an increase in Shannon H and Evenness from ~1.7 to 2.0 and ~0.2 to 0.36, respectively, before returning to background levels in the early Oligocene (Figure 4.4).

The relative abundance patterns show clear evidence for significant calcareous nannoplankton assemblage disruption across the EOT interval. Two distinct groups of taxa exemplify this dynamic assemblage record, the first showing increases and acmes, and the second characterised by declining abundance (Figure 4.5). The first group – *Cyclicargolithus floridanus, Reticulofenestra lockeri, Reticulofenestra daviesii,*

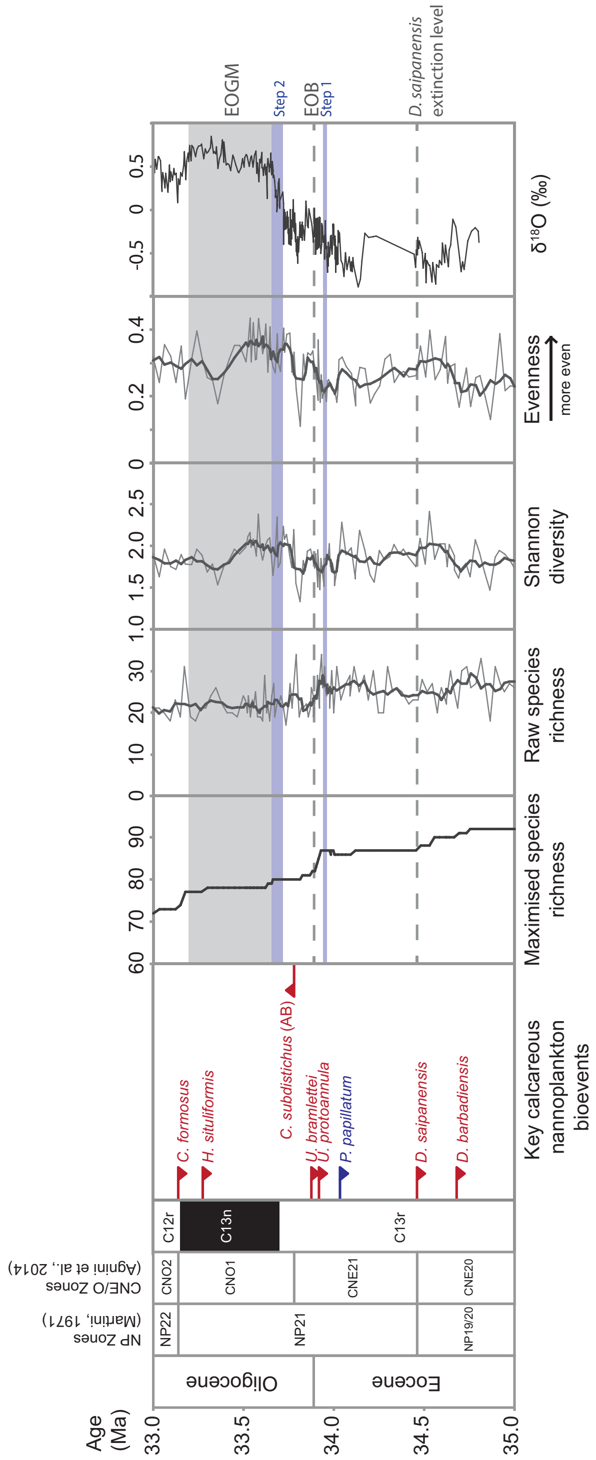

Figure 4.4: Site U1411 calcareous nannofossil bioevents, diversity indices and oxygen isotope records (Steve Bohaty, pers. comm. 2016). Bioevents detailed in text except *Pemma papillatum* which was not recorded at Site U1411 and the extinction level given is from Dunkley Jones et al. (2008) converted to GTS12. Diversity data from the quantitative counts are shown with a 3 point moving average. EOB = Eocene-Oligocene boundary, defined by the extinction of Hantkeninidae. Step 1, 2 and the EOGM = Eocene-Oligocene Glacial Maximum, are defined by the isotope records. Magnetostratigraphy is taken from the Expedition 342 shipboard records.

Clausicoccus subdistichus and *Sphenolithus predistentus* – display an asynchronous series of pulsed increases in abundance. Two pulses are identified in *Reticulofenestra daviesii*, with the major abundance increase close to the EOB, ~2 to 9 %. This is followed by the acme in *Clausicoccus subdistichus*, increasing from ~1.5 to 9 %, which is very closely tied to the second step recorded in the $\delta^{18}O$ record and then a major increase in *Reticulofenestra lockeri* (~4 to 14 %) occurs during the EOGM. *Cyclicargolithus floridanus* and *Sphenolithus predistentus* broadly increase from the base of the section into the EOGM (~18 to 50 % and ~0.3 to 2.6 %, respectively). The second group – *Coccolithus pelagicus,* large *Reticulofenestra dictyoda* (>8 µm), *Coccolithus formosus, Discoaster* spp. and *Umbilicosphaera bramlettei* – show declining abundance trends and, in a number of cases, terminal declines, which resulted in extinction. *Coccolithus pelagicus* shows steady decline from ~19 % in the late Eocene to ~11 % in the early Oligocene, whereas *Reticulofenestra dictyoda* (>8 µm), *Coccolithus formosus* and *Discoaster* spp. decrease significantly from ~8 %, ~4 % and ~2 % in the late Eocene to ~0.3 %, ~0.3% and ~0.3 % in the early Oligocene, respectively. *Umbilicosphaera bramlettei* is rare (on average 0.24 %) before its extinction following the EOB.

Other species which comprise a significant component of the assemblages include *Reticulofenestra dictyoda* 3-5 µm (~18 %), *Reticulofenestra dictyoda* 5-8 µm (~10 %), *Reticulofenestra bisecta* (*Reticulofenestra bisecta* and *Reticulofenestra stavensis*) (~3.3 %), *Blackites* spp. (~3 %) and *Sphenolithus moriformis* (~1.3 %) (Figure 4.5). These taxa show relatively little change through the study interval, although peaks in abundance are recorded in *Reticulofenestra dictyoda* (3-5 and 5-8 µm) close to the EOB and in *Blackites* spp. within the second step.

4.4 Discussion

4.4.1 Calcareous nannofossil palaeoecology

Although most calcareous nannoplankton species have very broad geographic distributions we are able to establish broad palaeoecological traits in many taxa, such as warm water oligotrophic and cold water eutrophic. An understanding of these palaeoecological preferences has primarily been established through biogeographic studies (Haq and Lohmann, 1976; Wei and Wise, 1990) and comparisons with other palaeoenvironmental proxies (Villa et al., 2008). Here we discuss the key Eocene-

Oligocene taxa and their palaeoecological affinities based on synthesis of previous work but also incorporating our own observations from this and other research.

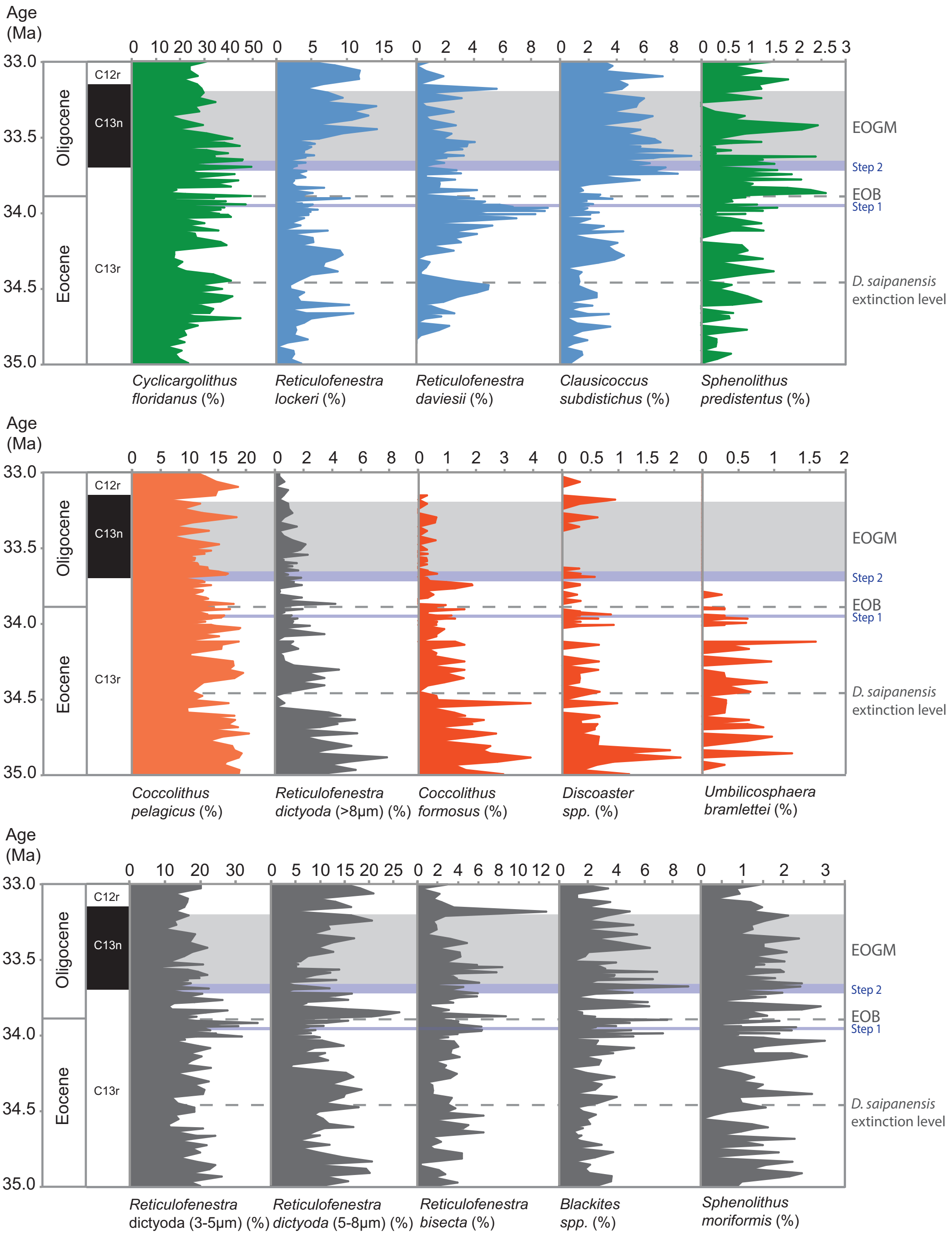

Figure 4.5: Key species relative abundance data. Some taxa are colour coded based on species strong palaeoecological preferences at the EOT; blue – cold water, orange – warm water, green – high productivity. EOB = Eocene-Oligocene boundary, defined by the extinction of Hantkeninidae. Step 1, 2 and the EOGM = Eocene-Oligocene Glacial Maximum, are defined by the isotope records. Magnetostratigraphy is taken from the Expedition 342 shipboard records.

Reticulofenestra daviesii

Reticulofenestra daviesii is especially abundant at high latitude sites and is considered a cold water taxon with eutrophic preferences (Fioroni et al., 2015; Monechi et al., 2000; Persico and Villa, 2004; Villa et al., 2014, 2008). It is particularly characteristic of EOT assemblages with records from the Southern Ocean showing a sharp increase in abundance of this taxon from ~20 to 90 % at ODP Site 748 (Villa et al., 2008) and ~10 to 70 % at ODP Site 689 (Persico and Villa, 2004). At lower latitudes, e.g., the Massignano section (Italy) and the Indian Ocean (ODP Site 711) this species shows a distinct increase in abundance in the late Eocene (Fioroni et al., 2015; Monechi et al., 2000). Such behaviour is also seen at Site U1411 during the EOT.

Reticulofenestra lockeri

Reticulofenestra lockeri is often grouped with *Reticulofenestra daviesii* as differentiation between the species may be difficult, especially when preservation is poor (Wei and Wise, 1990). The exceptional preservation at Site U1411 facilitates confident differentiation between these species but nevertheless *R. daviesii* and *R. lockeri* both display low abundances in the late Eocene with pulsed increases through the EOT, indicating *R. lockeri* also favours cold water eutrophic conditions (Wei and Wise, 1990). At Site U1411 *R. lockeri* increases in abundance across the EOT supporting this interpretation.

Clausicoccus subdistichus

Small *Clausicoccus* (*C. subdistichus* or *C. obrutus* of some authors - Fornaciari et al., 2010; Nocchi et al., 1988; occasionally included with *C. fenestratus* - Wei and Wise, 1990) dramatically increase in abundance close to the onset of the EOGM. This distinct acme is seen at Site U1411 and is considered a synchronous event of biostratigraphic utility (Agnini et al., 2014; Fornaciari et al., 2010; Nocchi et al., 1988; Wei and Wise, 1990). The timing of this shift indicates these taxa have a cold water and/or eutrophic preference, strongly responding to the shift into ‘icehouse world’ conditions of the early Oligocene.

Chiasmolithus spp.

The *Chiasmolithus* genus has long been distinguished as a cold water favouring group (Pea, 2010; Schneider et al., 2013; Villa et al., 2014, 2008; Wei and Wise, 1990) and has been used as a palaeotemperature index in conjunction with *Discoaster* (the *Discoaster/Chiasmolithus* ratio of Bukry, 1973). The group has also been interpreted as preferring moderate to high nutrient levels (Bralower, 2002; Gibbs et al., 2006;

Schneider et al., 2013, 2011; Tremolada and Bralower, 2004; Villa et al., 2014). *Chiasmolithus* is very low in abundance at Site U1411 across the EOT (<0.5 %) and there is some suggestion that the highest abundances are associated with southern rather than northern high latitudes (Haq et al., 1977), where they may comprise ~10-20 %.

Isthmolithus recurvus

The biogeography of *Isthmolithus recurvus* reveals a clear preference for higher latitudes and cooler waters and it is absent from most tropical sites (Bukry, 1975; Pea, 2010; Schneider et al., 2011; Shamrock and Watkins, 2012; Wei and Wise, 1990). At Site U1411 *I. recurvus* is rare (<2 %) but increases in abundance from its origination through the late Eocene and early Oligocene interval, supporting the cold water preference of this taxon.

Cyclicargolithus floridanus

During the Eocene *Cyclicargolithus floridanus* shows a clear preference for warmer water and is most abundant in low and mid latitudes (Schneider et al., 2011). Dunkley Jones et al. (2008) highlighted its increase in abundance through the EOT and considered this the result of higher productivity. Similar trends have also been recorded by Aubry (1992), Fioroni et al. (2015) and Monechi et al. (2000) and explained by increasing eutrophy across the EOT. A significant increase in abundance of this species is seen at Site U1411 across the EOT.

Sphenolithus spp.

Sphenolithus is a genus typically considered to have a warm water oligotrophic preference (Bralower, 2002; Gibbs et al., 2006; Schneider et al., 2013, 2011). Species within the group however may diverge from this, in particular, showing positive responses to increased eutrophy as suggested by records from the Middle Eocene Climatic Optimum (MECO) (Chapter 3; Toffanin et al., 2011), EOT (this study; Dunkley Jones et al., 2008; Fioroni et al., 2015) and Messinian Salinity Crisis (Wade and Bown, 2006). As cooling progressed across the EOT, an increase in abundance of *Sphenolithus predistentus* (this study; Dunkley Jones et al., 2008; Fioroni et al., 2015) is strongly indicative of a response to increasing eutrophic conditions. This is similar to the response seen in *Cyclicargolithus floridanus* which is also a predominantly warm water taxon clearly responding to another driver, most likely increased nutrients, during this interval of global cooling.

Discoaster spp.

Discoaster spp. is a warm water oligotrophic group (Bralower, 2002; Gibbs et al., 2006; Pea, 2010; Schneider et al., 2013, 2011; Tremolada and Bralower, 2004; Villa et al., 2014, 2008), largely absent from the high latitudes by the EOT (Villa et al., 2008; Wei and Wise, 1990) and decreasing in abundance through the EOT at low and mid latitude sites (this study; Bordiga et al., 2015; Dunkley Jones et al., 2008). The extinction of the rosette or helio-discoasters (*Discoaster barbadiensis* and *Discoaster saipanensis*) is a significant event, marking the loss of a major Paleogene group, classified as a separate genus by some authors (Aubry, 1984; Theodoridis, 1984). Nevertheless, three species of eu-discoasters survived through the EOT and Oligocene (*D. deflandrei, D. nodifer* and *D. tanii*), and this group flourished again in the Neogene.

Coccolithus formosus

The geographic distribution of *Coccolithus formosus* in the Eocene shows a preference for the low and mid latitudes, and warm water, oligotrophic conditions (Monechi et al., 2000; Pea, 2010; Villa et al., 2014; Wei and Wise, 1990; Wei et al., 1992). At Site U1411 it decreases in abundance through the late Eocene until its extinction in the early Oligocene. This preference for warmer water environments is particularly well illustrated by its premature disappearance from southern high latitude sites during the middle Eocene, some 6 myr prior to its extinction level in the tropics and this similar pattern of withdrawal to low latitude refugia prior to extinction is also shown by the rosette discoaster species (Villa et al., 2008; Wei et al., 1992).

Umbilicosphaera protoannula

Umbilicosphaera protoannula shows a clear decrease in abundance across the EOT at low and mid latitudes prior to an extinction level close to the EOB (Dunkley Jones, 2008; Dunkley Jones et al., 2008). At Site U1411, this species is rare (<0.5 %) and is extinct at 33.92 Ma. The species is more common at low and mid latitude sites, such as Tanzania (Bown et al., 2007) and St. Stephens Quarry (Alabama, Dunkley Jones, 2008). These results indicate warm water preference, restricted to low to mid latitudes and decreasing in abundance prior to extinction across the EOT.

Umbilicosphaera bramlettei

Umbilicosphaera bramlettei has not previously been used in palaeoecological studies, but shows similar trends to *U. protoannula* at the Expedition 342 sites, decreasing in abundance from the middle Eocene (~2.3 %) to the EOT (<0.5 %) with an extinction level close to the EOB. These similar trends suggest a preference for warmer water conditions.

Coccolithus pelagicus

Coccolithus pelagicus is a common component of Eocene assemblages at all latitudes but is currently restricted to cold, northern high latitudes and upwelling sites (McIntyre and Bé, 1967). This is a striking shift in ecological preference and even more so given its Paleocene and Eocene records suggest a preference for the low to mid latitudes (Gibbs et al., 2006; Haq and Lohmann, 1976; Pea, 2010; Persico and Villa, 2004; Villa et al., 2008). At Site U1411 and ODP Site 748 in the Southern Ocean (Villa et al., 2008) *C. pelagicus* shows a decrease through the EOT, suggesting a response to cooling ocean conditions.

Reticulofenestra bisecta

Reticulofenestra bisecta is a warm temperate taxon (Monechi et al., 2000; Villa et al., 2008; Wei and Wise, 1990) that originated in the low latitudes before becoming more widespread by the middle/late Eocene (Schneider et al., 2011). The species decreases across the early Oligocene at a number of locations (Dunkley Jones, pers. comm. 2014; Monechi et al., 2000; Villa et al., 2008) and although relatively rare at Site U1411, it does show an overall minor decrease during the EOGM. During the late Eocene *R. bisecta* has a similar distribution and trends to *Coccolithus pelagicus.*

4.4.1.1 Palaeoecological indices

Visual assessment of trends in these environmentally-diagnostic taxa form the basis of our palaeoenvironmental reconstructions but we have also used ratios of selected taxa in order to summarise the results from these multispecies records (Table 4.2).

We have used two indices to determine the relative trends in temperature and productivity change, as indicated by the relevant taxic groups.

$$Temperature\ index\ (TI)\ = \frac{cold}{(cold + warm + temperate)}$$

$$Productivity\ index\ (PI)\ = \frac{eutrophic}{(eutrophic + oligotrophic)}$$

Cold	Warm	Warm Temperate	Eutrophic	Oligotrophic
Reticulofenestra daviesii	*Discoaster* spp.	*Coccolithus pelagicus*	*Cyclicargolithus floridanus*	*Sphenolithus* spp. (excluding *S. predistentus*)
Reticulofenestra lockeri	*Sphenolithus* spp.	*Reticulofenestra bisecta*	*Sphenolithus predistentus*	*Discoaster* spp.
Clausicoccus subdistichus	*Coccolithus formosus*		*Reticulofenestra daviesii*	*Coccolithus formosus*
Chiasmolithus spp.	*Umbilicosphaera protoannula*		*Clausicoccus subdistichus*	
Isthmolithus recurvus	*Umbilicosphaera bramlettei*		*Reticulofenestra lockeri*	

Table 4.2: Summary table of the palaeoecological groups used in the temperature and productivity indices.

The temperature index shows an increase across the EOT (Figure 4.6) suggesting an initial response to cooling surface waters between 34.86 Ma to 34.53 Ma followed by a subsequent shift to colder conditions from 33.66 Ma to 33.36 Ma, with three small pulsed increases (0.1 to 0.18) at 34.22, 33.99, 33.72 Ma (Figure 4.6). The assemblage ratio is ~0.15 cold water taxa in the late Eocene rising to ~0.5 by the early Oligocene. The productivity index indicates increasing eutrophy from the base of the study interval to ~34.50 Ma but there is little variation following this, with the majority of the assemblage made up of meso/eutrophs (~0.95) and few oligotrophs (~0.05) (Figure 4.6).

4.4.1.2 Statistical analysis

Non-metric multidimensional scaling (NMDS) was performed in order to determine how nannofossil assemblage variation across the EOT relates to changing environmental parameters. Using the raw data (including *R. minuta*) a reduced relative abundance dataset has been produced; a total of 15 taxa which comprise on average 96 % of the assemblages. This reduces the variation in the analysis produced from the inclusion of rare taxa. NMDS was performed using the metaMDS function in the program R, which first transformed the dataset using both a square root transformation and a Wisconsin double standardisation to reduce the influence of dominant taxa, before performing the ordination using the Bray Curtis distance metric (Holland, 2008). This approach is the most effective for ecological datasets as it makes few assumptions on the nature of the data (McCune and Grace, 2002) and the Bray Curtis distance metric is a well regarded approach for abundance data. NMDS runs the ordination until the minimum distance between samples has been generated. The ordination space has a set number of axes, in

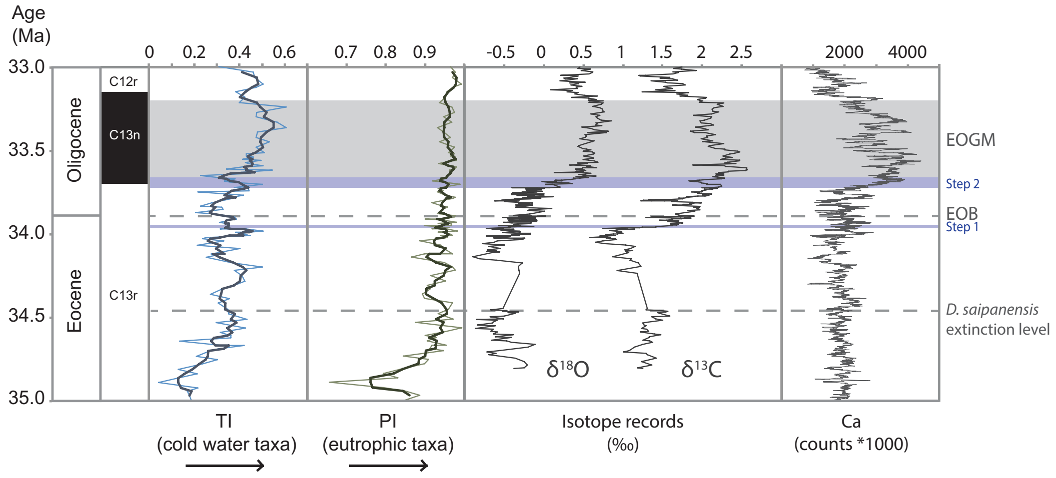

Figure 4.6: Palaeoenvironmental indices (temperature - TI and productivity - PI) plotted against Site U1411 oxygen and carbon isotope records (Steve Bohaty, Paul Wilson, pers. comm. 2016, National Oceanography Centre Southampton) and the Ca counts (Diederik Liebrand, Steve Bohaty, Paul Wilson, pers. comm. 2015, National Oceanography Centre Southampton). Palaeoenvironmental indices are shown with a 3 point moving average. EOB = Eocene-Oligocene boundary, defined by the extinction of Hantkeninidae. Step 1, 2 and the EOGM = Eocene-Oligocene Glacial Maximum, are defined by the isotope records. Magnetostratigraphy is taken from the Expedition 342 shipboard records.

this study the number of dimensions (axes; k) was set to 2. Samples with similar assemblage compositions plot close together and species scores distribution is based on abundance, plotting close to samples where they are highly abundant. Stress values produced reflect how good the ordination fit is, with the general rule of thumb >0.1 indicates a good fit, >0.2 an acceptable fit and >0.3 a poor fit, although this must be taken as provisory. Samples were divided into three time bins; late Eocene (red), EOT (blue) and early Oligocene (green), in order to establish changes in assemblage composition through time. The function ordisurf has been used to overlay carbon and oxygen isotope and age vectors on the sample scores. Ordisurf fits a smooth surface for the given variable and plots fitted contours on the ordination plot to assess the correlation between these variables and the sample scores. This is a preferred technique for overlaying vectors on NMDS ordinations as it does not constrain the relationship to be linear and is applicable as NMDS axes are not independent eigenvectors as they are in other multivariate techniques, such as principal component analysis (PCA).

The NMDS results give a reasonable fit with a stress of 0.266 and clearly indicate a temporal gradient with a shift from late Eocene to early Oligocene assemblages in NMDS axis 1, highlighted by the colour coded sample scores (Figure 4.7a).

Figure 4.7 (this page and the following page): NMDS ordination plots; a) samples (open circles) and species (stars) scores, b) sample scores with overlain age contours (Ma), c) sample scores with overlain oxygen isotope contours (‰), d) sample scores with overlain carbon isotope contours (‰). Samples are colour coded; red – late Eocene (35.00-33.96 Ma), blue – EOT (33.96-33.66 Ma), green – early Oligocene (33.66-33.00 Ma).

a) Samples and species scores

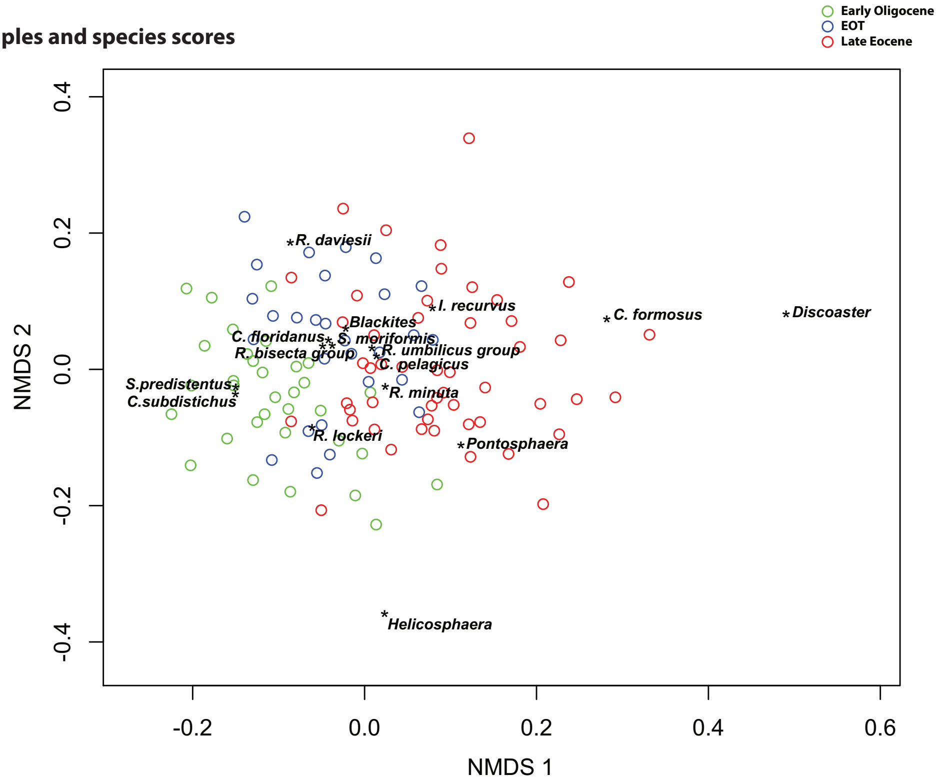

b) Age

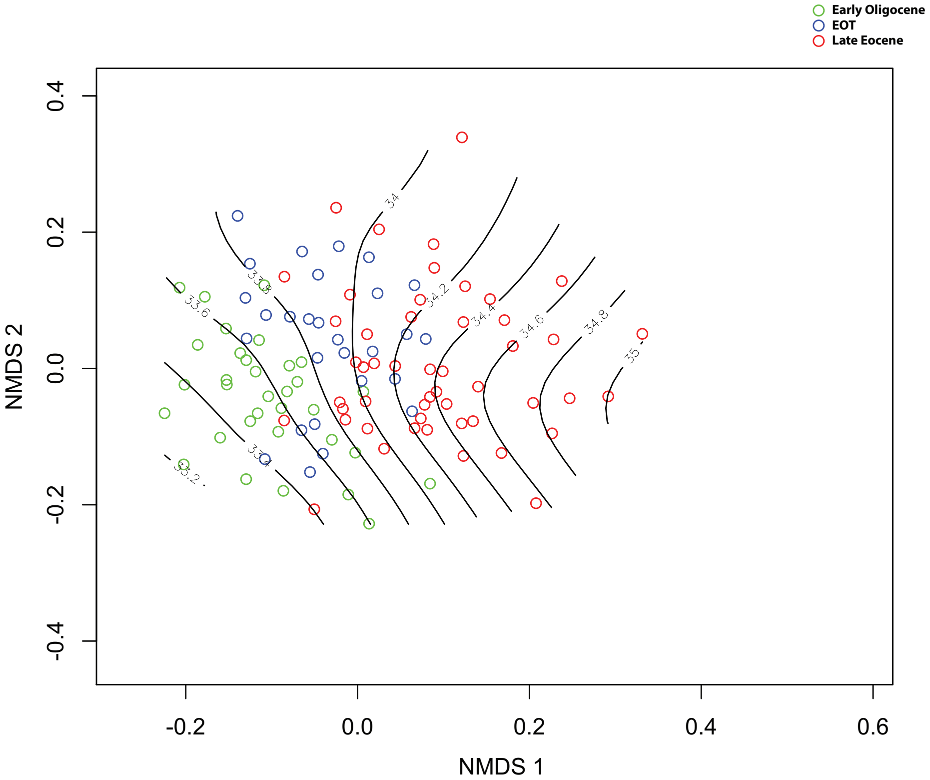

c) Oxygen isotopes

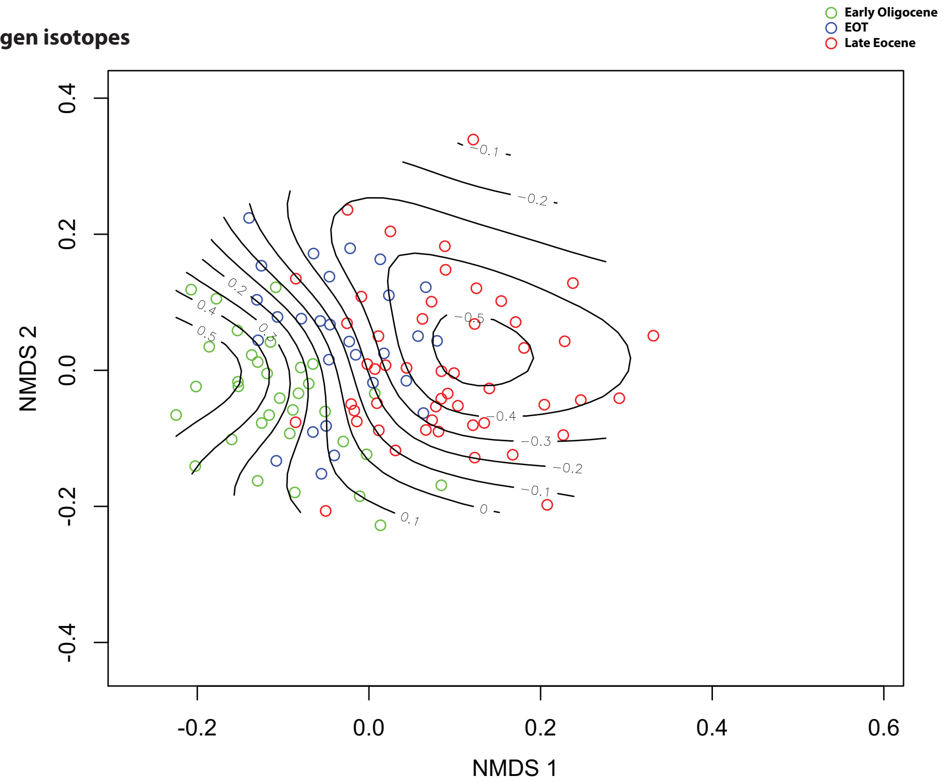

d) Carbon isotopes

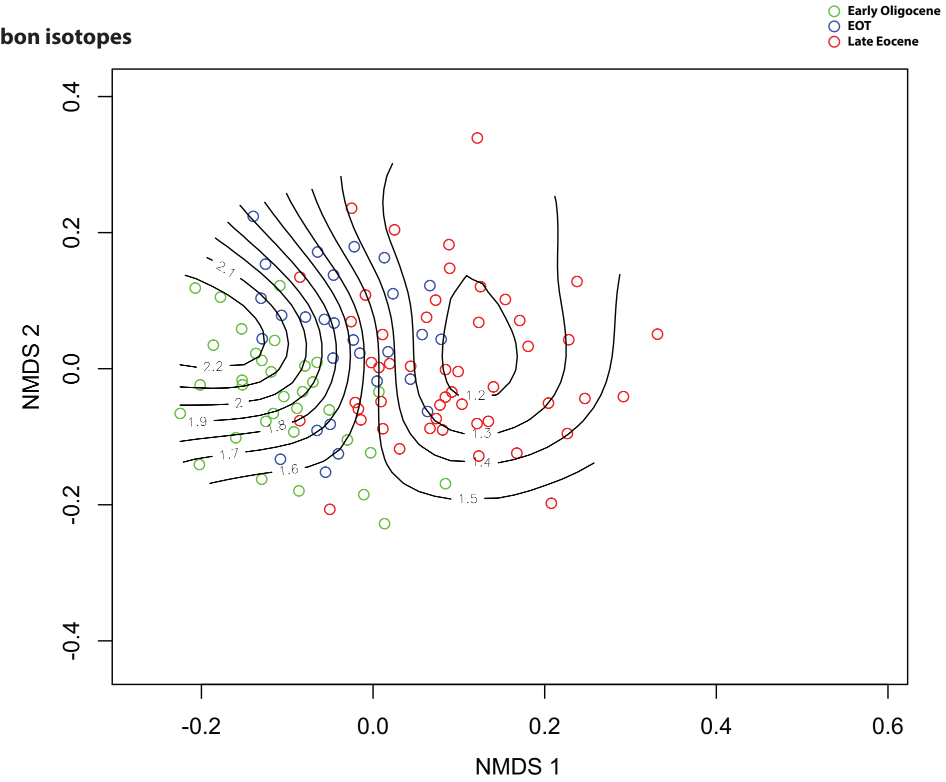

This is further shown by the ordisurf contours, indicating older samples plot with positive values and younger samples with negative values in NMDS axis 1 (Figure 4.7b). Species scores indicate the temporal gradient represents a shift in environmental conditions with *Discoaster* and *Coccolithus formosus,* warm water oligotrophs, plotting in the late Eocene sample space with positive NMDS 1 values and colder eutrophic taxa plotting with negative values within the early Oligocene sample space, *Clausicoccus subdistichus, Sphenolithus predistentus* and *Reticulofenestra lockeri.* Many species occupy broad ecological tolerances and plot within the centre of the ordination space, with the exception of those few taxa with strong environmental preference (warm oligotrophs positive values and cold eutrophs negative values in NMDS 1). The oxygen and carbon isotope variables have a non linear relationship with the sample scores but the general pattern indicates more increasingly positive oxygen and carbon isotope values within the early Oligocene (Figure 4.7c and d), signifying colder more nutrient rich conditions and supporting the distribution of species within the ordination.

4.4.2 Extinction and declines

The EOT extinctions at Site U1411 occur in taxa with preferences for warm and oligotrophic surface water conditions (*D. barbadiensis, D. saipanensis, U. protoannula, U. bramlettei, H. situliformis* and *C. formosus*). Many of these species were abundant during the warmer greenhouse conditions of the early and middle Eocene but declined preceding their extinction during the EOT (*C. formosus* ~2 % at 39 Ma to ~1 % at 34 Ma; *Discoaster* spp. ~1.5 % at 39 Ma to ~0.5 % at 34 Ma; *U. bramlettei* ~2 % at 39 Ma to ~0.5 % at 34 Ma). At Site U1411 their relatively low abundances even in the middle Eocene reflects the temperate meso/eutrophic conditions at this site, and contrasts with other sites where discoasters can comprise up to 6 % at Blake Nose (Newsam et al., in press), up to ~10 % at the Exmouth Plateau (Shamrock and Watkins, 2012) and ~33 % at Shatsky Rise (Schneider et al., 2011) in the middle Eocene.

The extinctions of the rosette or helio-discoasters, an important genus-equivalent group, is a key loss in the late Eocene followed by the *Coccolithus formosus* extinction in the early Oligocene. At Site U1411 the age for the top of the helio-discoasters is close to the Agnini et al. (2014) calibration ages, with the extinction of *Discoaster barbadiensis* within ~10 kyr of the calibration age and the *Discoaster saipanensis* extinction level ~90 kyr prior to the calibration age, indicating both likely represent true extinction levels, within error of the current age model. The extinction level of *Coccolithus formosus* at Site U1411 (33.14 Ma) is ~280 kyr older than the Agnini et al. (2014) calibration suggesting withdrawal from this mid to high latitude site to lower latitudes prior to the true extinction level (Blaj et al., 2009), rather than age model error. The extinction of the helio-discoasters is preceded by a significant decline in abundance from 35.15 Ma, suggesting the environment at this location was relatively hostile to this group well before their extinction (~690 kyr later). A similar pre-extinction decline is also recorded in *Coccolithus formosus*. More generally, both these taxa also exhibited major range retractions withdrawing from the high southern latitudes in the middle Eocene (helio-discoaster at 40.14 Ma and *C. formosus* at 39.14 Ma, respectively at ODP Site 748; Villa et al., 2008 converted to GTS12) ~5-6 myr prior to their extinction.

Umbilicosphaera protoannula, Umbilicosphaera bramlettei and *Hayella situliformis* are rare at Site U1411 prior to their extinctions, which occur close to the EOB, at 33.92 Ma (EOB -30 kyr), 33.88 Ma (EOB +10 kyr) and 33.28 Ma (EOB +610 kyr), respectively. The stratigraphic ranges of the *Umbilicosphaera* species and *Hayella situliformis* are relatively poorly documented but there is some evidence for latitudinal diachroneity in their extinction levels, with slightly younger ages reported from the tropical Tanzanian sites, with the *Umbilicosphaera protoannula* extinction at 33.07 Ma and *Umbilicosphaera bramlettei* and *Hayella situliformis* recorded to at least 33 Ma, the youngest sample at TDP Site 17 (Bown et al., 2007). There is no known record for these taxa in high southern latitudes however *Umbilicosphaera protoannula* is recorded until the late Eocene (NP20) in the higher latitudes of the North Atlantic (ODP Site 647; Firth, pers. comm. 2014).

As well as these disappearing taxa there are also significant abundance declines in *Coccolithus pelagicus* and large specimens of *Reticulofenestra dictyoda* (8-14 μm). *Coccolithus pelagicus* has a warm temperate water preference and its declining abundance (~19 to 11 %) is consistent with the cooling through this interval. *Reticulofenestra dictyoda* is typically considered to have a temperate water, meso/eutrophic preference (Villa et al., 2014) and so the decline of larger specimens may reflect competition with smaller, more opportunistic reticulofenestrids, which were able to better utilise the changing mixed layer conditions and in particular increases in nutrient levels.

4.4.3 Pulsed abundance increases and population shifts

The series of pulsed increases and population shifts at Site U1411 indicate profound changes in the surface water environment that occurred progressively and without recovery across the EOT. The taxa that manifest this change all share a preference for colder and/or more eutrophic environments and can be broadly thought of as opportunistic species. *Reticulofenestra daviesii* displays the first of these pulsed increases and its abundance through the EOT has been widely reported and it is considered a strong indicator of cold environments (Villa et al., 2008). At Site U1411 an initial pulse in *Reticulofenestra daviesii* occurs in the late Eocene (~34.6 Ma) peaking at 34.48 Ma, close to the helio-discoaster extinction, followed by a second larger pulse from 34.20 Ma with peak abundance at 33.97 Ma, within an interval considered to reflect a major phase of global cooling. *Reticulofenestra lockeri* is also considered to have a cold water eutrophic preference and has an increase through the late Eocene, peaking at 34.28 Ma followed by a larger second pulsed increase in abundance within the sustained cold conditions of the EOGM from 33.48 Ma. The sharp increase in *Clausicoccus subdistichus* at 33.78 Ma is a widely observed event and close to the onset of the EOGM (40 kyr) at Site U1411. There are sustained high abundances in this opportunistic species, with the acme lasting for ~250 kyr, extending 140 kyr into the EOGM. The acme top is within 70 kyr of the GTS12 calibration age (33.43 Ma). An increase in cold water taxa is supported by the temperature index which displays two distinct protracted increases, one in the late Eocene (0.13 at 34.86 to 0.39 at 34.53 Ma) and another following the EOB (0.31 at 33.66 to 0.55 at 33.36 Ma) and three sharp pulsed increases across the EOB (at 34.22 Ma, 33.99 Ma and 33.72 Ma).

Two other increasing groups *Cyclicargolithus floridanus* and *Sphenolithus predistentus* shed further light on the role of nutrients across the EOT as they show preferences for warmer water environments but also eutrophic conditions (Aubry, 1992; Dunkley Jones et al., 2008; Fioroni et al., 2015). Both show protracted and sometimes pulsed increases in abundance across the EOT and as warming is unlikely to be a major factor through this time interval, the primary driver of these increases must be related to nutrients. This is further supported by the productivity index data which shows sustained and high levels of eutrophy throughout the EOT at Site U1411.

4.4.4 Palaeoceanographic change across the EOT

The nannoplankton population record across the EOT at Site U1411 comprises a series of species abundance shifts and interspersed extinctions. The taxa involved strongly indicate the overarching controls of intensified surface water cooling and increasing and/or pulsed nutrient availability, as warm water taxa show stepped extinction and cold water opportunist taxa waxed and waned. This complex response cannot be attributed to a single forcing factor and was undoubtedly due to a range of species-specific ecological preferences in response to the interplay of a number of environmental controls across this two million years of climatic and oceanographic change.

The EOT saw the culmination of the shift from the stable warm oceans of the Eocene to the cooler, mixed oceans of the early Oligocene (Dunkley Jones et al., 2008). The oceanographic reorganisation included initiation of the Antarctic Circumpolar Current (ACC) and enhanced ‘modern’-like thermohaline circulation (Katz et al., 2008; Miller et al., 2009; Scher et al., 2015). This also resulted in increased ocean upwelling and nutrient-delivery to the mixed layer, with enhanced regional productivity documented at low, mid and high latitude sites (Coxall and Wilson, 2011; Cramer et al., 2009; Dunkley Jones et al., 2008; Salamy and Zachos, 1999). There is also biotic and geochemical evidence for increased seasonality (Diester-Haass and Zachos, 2003; Eldrett et al., 2009; Ivany et al., 2000; Wade et al., 2012). The EOT is characteristically defined by the +1.2-1.5 ‰ shift in oxygen isotope records, denoted as the ‘isotopic shift’ in Coxall and Pearson (2007), comprised of two prominent positive shifts separated by a plateau at Site 1218 (Coxall et al., 2005). The oxygen isotope record from U1411 records only one prominent shift at 33.72 Ma, the second step of the isotopic shift, yet a positive step shift in the carbon isotopes prior to the EOB represents significant environmental change and is considered to mark the first shift in the records. Following the second step of the isotopic shift there was a ~500 kyr interval of sustained high $\delta^{18}O$ values, the EOGM, recorded between 33.66 Ma and 33.20 Ma at Site U1411. Site U1411, which today is positioned within the path of two major Atlantic currents, the Deep Western boundary current and the Gulf Stream, would have been strongly influenced by these currents across the EOT and subsequent feedbacks, such as increased nutrient delivery, as they are considered to have flown along similar trajectories in the Paleogene (Norris et al., 2014).

4.4.4.1 Timing and causes of nannoplankton population response

As cooling intensified across the EOT isotopic shift, a critical threshold point was reached where warm water taxa were no longer able to endure the conditions and restriction of optimal habitat space resulted in abundance decline and ultimately extinction. At Site U1411 the majority of these taxa became extinct prior to the second isotopic shift and the EOGM but *Coccolithus formosus* persisted through the isotopic shift and the EOGM but was unable to sustain through the persistent glacial conditions of the emerging icehouse world. Latitudinal diachroneity between the southern high latitudes and Site U1411 and lower latitude sites with retractions in warm water taxa (discoasters and *Coccolithus formosus*) to lower latitudes during the middle Eocene, is consistent with increasing latitudinal sea surface temperature gradients in the late Eocene between equatorial sites and the North Atlantic (5°C) and South Atlantic (12°C) (Inglis et al., 2015). The early onset of major environmental change in the high latitudes, with cooling as great as 6 °C relative to 2.5°C at low to mid latitudes, which maintained more stable, greenhouse-like conditions (Inglis et al., 2015; Pearson et al., 2007), highlights why lower latitudes became a refugia for these typically warm water species.

The pulsed increase in cold water eutrophs within the EOT may be a species-specific response to the stepwise cooling through this interval (Lear et al., 2008), seasonal or episodic increases in productivity (Diester-Haass and Zachos, 2003) or a combination of these and/or other environmental factors. At Site U1411 *Reticulofenestra daviesii* shows the first surge in abundance and similar pulsed increases in this species have been identified at low latitude Indian Ocean ODP Site 711 (Fioroni et al., 2015), with the onset of this taxon as a key component in the late Eocene and a peak in abundance just after the EOB (within C13n) and in the high latitude Southern Ocean (ODP Site 748) *Reticulofenestra daviesii* also has an initial pulse in abundance in the late Eocene prior to the distinct increase in the earliest Oligocene (Villa et al., 2008). Persico and Villa (2004) highlight three pulses in cold water taxa (*Chiasmolithus* spp. and *Reticulofenestra daviesii*) in the Southern Ocean (ODP Site 689) through the late Eocene, with the last pulse in C13r prior to the EOB, which implies that cooling was a dominant control on nannofossil assemblages in the late Eocene prior to the EOB. Following the EOB, increases and peaks in eutrophic taxa (across 120 kyr) implies a response to enhanced productivity from episodic/pulsed nutrient delivery and seasonality was the dominant control on the assemblages. *Sphenolithus predistentus* peaks in abundance 30 kyr after the EOB, followed by the beginning of the acme in *Clausicoccus subdistichus* 60 kyr later, with the peak abundance in this taxon at the onset of the Site U1411 isotopic shift and *Cyclicargolithus floridanus* peaks at 33.70 Ma, 20 kyr after this. At TDP Sites 12 and 17 a distinct significant shift in *Cyclicargolithus floridanus* (<5 µm) and *Sphenolithus predistentus* occurs immediately following the EOB (Dunkley Jones et al., 2008), a prominent increase in *Sphenolithus predistentus* at ODP Site 711 is also recorded just after the boundary (Fioroni et al., 2015) and Bordiga et al. (2015) record an interval of high productivity between the EOB and the second step, supporting this analogy.

The results from Site U1411 provide strong evidence for a close link between plankton evolution and the climate-oceanographic changes associated with the EOT. This resulted in Oligocene nannoplankton assemblages quite distinct from those of the preceding Eocene. Taxa comprising early Oligocene post-EOT assemblages typically include *Cyclicargolithus floridanus, Sphenolithus predistentus, Sphenolithus moriformis, Reticulofenestra bisecta* and *Coccolithus pelagicus* (shipboard data from Sites U1406 and U1411 IODP Expedition 342 - Norris et al., 2014; ODP Site 1218 - Blaj et al., 2009). Assemblages from Southern Ocean Site 748 contain *Reticulofenestra bisecta* and *Coccolithus pelagicus* but are dominated by *Reticulofenestra daviesii* and *Chiasmolithus* (Villa et al., 2008) thus emphasizing the persistent cold glacial conditions in the southern hemisphere in the Oligocene.

4.4.5 Significant plankton response across the EOT

The EOT triggered dynamic restructuring within marine plankton, measured by high levels of turnover, speciation and extinction and accelerated diversity loss in the calcareous nannoplankton (Chapter 6; Bown et al., 2004; Dunkley Jones et al., 2008), planktonic foraminifera (Ezard et al., 2011; Pearson et al., 2008), benthic foraminifera (Cotton and Pearson, 2011) and radiolaria (Kamikuri et al., 2012). The planktonic foraminifera suffered extinctions in several species of the *Turborotalia cerroazulensis* group (*T. cerroazulensis, T. cocoaensis* and *T. cunialensis*) ~140 kyr (GTS12) prior to the EOB followed by dwarfing within the genus *Pseudohastigerina* synchronous with extinction of the planktonic foraminifera family, Hantkeninidae (Wade and Pearson, 2008) at the EOB (33.89 Ma; GTS12). The siliceous zooplankton group the radiolarians show high levels of turnover across the EOT with clustered extinctions in 11 species within ~180 kyr around the EOB and increased speciation in the early Oligocene (Kamikuri et al., 2012; Moore et al., 2015). In calcareous nannoplankton there are six species extinctions including a genera-equivalent group (the helio-discoasters), as identified across 1.55 myr at Site U1411, and the additional extinction of the neritic genus *Pemma papillatum* (Dunkley Jones et al., 2008; not recorded at Site U1411). The protracted nature of the calcareous nannoplankton extinctions across the transition is unlike the zooplankton groups, which show intense perturbation around the EOB (Kamikuri et al., 2012; Pearson et al., 2008). Although the extinctions in the three plankton groups differ slightly in timing and magnitude they nevertheless indicate a significant level of population disruption. Clearly, the evolving oceanographic conditions of the EOT is reflected in the disruption in the planktonic foraminifera, radiolaria and nannoplankton populations which led to multiple extinctions in these groups. By contrast, the siliceous phytoplankton group, the diatoms, underwent rapid diversification across the EOT (~50 to 80 species), peaking near the EOB (Lazarus et al., 2014; Rabosky and Sorhannus, 2009). The diatoms, which include highly efficient opportunists, were able to successfully exploit the newly emergent cold and highly eutrophic icehouse conditions in the early Oligocene and become the dominant phytoplankton group in the oceans.

4.5 Summary

The EOT calcareous nannofossil records from Site U1411 document significant population restructuring leading to distinct differences between late Eocene and early Oligocene assemblage compositions. There are declines and a series of extinctions in warm water oligotrophic and warm temperate mesotrophic favouring taxa as pulsed increases in cold water species and protracted increase in eutrophic taxa occur throughout the transition. This indicates an overarching control of intensified surface water cooling and increased and/or pulsed nutrient availability, with the EOT representing a critical threshold where reduced optimal habitat space for warm water taxa led to decline and ultimately extinction in many taxa. Records indicate cooling may have been the dominant control on assemblages in the late Eocene with increases and peaks in eutrophic taxa following the EOB suggesting a response to productivity. The evolving icehouse conditions across this transition led to severe disruption in many plankton groups, with dwarfing and major extinctions within the planktonic foraminifera and high turnover within radiolaria also recorded at this time, although the opportunistic diatoms were better adapted in these newly emerging surface water environments and proliferated in the icehouse world.

Chapter 5

Evidence for widespread disruption to surface ocean environments during the Eocene-Oligocene transition from global calcareous nannoplankton population shifts

5.1 Introduction

The Eocene-Oligocene transition (EOT) was a fundamental event in Cenozoic Earth's history, associated with widespread climatic and oceanographic change, including climatic cooling, Antarctic ice sheet formation and expansion, deepening of the calcite compensation depth (CCD), sea level fall, changes in ocean chemistry and elevated marine biotic disruption and extinction. Calcareous nannoplankton (marine calcifying algae) were the dominant phytoplankton group in the early Paleogene surface oceans but underwent a significant diversity decline through the late Eocene with accelerated loss and significant population shifts across the EOT (Chapters 4 and 6; Bordiga et al., 2015; Bown et al., 2004; Dunkley Jones, 2008; Dunkley Jones et al., 2008; Persico and Villa, 2004). Aside from the singular Cretaceous-Paleogene mass extinction event, this interval saw the greatest evolutionary change in the history of this phytoplankton group and is indicative of a major role for climate change in their evolutionary history.

Here we provide the first synthesis of EOT nannofossil data from a series of global sites in order to document the timing and nature of the widely observed population and evolutionary shifts and to determine the causal factors. The abundant, geographically widespread and continuous fossil record of this phytoplankton group enable the reconstruction of palaeoenvironments using the distribution of species or groups with strong palaeoecological affinities. Our aim is to identify palaeoecologically diagnostic assemblage responses from each site and to look for common characteristics of environmental change and distinguish these from potential site-specific response. This will provide us with a comprehensive biotic proxy for surface water ocean dynamics through this critical event.

5.2 Materials and methods

5.2.1 Global sites

The acquisition of expanded, continuous EOT sections containing well preserved calcareous nannofossils (from Ocean Drilling Program – ODP, Integrated Ocean Drilling Program – IODP and land-based drilling projects) provide detailed site-specific population records across this critical event. For this study EOT calcareous nannofossil data has been compiled from five sites: IODP Site 1411 (IODP Expedition 342; Chapter 4) and four previously studied global sites; SSQ (St. Stephen's Quarry; Dunkley Jones, 2008), IODP Site 1334 (IODP Expedition 320; Dunkley Jones, pers. comm. 2014), Tanzania Drilling Project 12/17 (TDP 12/17 – sites 12 and 17 combined to form a continuous stratigraphy across the EOT; Dunkley Jones et al., 2008) and ODP Site 748 (ODP Leg 120; Villa et al., 2008) (Figure 5.1; Table 5.1). The main criteria for site selection were high resolution (~20-50 kyr) and high quality EOT nannofossil records from varying latitudes, ocean basins and oceanographic settings, which provide a representative overview of global nannoplankton dynamics through the interval. Sediments range from glauconitic sandy marls (SSQ) to clayey nannofossil ooze (1411) with the calcareous nannofossil preservation moderate to exceptionally well preserved as shown in Table 5.1.

5.2.1.1 Age Models

The age model for Site 1411 uses the Geological Time Scale 2012 (GTS12; Gradstein et al., 2012) calibration ages integrating bio- and magnetostratigraphic shipboard data (see Chapter 4). We have used published age models for the other sites (SSQ – Wade et al., 2012; 1334 – Westerhold et al., 2014; TDP 12/17 – Pearson et al., 2008; 748 – Villa et al., 2008) but have converted ages to GTS12 to enable comparison. Sites 1411, TDP 12/17 and 748 provide records from 33-35 Ma, with ~20 kyr sampling resolution. Site 1334 has a lower resolution record with sample spacing every ~50 kyr across the interval and site SSQ has a sampling resolution of ~10 kyr across 33.72-34.24 Ma. The records span the nannofossil NP Zones 19/20 to 22.

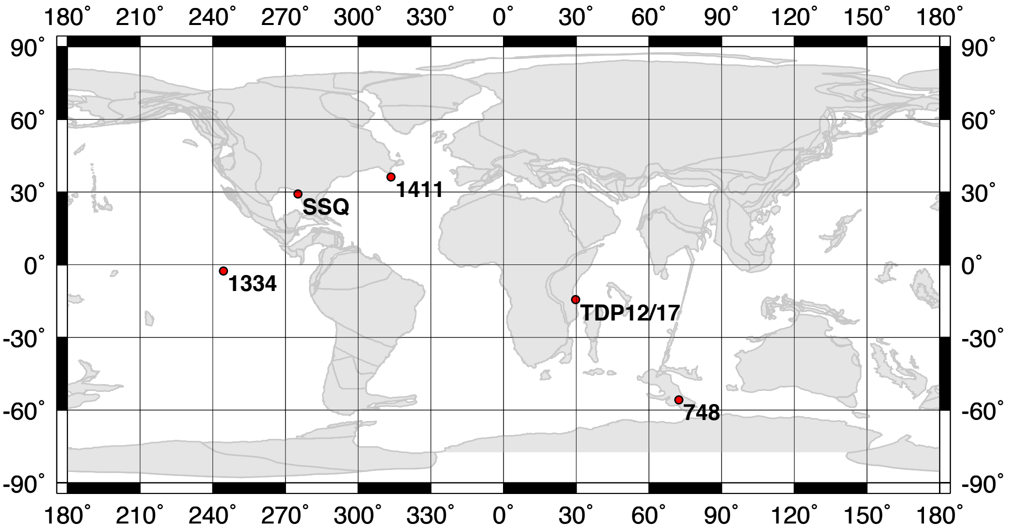

Figure 5.1: Plate tectonic reconstruction (www.odsn.de) for the late Eocene (34 Ma) displaying the locations of the global sites used in this study (1411 – IODP Site 1411, Expedition 342; SSQ – St. Stephens Quarry, Alabama; 1334 – IODP Site 1334, Expedition 320; TDP12/17 – Tanzania Drilling Project; 748 – ODP Site 748B, Leg 120).

Site	Latitude	Palaeo-water depth (m)	Sediments	Nannofossil preservation	Publication
1411	41°37’N 48°6'W	~2800	Nannofossil clay and clayey nannofossil ooze	Good to exceptional	This thesis, Chapter 4
SSQ	31°33’N 88°02’W	~125	Glauconitic sandy marls	Good to exceptional	Dunkley Jones, 2008
1334	7°59’N 131°58’W	~3500	Nannofossil ooze and nannofossil chalk	Moderate to good	Dunkley Jones, pers. comm. 2014
TDP 12/17	9°11’S 39°39’E	~300-500	Clays with occasional limestone interbeds	Exceptional	Dunkley Jones et al., 2008
748	58°26’S 78°59’E	~600-900	Nannofossil ooze	Moderate to good	Villa et al., 2008

Table 5.1: Detailed description of the global sites used in this study.

5.2.2 Analytical techniques

Nannofossil abundance data from all sites have been collated from 33 to 35 Ma (with the exception of SSQ – 33.72 to 34.24 Ma) and where possible additional biostratigraphic information has been provided. 300-500 specimens were counted for each sample at all sites, which provides a statistically significant value as 300 counts account for taxa that comprise 1 % of the assemblages at the 95 % confidence level. Count data was subsequently converted to relative abundances which allows for comparisons between sites. Consistent taxonomic concepts have been used for Sites 1411, SSQ, 1334 and TDP 12/17 as studies come from the same working group, following Bown (2005a), Bown and Dunkley Jones (2006) and Dunkley Jones et al. (2009). Only records from Site 748 may have slightly divergent taxonomic concepts. Plots of species and grouped abundance have been generated for key taxa through the interval to test for synchrony/diachrony between sites and to observe widespread abundance declines and increases, acmes and extinctions.

5.2.2.1 Palaeoecology

The majority of calcareous nannoplankton are eurytopic and widely distributed. Despite this, many species and groups display an affinity for more specific environmental conditions ranging from warm water oligotrophs to cold water eutrophs. Palaeoecological preferences of Paleogene taxa are relatively well established from previous biogeographic and palaeoecological studies (e.g. Haq and Lohmann, 1976; Schneider et al., 2013; Villa et al., 2008; Wei and Wise, 1990). Here we use key EOT taxa with relatively strong palaeoenvironmental preferences (temperature and nutrient affinities) and infer the strength of their association to these parameters across this interval (Table 5.2).

5.2.2.2 Non-metric multidimensional scaling

Multivariate analysis, non-metric multidimensional scaling (NMDS), has been performed in the program R on a reduced set of 16 species from the assemblages at all sites. The metaMDS function was used, which applied a square root transformation and Wisconsin double standardization to the relative abundance data, which down weighs the abundant taxa, prior to performing the ordination using the Bray-Curtis metric. This technique aims to explain the variance in the dataset by plotting the minimal distance between samples on an ordination space with a given number of axes. Samples with similar assemblage compositions plot close together and species scores distribution is based on abundance, plotting close to samples where they are highly abundant. In this study the number of dimensions (axes; k) was set to 2. Stress values provide a measure of goodness of fit, with a general rule that >0.1 indicates a good fit, >0.2 an acceptable fit and >0.3 a poor fit. We have used the ordisurf function to assess the influence of variables, latitude and age, on the assemblages (for further explanation on these techniques see Chapter 4).

	Temperate	Subtropical	Tropical		Polar
Group 1	**1411**	**SSQ**	**1334**	**TDP 12/17**	**748**
Coccolithus formosus	🟥🟧	🟥🟧	🟥🟧		
Discoaster	🟥🟧		🟥🟧	🟥🟧	
Umbilicosphaera bramlettei	🟥				
Umbilicosphaera protoannula		🟥		🟥	
Reticulofenestra bisecta		🟥	🟥		🟥
Coccolithus pelagicus	🟥				🟥
Pemma papillatum				🟥	
Bramletteius serraculoides		🟥			
Reticulofenestra dictyoda	🟨	🟨	🟨	🟨	🟨
Group 2	**1411**	**SSQ**	**1334**	**TDP 12/17**	**748**
Cyclicargolithus floridanus	🟩	🟩	🟩	🟩	
Sphenolithus predistentus	🟩	🟩	🟩	🟩	
Clausicoccus subdistichus	🟦🟩	🟦🟩	🟦🟩	🟦🟩	
Reticulofenestra daviesii	🟦🟩		🟦		🟦🟩
Reticulofenestra lockeri	🟦				
Reticulofenestra macmillani				🟦	
Chiasmolithus					🟦
Isthmolithus recurvus					🟦

Table 5.2: Key EOT taxa with assigned palaeoecological preferences (temperature and/or nutrient preferences). Red – warm; pink – warm temperate; blue – cold; orange – oligotrophic; yellow – mesotrophic; green – eutrophic. For species/groups with both temperature and nutrient preferences controlling their abundance in the EOT assemblages, the area of the square for each preference denotes which controls that species/group across the EOT. Size of the square is equal to our confidence that the species/group exhibits and is controlled by that preference across the EOT; large – strong, small – moderate. Species shown for each site only include those that show a significant change in abundance through the EOT interval.

5.3 Results

5.3.1 Nannoplankton population restructuring

There are significant nannofossil assemblage shifts seen globally across the EOT interval with two distinct groups identified at each site (Table 5.2; Figure 5.2). The first group includes taxa that consistently decline in abundance - *Coccolithus formosus, Discoaster* spp., *Reticulofenestra dictyoda* and *Reticulofenestra bisecta* - and the second group that increase in abundance - most commonly comprising *Cyclicargolithus floridanus, Reticulofenestra daviesii, Clausicoccus subdistichus* and *Sphenolithus predistentus*. The decreasing taxa comprise warm water oligotrophs, which display an overall gradual decline in abundance through the interval at all sites (1411 - 33 to 13 %; SSQ – 6.5 to 1 %, following two initial peaks of ~10 %; 1334 - 70 to 5 %; TDP 12/17 - 26 to 0.25 %; 748 – increasing from ~25 to 69 % then decreasing to 6 %). The increasing taxa are cold water eutrophs, which increase overall throughout the EOT (1411 - 23 to 40 % with a peak of 60 %; SSQ - 15 to 70 %; 1334 - 1 to 56 %; TDP 12/17 - 30 to 80 %; 748 - 70 to 90 %, with a decrease to 30 % prior to the Eocene-Oligocene boundary) but with a significant step-shift seen at each site close to the Eocene-Oligocene boundary (EOB). The components of the two groups and details of the abundance change (magnitude and timing) vary from site-to-site but this interval of atypically strong population shifts is evident at each location.

The warm water oligotrophs, *Coccolithus formosus* and *Discoaster*, consistently display significant gradual declines prior to their extinction levels (Figure 5.3). This is most prominent in the low latitude open ocean at Site 1334 (*Coccolithus formosus* - 10 % to 0.5 % and *Discoaster* - 50 % to 0 %), where these taxa would typically thrive. In the more eutrophic and slope/shelf settings they occur at much lower abundances but still display the declines in abundance (*Coccolithus formosus:* SSQ - 1.8 % to 0.2 % and 1411 - 3.2 % to 0.2 %; *Discoaster:* TDP 12/17 - 3 % to 0.2 % and 1411 - 1.7 % to 0.2 %). The cold water species *Reticulofenestra daviesii* is most dominant in the Southern Ocean at Site 748, comprising 30 % in the late Eocene and increasing to 90 % across the EOB. Pulsed increases in this species are seen in the late Eocene at Site 1411 and in the early Oligocene at 1334 but with lower abundances, peaking at 5 % and 9 %, respectively. *Clausicoccus subdistichus* displays a widely recognised prominent acme across the EOT, identified at Sites 1411, SSQ and 1334 (0.3 to 7 %, 1 to 6 % and 0 to 6 %, respectively) with a more gradual increase at TDP 12/17 (0 to 2 %). *Cyclicargolithus*

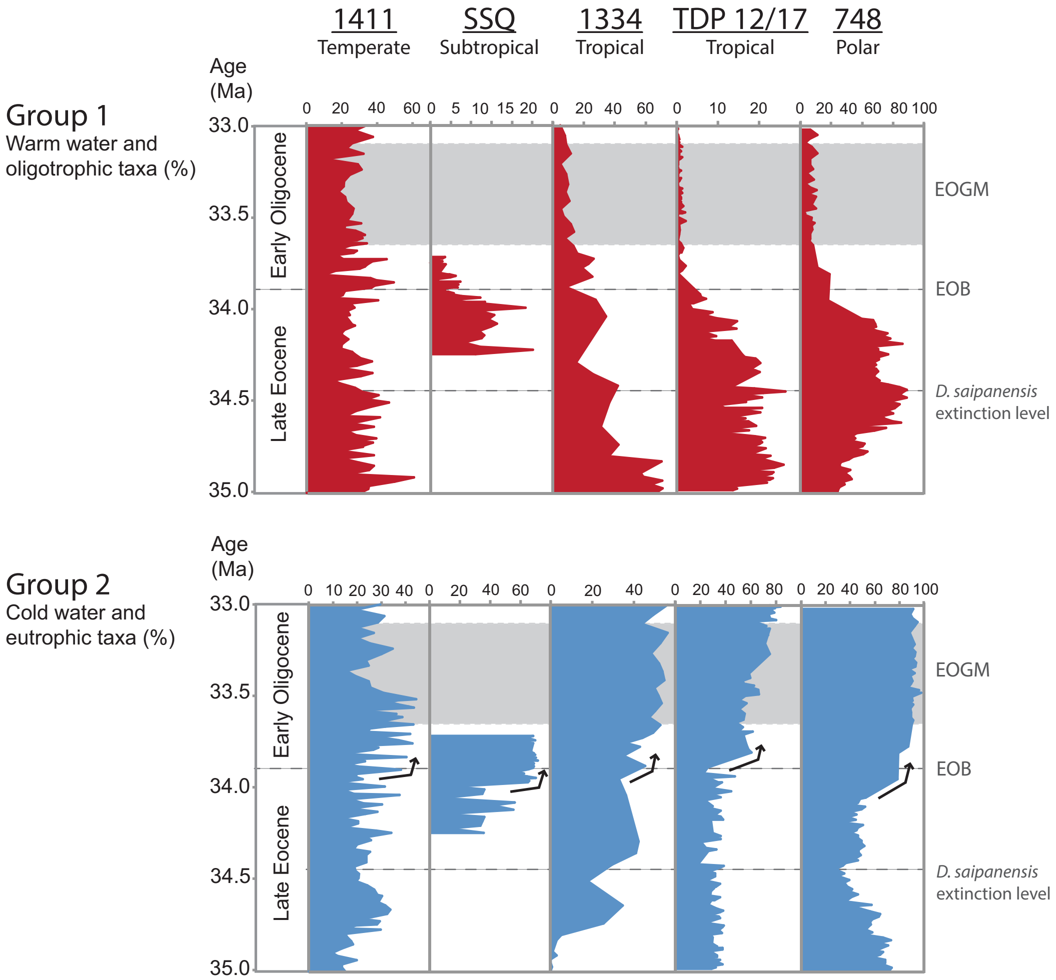

Figure 5.2: Relative abundance data of warm water oligotrophic (Group 1) and cold water eutrophic (Group 2) taxa (as shown in Table 5.2) for each site. Arrows indicate a step shift in abundance. *D. saipanensis* extinction level (34.44 Ma GTS12). EOB = Eocene-Oligocene boundary (33.89 Ma GTS12). EOGM = Eocene-Oligocene Glacial Maximum, defined using an oxygen isotope compilation.

floridanus and *Sphenolithus predistentus* are key productivity indicators, and show widespread increases across a range of oceanographic setting (*C. floridanus:* 1411 - 9 to 37 %; SSQ - 33 to 68 %; 1334 - 0.2 to 42 %; TDP 12/17 - 27 to 75 %; *S. predistentus:* 1411 - 0.1 to 1.9 %; SSQ - 0.2 to 2.7 %; 1334 - 0 to 18 %; TDP 12/17 - 0.5 to 11 %).

5.3.2 Global sites statistical comparison

The NMDS ordination shows a good fit, stress = 0.109, with samples arranging along the NMDS 1 axis based on site locality (Figure 5.4). Sample scores from the low latitude sites (TDP 12/17, 1334, SSQ) have positive values and plot close together, with overlap, mid-latitude Site 1411 plots close to these low latitude sites, near the centre of the

Figure 5.3 (this page and the following page): Key species abundance data. Colour coded base on palaeoecological preference (Table 5.2). *D. saipanensis* extinction level (34.44 Ma GTS12). EOB = Eocene-Oligocene boundary (33.89 Ma GTS12). EOGM = Eocene-Oligocene Glacial Maximum, defined using an oxygen isotope compilation.

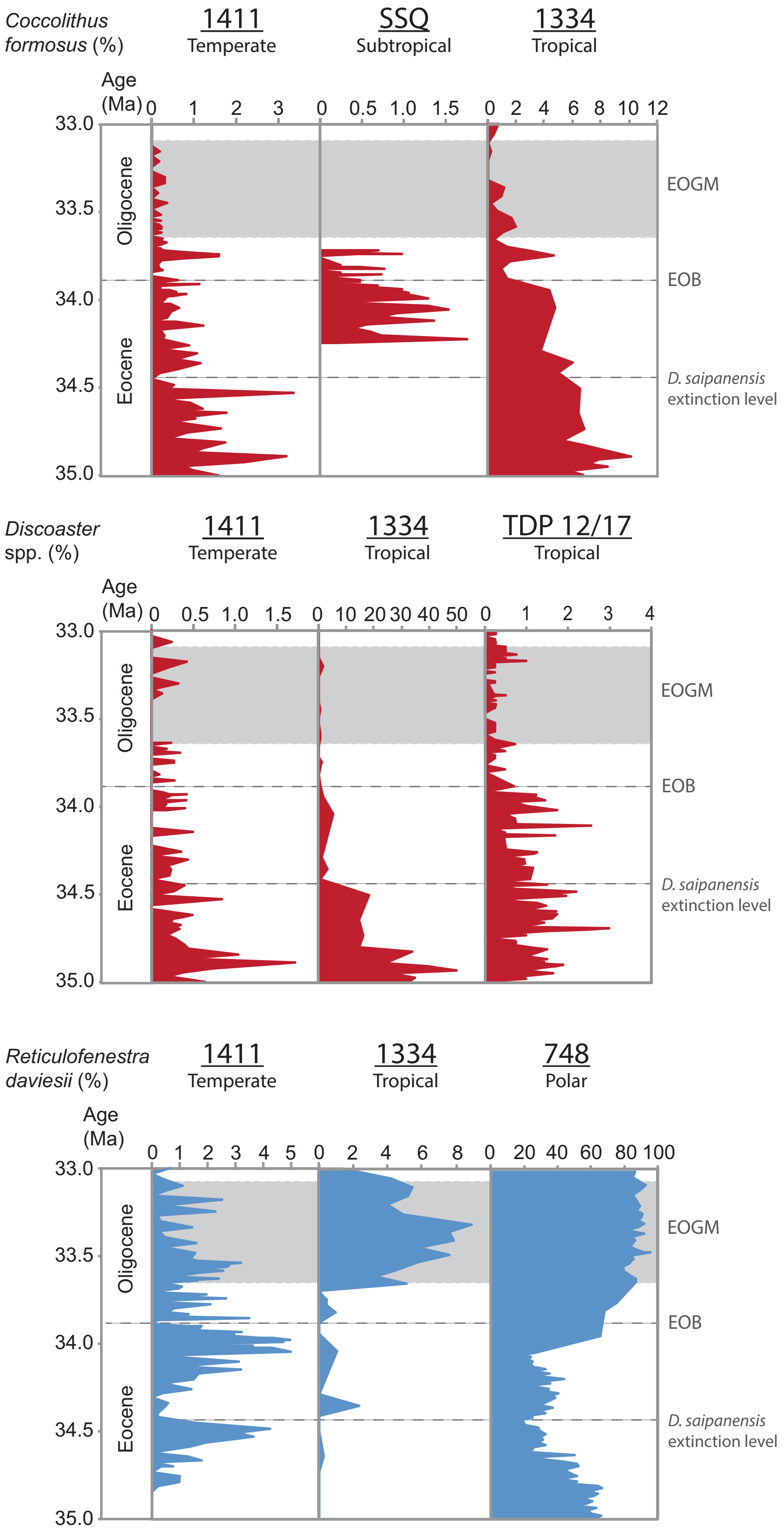

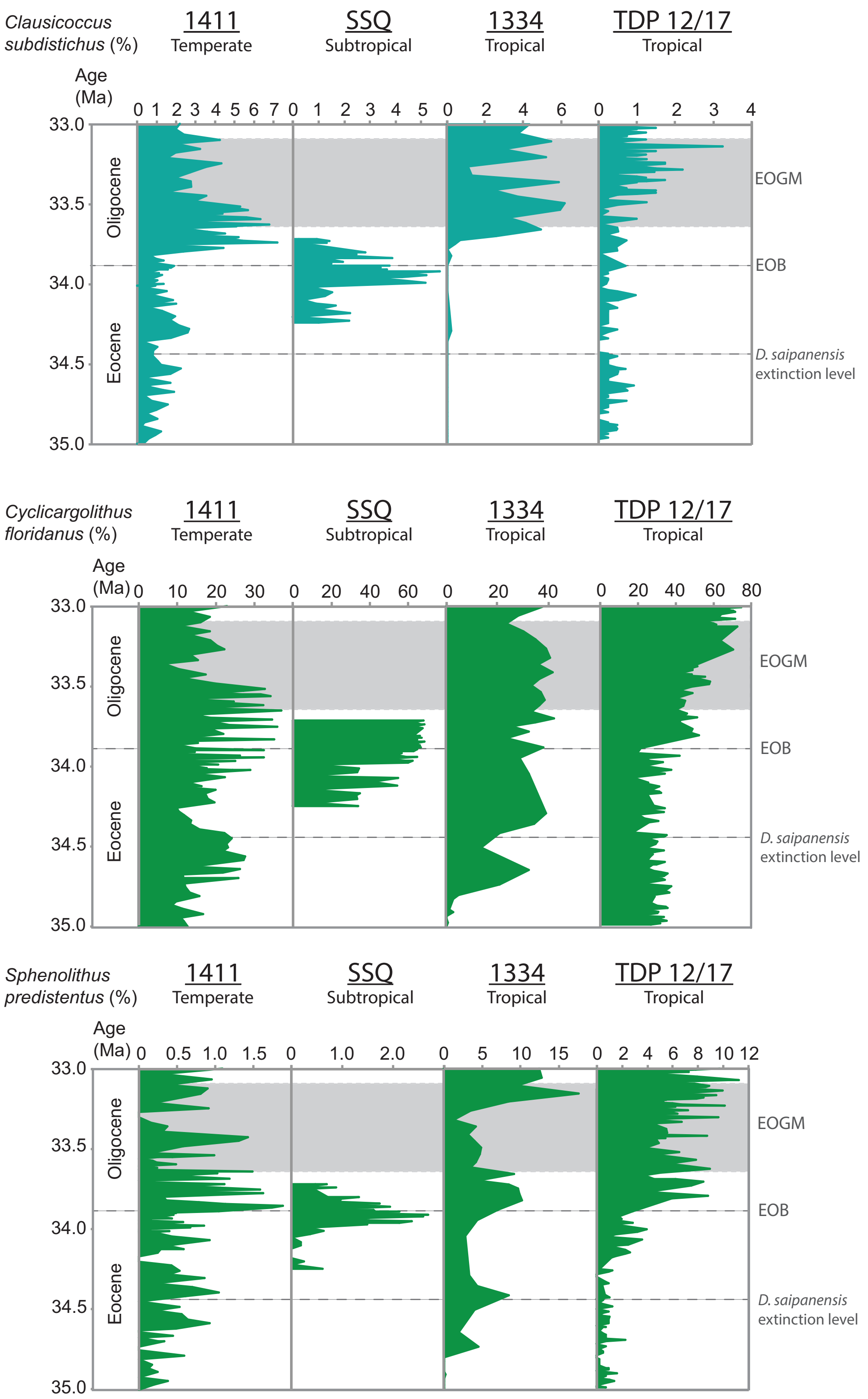

ordination space, and high latitude Site 748 plots with negative values on the NMDS 1 axis. The cool water taxa, *Chiasmolithus*, *Isthmolithus recurvus* and *Reticulofenestra daviesii*, plot within the Southern Ocean site sample scores, with negative values in

NMDS 1 (Figure 5.4a). The temperate and warm temperate mesotrophic taxa (e.g. *R. dictyoda, C. pelagicus*) plot in the centre of the ordination space, and warm water taxa (e.g. *Discoaster* and sphenoliths) have positive values in NMDS 1, plotting within the low latitude sites sample space (Figure 4a). This is corroborated by the overlay of the ordisurf function, which highlights a strong latitudinal control on the assemblages (r^2 = 0.91, 91.2 % deviance explained), within the NMDS 1 axis (Figure 4b). There is a weaker relationship between the sample scores and age (r^2 = 0.564, 57.1% deviance explained) (Figure 4c).

Figure 5.4: NMDS ordination plots. a) sample (open circles) and species (stars) scores b) sample scores with overlain latitude contours (+/- °), c) sample scores with overlain age contours (Ma). Samples are colour coded based on site locality (grey – 748, yellow – 1411, blue – SSQ, green – 1334 and red – TDP).

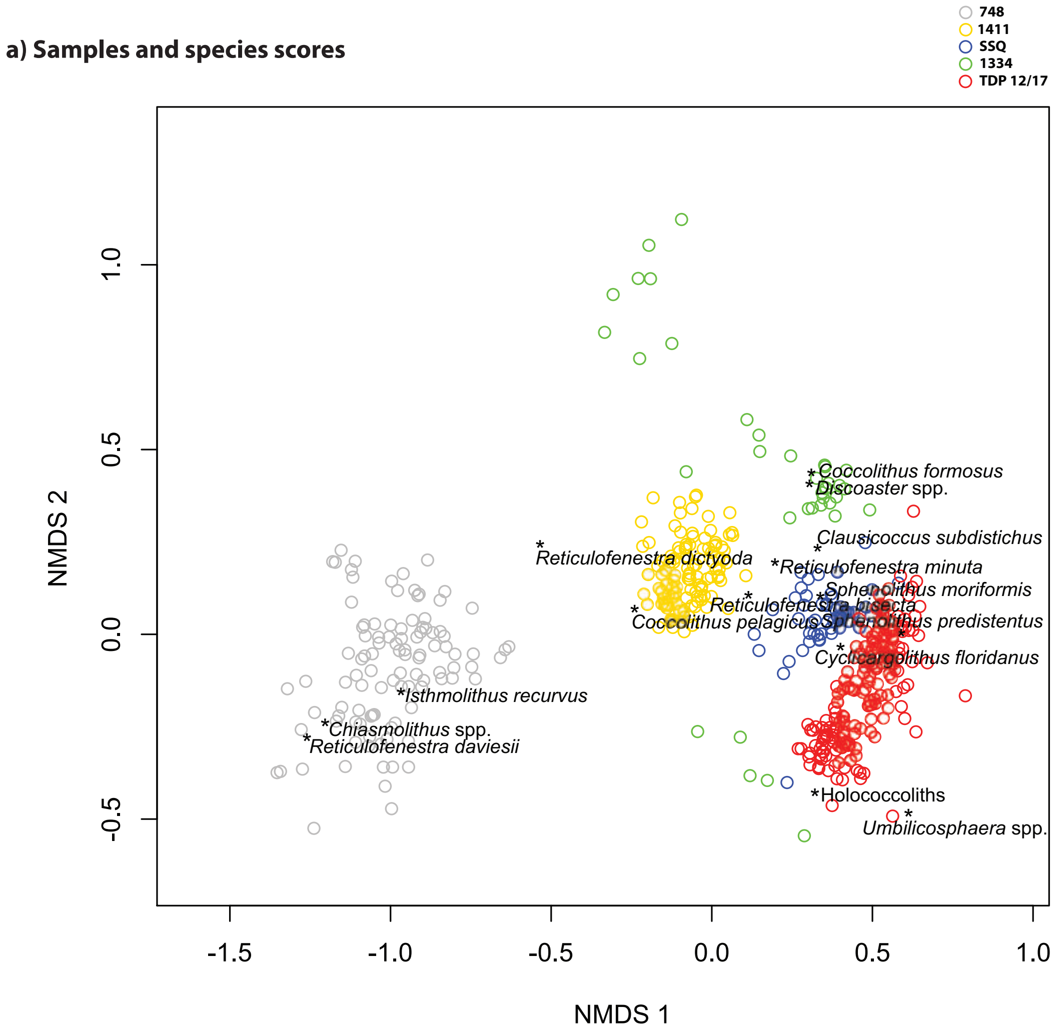

b) Latitude

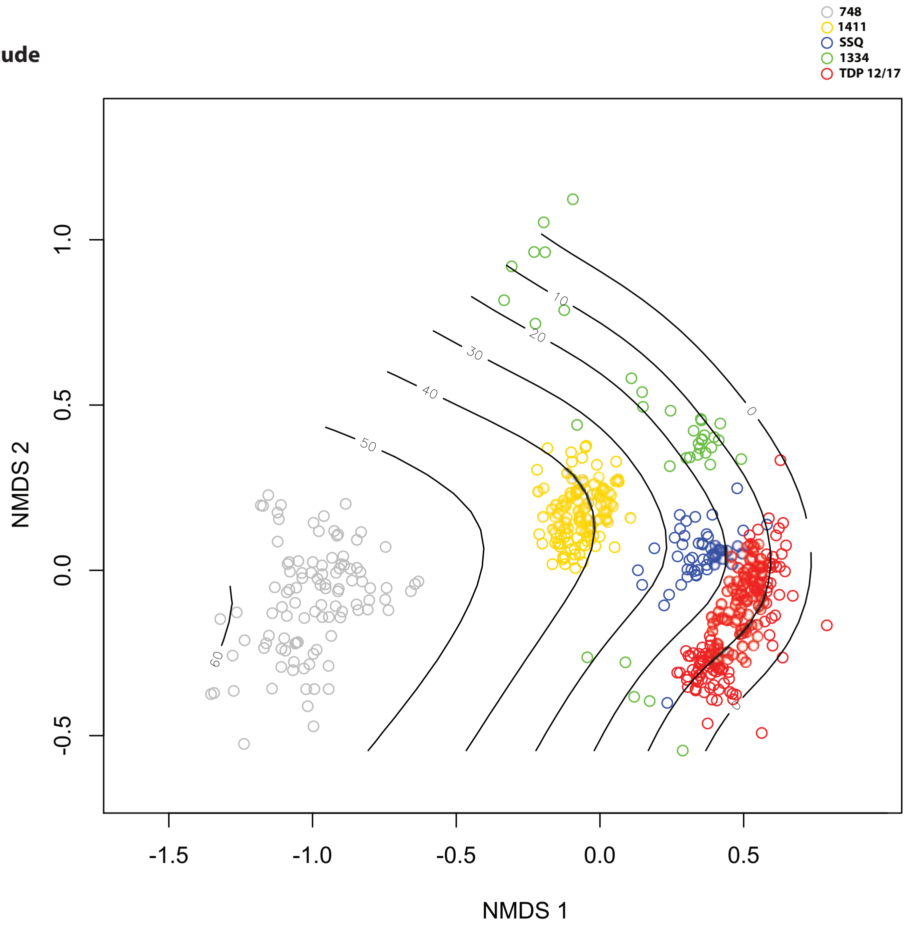

c) Age

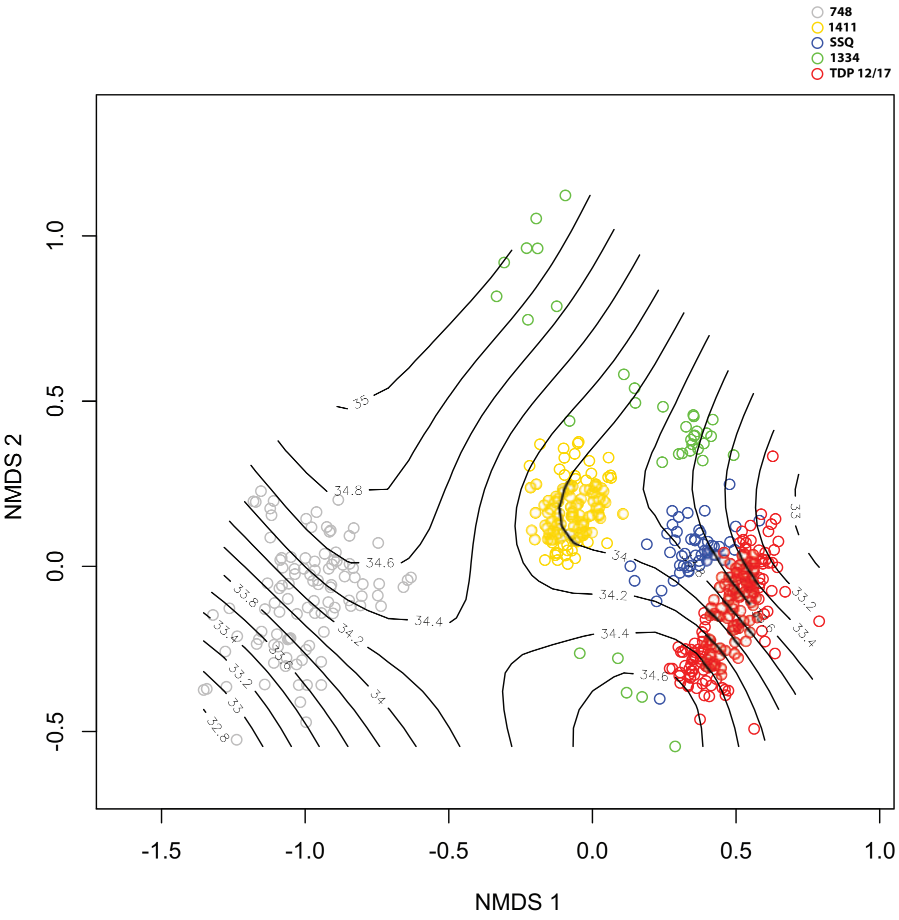

5.4 Discussion

5.4.1 Timing of global assemblage shifts

The nature and timing of the nannoplankton assemblage shifts at each site is an important indicator of global EOT palaeoceanographic change. The warm water oligotrophs show gradual, protracted decline at Sites 1411, 1334 and TDP, and distinct decreases at Sites SSQ and 748 at 34.22 Ma and 34.18 Ma, respectively. The increasing taxa demonstrate significant step-shifts occurring close to the EOB (33.89 Ma) and within ~160 kyr of each other. This succession of shifts is preceded by the conspicuous increase in cold water taxa from 34.06 Ma at Site 748, and slightly later but in quick succession at SSQ, 1334, 1411 and TDP 12/17 (34.01 Ma, 33.95 Ma, 33.90 Ma and 33.90 Ma, respectively). These population changes in nannoplankton, within ~10-170 kyr years of the EOB, coincide with an interval of planktonic foraminifera extinctions, notably the loss of the *Turborotalia cerroazulensis* group (34.03 Ma) and the Hantkeninidae family (33.89 Ma), and elevated radiolarian turnover (Kamikuri et al., 2012). The planktonic foraminifera extinctions are considered to have been influenced by changing productivity levels in response to changing water column stratification (Wade and Pearson, 2008), which could also have influenced population composition within the calcareous nannoplankton. The disturbance across marine plankton groups represents a distinct ecological event and this perturbation appears coincident with the first step of the oxygen isotope excursion as noted by Dunkley Jones et al. (2008). This first step is thought to primarily reflect significant cooling (Lear et al., 2008) and is accompanied by a distinct pulse in weathering in the Southern Ocean (Scher et al., 2011) and is coincident with more vigorous ocean circulation driven by strengthened thermal gradients which drove cool nutrient rich waters from the Southern Ocean globally. The biotic response in the late Eocene, precedes the second step of the oxygen isotope shift and EOGM, by ~250-400 kyr and by and large this interval shows little response with cold eutroph dominated assemblages well established and prevailing. This is consistent with the second isotope step primarily reflecting changes in ice volume (Lear et al., 2008) and therefore having a less direct influence on surface water environments and the plankton assemblages. The early disturbance recorded in the plankton groups suggests they rapidly responded to environmental perturbation, passing a critical threshold and are therefore useful proxies for determining the initial onset of major climatic and oceanographic change (Bordiga et al., 2015).

5.4.2 Ecological signals and response in global nannofossil assemblages

We identify significant global response in the calcareous nannoplankton assemblages across the EOT reflecting environmentally forced restructuring of populations at each site, with a definitive change towards assemblages rich in cool water favouring, eutrophic taxa. The timing of this significant step-shift in populations occurred within ~10-170 kyr of the EOB at all sites. The population restructuring is most evident in the decline and extinction of warm water oligotrophs and the increased abundance of cold water and/or eutrophic favouring taxa, such as *Cyclicargolithus floridanus*, *Sphenolithus predistentus* and *Reticulofenestra daviesii*. These taxa which were able to exploit the emerging icehouse oceanographic conditions went on to dominate the nannoplankton assemblages for much of the Oligocene. The influence of both temperature and productivity controls on the nannofossil assemblages indicate the interplay of various oceanographic parameters was a global phenomenon.

Much of this evidence points towards the reduction of warm water oligotrophic habitats, which in the Paleogene, and at present, support the highest nannoplankton diversities. This is evident in the decline and extinction of taxa with strong preference for warm water environments (*Discoaster*, *Coccolithus formosus*, *Umbilicosphaera bramlettei* and *Umbilicosphaera protoannula)* and in the decreasing abundance of a number of taxa with probable warm water (*Pemma papillatum* and *Bramletteius serraculoides*) and warm temperate preference (*Reticulofenestra bisecta* and *Coccolithus pelagicus*). There is further support from the spread and increasing abundance of cold water taxa, most strongly identified in the grilled reticulofenestrids, the *Reticulofenestra lockeri* group (*Reticulofenestra daviesii, Reticulofenestra lockeri, Reticulofenestra macmillani*) and *Chiasmolithus* and *Isthmolithus recurvus* in high southern polar latitudes. The initiation of this reduction in warmer water, oligotrophic habitats is particularly evident in the southern high latitudes where warm water oligotrophs began withdrawing from these regions in the middle Eocene, with last occurrences of *Discoaster* spp. and *Coccolithus formosus*, ~5 myr and ~6 myr prior to their final extinction levels, respectively (Persico et al., 2012). This earlier onset of cooling at southern high latitudes is supported by geochemical palaeothermometry (TEX_{86}), which indicates significant latitudinal temperature gradients as great as $14^{o}C$ between South Atlantic and equatorial Atlantic sites by the late middle Eocene (41.3 to 38 Ma) (Inglis et al., 2015), as the tropics maintained stable warmth through the Eocene (Pearson et al., 2007). Overall, sea surface temperature cooling is estimated to have been $6^{o}C$ in high latitudes, relative to $2.5^{o}C$ at low latitudes between the early and late Eocene (Inglis et al., 2015), with intensified global cooling across the EOT (Lear et al., 2008; Liu et al., 2009). The Site 748 species abundance plots and the NMDS ordination further indicate a strong temperature control, with *Reticulofenestra daviesii* dominating the EOT assemblages at this site and the cool water taxa plotting within the Site 748 sample space. This strong latitudinal control on the assemblages displayed in the NMDS ordination, with the polar Southern Ocean Site 748 most distinct from low latitude and mid to high northern latitude sites, is undoubtedly due to a higher degree of climatic forcing in the southern hemisphere with progressive cooling and thermal isolation relating to Antarctic ice sheet expansion and changes in ocean circulation from the opening of the Southern Ocean gateways leading to the initiation of the Antarctic Circumpolar Current (Kennett, 1977; Plancq et al., 2014).

In addition to the influence of decreasing temperatures, there is also strong evidence for widespread increases in surface water productivity. The increasing abundances of warmer water taxa *Cyclicargolithus floridanus* and *Sphenolithus predistentus* at sites 1411, SSQ, 1334 and TDP 12/17 indicate the strong influence of increasing productivity control on low and mid latitude assemblages in both shelf and open ocean settings. In addition, *Clausicoccus subdistichus,* a cool eutrophic species, also increases across the EOT at these sites and exhibits a globally recognised acme for ~300-400 kyr up to 33.50 Ma (GTS12). At the tropical and subtropical sites (SSQ, 1334 and TDP) the increasing taxa are dominated by these eutrophic species, while the temperate Site 1411 sees increases in both eutrophic and cold water taxa. The loss of oligotrophic taxa, *C. formosus* and *Discoaster*, is seen at all four sites. Site 748 lacks the warmer water eutrophic taxa *C. floridanus* and *S. predistentus* but likely the strong increase in *R. daviesii* represents a response to both cooling and increasing productivity (Fioroni et al., 2015) and nannofossil records suggest highly eutrophic assemblages were already established by the late Eocene in the Southern Ocean (Villa et al., 2014). The spread of more productive surface waters, with eutrophic assemblages proliferating through into the early Oligocene, is also supported by evidence for increasing productivity from other proxies, such as increased benthic foraminifera accumulation rates, increased dissolution and fragmentation of planktonic foraminifera and maximum accumulation rates of radiolaria, across the EOT at low, mid and high latitude sites (Coxall and Wilson, 2011; Diester-Haass, 1995; Diester-Haass and Zachos, 2003; Salamy and Zachos, 1999). Increased nutrient availability was likely driven by intensified ocean and atmospheric vertical mixing created by a strong temperature gradient and enhanced wind driven upwelling which led to the spinning up of the oceans (Diester-Haass, 1995; Houben et al., 2013; Miller et al., 2009) and strengthened ocean circulation from the early Oligocene transporting nutrient rich waters from the Southern Ocean.

5.5 Summary

This chapter has shown comparable nannofossil trends at all global localities across the EOT, with protracted decline in warm water oligotrophic taxa and a significant step shift increase in cold water eutrophic taxa within 10-170 kyr of the EOB, an interval which also exhibits major extinctions in the planktonic foraminifera and a high level of turnover in the radiolaria. This suggests widespread perturbation to surface water environments, with clear evidence for surface water cooling and increased productivity driving the response in the plankton groups. However, the calcareous nannoplankton records do display a strong latitudinal control on the assemblages, particularly evident between the Southern Ocean and low to mid latitude sites, suggesting earlier onset of climatic cooling at southern polar latitudes, which is supported by evidence for range retractions in warm water taxa from the middle Eocene.

Chapter 6

Calcareous nannoplankton diversity decline through the Paleogene greenhouse to icehouse transition in the North Atlantic

6.1 Introduction

The abundant and global occurrence of calcareous nannofossils within deep sea pelagic sediments provides an extensive and exceptionally complete fossil record from which palaeodiversity estimates can be extracted. The phytoplanktonic calcareous nannoplankton (predominantly coccolithophorid algae) are a key component of modern ocean ecosystems and dominated the surface oceans in the early Cenozoic. Low resolution (three million year) Cenozoic global records of calcareous nannoplankton diversity have highlighted rapid diversification in the early Paleogene following catastrophic diversity loss at the Cretaceous-Paleogene boundary (~93 % species extinction rate; Bown et al., 2008, 2004). Peak diversities were reached in the middle Eocene (~45 Ma) but a significant long term decline in species richness occurred through the middle to late Eocene greenhouse to icehouse transition (~45 to 33 Ma), from which the calcareous nannoplankton never fully recovered. The middle Eocene to early Oligocene therefore marks a key interval within the evolutionary history of the calcareous nannoplankton. Recent discoveries of exceptionally preserved Paleogene calcareous nannofossil assemblages (e.g. Tanzania Drilling Project) have unearthed a wealth of new taxa and provide more reliable stratigraphic records (Bown, 2005a; Bown and Dunkley Jones, 2006; Dunkley Jones et al., 2009), resulting in higher Paleogene species richness estimates (Bown et al., 2008) and extending the evolutionary history of many Neogene and modern groups back into this interval. These records emphasise the need to reassess long term Paleogene nannofossil diversity and in particular the value of records with exceptional preservation, as the pervasive dissolution and/or overgrowth, which typifies most carbonate-rich deep sea nannofossil assemblages, has led to misleadingly reduced estimates of diversity, and this is especially so in the Paleogene (Bown et al., 2008).

Here we present a high resolution long term record of calcareous nannoplankton diversity through this critical Paleogene greenhouse to icehouse transition using Integrated Ocean Drilling Program (IODP) Expedition 342 cores that specifically targeted the recovery of exceptionally preserved microfossils. This was achieved by drilling shallow sections in supra-CCD drift sediments that were clay-rich. IODP Sites U1408 and U1411 (IODP Expedition 342) provide a near-continuous middle Eocene to early Oligocene section of sediments, which display minimal effects of diagenetic modification and good to exceptionally preserved calcareous nannofossils. We document the structure and timing of the calcareous nannoplankton diversity decline and compare these new records with global records of nannoplankton diversity to examine regional versus global trends. We also compare them with palaeoceanographic parameters (e.g., oxygen isotopes, CO_2) to assess whether climatic shifts played a significant role in the evolution of this phytoplankton group, as previous low resolution records suggest a possible link to the dynamic nature of the climate at this time.

6.2 Materials and Methods

6.2.1 Geological setting

Sites U1408 and U1411 are located 74 km apart (41°26’N 49°47’W and 41°37’N 48°6’W, respectively) on the Southeast Newfoundland Ridge in the western North Atlantic (Figure 6.1). These bathyal sites (~2600-2850 mbsl in the Eocene) comprise expanded sections of Paleogene drift sediment packages with high sedimentation rates (between 1.4 to 3 cm/kyr on average), typically consisting of clay-rich nannofossil oozes, which have facilitated the exceptional preservation of the calcareous microfossils within. Revised bio- and magnetostratigraphic shipboard datums have been used to produce age models for each site (detailed in Chapter 2) and these indicate a near-continuous composite record is present, with a minor gap of around 10 kyr between the two sections (38.20 to 38.21 Ma). For this study we focused on the section from 32.51 to 45.26 Ma. This interval is of particular interest as it represents the last interval of high nannofossil diversity shown in the recent global nannofossil diversity compilation (Bown, pers. comm. 2016) and spans the long term diversity decline into the Oligocene.

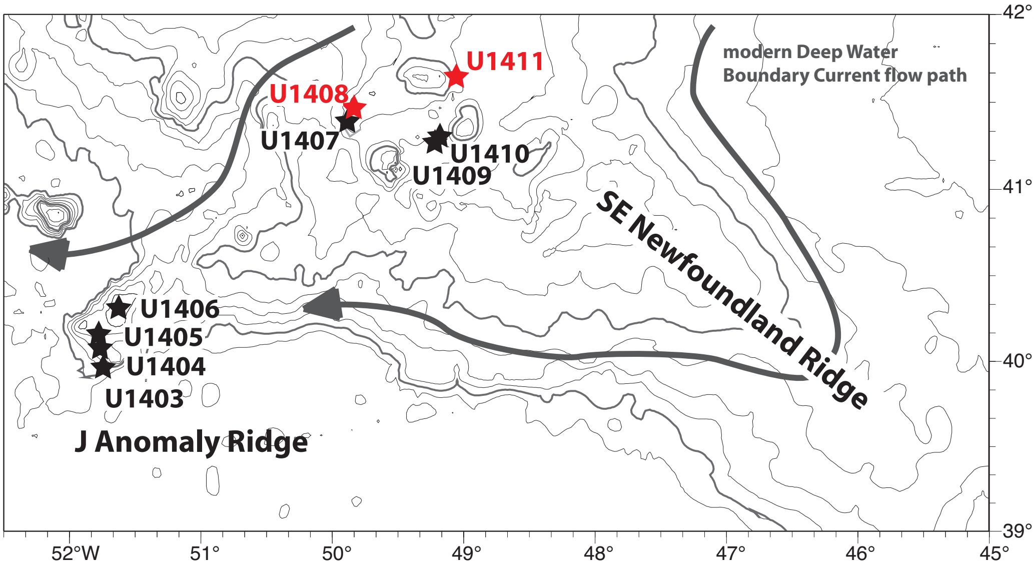

Figure 6.1: Location map of Site U1408 and Site U1411 used in this study. Modified from Norris et al. (2014).

6.2.2 Data collection

430 samples have been analysed from the middle Eocene to the early Oligocene, 45.26 Ma to 32.51 Ma (45.26 Ma to 38.21 Ma from Site U1408 and 38.20 to 32.51 Ma from Site U1411). Low resolution samples (~30-35 kyr) were studied across the entire interval with higher resolution sampling at the key transient climatic events, the MECO (~17 kyr sampling across 41.5 to 39 Ma) and the EOT (~10 kyr across 34 to 33.5 Ma). Standard procedures were used to produce smear slides and to generate count data, counting 300 nannofossil specimens to species level, per smear slide, viewed using transmitted light microscopy at x1000 magnification on an Olympus BX40 under cross polarized, bright field and phase contrast light (Bown and Young, 1998). Counts of 300 specimens were performed as this represents a statistically significant value accounting for taxa that comprise 1 % of the assemblages at the 95 % confidence level. Extended counts were performed, excluding the dominant taxa (reticulofenestrids <5 µm and *Coccolithus pelagicus* <5 µm at Site U1408, and *Reticulofenestra minuta* at Site U1411) and counting until the total of other taxa equalled a minimum of 300 to ensure rare species were accounted for. Relative abundances were generated from the count data. Species accumulation curves (Figure 6.2) display a logarithmic trend, yet despite the first four to five fields of view capturing a large number of the species present in each sample, continued counting increases species richness due to the extremely high number of rare taxa, which cannot be quantified within the relative abundance counts. Due to the

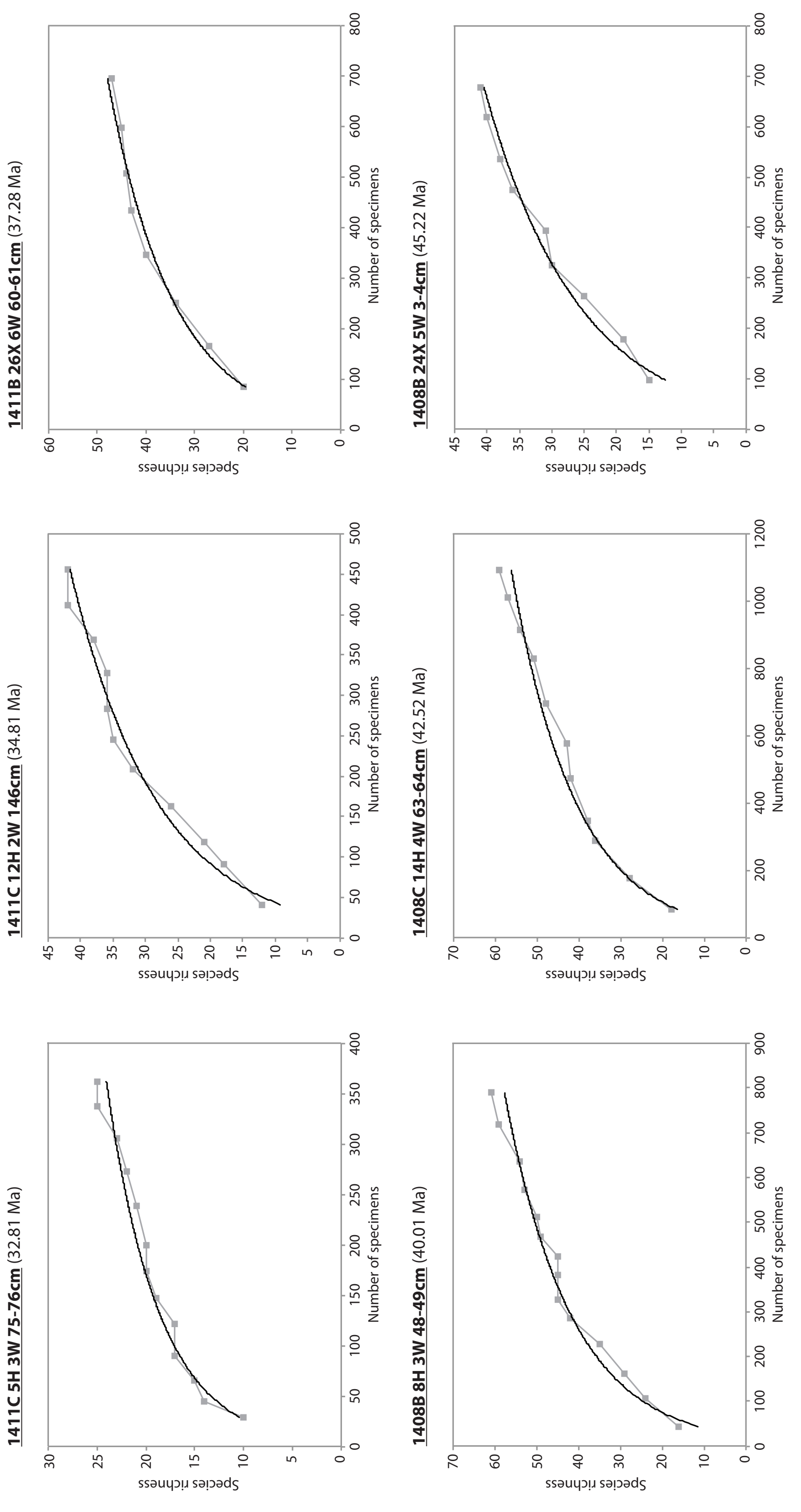

Figure 6.2: Species accumulation curves from six intervals through the studied interval.

large number of rare taxa (<0.5-1 %) within the assemblages, supplementary semi-quantitative analysis was also performed, scanning three complete traverses per slide (around 300 extra fields of view), to provide documentation of these species. It is important to note that species richness estimates can alter depending on species concepts so here we use the same taxonomic concepts as those used in the recent compilation (Bown, pers. comm. 2016) following Bown (2005a), Bown and Dunkley Jones (2006), Dunkley Jones et al. (2009), Bown and Dunkley Jones (2012) and Nannotax (http://ina.tmsoc.org/Nannotax3/), so our records are consistent and comparable with this recent work and the previously published records in Bown et al. (2004).

6.2.3 Analytical techniques

6.2.3.1 Diversity metrics

A range of different metrics are used to represent and assess the diversity of calcareous nannoplankton assemblages through this key interval, including raw count richness, raw semi-quantitative richness and maximised richness.

Raw species richness records are sourced from the quantitative counts and semi-quantitative logging to provide a presence/absence analysis of diversity. Maximised species richness is generated from the semi-quantitative species ranges but interpolates presence between observed occurrences thus reducing noise created by the relatively large numbers of rare (and sporadically distributed) taxa and generates an upper limit diversity estimate for these sites. An assumption is made that absence is primarily due to rarity rather than population shifts in and out of the area. In order to minimise the edge effects at the top and bottom of the time series, we have interpolated continued presence if published ranges indicate first or last occurrences beyond the uppermost or lowermost samples. In general, taxa recorded in only one sample have been excluded and we have removed unidentified and reworked specimens from diversity calculations.

6.2.3.2 Holococcoliths

Holococcoliths have not been included in the main diversity records because they likely include life cycle representatives already documented in the heterococcolith record. They are also predominantly extremely fragile coccoliths and their fossil records are particularly sensitive to varying preservation. Their exclusion from the main diversity dataset follows the protocols of previous studies and provides a more reliable comparison with these records (Bown et al., 2004; Bown, pers. comm. 2016).

6.2.3.3. Evolutionary rates

We have applied several measures to assess evolutionary rates per unit time, including the rate of speciation, rate of extinction, rate of turnover and rate of diversification. The methods used to assess these parameters follow Bown et al. (2004):

$$Rate\ of\ speciation\ (Rs)\ = \left(\frac{1}{D}\right)\left(\frac{FO}{t}\right) \times 100$$

$$Rate\ of\ extinction\ (Re)\ = \left(\frac{1}{D}\right)\left(\frac{LO}{t}\right) \times 100$$

$$Rate\ of\ turnover\ (Rt) = Rs + Re$$

$$Rate\ of\ diversification\ (Rd) = Rs - Re$$

D = maximised species richness, FO = number of first occurrences, LO = number of last occurrences and t = time interval.

Time bins of 1 myr have been used across the whole interval, a comparable resolution to recently compiled long term global records (Bown, pers. comm. 2016), with end values given for each time bin (e.g. 45 Ma for the 44-45 Ma time bin). The species richness was averaged for all samples within each time bin.

6.3 Results

6.3.1 Species richness

Species richness plots from the quantitative, semi-quantitative and maximised range records all show similar trends across the greenhouse to icehouse transition with peak diversity in the middle Eocene (~49, 77 and 125 respectively) and a decrease in diversity through to the early Oligocene (~17, 32 and 49, respectively) (Figure 6.3). A diversity decrease and rapid increase is recorded at the peak-MECO interval in the quantitative record and identified to a lesser degree in the semi-quantitative record but is not observed in maximised range records. The maximised species richness data highlight the high number of rare taxa present within the assemblages but provide a relatively realistic estimate of overall diversity through the interval at this location (despite sporadic occurrence of some taxa, see below), and we will focus on these data here. These records show consistently high species richness levels in the middle Eocene (between ~100 and 125 species), with peak richness at ~41 Ma (125 species), followed by a gradual decline in species richness throughout the late Eocene to 90 species by the EOT. There is then an accelerated decline in species richness (~90 to 70 species) over ~1 myr, which continues into the early Oligocene with only 49 species recorded at the top of the study interval.

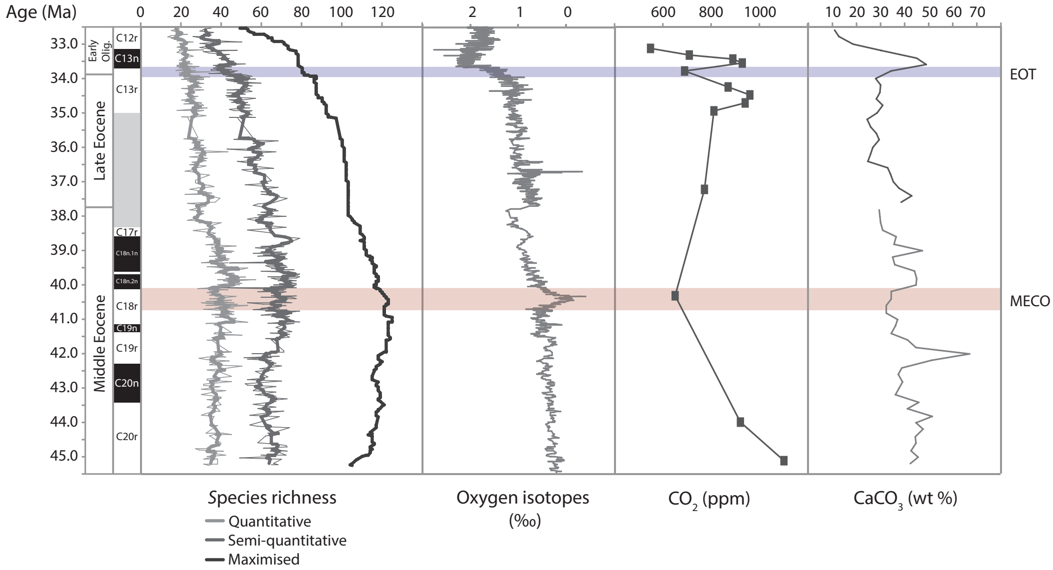

Figure 6.3: Species richness plots (quantitative, semi-quantitative and maximised richness) from Expedition 342 sites plotted against a global oxygen isotope compilation (5 point moving average) (Cramer et al., 2009; converted to GTS12), CO_2 (Anagnostou et al., 2016; converted to GTS12) and $CaCO_3$ (Expedition 342) records. Quantitative and semi-quantitative data are shown with a 3 point moving average. The blue shaded EOT interval is taken from the 'first step' to the onset of the EOGM (Chapter 4) and the red shaded MECO interval is defined by the onset to the top of the peak-MECO from the Expedition 342 sites (Chapter 3). Magnetostratigraphy is taken from the Expedition 342 shipboard records.

A number of nannofossil groups (rhabdoliths, pontosphaerids and helicosphaerids) are unusually diverse at the Expedition 342 sites, primarily due to the exceptional preservation in the clay-rich drift sediments. Even so, many of these species are recorded only rarely and sporadically and as these fragile species are typically not preserved in deep sea sediments and many are recently described, their stratigraphic ranges are poorly characterised. We have separated these taxa from those with well-established and continuous ranges to compare the diversity trends with and without the inclusion of these taxa (Figure 6.4). We note taxa with sporadic records are most dominant in the middle Eocene, significantly contributing to the middle Eocene 'peak' in diversity at ~41 Ma (in particular reflecting the high diversity in the genus *Blackites* with poorly documented ranges due to their occurrence only in exceptionally preserved material), but decrease to account for only ~10-20 in the early Oligocene. Qualitative observations of preservation indicate this does not have an affect on the assemblages.

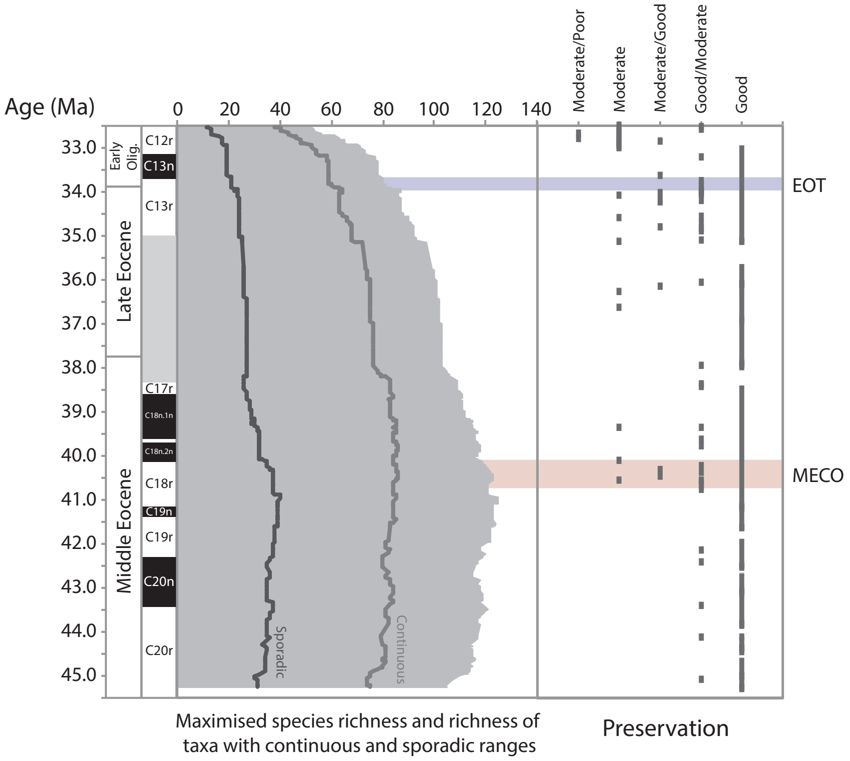

Figure 6.4: Maximised species richness overlain by continuous and sporadic ranges and qualitative preservation records. The blue shaded EOT interval is taken from the 'first step' to the onset of the EOGM (Chapter 5) and the red shaded MECO interval is defined by the onset to the top of the peak MECO from the Expedition 342 sites (Chapter 4). Magnetostratigraphy is taken from the Expedition 342 shipboard records.

Species richness records for selected groups have been plotted (Figure 6.5) to test for different trends within major groups that may have contrasting ecological or evolutionary characters. The meso/eutrophic reticulofenestrids are the only taxonomic group to show an increase in diversity through the middle Eocene increasing to 20 species in the late middle Eocene and early late Eocene before declining slightly through the EOT to ~15 species in the early Oligocene. Calcidiscaceae, *Coccolithus* and *Chiasmolithus* all record peak species richness in the middle Eocene (11, 9 and 7, respectively) decreasing through the late Eocene (2, 2 and 1 species, respectively, by the early Oligocene). *Coccolithus* shows a distinct decrease in species richness through the EOT and early Oligocene coincident with the large negative shift in oxygen isotope values. Helicosphaerids, pontosphaerids and *Blackites* are fragile taxa but the exceptional preservation at these sites is reflected in the high species richness documented here. *Helicosphaera* species richness is relatively stable throughout (~8) and *Pontosphaera* is comprised of on average 15 species, with gradually decreasing richness through the interval (18 to 14) and accelerated loss through the early Oligocene. *Blackites* has a peak of 22 species in the middle Eocene before declining through the late Eocene to 3 species by the top of the study interval. At least half of the species within *Blackites* have poorly documented stratigraphic ranges, with many of the species seen here only having been described in the last 10 years or so. Discoasters and sphenoliths have low species richness at these sites but show decreasing species richness through the study interval (8 to 3 and ~7 to 4, respectively).

In order to test for diversity trends related to specific ecological adaptations, we plotted groups of taxa with similar temperature preferences: warm – discoasters, sphenoliths, Calcidiscaceae; warm temperate – *Reticulofenestra bisecta* group, *Reticulofenestra reticulata* group, *Cyclicargolithus*, *Coccolithus*; and cool – *Reticulofenestra umbilicus* group, *Reticulofenestra lockeri* group, chiasmoliths, *Clausicoccus, Isthmolithus* (Figure 6.5). The warm water taxa show decreasing species richness from the middle Eocene (40.89 Ma) to late Eocene with an accelerated loss of this group from 35.77 Ma. Warm temperate water taxa increase in diversity at 40.59 Ma into the late Eocene and maintain a stable species richness through the late Eocene with accelerated diversity loss through the early Oligocene from 33.15 Ma. The cool water taxa generally have stable species richness with turnover in the late middle Eocene and a further decrease in the early Oligocene.

6.3.1.1 Holococcoliths

Despite the removal of the holococcoliths from the main diversity records, the consideration of holococcolith diversity is still informative and at these sites there are 8-10 species in the middle Eocene (Zone NP15), peaking in upper Zone NP16 to lower Zone NP17 with 13 species. This is followed by a sudden loss of 4 species from 39.57 to 38.62 Ma and then a gradual decrease to 6 species in the early Oligocene (Figure 6.5). The holococcoliths at the Expedition 342 sites include species from six genera;

Lanternithus, Zygrhablithus, Daktylethra, Holodiscolithus, Orthozygus and *Clathrolithus.*

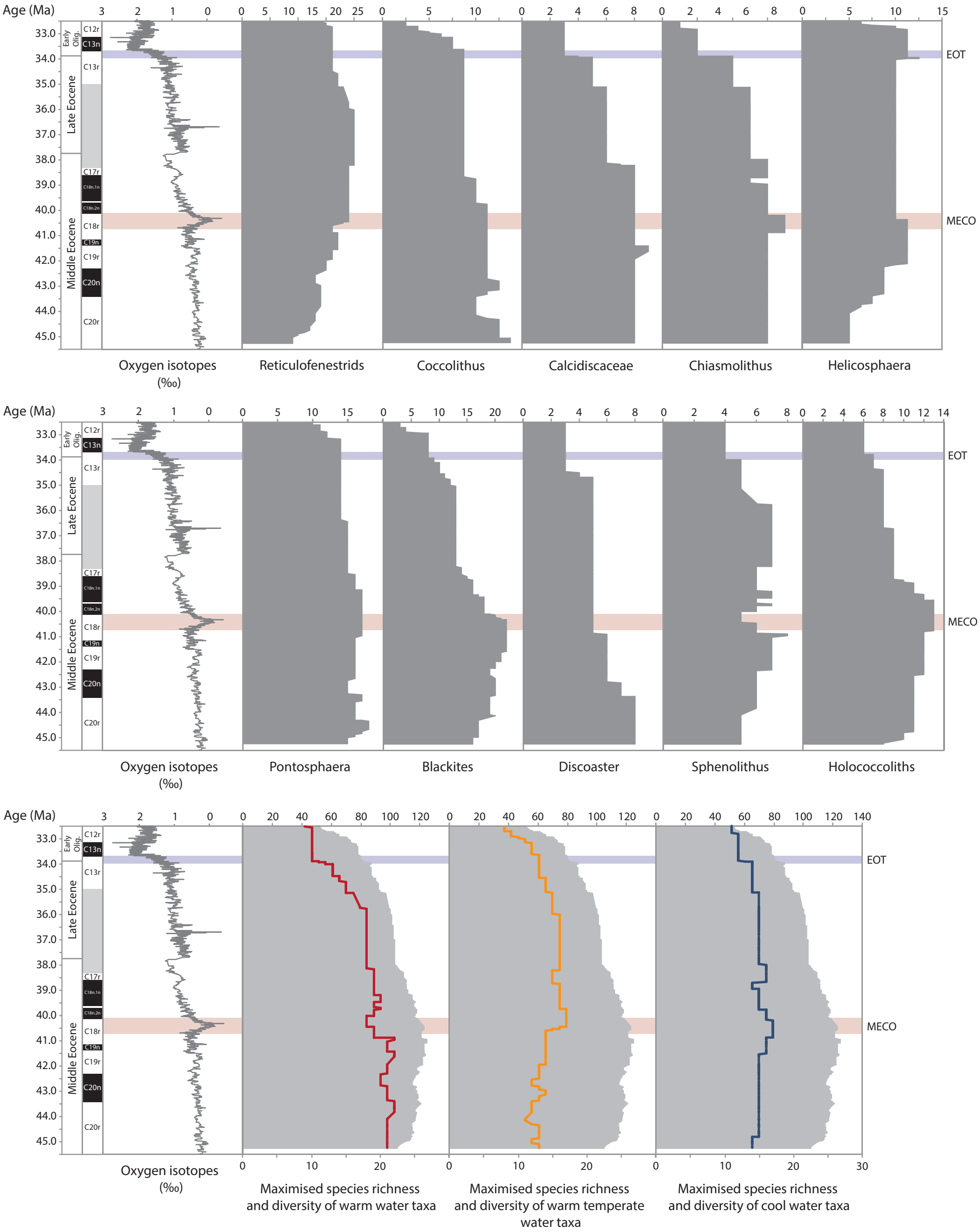

Figure 6.5: Selected taxa species richness and temperature groups' species richness plotted against a global oxygen isotope compilation (5 point moving average) (Cramer et al., 2009; converted to GTS12). The blue shaded EOT interval is taken from the 'first step' to the onset of the EOGM (Chapter 4) and the red shaded MECO interval is defined by the onset to the top of the peak-MECO from the Expedition 342 sites (Chapter 3). Magnetostratigraphy is taken from the Expedition 342 shipboard records.

6.3.2 Evolutionary rates

Across the middle to late Eocene extinction rates average 9 with a drop in values at 42 Ma to 2.5 and accelerated rates are identified from 35 Ma, peaking at 33 Ma with values of 42.5 (Figure 6.6). Speciation is highest in the middle Eocene at 45 and 42 Ma, with values of 11.8 and 9.3. These values significantly decrease through the late Eocene with speciation rate at 0 at 37, 36, 35 and 33 Ma (Figure 6.6). Rates of turnover are constant (~13) through the middle and late Eocene, decreasing to 1 at 37 Ma before dramatically increasing to 16.8 and 42.5 across the EOT and early Oligocene, due to the accelerated rates of extinction. Diversification declines through the interval from 8.2 to -42.5, reflecting decreasing speciation through the middle and late Eocene and rapidly increasing extinction rates in the early Oligocene (Figure 6.6).

Similar evolutionary rates and first and last occurrence trends are shown in the global nannofossil data (Bown, pers. comm. 2016) (Figures 6.6 and 6.7). Highest speciation rates occur in the middle Eocene, NP15 (11.8 Expedition 342; 9.6 global) and decrease to extremely low rates through the late Eocene and early Oligocene at the Expedition 342 sites but global records show pulsed speciation at 42, 37 and 33 Ma. Extinction rates fluctuate (on average 7 Expedition 342; 8 global) with an elevated rate from the EOT (42.5 Expedition 342; 18.4 global). Subtle differences in the global records include noticeably higher extinction rates at 42 Ma and speciation in the late Eocene and early Oligocene, 37 Ma and 33 Ma, but these may reflect an artefact of temporal resolution.

6.4 Discussion

The high sedimentation rates and exceptional preservation of calcareous nannofossils within the Expedition 342 sediments across this 13 myr middle Eocene to early Oligocene section has allowed us to generate high quality, high resolution records of nannoplankton diversity change through this interval of profound palaeoclimate change. The extremely high species richness values indicate that these sites, situated between mid and high latitudes in the North Atlantic, are well placed to document a high proportion of the global nannofossil diversity, including a virtually complete census of polar, temperate and tropical taxa. This is supported by values that are comparable with global compilations.

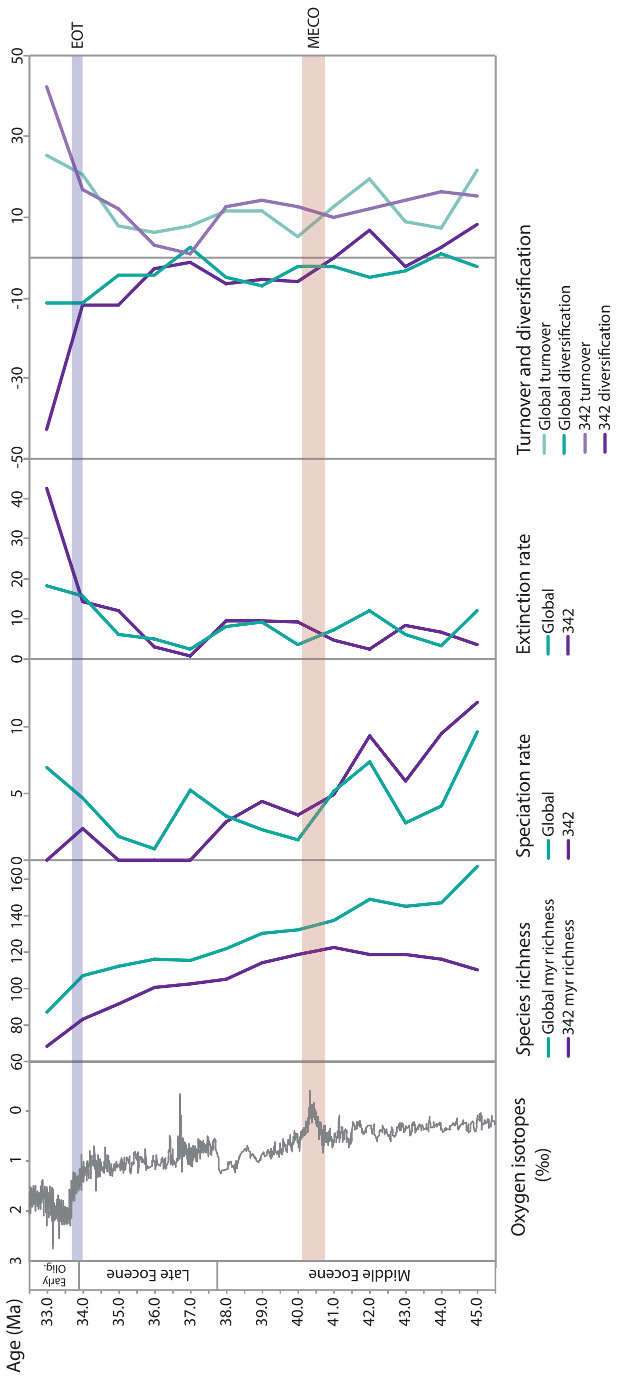

Figure 6.6: Evolutionary rates (extinction, speciation, turnover and diversification) in one million year time bins from Expedition 342 sites and the global compilation (Bown, pers. comm. 2016) plotted against a global oxygen isotope compilation (5 point moving average) (Cramer et al., 2009; converted to GTS12). The blue shaded EOT interval is taken from the 'first step' to the onset of the EOGM (Chapter 4) and the red shaded MECO interval is defined by the onset to the top of the peak-MECO from the Expedition 342 sites (Chapter 3). Magnetostratigraphy is taken from the Expedition 342 shipboard records.

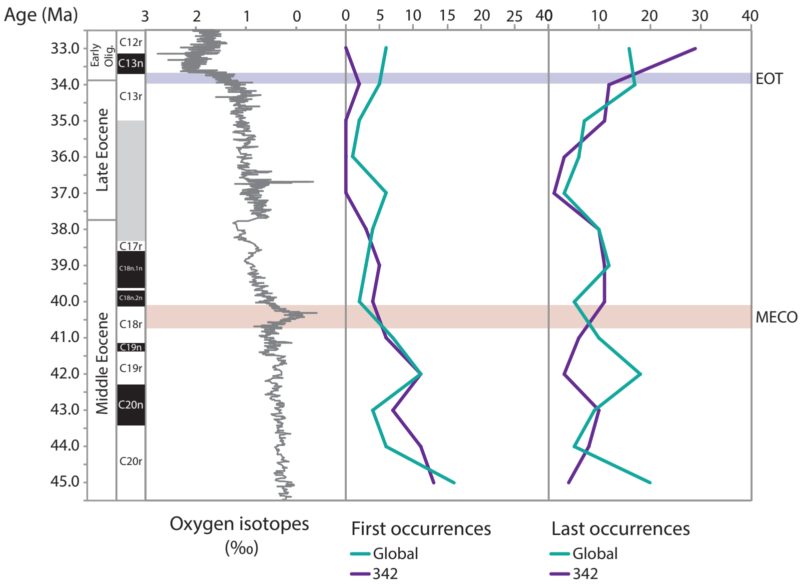

Figure 6.7: First and last occurrence data from Expedition 342 sites and the global compilation (Bown, pers. comm. 2016) plotted against a global oxygen isotope compilation (5 point moving average) (Cramer et al., 2009; converted to GTS12). The blue shaded EOT interval is taken from the 'first step' to the onset of the EOGM (Chapter 4) and the red shaded MECO interval is defined by the onset to the top of the peak-MECO from the Expedition 342 sites (Chapter 3). Magnetostratigraphy is taken from the Expedition 342 shipboard records.

The unusually diverse assemblages from the Expedition 342 sites are a reflection of the exceptional preservation of the calcareous nannofossils preserved within the clay-rich Paleogene drift sediments. This standard of preservation has resulted in high species richness values that are comparable to benchmark localities, such as the Kilwa Group lagerstätte of coastal Tanzania which are significantly elevated compared to typical deep sea records. Expedition 342 species richness values of 113 in the middle Eocene (Zone NP15) and 99 in the late Eocene (Zone NP19/20) are comparable to the Tanzania values of 145 and 79, respectively, and both are substantially higher than values recorded at other localities, for example, open ocean - Shatsky Rise (48 species NP15 and 26 species NP19/20), Allison Guyot (61 species NP15 and 32 species NP19/20) and shelf sites – Blake Nose (62 species NP15), Kerguelen Plateau (46 species NP15) (Bown et al., 2008). In comparison to global compilations of nannofossil diversity records, the overall gradient of species richness decline is flatter at the Expedition 342 sites, with no evident step-like changes as seen in the lower resolution records (3 myr spacing) of Bown et al. (2004). This likely represents the effect of the time bin size in the global compilation, capturing only broad changes through the interval. The most recent global compilation (Bown, pers. comm. 2016. – shown here in Figure 6.6), includes recently described species, improved species range estimates and samples over narrower time bins (1 myr), and shows a more gradual diversity decline, from 167 species at 45 Ma to 87 species at 33 Ma. This is comparable with Expedition 342 records, on average 110 to 68 species, respectively and highlights the high quality of these data from these North Atlantic sites.

6.4.1 Structure and timing of the nannofossil diversity decline

The long term Eocene diversity decline in nannofossils is known from low stratigraphic resolution records (Bown et al., 2004, 1992; Knoll, 1989; Spencer-Cervato, 1999), but this is the first study to document species richness at high resolution from one locality. We are thus able to examine the structure and timing of this decline in detail. The record shows an average species richness of 113 in the early middle Eocene (Zone NP15) increasing to a peak of 125 species at ~41 Ma, reflecting high diversities in many groups but is particularly influenced by peak diversity within the *Blackites* genus within Zone NP16. Diversity then declines across seven myr of the middle to late Eocene interval (~41 to 34 Ma) from 125 to 86 species. The decline is gradual and notably reveals little effect at the MECO (~40 Ma) and Middle/Late Eocene Turnover (MLET; ~38 Ma) events. The MECO saw only moderate turnover with the loss of seven species and origination of three (e.g. *Sphenolithus predistentus, Sphenolithus obtusus*) (see Chapter 3). At the MLET there is similar turnover with the loss of a seven species and origination of three, however this does not represent above-background diversity change, despite this event being associated with significant zooplankton extinctions (Kamikuri and Wade, 2012; Wade, 2004). An acceleration of diversity loss is only evident from the EOT into the earliest Oligocene, when >20 species were lost within ~1.5 myr. This marks a key interval in the nannofossil diversity record, with the rate of diversity loss at ~15 species/myr, which is much higher than rates of ~5.5 species/myr during the middle and late Eocene.

6.4.2 Character of evolutionary rates

The principal driver of this diversity decline is clearly revealed in the evolutionary rates data, with comparable trends in both the Expedition 342 and global records. Moderately high rates of extinction are documented throughout the middle Eocene to early Oligocene interval but the highest values occur over the EOT. This contrasts dramatically with speciation rates, which are high in the middle Eocene but drop to very low or zero rates in the late Eocene and early Oligocene. This combination of relatively high extinction rates with little or no speciation lies behind the long term diversity decline, and is reflected in decreasing and negative rates of diversification (speciation minus extinction). These diversification rates are amongst the lowest in the evolutionary history of the group, only exceeded by the Cretaceous-Paleogene boundary and the Triassic-Jurassic boundary (Bown, 2005b; Bown et al., 2004). High turnover rates characterise the EOT, reflecting the high number of extinctions, although diversity loss is not comparable to the severe mass extinction events and the EOT lies at the high end of the spectrum of background extinction rates (Bown, 2005b).

6.4.3 Selectivity of different groups

Expedition 342 species richness is principally driven by highly diverse select groups, most notably the reticulofenestrids, coccolithaceans, rhabdoliths and pontosphaerids, with intervals of moderately high richness in the helicosphaerids and holococcoliths. The grouped taxa species richness records highlight distinct patterns across the interval with contrasting trends in groups of different ecological preference. The reticulofenestrids are the only group to show an increase in diversity through the interval suggesting that adaption to cooler, meso/eutrophic conditions and opportunistic behaviour was advantageous as climate cooled, ocean circulation was invigorated and seasonality increased (Diester-Haass and Zachos, 2003; Lear et al., 2008; Miller et al., 2009). These environmental changes most likely led to an increasing range of mixed layer habitats, including both warm and cool water eutrophic conditions which were effectively exploited by the reticulofenestrids and led to increasing diversity. The increase in reticulofenestrid species richness was stepped and in particular at the appearance of the *Reticulofenestra reticulata* group from 42.48 Ma and the *Reticulofenestra bisecta* group from 40.57 Ma, during the MECO (see Chapter 3).

Warm water taxa decrease in diversity through the interval, suggesting that the warm, oligotrophic habitats which supported the highest diversities of these taxa, were shrinking during this time. The greenhouse to icehouse transition was climatically and oceanographically dynamic, recording persistent global ocean cooling over a 17 million year interval (Zachos et al., 2008) which would have led to long term reduction of habitat space for these taxa, with intensified surface water cooling and increasing eutrophy across the EOT eventually driving extinction. Accelerated diversity loss in the early Oligocene is identified within the warm temperate taxa, indicating that the significant environmental change also forced these taxa beyond a critical threshold and drove them into decline. The response in this warm temperate group likely represents a response to the intensified surface water cooling from the EOT, as these taxa exhibit mesotrophic preferences and would presumably have been able to adapt to higher productivity conditions of the early Oligocene. The relatively stable species richness record seen in the cool water group indicates that in the middle Eocene, although low in abundance, these species were already present within the assemblages. The middle Eocene therefore represents an interval when both warm and cool water groups were present, previously referred to as an evolutionary ecotone in an analysis of Paleogene foraminiferal diversity (Bown et al., 2004; Hallock et al., 1991), and is another reason for the highest diversities that characterize this interval.

6.4.4 Palaeoclimatic control on Paleogene nannofossil diversity

Evolution is controlled by the interplay of biotic (species competition, etc.) and abiotic (temperature, nutrients, etc.) factors but the relative contributions of these variables is often difficult to determine, and especially so in the fossil record. The long term Eocene diversity decline is one of the most profound periods of evolutionary change in calcareous nannoplankton history and the close coincidence with trends seen in the very significant climatic and oceanographic change is strongly suggestive of a cause and effect relationship. The protracted global cooling of the Paleogene greenhouse to icehouse transition and its associated effects on the marine habitat, such as more vigorous ocean circulation (Miller et al., 2009), restructuring of global circulation and onset of the Antarctic Circumpolar Current (Scher et al., 2015), increased continental weathering and enhanced productivity and seasonality (Diester-Haass and Zachos, 2003; Salamy and Zachos, 1999; Scher et al., 2011; Wade et al., 2012), are all factors which will have impacted calcareous nannoplankton by varying degrees, and especially those which had evolved and diversified in the warm stable oligotrophic environments of the Mesozoic and early Paleogene (Bown, 2005b).

Here we compare the Expedition 342 nannofossil diversity record with palaeoclimatic proxies in order to look for possible drivers of evolution through this time interval and in particular to determine the causes of the declining species richness through the middle Eocene to early Oligocene time interval. We will use oxygen isotopes as a proxy for palaeotemperature, consider changes in CO_2 using records from boron isotopes, which has been proposed as a forcing parameter of global cooling through the Eocene and discuss changes to stratification through the greenhouse to icehouse interval as possible parameters driving nannoplankton diversity loss.

The link between declining nannofossil diversity and long term Eocene cooling has been highlighted in previous low resolution data compilations, which show diversity broadly tracking oxygen isotope records through this interval (Bown et al., 2004). The maximised species richness record from Expedition 342 provides further support for the relationship between global cooling and diversity with a strong positive correlation (r^2=0.7796) seen between species richness and global oxygen isotope records (Cramer et al., 2009) (Figure 6.8). The relationship is strongest through the middle and late Eocene, with deviation from the trend in the earliest Oligocene, where extremely high isotopic values reflect both intensified global cooling and the growth of continental ice sheets on Antarctica (Lear et al., 2008). The strong correlation between climate proxies (oxygen isotopes) and nannofossil diversity shown here supports a strong abiotic control on assemblage composition and evolution during the Paleogene.

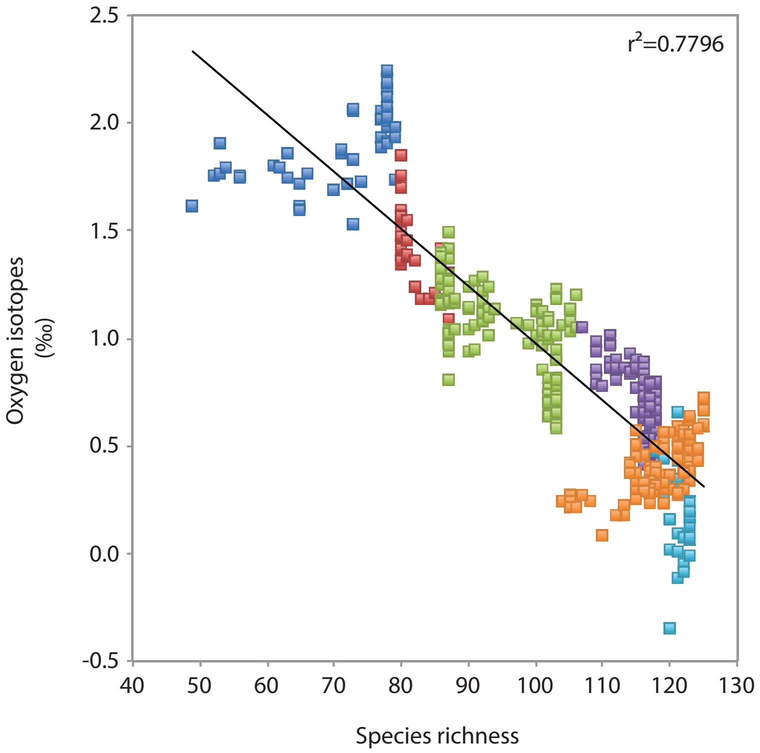

Figure 6.8: Correlation between Expedition 342 nannofossil diversity and a global oxygen isotope compilation (Cramer et al., 2009; converted to GTS12). Colours represent different time intervals; orange – middle Eocene (45.26 to 40.75 Ma), turquoise – MECO (40.73 to 40.10 Ma), purple – late middle Eocene (40.08 to 37.93 Ma), green – late Eocene (37.86 to 33.97), red – EOT (33.96 to 33.67) and blue – early Oligocene (33.66 to 32.51 Ma).

Current CO_2 records through the Eocene are extremely low in resolution, but a significant drop in CO_2 has been identified between ~34.2 and 33.6 Ma (Pearson et al., 2009) and this broadly coincides with the interval of accelerated loss in nannofossil diversity at ~33.9 Ma. Spot records through the middle and late Eocene suggest long term decrease in CO_2 from the middle Eocene through to the early Oligocene (~1100 to 550 ppm - Anagnostou et al., 2016). Henderiks and Pagani (2008) suggest declining atmospheric CO_2 levels limited the diffusive uptake of aqueous CO_2 in larger nannofossil species affecting their growth and photosynthesising ability, which led to smaller species being advantaged during the EOT as CO_2 levels dropped. However, due to the scarcity of data we are unable to correlate or attribute the nannofossil diversity decline to decreasing CO_2, although it must be considered as a potential forcing factor.

Decreasing vertical stratification through the greenhouse to icehouse transition has also been identified as a significant environmental factor at this time with the stable stratified oceans of the early Eocene giving way to more unstable and vertically mixed oceans, with the ‘spinning up’ of the oceans by the early Oligocene (Miller et al., 2009). Changing vertical water column structure as well as increased latitudinal thermal gradients are considered to cause changing evolutionary patterns within plankton groups (Lipps, 1970) and in particular calcareous nannoplankton species are shown to be highly sensitive to surface water stratification in the modern day (Dunkley Jones et al., 2008). Schneider et al. (2011) suggest early Eocene turnover within the nannoplankton group was related to destratification, providing independent evidence for the influence of this factor on Paleogene nannoplankton. Further, the declining diversity within photosymbiotic planktonic foraminifera through the Eocene has also been linked with changing thermal and nutrient stratification (Moore et al., 2014).

The long term loss of warm water taxa and declining abundances of warm temperate species through the early Oligocene as cool water favouring, meso/eutrophic reticulofenestrids sustain high species richness suggest that the changes in surface water environments, the initiation of cold polar oceans and increases in productivity, were favoured by opportunistic nannofossil taxa. The contraction of warm oligotrophic regions drove range retractions in many warm water favouring taxa and ultimately their extinction, particularly evident in the southern high latitudes with the loss of *Discoaster* and *Coccolithus formosus* from Southern Ocean assemblages ~5-6 myr earlier than the global extinction ages of these taxa (Persico et al., 2012; Villa et al., 2008). Ezard et al. (2011) assessed the interplay of biotic and abiotic factors in the macroevolutionary dynamics of planktonic foraminifera and identified that species’ ecological preferences had a strong control on diversity. The decline in calcareous nannoplankton from the middle Eocene coincided with a similar pattern of diversity in the planktonic foraminifera, with a loss of thermophilic species and increase in opportunistic taxa also identified in this zooplankton group (Boersma and Premoli Silva, 1991; Ezard et al., 2011). This suggests an overarching abiotic control on evolution and diversity in these calcareous plankton groups. A rise in the diversity of oceanic diatoms in the late Eocene, identified particularly in the endemic high latitude taxa and within high productivity areas (Lazarus et al., 2014), suggests an expansion of habitats for this siliceous phytoplankton group, which were better adapted to the emerging icehouse conditions, and especially cooler and/or nutrient rich waters. The loss of calcareous plankton as the diatoms proliferated does not necessarily reflect outcompetition by the siliceous group, but highlights the overall ecological preferences of each plankton group.

6.5 Summary

In this chapter we have documented the first high resolution long term record of Paleogene calcareous nannoplankton diversity from the middle Eocene, where Cenozoic nannofossil species richness reached its peak, through the long term diversity decline in this group to the early Oligocene. The Expedition 342 sites, situated at mid to high latitudes in the North Atlantic with exceptionally preserved nannofossils, provide a complete assemblage and allow for an extremely accurate representation of nannofossil diversity through this interval. We record a gradual decline in species richness through the middle to late Eocene with accelerated loss from the EOT, driven by low speciation and high extinction rates, which is in keeping with global trends. Species ecology appears to play a key role in the pattern of species richness records with the opportunistic reticulofenestrids increasing whilst all other groups decline and palaeoecological groups display a decline in warm and warm temperate taxa with diversity values remaining stable in cold water taxa. We highlight a strong correlation between our nannofossil diversity records and the global isotope compilation implying palaeoclimatic cooling was a significant control on declining diversity, however we cannot rule out other environmental parameters until higher resolution proxy data is obtained. Similar loss and decline in planktonic foraminifera strongly suggests an abiotic control on these plankton groups and increasing diversity in oceanic diatoms indicates this siliceous phytoplankton group were better adapted to the cooler, more eutrophic conditions proliferating from the early Oligocene.

Chapter 7

Middle Eocene to early Oligocene calcareous nannoplankton population trends: a proxy for long term surface water palaeoenvironmental change in the North Atlantic

7.1 Introduction

The Eocene epoch saw the transition from greenhouse to icehouse climate modes, during which terrestrial and marine environments were subjected to major physical, chemical and biological change. Peak Paleogene temperatures were reached during the Early Eocene Climatic Optimum (53-51 million years ago (Ma); EECO) followed by long term (17 million years (myr)) cooling, interspersed with short but significant pulses of warming and cooling (Villa et al., 2008; Zachos et al., 2008, 2001). Two prominent climate events, the Middle Eocene Climatic Optimum (MECO) and Eocene-Oligocene transition (EOT) exhibit extensive biotic and/or climatic change over short timescales and have attracted a high level of focus in palaeoclimatic and palaeoceanographic studies. Other events, such as the biotic Middle/Late Eocene Turnover (MLET; Kamikuri and Wade, 2012) and the late Eocene warming event (Bohaty and Zachos, 2003) display significant geochemical perturbation and biotic response but are relatively unstudied due to the lower magnitude of climatic change and recent discovery.

Calcareous nannoplankton provide a useful tool for reconstructing past surface water environments due to their abundant, widespread fossil record and well-established palaeoecological preferences for certain species and groups. Previous Paleogene work has tended to focus on high resolution quantitative analysis over critical climate change intervals that are of relatively short duration, e.g., the PETM (Bralower, 2002; Gibbs et al., 2006), MECO (Chapter 3, Toffanin et al., 2011) and EOT (Chapter 4 and 5, Dunkley Jones et al., 2008). However, the record of longer-term population dynamics is much less well known despite these intervals representing the majority of Earth's history. For the Paleogene there are a number of long term nannoplankton assemblage studies (Gibbs et al., 2012; Schneider et al., 2011; Shamrock and Watkins, 2012; Villa et al., 2008) revealing intriguing links between environmental change and population trends. Nevertheless, temporal resolutions are generally relatively low, particularly in the northern hemisphere and further research is required to build on these studies to establish the global response in nannoplankton across the greenhouse to icehouse transition, which will help to constrain surface water palaeoenvironmental change through this key interval. Here we present the first high resolution population record from the northern high latitudes focussed on the middle Eocene to early Oligocene interval, incorporating the MECO and EOT transient events as well as the intervening intervals of less prominent environmental change. The temporal resolution is sufficient to capture relatively short environmental change and the standard of preservation is such that we are confident that these represent highest quality data.

7.2 Materials and methods

7.2.1 IODP Expedition 342: Sites U1408 and U1411

In order to study this relatively long time interval at high resolution we have used two closely located sites, Integrated Ocean Drilling Program (IODP) Sites U1408 and U1411, which provide a near-continuous composite middle Eocene to early Oligocene section (Site U1408 – middle to late Eocene; Site U1411 – late Eocene to early Oligocene). The sites were drilled during IODP Expedition 342 on the Southeast Newfoundland Ridge in the Northwest Atlantic (Figure 7.1) and comprise predominantly clay-rich nannofossil ooze drift sediments deposited above the CCD at bathyal mid-depth (~2600-2850 mbsl). These sections are ideal for a study of this kind as they were deposited relatively rapidly, providing an expanded stratigraphic record, and the clay-rich lithologies and shallow burial depths have resulted in exceptionally good nannofossil preservation. The composite section runs from sample 1408B-24X-5W, 123-124 cm to 1408B-5H-3W, 63-64 cm (228.62 to 32.88 mcd) at Site U1408 and 1411B-28X-7H, 22 cm to 1411B-12H-6W, 135-136 cm (273.25 to 107.87 mcd) at Site U1411. There is a minor core gap of ~570 kyr (17.8 m) between samples 1411C-15X-1W, 10-11 cm to 1411B-20H-4W, 96-97 cm. We use revised shipboard age models (based on bio- and magnetostratigraphic datums; Chapter 2) which indicate that the samples range from 45.26 to 32.51 Ma in age. Sample spacing is at 30-35 kyr across the background intervals, 17 kyr across the MECO (39 to 41.5 Ma) and 10 kyr across the EOT (33.5 to 34 Ma), providing appropriate temporal resolution relative to the rate of climatic change for each interval.

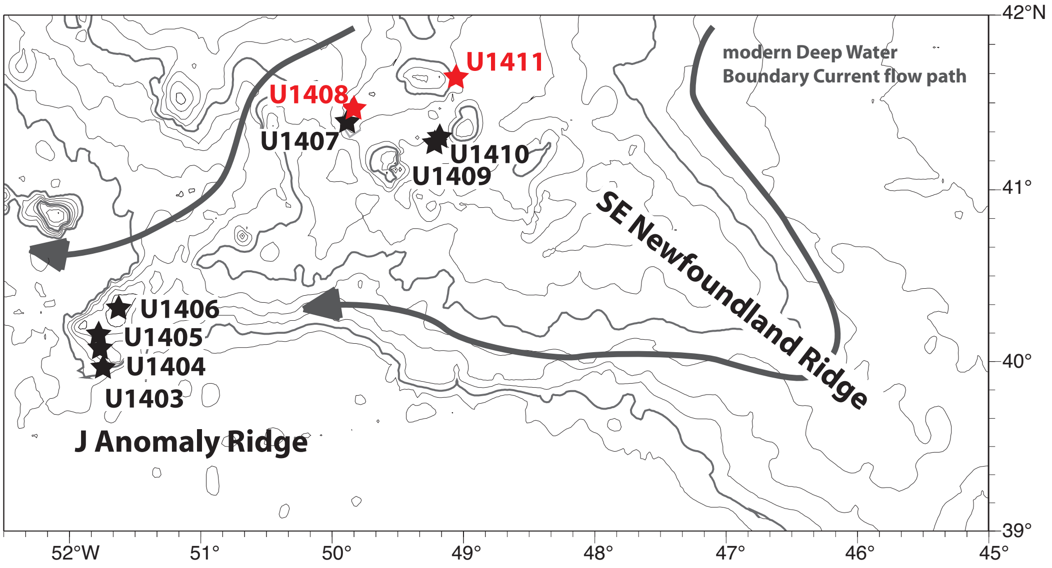

Figure 7.1: Location map of Sites U1408 and U1411 from Expedition 342 in the Northwest Atlantic Ocean. Modified from Norris et al. (2014).

7.2.2 Data collection

430 samples have been prepared as smear slides using standard procedures (Bown and Young, 1998). Samples were analysed using an Olympus BX40 microscope at 1000x magnification using transmitted light microscopy under cross polarized, bright field and phase contrast light. Simple abundance counts were performed, counting a minimum of 300 specimens across a random traverse of each slide, with extended counts excluding the dominant species (small reticulofenestrids <5 µm and *Coccolithus pelagicus* <5 µm at Site U1408, and *Reticulofenestra minuta* at Site U1411) and counting all other species until they totalled a minimum 300 specimens. All count data have been converted into relative abundances to account for the differences in sample size. The dominant small reticulofenestrids have been removed from grouped plots (*R. umbilicus* group and *Cyclicargolithus*) and from the cumulative plot as these small taxa dampen the trends recorded in the larger specimens. Additional data presented from Goban Spur (ODP 549) and Exmouth Plateau (ODP 762) as comparison study sites to our Expedition 342 data has been provided by Leah LeVay (pers. comm. 2016) and is presented in Schneider et al. (2011).

7.2.3 Palaeoecological analysis

Calcareous nannofossil palaeoenvironmental groupings and indices have previously been used as proxies for surface water change during the Paleogene (Gibbs et al., 2006; Persico and Villa, 2004; Villa et al., 2008). This approach sums the abundances of taxa with diagnostic palaeoecological preferences (e.g. warm water oligotrophs or cool water eutrophs), which have been determined primarily from biogeographic studies (Haq and Lohmann, 1976; Wei and Wise, 1990) and comparison with palaeoenvironmental proxies, such as oxygen isotope records (Villa et al., 2008). The palaeoecological preferences applied here are based on previous work (Fioroni et al., 2015; Gibbs et al., 2006; Schneider et al., 2013; Villa et al., 2014, 2008; Wei and Wise, 1990) and our own observations (see Chapters 3, 4 and 5; Newsam et al., in press). The groups used are: 1. warm water oligotrophs – *Discoaster, Sphenolithus, Umbilicosphaera protoannula, Umbilicosphaera bramlettei, Coccolithus formosus*; 2. warm temperate mesotrophs – *Reticulofenestra bisecta, Reticulofenestra reticulata, Coccolithus pelagicus*; 3. cold water taxa – *Chiasmolithus, Clausicoccus subdistichus, Isthmolithus recurvus, Reticulofenestra lockeri* group; and 4. eutrophic taxa - *Reticulofenestra dictyoda, Reticulofenestra umbilicus, Cyclicargolithus floridanus* (>5 µm), *Sphenolithus predistentus.* Further to this we apply a palaeoenvironmental index (PEI) which integrates the records of these palaeoecological groups.

$$PEI = \frac{(cold\ water + eutrophs)}{(cold\ water + eutrophs + warm\ temperate\ mesotrophs + warm\ oligotrophs)}$$

7.2.4 Shannon H and Evenness

The Shannon H index and Evenness are diversity metrics which provide an indication of changing assemblage structure incorporating both occurrence (species richness) and abundance data. Shannon H is calculated from the equation $H = -\sum p_i \ln p_i$ (where p_i represents the proportion of individuals found in the ith species) and Evenness is calculated by $E = e^H/S$ and measures the distribution of species within a sample, where 1 represents all species in equal proportions and 0 represents one species dominating the assemblage. For Shannon H and Evenness the relative abundance records were re-summed to 100 % after the removal of unidentified and reworked specimens.

7.3 Results

Calcareous nannofossils are very abundant within all the samples and good to exceptionally well preserved with extremely high species richness (125 to 49) throughout the study section (Chapter 6). The relative abundance data is relatively noisy undoubtedly reflecting natural variability, however Milankovitch forcing may be accountable for some variability within the records, although in this study we focus only on the longer term trends. Reticulofenestrids (*Reticulofenestra* 66 % and *Cyclicargolithus* 13 %) dominate the assemblages throughout the middle Eocene to early Oligocene (Figure 7.2). The small reticulofenestrids (*Reticulofenestra minuta* and *Cyclicargolithus floridanus* (<5 µm)) are dominant throughout (~45 %) with highest abundances in the latest middle Eocene and EOT (66 and 69 %). *Reticulofenestra* has been split into key groups of taxa (groupings taken from Chapter 2) with *R. minuta* removed from the *R. umbilicus* group due to its exceptionally high abundance. The *R. umbilicus* group are highly abundant throughout the interval (~25-30 %) and increase to higher values, up to 50 %, in the early Oligocene (from ~33 Ma), primarily the smaller *Reticulofenestra dictyoda* (3-8 µm) (Table 7.1). Two intervals record a decrease in this group, ~38 to 37 Ma and across the EOT (particularly in larger specimens of *R. dictyoda* 8-14 µm), where average values are less than 20 %. The *Reticulofenestra lockeri* group and *Cyclicargolithus* >5 µm record a rapid increase across the EOT, from ~2 to 10 % and ~4 to 40 %, respectively.

Coccolithus also comprise a large component of the assemblages (9 %), with other coccolithaceans, *Umbilicosphaera* and *Clausicoccus*, contributing significant proportions in the middle Eocene and early Oligocene, reaching peaks of 5 and 9 %, respectively (Figure 7.3). *Chiasmolithus, Calcidiscus* and *Cruciplacolithus* are rare with highest abundances in the middle Eocene decreasing through the late Eocene (2.4 to 0.2 %, 1 to 0.15 % and 1 % to 0.2 %, respectively). The relatively fragile taxa, *Helicosphaera* and *Pontosphaera*, are consistently present but very low in abundance (~0.5 % and 0.74 % on average), whereas *Blackites* are a significant component of middle Eocene assemblages (10.5 %), declining in abundance through the interval to low abundance in the early Oligocene (1 %) (Figure 7.3). Nannoliths have low abundances at these sites – *Discoaster* ~3 % in the middle Eocene, peaking at 4.3 % at the MECO, to 0.5 % in the early Oligocene; and *Sphenolithus* maintains an average abundance of ~1.6 %. Holococcoliths are rare (4.3 % to 0.3 % middle Eocene to early Oligocene) and primarily represented by *Zygrhablithus bijugatus* (Figure 7.3).

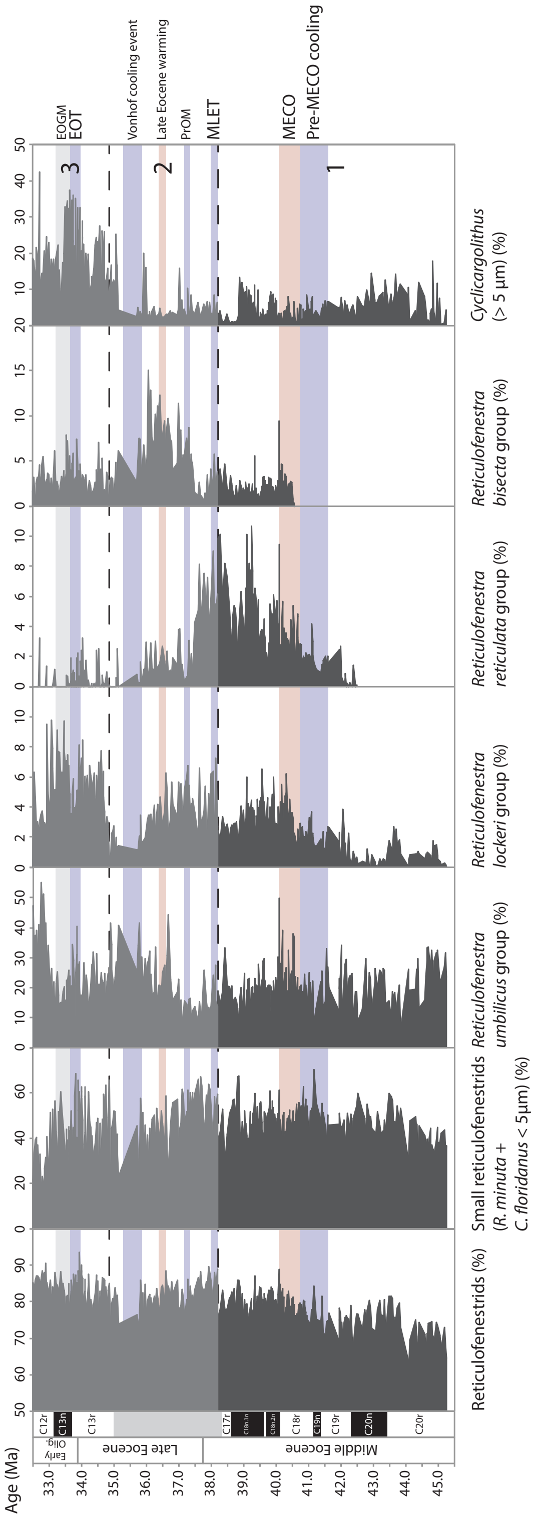

Figure 7.2: Middle Eocene to early Oligocene relative abundance data for the reticulofenestrids from the Expedition 342 sites. Dark grey = Site U1408, light grey = Site U1411. 1: Middle Eocene stability, 2: Late Eocene transitional phase, 3: EOT and early Oligocene population restructuring. Key palaeoclimatic events (converted to GTS12) are shown as red (warming), blue (cooling) and grey (glacial) bands. Magnetostratigraphy is taken from Expedition 342 shipboard records.

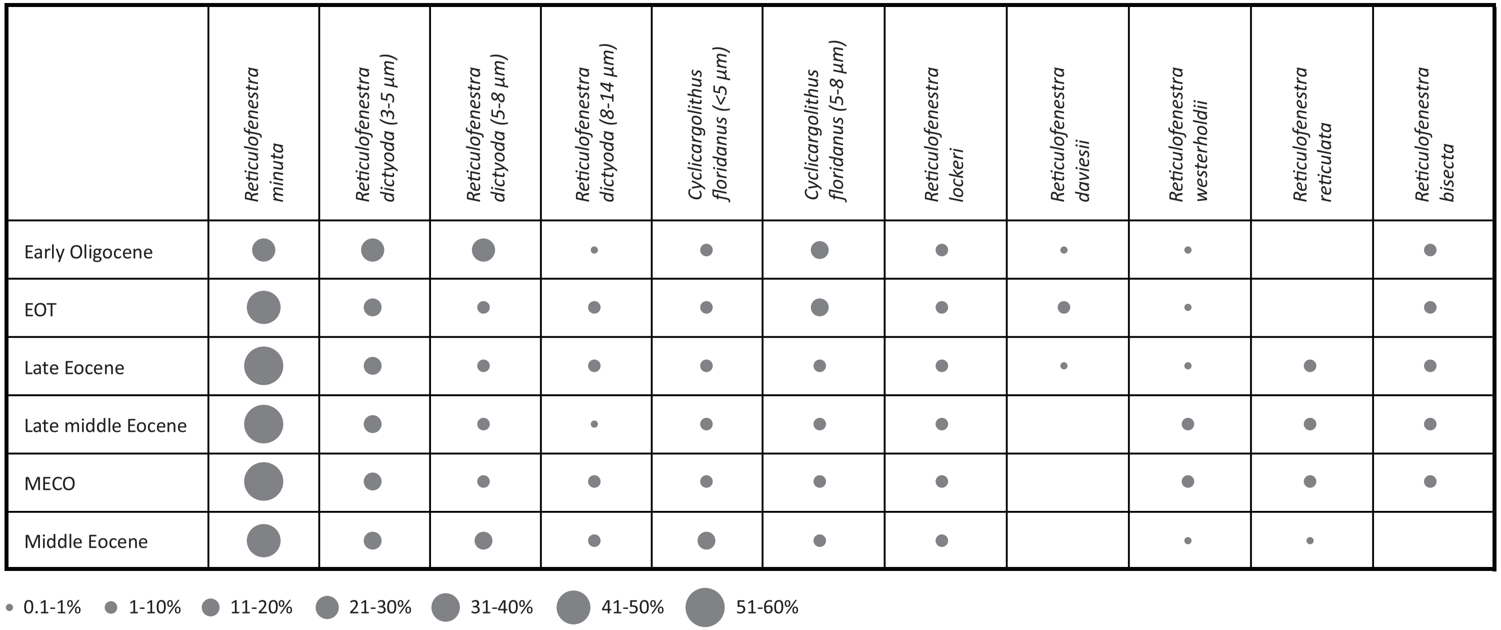

	Reticulofenestra minuta	*Reticulofenestra dictyoda (3-5 µm)*	*Reticulofenestra dictyoda (5-8 µm)*	*Reticulofenestra dictyoda (8-14 µm)*	*Cyclicargolithus floridanus (<5 µm)*	*Cyclicargolithus floridanus (5-8 µm)*	*Reticulofenestra lockeri*	*Reticulofenestra daviesii*	*Reticulofenestra westerholdii*	*Reticulofenestra reticulata*	*Reticulofenestra bisecta*
Early Oligocene	21-30%	21-30%	21-30%	0.1-1%	1-10%	11-20%	1-10%	0.1-1%	0.1-1%		1-10%
EOT	41-50%	11-20%	1-10%	1-10%	1-10%	11-20%	1-10%	1-10%	0.1-1%		1-10%
Late Eocene	51-60%	11-20%	1-10%	1-10%	1-10%	1-10%	1-10%	0.1-1%	0.1-1%	1-10%	1-10%
Late middle Eocene	51-60%	11-20%	1-10%	0.1-1%	1-10%	1-10%	1-10%		1-10%	1-10%	1-10%
MECO	51-60%	11-20%	1-10%	1-10%	1-10%	1-10%	1-10%		1-10%	1-10%	1-10%
Middle Eocene	41-50%	11-20%	11-20%	1-10%	11-20%	1-10%	1-10%		0.1-1%	0.1-1%	

Table 7.1: Relative abundance of key reticulofenestrid species from Expedition 342 sites across the middle Eocene to early Oligocene.

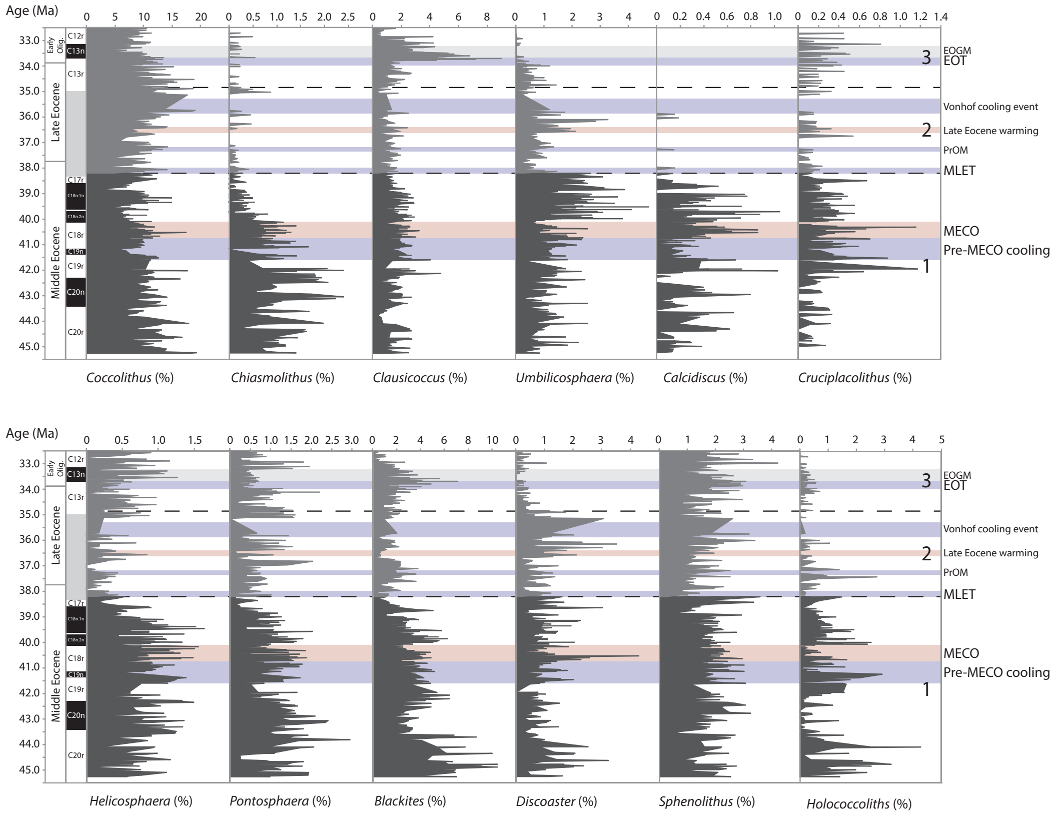

Figure 7.3: Middle Eocene to early Oligocene relative abundance data for key nannofossil groups from the Expedition 342 sites. Dark grey = Site U1408, light grey = Site U1411. 1: Middle Eocene stability, 2: Late Eocene transitional phase, 3: EOT and early Oligocene population restructuring. Key palaeoclimatic events (as detailed in the text, converted to GTS12) are shown as red (warming), blue (cooling) and grey (glacial) bands. Magnetostratigraphy is taken from Expedition 342 shipboard records.

In other taxa a number of major shifts are seen across the study interval (Figure 7.4), with some species declining in abundance (*Coccolithus formosus* – 2.5 to 0.15 %, *Zygrhablithus bijugatus* - 4 to 0.22 %), others increasing (*Reticulofenestra daviesii* – 0.1 to 5 %, *Clausicoccus subdistichus* – 1.5 to 7.2 %) and some taxa displaying peaks in abundance (*Bramletteius serraculoides* – 1.65 % at 39.14 Ma). Some taxa have relatively stable abundances throughout (e.g. *Sphenolithus moriformis*), but the majority display some degree of variability most likely reflecting evolutionary and/or environmental change.

The palaeoecological groups display distinct trends which broadly mirror known patterns in long term climatic change (Figure 7.5). The warm water oligotrophs, although relatively rare overall, decrease in abundance across the interval from 9 to 0.95

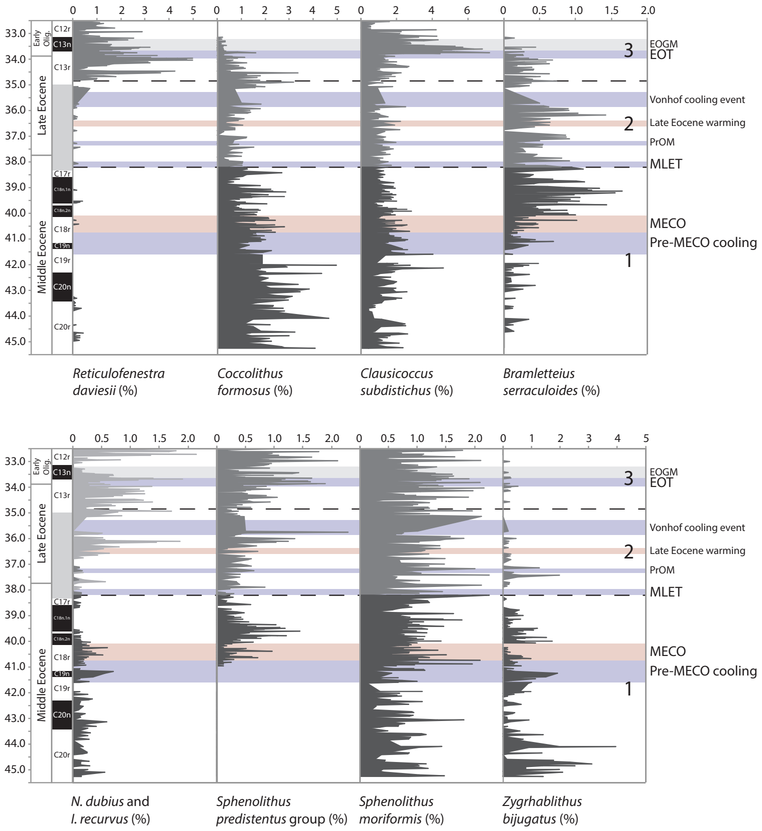

Figure 7.4: Middle Eocene to early Oligocene relative abundance data for key nannofossil species from Expedition 342 sites. Dark grey = Site U1408, light grey = Site U1411. *Neococcolithes dubius* shown in standard colours, *Isthmolithus recurvus* shown in very light grey. 1: Middle Eocene stability, 2: Late Eocene transitional phase, 3: EOT and early Oligocene population restructuring. Key palaeoclimatic events (as detailed in the text, converted to GTS12) are shown as red (warming), blue (cooling) and grey (glacial) bands. Magnetostratigraphy is taken from Expedition 342 shipboard records.

%, with a staggered decline. The records highlight an average of 5 % maintained through the middle Eocene with a decrease through the MECO of ~2 %. There is a large decrease from 9 to 1 % from 38.21 Ma followed by a slight increase over 1.8 myr to ~7 % at 36.15 Ma. Following a final peak in richness at 34.89 Ma there is decline to ~ 1 % by the early Oligocene. Warm temperate mesotrophs display a broad increase from ~7% in the middle Eocene to a peak of 27 % in the late Eocene at 36.42 Ma. This is followed by a decline to ~11 % by 34.81 Ma which maintains through the EOT and early Oligocene. Cold water taxa have relatively low abundances in the middle Eocene but increase from ~2.5 % to 9 % by 40.32 Ma and these values are sustained through the middle and early late Eocene. There is a decrease from 36.05 Ma to <4 % until 34.84 Ma then a series of pulsed increases to 14 % by the earliest Oligocene. Eutrophs are abundant throughout the interval ranging from 23 to 67 % but show stable abundance of

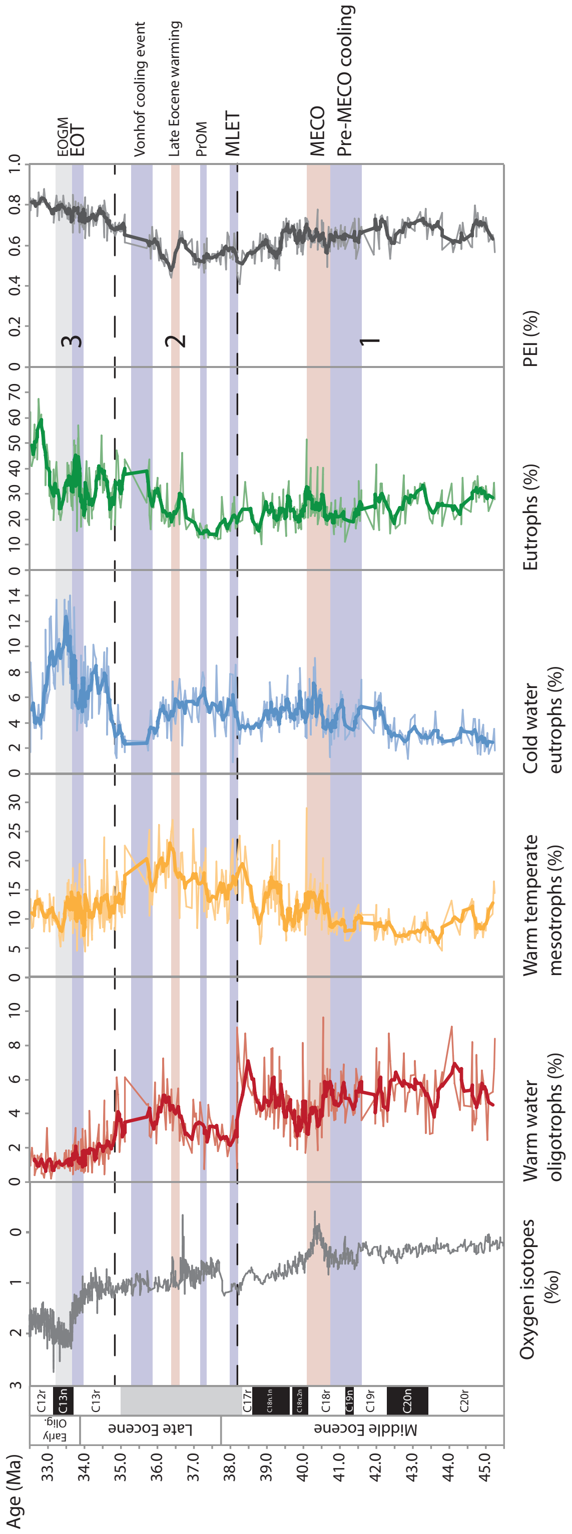

Figure 7.5: Palaeoecological groups and the palaeoenvironmental index plotted against a global oxygen isotope compilation (Cramer et al., 2009; converted to GTS12). 1: Middle Eocene stability, 2: Late Eocene transitional phase, 3: EOT and early Oligocene population restructuring. Key palaeoclimatic events (converted to GTS12) are shown as red (warming), blue (cooling) and grey (glacial) bands. Magnetostratigraphy is taken from Expedition 342 shipboard records.

~25 % in the middle Eocene, increasing from ~37 Ma, with a series of stepped increases from ~35 Ma across the EOT and early Oligocene to peak abundance of 67 % at 32.76 Ma. The palaeoenvironmental index indicates consistently highly eutrophic assemblages, on average 0.67, peaking in the early Oligocene to 0.88.

Shannon H and Evenness do not show a high degree of change across the greenhouse to icehouse transition at these sites (Figure 7.6). Shannon H values remain, on average, between ~1.7 and 2.2, with values increasing from 1.86 to 2.23 (by 39.08 Ma) in the middle Eocene, followed by a sudden decrease to 1.81 by 38.65 Ma. They remain at ~1.85 through the late Eocene with a final decrease to 1.67 by the early Oligocene. Evenness maintains an average of 0.2 throughout the middle Eocene, indicating an assemblage dominated by a few species but from ~37.24 Ma the Evenness increases and is highly variable from ~35 Ma, reaching on average 0.3 by the top of the interval, implying species proportions become more even through the late Eocene and EOT interval.

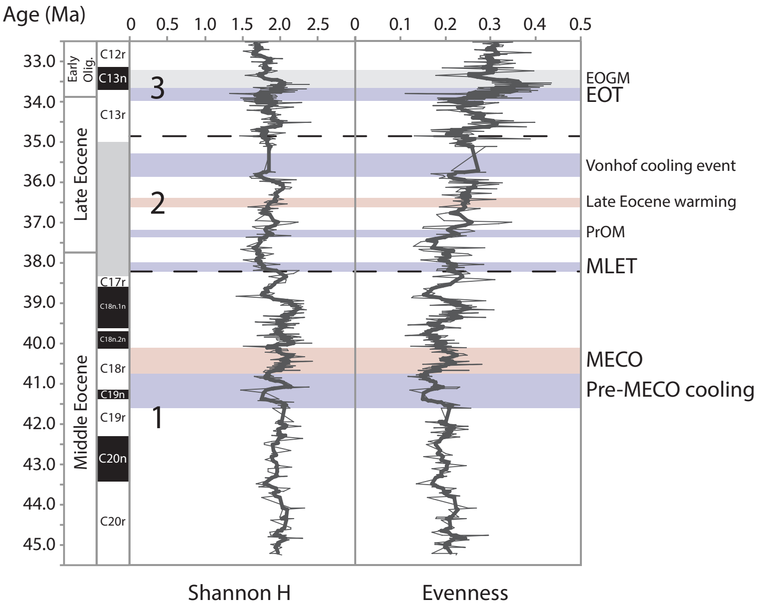

Figure 7.6: Shannon H and Evenness through the middle Eocene to early Oligocene at the Expedition 342 sites. 1: Middle Eocene stability, 2: Late Eocene transitional phase, 3: EOT and early Oligocene population restructuring. Key palaeoclimatic events (converted to GTS12) are shown as red (warming), blue (cooling) and grey (glacial) bands. Magnetostratigraphy is taken from Expedition 342 shipboard records.

7.4 Discussion

7.4.1 Global calcareous nannoplankton assemblage data from long time series

Long time series population records can provide a quantitative evaluation of biotic variability which helps to elucidate surface water palaeoenvironmental change. Moreover the assessment of assemblage data from a number of geographically distinct localities can suggest overarching global controls relating to palaeoclimatic and oceanographic evolution. Through the Paleogene greenhouse to icehouse transition data is limited and relatively low resolution in many sections. Nevertheless previously published assemblage data has shown comparable population structure at generic level across similar latitudinal zones through the Eocene, although distinct differences are evident between low, mid and high latitude sites from low resolution records (Schneider et al., 2011). A comparison between our high resolution Expedition 342 data to lower resolution records from other Eocene sites from a similar latitudinal zone, such as Goban Spur (DSDP 549 – North East Atlantic) and Exmouth Plateau (ODP 762 – Indian Ocean) (Schneider et al., 2011) highlights remarkable similarities with high abundance of reticulofenestrids, a significant component of *Coccolithus* and low abundances of the warm water oligotrophs, such as *Discoaster, Sphenolithus* and *Coccolithus formosus* (Figure 7.7). A distinct signal recorded at all these temperate sites is the increasingly high abundance of the warm temperate mesotroph *Reticulofenestra bisecta* from ~37 Ma to peak abundance. There are some minor discrepancies between sites with a higher percentage of *Cyclicargolithus* at the Expedition 342 sites, compared to Goban Spur, but this likely reflects the specifics of the site locality, with the Expedition 342 sites lying in the path of the warm, nutrient rich Gulf Stream, which may have led to higher abundances of this group. A similar explanation may also account for the similarly high abundances of *Cyclicargolithus* at Exmouth Plateau. *Zygrhablithus bijugatus* comprises a much higher percentage of the assemblages at Goban Spur and Exmouth Plateau, but this likely represents a preservational difference between the sites (LeVay, pers. comm. 2016). Although a holococcolith, *Z. bijugatus* is prone to overgrowth a forms large single crystals which are subsequently extremely resistant to dissolution. When preservation is moderate and both overgrowth and dissolution modified assemblages, as is typical in many deep-sea oozes, *Z. bijugatus* is frequently preferentially concentrated and increases substantially in relative abundance. The higher proportion of 'other taxa' at Expedition 342 sites is also most likely due to the better preservation at this locality, conserving higher abundances of *Blackites, Umbilicosphaera, Clausicoccus, Helicosphaera* and *Pontosphaera* and reflected in the contrasting quantitative diversity records at each site (57 species at the Expedition 342 sites, 27 species at Goban Spur and 26 species at Exmouth Plateau (LeVay, pers. comm. 2016).

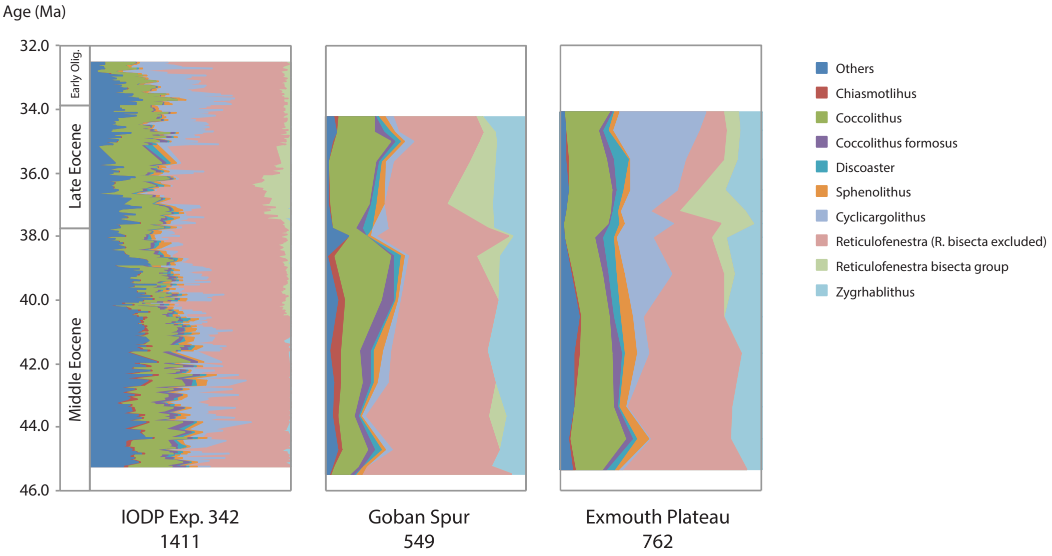

Figure 7.7: Cumulative relative abundance data of key nannofossil groups from temperate sites (IODP Expedition 342 – this study; Goban Spur and Exmouth Plateau – Schneider et al., 2011, converted to GTS12) across the middle Eocene to early Oligocene. Small reticulofenestrids <5 µm have been removed from the Expedition 342 plot as discussed in the methods section.

By contrast to these mid latitude sites, low latitude sites (Shatsky Rise – ODP 1210; Walvis Ridge – 1263) record the highest percentages of discoasters and sphenoliths and lowest abundances of reticulofenestrids (Schneider et al., 2011) although abundances of *Cyclicargolithus floridanus* (ODP 711; Fioroni et al., 2015) can be comparable to the mid latitudes. On the other hand, the southern high-latitude polar sites (Kerguelen Plateau – ODP 1135/1137 and ODP 748B; Maud Rise – ODP 689/690) have assemblages dominated by extremely high percentages of *Reticulofenestra* and display much higher abundances of *Chiasmolithus,* reflecting the cooler conditions at these sites (Schneider et al., 2011; Villa et al., 2008). Distinct trends at generic level from tropical, temperate and polar sites reflect surface ocean palaeoenvironmental conditions at different latitudinal zones.

7.4.2 Expedition 342 long time series population data

Grouped generic level records provide an overview of assemblage dynamics through long time series, yet to determine surface water palaeoenvironmental conditions in the North Atlantic through the middle Eocene to early Oligocene more comprehensive analysis is required. At the Expedition 342 sites the dominance of the reticulofenestrids, particularly *Reticulofenestra minuta,* the moderate abundance of *Coccolithus* and high values of the palaeoenvironmental index are all indicative of a meso/eutrophic photic zone throughout the study interval, with low abundances of oligotrophic taxa, such as *Discoaster* and *Sphenolithus,* further supporting this interpretation. Warm water taxa decrease as cold water taxa increase and the warm temperate mesotrophs increase to peak abundance in the late Eocene. Within the warm temperate group, different taxa dominate at different times, with *Reticulofenestra reticulata* reaching overall highest abundance at 38.27 Ma, followed by *R. bisecta* (36.05 Ma) and then *C. pelagicus* (35.13 Ma). These taxic shifts alongside the significant long term diversity decline are not however reflected in the Shannon H index, suggesting this is not the best metric to reflect changes in assemblage structure through this interval. This may be due to the high level of population restructuring, i.e. species replacing one another but diversity remaining relatively constant, although relatively low values of evenness do reflect the consistent dominance of small reticulofenestrids from the middle Eocene until the late Eocene. Grouped and species data (Figures 7.2, 7.3 and 7.4; Table 7.1) therefore provide a more comprehensive expression of changes to nannofossil assemblages through this interval.

7.4.2.1 Restructuring of the reticulofenestrids

The reticulofenestrids are the dominant Paleogene coccolithophore group following their origination in the early Eocene (~55 Ma) and they dominate the nannofossil assemblages at Sites U1408 and U1411 throughout the middle Eocene to early Oligocene (Figure 7.2). Although considered opportunistic as a group, the different groups within the reticulofenestrids, the *Reticulofenestra umbilicus, Reticulofenestra lockeri, Reticulofenestra reticulata*, *Reticulofenestra bisecta* and *Cyclicargolithus* groups show distinct patterns in their abundance (Figure 7.2; Table 7.1). Each group likely favoured a distinct environmental niche that accounts for the significant restructuring within the reticulofenestrids through this interval of dynamic climatic and oceanographic change. The *Reticulofenestra umbilicus* group are the most dominant (minus the small reticulofenestrids), with consistently moderate to high abundances throughout. They are considered to have a cool temperate water, meso/eutrophic preference (Villa et al., 2014, 2008) allowing this group to prevail in the surface water conditions at the Expedition 342 sites. The *Reticulofenestra reticulata* and *Reticulofenestra bisecta* groups show distinct increases following their first appearances at 42.46 Ma and 40.58 Ma respectively. *R. reticulata* peaks in abundance at 38.27 Ma, where they comprise 10 % of the assemblages and *R. bisecta* peaks at 36.05 Ma at 15 %. These taxa have a warm temperate, mesotrophic preference (Chapter 3; Newsam et al., in press) supported by the origination of both groups during middle Eocene warmth and peaks in abundance through the transient warming of the MECO. The extinction of *R. reticulata* and decline in *R. bisecta* leading into the EOT, further suggests these groups were unable to thrive in the cooler conditions. The *R. bisecta* group did continue into the early Oligocene, likely due to broad temperature tolerance and ability to exploit higher nutrient conditions, but they declined soon after becoming extinct in the late Oligocene (Agnini et al., 2014; Bown and Dunkley Jones, 2012). The more opportunistic reticulofenestrids such as *Cyclicargolithus floridanus* and the *Reticulofenestra lockeri* group, increase and rise to dominance during the late Eocene through to the early Oligocene. The pulsed increases in these eutrophic and cold water groups reflects the accelerated global cooling and ice growth in the emerging icehouse oceanographic conditions (see Chapter 4).

7.4.3 Calcareous nannoplankton response across key palaeoclimatic intervals

Significant calcareous nannoplankton assemblage shifts through the middle Eocene to early Oligocene and, in particular, the distinct trends seen in the palaeoenvironmentally diagnostic groups and taxa at the Expedition 342 sites can be broadly categorised into three key intervals; 1: Middle Eocene stability, 2: Late Eocene transitional phase and 3: EOT and early Oligocene population restructuring. These intervals have been defined by broad trends observed in the abundance data, with middle Eocene stability representing an interval with relatively consistent abundances in the groups and species data, the late Eocene transitional phase marking an interval of highly variable population records with a number of taxa going into decline at the onset of this phase and the EOT and early Oligocene population restructuring documenting major assemblage shifts leading to distinctly different assemblage compositions than recorded in the Eocene. Previous geochemical and biotic records have also identified a number of key warming and cooling events overlain on the long term cooling record through the greenhouse to icehouse transition (Bohaty and Zachos, 2003; Bohaty et al., 2009; Villa et al., 2008). Assessing changes in our calcareous nannofossil records in relation to these events enable us to better understand the link between climatic and biotic response and allow us to interpret palaeoceanographic change in the North Atlantic through this interval.

7.4.3.1 Middle Eocene stability

The nannofossil abundance records from the middle Eocene show an interval of relative stability, with warm water oligotrophs, cold water taxa and eutrophs displaying constant average values and stable PEI values, with only a minor decrease from 39.46 Ma reflecting the gradual increase in warm temperate taxa. Two short term climatic events are known to occur within this interval, the pre-MECO cooling and the MECO.

Pre-MECO cooling

In the pre-MECO phase an interval of cooling has been identified from ~41.5 Ma at equatorial and high southern hemisphere sites (Bohaty et al., 2009; Villa et al., 2008). Edgar et al. (2007) identified cooling of surface and bottom waters in the equatorial Atlantic using geochemical proxy evidence and the prevalence of cool water nannofossil assemblages in the Southern Ocean support the widespread nature of this event (Villa et al., 2014). The Expedition 342 nannofossil records show little response at this time, although an increase and peak (~63 %) in *Reticulofenestra minuta* and minor decreases in the warm and warm temperate taxa, *Coccolithus formosus* and *Coccolithus pelagicus,* are consistent with cooler conditions at this time. This muted response implies the cooling signal was not as strong at this location in the North Atlantic.

MECO

The MECO was a transient reversal in the climate state, with a positive excursion in the oxygen isotope records indicating 4-6°C of surface water warming (Southern Ocean - Bohaty et al., 2009). The lack of response in warm water nannofossils at Site U1408 (discussed in Chapter 3) suggests warming during this interval had little effect on the assemblages or there was a lesser degree of warming at this site, which is suggested by preliminary TEX_{86} records showing only ~2°C increase from pre to peak-MECO (Cramwinckel, pers. comm. 2015). Short peaks in abundance of *Discoaster* (4.29 %, the peak value recorded through the whole transition), *Umbilicosphaera bramlettei* and *Coccolithus formosus* are recorded in the onset of the event, however they are minor components of the assemblages through this interval and overall show declining abundances. The main feature of the MECO assemblages at Site U1408 is the dominance of warm temperate and cool meso/eutrophs (e.g. *Reticulofenestra reticulata* group, *Reticulofenestra dictyoda*) and we attribute this to increased nutrient availability related to influence from the Gulf Stream. A similar response to increased nutrients has been identified at nearby Blake Nose (O'Dea, 2013) and the Alano section (Toffanin et al., 2011). The MECO therefore does not stand out from the long term trend as an exceptional event and suggests nannofossil assemblage dynamics through this interval are similar to background rates of change. These results suggest the lower degree of temperature change recorded at Site U1408 (observed in the preliminary TEX_{86} results) did not past the threshold of climatic perturbation required to promote a significant response in the calcareous nannoplankton, as previous studies have highlighted a certain magnitude of climatic change is required for marine plankton disturbance, particularly in calcareous nannoplankton which are more resilient to environmental change than other plankton groups (Gibbs et al., 2012; Newsam et al., in press).

7.4.3.2 Late Eocene transitional phase

In the late Eocene the nannofossil records display a broad increase in warm temperate mesotrophic taxa and a muted increase in eutrophic taxa but the prominent feature is extreme variability in the records, with fluctuating values in all groups of taxa and the PEI, suggesting significant perturbation of the photic zone environment and reflecting the dynamic nature of the climatic and oceanographic change during this interval. As well as high variability in the abundance records, this transitional phase also sees a major decline of many groups; *Umbilicosphaera, Calcidiscus, Helicosphaera, Pontosphaera* and *Blackite*s at the base of the interval, following stable abundances in the middle Eocene and following this decline many of these groups have relatively inconsistent records. This interval also records the evolution of the cold water taxon *Isthmolithus recurvus*. Moreover, through this interval a number of palaeoclimatic events have been previously recorded. The MLET lies at the beginning of this transitional interval and is followed by some minor warming and cooling events (PrOM, late Eocene warming event, Vonhof cooling event), which have only been recorded in the Southern Ocean to date. We assess our nannofossil records across these intervals with caution, as they may only be a feature of the Southern Ocean, where a higher degree of climatic and oceanographic disruption occurred through the interval.

<u>MLET</u>

The MLET is a short interval of major zooplanktonic turnover and extinction associated with a minor cooling event. It was first identified in the low latitude western North

Atlantic Ocean (Kamikuri and Wade, 2012; Wade, 2004). Due to the low resolution Expedition 342 shipboard foraminiferal biostratigraphy this event is currently hard to place but using the last occurrence of *Morozovelloides* (shipboard age 38.20 Ma, 273.25 mcd) and nannofossil observations from this thesis and other work (Newsam et al., in press) we tentatively place the MLET between 38.20 Ma and 37.98 Ma. The MLET therefore occurs within the interval where our records switch from Site U1408 to U1411. Although these sites are located close to one another there may be slight variations in assemblages between the two localities and so we interpret this interval with caution.

The principal shift across the MLET is recorded at the base of the event with a decline in the warm water group from 9 to 1 %, although these are relatively minor components of the assemblages. *Umbilicosphaera* a component of this group decreases from 2.66 to 1 % contributing to this significant decline in abundances. This may reflect cooler and/or more eutrophic conditions proliferating. Also recorded in this interval is an increase in the cool water *R. lockeri* group, but also peak abundances of the warmer water *R. reticulata* group (at 37.50 to 38.27 Ma), however these may reflect increasing nutrient availability at this time. Although caution should be taken due to the tentative placement of this event, it still stands out as an interval with significant shifts in the warm water group at the onset of the transitional phase.

PrOM

Villa et al. (2014, 2008) identify a middle/late Eocene cooling event in the Southern Ocean (ODP Site 748) at ~37.3 Ma using oxygen isotope records and nannofossil assemblage data, recording a sharp decrease in the temperature index suggesting cooling surface water conditions. Scher et al. (2014) confirm this event at ODP Site 738 and title it the late Priabonian oxygen isotope minimum (PrOM). At the Expedition 342 sites, this interval sees cold water taxa reach ~6.5 % in abundance, comparable to values at the MLET, but they are still low in abundance and the shifts do not clearly stand out above the background noise, which suggests that this event was a Southern Ocean phenomenon or less significant in the Northwest Atlantic, and below the threshold sensitivity required to trigger major shifts in calcareous nannoplankton.

Late Eocene warming event

The late Eocene warming interval was first documented in oxygen isotope records from the Southern Ocean by Bohaty and Zachos (2003). It was subsequently identified in calcareous nannofossil assemblages at ODP Site 748 (Villa et al., 2008). At Site U1411 there are relatively high abundances of the warm temperate *R. bisecta* group across the interval (~12 %), decreasing abundances of the *R. umbilicus* (44 to 21 %) and *R. lockeri* groups (6.3 to 4.7 %) and low values in the palaeoenvironmental index (0.46). This is consistent with warming and may indicate the widespread nature of this warming event, although these shifts are not strongly delineated from background variability. The interval has also been regarded as highly eutrophic (Villa et al., 2014) which while consistent with the high abundance of the mesotrophic *R. bisecta* group at the Expedition 342 sites, is not supported by the rest of our assemblage data.

Vonhof cooling event

Vonhof et al. (2000) identified a cooling event in the Southern Ocean at ~35.5 Ma (Villa et al., 2008) using oxygen isotope analysis which was also associated with a marked productivity increase shown by an increase in fine fraction $\delta^{13}C$ and reflected in a peak in calcareous dinocysts. Further geochemical and nannofossil assemblage records from Maud Rise and Kerguelen Plateau support this cooling event (Bohaty and Zachos, 2003; Villa et al., 2008). In our records this interval corresponds to the coring gap at Site U1411, however it appears to occur during an interval of lowest abundance in cold water taxa and peaks in the warm and warm temperate water taxa, *Discoaster* and *Coccolithus pelagicus,* suggesting this event was limited to the Southern Ocean and was not global in extent.

7.4.3.3 EOT and early Oligocene population restructuring

The final phase marks an interval of significant population restructuring reflected in all groups and species abundance data. From 34.84 Ma there are profound changes, with a decline in warm water taxa following a final peak in this group and the onset of a series of pulsed increases in cold water and eutrophic taxa. This is reflected in the extremely high values of the PEI, with a marked increase to 0.8.

This interval incorporates the EOT and our nannofossil records across this interval are extensively discussed in Chapter 4. In brief the warm water group decreases significantly to very low abundances (<2 %) and many warm water groups and species are lost to extinction (*Reticulofenestra reticulata*, *Umbilicosphaera bramlettei, Umbilicosphaera protoannula*, *Bramletteius serraculoides* and *Coccolithus formosus*). At the same time there are pulsed increases in cold water taxa, such as *Reticulofenestra daviesii* and *Clausicoccus subdistichus* and increases and dominance of eutrophic groups, particularly *Cyclicargolithus floridanus* (>5 µm). The population shifts across the EOT reflect the intensified global cooling and increasing productivity levels

(Chapter 4, Dunkley Jones et al., 2008). The response is striking compared to other transient events within the long term greenhouse to icehouse transition (discussed above) and pre-EOT assemblage compositions are not recovered. This indicates photic zone habitats underwent a profound state change with threshold-type behaviour seen in the nannoplankton driving extinctions and establishing new population structures which are distinct from those of the pre-EOT interval.

7.4.4 Palaeoenvironmental implications from nannofossil population data

The calcareous nannoplankton assemblages at the Expedition 342 sites display clear trends and indicate profound changes in oceanographic conditions in the Northwest Atlantic, with distinct assemblage compositions in the early Oligocene from those recorded in the middle Eocene. The middle Eocene stability, followed by high variability from the late Eocene and subsequently major population restructuring at the EOT and into the early Oligocene indicates a progressive intensification of environmental perturbation through the Paleogene greenhouse to icehouse transition. The relative stability and high diversity (Chapter 6) in the nannofossil populations through the middle Eocene suggest optimal conditions for this phytoplankton group, with the highest percentage of warm water oligotrophs, as well as hosting cold water and eutrophic taxa indicating the North Atlantic was habitable for all nannoplankton groups. Fluctuations in the assemblages during the late Eocene transitional phase reflects a preliminary response in the calcareous nannoplankton assemblages to changing surface water conditions implying a lower limit of perturbation had been reached following ~13 myr of long term cooling from the EECO and also likely reflect the mid to high latitude location of the Expedition 342 sites. The assemblages have an increasing component of warm temperate mesotrophs with a lesser component of warm water oligotrophs than the middle Eocene indicating the surface waters were becoming cooler and more nutrient rich. The severe population restructuring which follows from the EOT indicates a critical threshold in climatic and/or oceanographic conditions had been passed which led to major assemblage response in the calcareous nannoplankton. Pulsed increases in cold water and eutrophic taxa highlight a profound shift in the North Atlantic to cool, higher productivity surface water conditions.

These records suggest calcareous nannoplankton have relatively low sensitivity to minor climatic perturbation and require specific climatic thresholds to be surpassed in order for this group to exhibit a significant response. Particularly notable is the muted response to the global transient warming event, the MECO, suggesting resilience in this phytoplankton group to a lower magnitude of climatic perturbation at the Expedition 342 sites during this interval or due to the MECO lying within the long term cooling trend. Calcareous nannoplankton have previously been shown to exhibit a lower sensitivity than other plankton groups across minor warming and cooling events in the Paleogene (Gibbs et al., 2012; Newsam et al., in press). Major changes in calcareous nannoplankton assemblages therefore provide a strong indication for significant surface water environmental perturbation, as recorded at key Paleogene events with a high magnitude of climatic change such as the PETM (Bown and Pearson, 2009; Bralower, 2002; Gibbs et al., 2006) and the EOT (this thesis; Dunkley Jones et al., 2008).

7.5 Summary

The long time series presented in this chapter provides one of few long term assemblage records through the Paleogene and the first high resolution record from the North Atlantic. These Expedition 342 records compliment previous long term lower resolution work from mid latitude temperate sites, showing comparable assemblage composition. We divide our records into three key intervals. The first, the middle Eocene stability, which records relatively consistent abundances in all species, groups and indices. This is followed by a period of high variability during the late Eocene transitional phase, with fluctuating abundances recorded in taxa but only minor assemblage response to palaeoclimatic events previously noted during this interval. The final stage, the EOT and early Oligocene population restructuring, shows a distinct assemblage response with a significant shift in assemblage composition with a loss of warm oligotrophs and warm temperate mesotrophs as cold water eutrophic taxa proliferate and persist through the glacial conditions of the EOGM. These records suggest a higher degree of climatic and oceanographic perturbation was required to drive this phytoplankton group beyond a critical threshold and suggest that significant assemblage response recorded in calcareous nannoplankton is a useful proxy in determining a high magnitude of surface water environmental change.

Chapter 8

Conclusions

The principal objective of this thesis was to document the timing and structure of diversity loss and population response in calcareous nannoplankton through the Paleogene greenhouse to icehouse climate-mode transition. The stratigraphically expanded sections at the Integrated Ocean Drilling Program (IODP) Expedition 342 sites and the clay-rich nature of the sediments yielding exceptionally preserved calcareous nannofossils have allowed the documentation of high resolution assemblage records which further our understanding of the evolutionary and ecological response in this phytoplankton group through intervals of profound climatic and oceanographic change in Earth's history. The near-continuous sections at Sites U1408 and U1411 covering a wide stratigraphic range allow the two themes of this thesis to be addressed; calcareous nannoplankton response across long time series relative to intervals of transient change.

8.1 IODP Expedition 342

The IODP Expedition 342 sediments utilised in this research are some of the most complete stratigraphically expanded Paleogene sections recovered and provide a new insight into biotic and oceanographic change in the North Atlantic, a relatively understudied locality for Paleogene climatic research. The position of the sites lying within the flow-path of both the Gulf Stream and the Deep Western Boundary Current and their mid to high latitude location means they are well suited to document changes through the middle Eocene to early Oligocene.

The exceptionally preserved calcareous nannofossils in these clay-rich drift sediments from the IODP Expedition 342 sites presented in this thesis (Chapter 2) rival other deep sea records and provide comparable taxonomic records to those documented from the Kilwa Group, Tanzania, providing new sections coeval in age but from a truly oceanic setting. The dominance of small reticulofenestrids, the presence and high diversity of larger fragile taxa (*Helicosphaera, Pontosphaera, Blackites,* holococcoliths) and the morphological characteristics consistently preserved, such as central area grills, bars, crosses and ornamentation on spines highlight the complete nature of the assemblages at the Expedition 342 sites. The high standard of preservation at these sites and previously documented at Tanzania highlight the need to reassess previous estimates of calcareous nannoplankton diversity and assemblage response through the Paleogene.

8.2 Intervals of abrupt climatic change

Two critical abrupt events of climatic change lie within the Paleogene greenhouse to icehouse transition, the Middle Eocene Climatic Optimum (MECO) and the Eocene-Oligocene transition (EOT). High resolution records (10-17 thousand years (kyr)) across these key intervals (Chapters 3 and 4) provide detailed records of calcareous nannoplankton response; determining the precise timing of key bioevents (originations, extinctions and acmes), highlighting diversity patterns and identifying population shifts, in order to examine the relationship between plankton evolution and palaeoecology with the strongly shifting palaeoceanographic conditions in the North Atlantic.

Calcareous nannoplankton record a minor evolutionary and population response to the transient warming at the MECO (Chapter 3), with only minor peaks in abundance of warm water taxa (*Discoaster* spp*.*, *Coccolithus formosus* and *Umbilicosphaera*) at the onset of the event and two key evolutionary events within warmer water taxa (*Reticulofenestra bisecta* group and sphenoliths) suggesting a broader temperature influence. However, the dominant response in the assemblages is the increasing affinity to eutrophic conditions throughout the onset and peak of the event, documented by high and increasing values of the palaeoenvironmental index. Site U1408 appears to have been meso/eutrophic in nature, demonstrated by the high abundance of reticulofenestrids within the assemblages and the addition of nutrients, likely transported downstream by the Gulf Stream, undoubtedly suited this dominant group allowing them to thrive. Previous work has highlighted highly eutrophic calcareous nannoplankton assemblages through the interval as a relatively geographically widespread phenomenon.

The EOT marks a profound transition into the Cenozoic icehouse world with a high degree of climatic and oceanographic change. Major calcareous nannoplankton assemblage response is recorded at Site U1411 across the EOT (Chapter 4) with a distinct diversity decline, elevated rates of extinction and significant population restructuring. The increasing abundance of opportunistic taxa associated with cool and/or eutrophic surface waters (e.g. *Reticulofenestra daviesii, Clausicoccus* *subdistichus*, *Cyclicargolithus floridanus*) whilst warm water oligotrophs (e.g. *Discoaster* spp., *Coccolithus formosus, Umbilicosphaera*) went into decline, with many becoming extinct, suggests a reduction of optimal habitat space for these species through the emerging icehouse conditions in the North Atlantic. The assemblages at Site U1411 suggest a temperature control in the late Eocene, with peaks in eutrophic taxa (*Sphenolithus predistentus* and *Cyclicargolithus floridanus*) following the Eocene-Oligocene boundary (EOB) indicating a strong productivity influence.

A protracted decline in warm water oligotrophs and a step shift increase in cold water eutrophs is a trend displayed in calcareous nannoplankton at all global sites across the EOT, reflecting the widespread nature of intensified cooling and increasing productivity levels (Chapter 5). The succession of step shifts occur within 10-170 kyr of the EOB, an interval also associated with high levels of extinction and turnover in other plankton groups. Disturbance was most prominent close to the EOB and prior to the 'second step', implying plankton groups were sensitive to the initial perturbation of climatic and oceanographic change and suggesting these biota were not well adapted to the emerging icehouse conditions. A latitudinal control on the calcareous nannoplankton assemblages is evident, with nannofossil records from the Southern Ocean showing marked differences to mid and low latitudes, suggesting a higher degree of climatic forcing at this locality. This is further supported by earlier onset of climatic cooling shown by range retractions in warm water taxa at this locality, ~5-6 million years (myr) prior to their true extinction age.

These calcareous nannoplankton records document evolutionary and taxic change across these transient climatic events yet the response in calcareous nannoplankton at the EOT is more distinct than at the MECO. The minor response to the transient warming at the MECO may represent the nature of this event lying amidst the long term greenhouse to icehouse cooling trend. In contrast, extensive population restructuring and significant diversity loss occurred across the EOT, due to the high magnitude of surface water perturbation. These results imply a higher degree of environmental change was required to drive calcareous nannoplankton beyond a critical threshold.

8.3 Long time series

The detailed documentation of diversity change and palaeoecological response in the calcareous nannoplankton through the ~13 myr transition interval presented in this thesis provides the first record of this nature from the northern hemisphere at such high resolution. There are few records of long term diversity and population dynamics as work is typically focussed on intervals of critical climatic change, yet these background intervals represent vast periods within Earth's history and this thesis has attempted to establish the link between the calcareous nannoplankton response and changes to climatic and/or oceanographic parameters over long time series as well as key intervals of abrupt climatic change, discussed above.

The nature and timing of the diversity loss through the Paleogene has previously been poorly constrained due to the low resolution records available, but marks a key evolutionary event in calcareous nannoplankton history, with this group never fully recovering from long term diversity loss following the last interval of high diversity in the middle Eocene. At the Expedition 342 sites extremely high species richness undoubtedly reflects the exceptional standard of nannofossil preservation and the location of the sites mean a complete census of polar, temperate and tropical taxa are recorded. The diversity decline is documented at a higher resolution than previous compilations and this thesis endeavours to explain the relationship between nannoplankton and palaeoclimatic forcing which has been attributed to declining species richness (Chapter 6). A gradual loss in species richness is recorded, following maximum diversity in the middle Eocene (125 species), with accelerated loss from the EOT into the early Oligocene (49 species), driven by relatively high extinction rates and extremely low speciation rates which is reflected by the lowest diversification rates in the evolutionary history of the group, aside from the Cretaceous-Paleogene and Triassic-Jurassic boundary. This structure of diversity decline and the evolutionary rates from the Expedition 342 sites show a remarkable similarity to global compilations. The strong correlation demonstrated between climatic parameters (oxygen isotopes) and nannofossil species richness suggests abiotic forcing had a strong control on the declining diversity.

In addition to these records of diversity loss the middle Eocene to early Oligocene longer term population records display three broad intervals of assemblage response (Chapter 7); 1: Middle Eocene stability, with relatively constant nannofossil abundance records, 2: Late Eocene transitional phase, where there is high variability in all groups of taxa and 3: EOT and early Oligocene population restructuring, where there are profound assemblage shifts. The long time series of calcareous nannoplankton diversity and population data suggest strong ecological control on the assemblages through this interval, shown by selectivity of certain groups in response to the transition from a greenhouse into an icehouse world. These records show a gradually increasing response, not a stepwise change as previously proposed, suggesting environmental perturbation was intensifying through the interval, with severe climatic and oceanographic change from the EOT promoting the greatest evolutionary and ecological response in the calcareous nannoplankton. This phytoplankton group is therefore a useful proxy for documenting the onset of major surface ocean change.

8.4 Future work and concluding remarks

The research presented in this thesis is part of an ongoing project and will benefit from additional proxy data currently being generated by the IODP Expedition 342 shipboard and shore-based scientists. In particular, assemblage data for other plankton groups, high resolution isotope records, TEX_{86} and alkenone records, once available, will provide a complete synthesis of palaeobiotic and palaeoceanographic change in the North Atlantic through the Paleogene greenhouse to icehouse transition. The IODP Expedition 342 material is exemplary for research of this nature and in the future acquisition of similar high quality sections of stratigraphically complete, highly expanded sediments containing exceptionally well preserved microfossils from alternative oceanographic settings will further enhance our understanding of biotic response through intervals of severe climatic and oceanographic change.

The work presented in this thesis has addressed key evolutionary and ecological questions in Paleogene calcareous nannoplankton research, and has attempted to unravel the implications of transient and long term climatic and oceanographic perturbation on calcareous nannoplankton assemblages. The high resolution assemblage records presented here have detailed the structure and constrained the timing of the Paleogene diversity decline and population shifts and have given insight into potential environmental controls on the calcareous nannoplankton through this interval. Conclusions drawn in this thesis suggest that environmental perturbation beyond a critical threshold is required for nannofossil assemblages to display above background evolutionary response and major population shifts. This thesis provides a synthesis of nannofossil assemblage change in the North Atlantic, building on previous diversity and palaeoecological studies and laying the foundations for future research into diversity and population structure at high resolution using exceptionally preserved calcareous nannoplankton through the Paleogene greenhouse to icehouse transition.

References

Agnini, C., Fornaciari, E., Raffi, I., Catanzariti, R., Pälike, H., Backman, J., Rio, D., 2014. Biozonation and biochronology of Paleogene calcareous nannofossils from low and middle latitudes. Newsletters on Stratigraphy 47, 131–181. doi:10.1127/0078-0421/2014/0042

Anagnostou, E., John, E.H., Edgar, K.M., Foster, G.L., Ridgwell, A., Inglis, G.N., Pancost, R.D., Lunt, D.J., Pearson, P.N., 2016. Changing atmospheric CO_2 concentration was the primary driver of early Cenozoic climate. Nature 0, 1–19. doi:10.1038/nature17423

Aubry, M.-P., 1992. Late Paleogene calcareous nannoplankton evolution: a tale of climatic deterioration, in: Prothero, D.R., Berggren, W.A. (Eds.), Eocene-Oligocene Climatic and Biotic Evolution. Princeton University Press, Princeton, pp. 272–309.

Aubry, M.-P., 1984. Handbook of Cenozoic calcareous nannoplankton, Book 1: Ortholithae (Discoasters). Micropaleontology Press, American Museum of Natural History, New York, pp. 263.

Aubry, M.-P., Bord, D., 2009. Reshuffling the cards in the photic zone at the Eocene/Oligocene boundary. Geological Society of America Special Paper 452, 279–301. doi:10.1130/2009.2452(18)

Baba, C.C., 2014. The Middle Eocene Climatic Optimum at Site U1408 in the North Atlantic. Undergraduate thesis, University of California.

Backman, J., Hermelin, J.O.R., 1986. Morphometry of the Eocene nannofossil *Reticulofenestra umbilicus* lineage and its biochronological consequences. Palaeogeography Palaeoclimatology Palaeoecology 57, 103–116. doi:10.1016/0031-0182(86)90009-X

Bambach, R.K., 2006. Phanerozoic Biodiversity Mass Extinctions. Annual Review of Earth and Planetary Sciences 34, 127–155. doi:10.1146/annurev.earth.33.092203.122654

Beerling, D.J., Royer, D.L., 2011. Convergent Cenozoic CO_2 history. Nature Geoscience 4, 418–420. doi:10.1038/ngeo1186

Bijl, P.K., Houben, A.J.P., Schouten, S., Bohaty, S.M., Sluijs, A., Reichart, G.-J., Sinninghe Damsté, J.S., Brinkhuis, H., 2010. Transient Middle Eocene Atmospheric CO_2 and Temperature Variations. Science 330, 819–821.

Bijl, P.K., Schouten, S., Sluijs, A., Reichart, G.-J., Zachos, J.C., Brinkhuis, H., 2009. Early Palaeogene temperature evolution of the southwest Pacific Ocean. Nature 461, 776–779.

Blaj, T., Backman, J., Raffi, I., 2009. Late Eocene to Oligocene preservation history and biochronology of calcareous nannofossils from paleo-equatorial Pacific Ocean sediments. Rivista Italiana di Paleontologia e Stratigrafia (Research In Paleontology and Stratigraphy 115, 67-85. doi:10.13130/2039-4942/5920

Boersma, A., Premoli Silva, I., 1991. Distribution of Paleogene planktonic foraminifera - analogies with the Recent. Palaeogeography Palaeoclimatology Palaeoecology 83, 29–47. doi:10.1016/0031-0182(91)90074-2

Bohaty, S.M., Zachos, J.C., Delaney, M.L., 2012. Foraminiferal Mg/Ca evidence for Southern Ocean cooling across the Eocene-Oligocene transition. Earth and Planetary Science Letters 317-318, 251–261. doi: 10.1016/j.epsl.2011.11.037

Bohaty, S.M., Zachos, J.C., Florindo, F., Delaney, M.L., 2009. Coupled greenhouse warming and deep-sea acidification in the middle Eocene. Paleoceanography 24. doi:10.1029/2008PA001676

Bohaty, S.M., Zachos, J.C., 2003. Significant Southern Ocean warming event in the late middle Eocene. Geology 31, 1017–1020. doi:10.1130/G19800.1

Bordiga, M., Henderiks, J., Tori, F., Monechi, S., Fenero, R., Legarda-Lisarri, A., Thomas, E., 2015. Microfossil evidence for trophic changes during the Eocene-Oligocene transition in the South Atlantic (ODP Site 1263, Walvis Ridge). Climate of the Past 11, 1249–1270. doi:10.5194/cp-11-1249-2015

Boscolo Galazzo, F., Thomas, E., Pagani, M., Warren, C., Luciani, V., Giusberti, L.,

2014. The middle Eocene climatic optimum (MECO): A multiproxy record of paleoceanographic changes in the southeast Atlantic (ODP Site 1263, Walvis Ridge). Paleoceanography 29, 1143–1161. doi:10.1002/2014PA00267

Boscolo Galazzo, F., Giusberti, L., Luciani, V., Thomas, E., 2013. Paleoenvironmental changes during the Middle Eocene Climatic Optimum (MECO) and its aftermath: The benthic foraminiferal record from the Alano section (NE Italy). Palaeogeography Palaeoclimatology Palaeoecology 378, 22–35. doi:10.1016/j.palaeo.2013.03.018

Bown, P.R., 2005a. Palaeogene calcareous nannofossils from the Kilwa and Lindi areas of coastal Tanzania (Tanzania Drilling Project 2003-4). Journal of Nannoplankton Research 27, 21–95.

Bown, P.R., 2005b. Calcareous nannoplankton evolution: a tale of two oceans. Micropaleontology 51, 299–308. doi:10.2113/gsmicropal.51.4.299

Bown, P.R., 2005c. Early to mid-Cretaceous calcareous nannoplankton from the Northwest Pacific Ocean, Leg 198, Shatsky Rise. in: Bralower, T. J., Premoli Silva, I., Malone, M. J. (Eds.), Proceedings of the Ocean Drilling Program, Scientific Results 198.

Bown, P.R., Newsam, C., in review. Calcareous nannofossils from the Eocene North Atlantic Ocean (IODP Expedition 342 Sites U1403-1411). Journal of Nannoplankton Research.

Bown, P.R., Dunkley Jones, T., 2012. Calcareous nannofossils from the Paleogene equatorial Pacific (IODP Expedition 320 Sites U1331-1334). Journal of Nannoplankton Research 32, 3–51.

Bown, P., Pearson, P., 2009. Calcareous plankton evolution and the Paleocene/Eocene thermal maximum event: New evidence from Tanzania. Marine Micropaleontology 71, 60–70.

Bown, P.R., Dunkley Jones, T., Lees, J.A., Randell, R.D., Mizzi, J.A., Pearson, P.N., Coxall, H.K., Young, J.R., Nicholas, C.J., Karega, A., Singano, J., Wade, B.S., 2008. A Paleogene calcareous microfossil Konservat-Lagerstätte from the Kilwa

Group of coastal Tanzania. Geological Society of America Bulletin 120, 3–12. doi:10.1130/B26261.1

Bown, P. R., Jones, T. D., Young, J. R., 2007. *Umbilicosphaera jordanii* Bown, 2005 from the Paleogene of Tanzania: confirmation of generic assignment and a Paleocene origination for the Family Calcidiscaceae. Journal of Nannoplankton Research 29, 25–30.

Bown, P.R., Dunkley Jones, T., 2006. New Palaeogene calcareous nannofossil taxa from coastal Tanzania : Tanzania Drilling Project Sites 11 to 14. Journal of Nannoplankton Research 28, 17–34.

Bown, P.R., Lees, J.A., Young, J.R., 2004. Calcareous nannofossil evolution and diversity through time, in: Thierstein, H.R., Young, J.R. (Eds.), Coccolithophores: From Molecular Processes to Global Impact. Springer-Verlag, pp. 481–508.

Bown, P.R., Young, J.R., 1998. Techniques, in: Bown, P.R. (Ed.), Calcareous Nannofossil Biostratigraphy. Kluwer Academic, London, pp. 16–28.

Bown, P.R., Burnett, J.A., Gallagher, L.T., 1992. Calcareous nannofossil evolution. Memorie di Scienze Geologiche 43, 1–17.

Bralower, T.J., 2002. Evidence of surface water oligotrophy during the Paleocene-Eocene thermal maximum: Nannofossil assemblage data from Ocean Drilling Program Site 690, Maud Rise, Weddell Sea. Paleoceanography 17. doi:10.1029/2001PA000662

Broecker, W.S., 1991. The Great Ocean Conveyor. Oceanography 4, 79–89.

Bukry, D., 1975. Coccolith and silicoflagellate stratigraphy, Northwestern Pacific Ocean, Deep Sea Drilling Project Leg 32, in: Deep Sea Drilling Project Initial Reports. pp. 677–701. doi:10.2973/dsdp.proc.32.124.1975

Bukry, D., 1973. Coccolith and silicoflagellate stratigraphy, Tasman Sea and Southwestern Pacific Ocean, Deep Sea Drilling Project Leg 21, in: Deep Sea Drilling Project Initial Reports. pp. 885–893. doi:10.2973/dsdp.proc.21.127.1973

Cotton, L.J., Pearson, P.N., 2011. Extinction of larger benthic foraminifera at the Eocene/Oligocene boundary. Palaeogeography Palaeoclimatology Palaeoecology 311, 281–296. doi:10.1016/j.palaeo.2011.09.008

Coxall, H.K., Wilson, P.A., 2011. Early Oligocene glaciation and productivity in the eastern equatorial Pacific: Insights into global carbon cycling. Paleoceanography 26, doi:10.1029/2010PA002021

Coxall, H.K., Pearson, P.N., 2007. The Eocene-Oligocene transition, in: Williams, M., Hayward, A., Gregory, J., Schmidt, D.N. (Eds.), Deep Time Perspectives on Climate Change: Marrying the Signal from Computer Models and Biological Proxies. Geological Society Special Publication, pp. 351–387.

Coxall, H.K., Wilson, P.A., Pälike, H., Lear, C.H., Backman, J., 2005. Rapid stepwise onset of Antarctic glaciation and deeper calcite compensation in the Pacific Ocean. Nature 433, 53–57.

Cramer, B.S., Toggweiler, J.R., Wright, J.D., Katz, M.E., Miller, K.G., 2009. Ocean overturning since the Late Cretaceous: Inferences from a new benthic foraminiferal isotope compilation. Paleoceanography 24. doi:10.1029/2008PA001683

Davies, R., Cartwright, J., Pike, J., Line, C., 2001. Early Oligocene initiation of North Atlantic Deep Water formation. Nature 410, 917–920.

DeConto, R.M., Pollard, D., 2003a. Rapid Cenozoic glaciation of Antarctica induced by declining atmospheric CO_2. Nature 421, 245–249.

DeConto, R.M., Pollard, D., 2003b. A coupled climate-ice sheet modeling approach to the Early Cenozoic history of the Antarctic ice sheet. Palaeogeography Palaeoclimatology Palaeoecology 198, 39–52. doi:10.1016/S0031-0182(03)00393-6

Diester-Haass, L., Zachos, J., 2003. The Eocene-Oligocene Transition in the Equatorial Atlantic (ODP Site 925): Paleoproductivity Increase and Positive $\delta^{13}C$ Excursion, in: Prothero, D.R., Ivany, L.C., Nesbitt, E.A. (Eds.), From Greenhouse to Icehouse: The Marine Eocene-Oligocene Transition. Columbia University Press, New York, pp. 397–416.

Diester-Haass, L., 1995. Middle Eocene to early Oligocene paleoceanography of the Antarctic Ocean (Maud Rise, ODP Leg 113, Site 689): change from a low to a high productivity ocean. Palaeogeography Palaeoclimatology Palaeoecology 113, 311–334. doi:10.1016/0031-0182(95)00067-V

Dunkley Jones, T., Bown, P.R., Pearson, P.N., 2009. Exceptionally well preserved upper Eocene to lower Oligocene calcareous nannofossils (Prymnesiophyceae) from the Pande Formation (Kilwa Group), Tanzania. Journal of Systematic Palaeontology 7, 359–411. doi:10.1017/S1477201909990010

Dunkley Jones, T., 2008. The response of low-latitude calcareous phytoplankton to global change through the Eocene-Oligocene transition. PhD thesis, University College London.

Dunkley Jones, T., Bown, P.R., Pearson, P.N., Wade, B.S., Coxall, H.K., Lear, C.H., 2008. Major shifts in calcareous phytoplankton assemblages through the Eocene-Oligocene transition of Tanzania and their implications for low-latitude primary production. Paleoceanography 23. doi:10.1029/2008PA001640

Edgar, K.M., Bohaty, S.M., Gibbs, S.J., Sexton, P.F., Norris, R.D., Wilson, P.A., 2013. Symbiont “bleaching” in planktic foraminifera during the Middle Eocene Climatic Optimum. Geology 41, 15–18. doi:10.1130/G33388.1

Edgar, K.M., Wilson, P.A., Sexton, P.F., Gibbs, S.J., Roberts, A.P., Norris, R.D., 2010. New biostratigraphic, magnetostratigraphic and isotopic insights into the Middle Eocene Climatic Optimum in low latitudes. Palaeogeography Palaeoclimatology Palaeoecology 297, 670–682. doi:10.1016/j.palaeo.2010.09.016

Edgar, K.M., Wilson, P.A., Sexton, P.F., Suganuma, Y., 2007. No extreme bipolar glaciation during the main Eocene calcite compensation shift. Nature 448, 908–911. doi:10.1038/nature06053

Eldrett, J.S., Greenwood, D.R., Harding, I.C., Huber, M., 2009. Increased seasonality through the Eocene to Oligocene transition in northern high latitudes. Nature 459, 969–973.

Ezard, T.H.G., Aze, T., Pearson, P.N., Purvis, A., 2011. Interplay Between Changing

Climate and Species' Ecology Drives Macroevolutionary Dynamics. Science 332, 349–351.

Fioroni, C., Villa, G., Persico, D., Jovane, L., 2015. Middle Eocene-Lower Oligocene calcareous nannofossil biostratigraphy and paleoceanographic implications from Site 711 (equatorial Indian Ocean). Marine Micropaleontology 118, 50–62. doi:10.1016/j.marmicro.2015.06.001

Fornaciari, E., Agnini, C., Catanzariti, R., Rio, D., Bolla, E.M., Valvasoni, E., 2010. Mid-latitude calcareous nannofossil biostratigraphy and biochronology across the middle to late Eocene transition. Stratigraphy 7, 229–264.

Galeotti, S., Coccioni, R., Gersonde, R., 2002. Middle Eocene-Early Pliocene Subantarctic planktic foraminiferal biostratigraphy of Site 1090, Agulhas Ridge. Marine Micropaleontology 45, 357–381. doi:10.1016/S0377-8398(02)00035-X

Gibbs, S.J., Bown, P.R., Murphy, B.H., Sluijs, A., Edgar, K.M., Pälike, H., Bolton, C.T., Zachos, J.C., 2012. Scaled biotic disruption during early Eocene global warming events. Biogeosciences 9, 4679–4688. doi:10.5194/bg-9-4679-2012

Gibbs, S.J., Bralower, T.J., Bown, P.R., Zachos, J.C., Bybell, L.M., 2006. Shelf and open-ocean calcareous phytoplankton assemblages across the Paleocene-Eocene Thermal Maximum: Implications for global productivity gradients. Geology 34, 233–236. doi:10.1130/G22381.1

Gradstein, F.M., Ogg, J.G., Schmitz, M.D., Ogg, G.M. (Eds.), 2012. The Geologic Time Scale 2012. Elsevier, Amsterdam pp. 1144. doi:10.1016/B978-0-444-59425-9.01001-5

Hallock, P., Premoli Silva, I., Boersma, A., 1991. Similarities between planktonic and larger foraminiferal evolutionary trends through Paleogene paleoceanographic changes. Palaeogeography Palaeoclimatology Palaeoecology 83, 49–64. doi:10.1016/0031-0182(91)90075-3

Haq, B.U., Lohmann, G.P., Wise Jr., S.W., 1977. Calcareous nannoplankton biogeography and its paleoclimate implications: Cenozoic of the Falkland Plateau (DSDP Leg 36) and Miocene of the Atlantic Ocean, in: Deep Sea Drilling Project

Initial Reports. pp. 745–760. doi:10.2973/dsdp.proc.36.114.1977

Haq, B.U., Lohmann, G.P., 1976. Early Cenozoic calcareous nannoplankton biogeography of the Atlantic Ocean. Marine Micropaleontology 1, 119–194. doi:10.1016/0377-8398(76)90008-6

Henderiks, J., Pagani, M., 2008. Coccolithophore cell size and the Paleogene decline in atmospheric CO_2. Earth and Planetary Science Letters 269, 575–583. doi:10.1016/j.epsl.2008.03.016

Hohbein, M.W., Sexton, P.F., Cartwright, J.A., 2012. Onset of North Atlantic Deep Water production coincident with inception of the Cenozoic global cooling trend. Geology 40, 255–258. doi:10.1130/G32461.1

Holland, S.M., 2008. Non-metric Multidimensional Scaling (MDS). R Manual, pp.7.

Houben, A.J.P., Bijl, P.K., Pross, J., Bohaty, S.M., Passchier, S., Stickley, C.E., Röhl, U., Sugisaki, S., Tauxe, L., van de Flierdt, T., Olney, M., Sangiorgi, F., Sluijs, A., Escutia, C., Brinkhuis, H., Scientists, E. 318, 2013. Reorganization of Southern Ocean Plankton Ecosystem at the Onset of Antarctic Glaciation. Science 340, 341–344. doi:10.1126/science.1223646

Hull, P., 2015. Life in the Aftermath of Mass Extinctions. Current Biology Review 25, 941–952. doi:10.1016/j.cub.2015.08.053

Inglis, G.N., Farnsworth, A., Lunt, D., Foster, G.L., Hollis, C.J., Pagani, M., Jardine, P.E., Pearson, P.N., Markwick, P., Galsworthy, A.M.J., Raynham, L., Taylor, K.W.R., Pancost, R.D., 2015. Descent toward the Icehouse: Eocene sea surface cooling inferred from GDGT distributions. Paleoceanography 30, 1000–1020. doi:10.1002/2014PA002723

Ivany, L.C., Patterson, W.P., Lohmann, K.C., 2000. Cooler winters as a possible cause of mass extinctions at the Eocene/Oligocene boundary. Nature 407, 887–890. doi:10.1038/35038044

Kamikuri, S., Moore, T.C., Ogane, K., Suzuki, N., Pälike, H., Nishi, H., 2012. Early Eocene to early Miocene radiolarian biostratigraphy for the low-latitude Pacific

Ocean. Stratigraphy 9, 77–108.

Kamikuri, S., Wade, B.S., 2012. Radiolarian magnetobiochronology and faunal turnover across the middle/late Eocene boundary at Ocean Drilling Program Site 1052 in the western North Atlantic Ocean. Marine Micropaleontology 88-89, 41–53. doi:10.1016/j.marmicro.2012.03.001

Katz, M.E., Cramer, B.S., Toggweiler, J.R., Esmay, G., Liu, C., Miller, K.G., Rosenthal, Y., Wade, B.S., Wright, J.D., 2011. Impact of Antarctic Circumpolar Current development on late Paleogene ocean structure. Science 332, 1076–1079. doi:10.1126/science.1202122

Katz, M.E., Miller, K.G., Wright, J.D., Wade, B.S., Browning, J. V, Cramer, B.S., Rosenthal, Y., 2008. Stepwise transition from the Eocene greenhouse to the Oligocene icehouse. Nature Geoscience 1, 329–334.

Keller, G., 1986. Stepwise mass extinctions and impact events: Late Eocene to early Oligocene. Marine Micropaleontology 10, 267–293. doi:10.1016/0377-8398(86)90032-0

Kennett, J.P., 1977. Cenozoic Evolution of Antarctic Glaciation, the Circum-Antarctic Ocean, and Their Impact on Global Paleoceanography. Journal of Geophysical Research 82, 3843–3860.

Knoll, A.H., 1989. Evolution and Extinction in the Marine Realm: Some Constraints Imposed by Phytoplankton. Philosophical Transactions of the Royal Society 325, 279–290.

Lazarus, D., Barron, J., Renaudie, J., Diver, P., Türke, A., 2014. Cenozoic planktonic marine diatom diversity and correlation to climate change. PLoS One 9. doi:10.1371/journal.pone.0084857

Lear, C.H., Bailey, T.R., Pearson, P.N., Coxall, H.K., Rosenthal, Y., 2008. Cooling and ice growth across the Eocene-Oligocene transition. Geology 36, 251–254. doi:10.1130/G24584A.1

Lear, C.H., Elderfield, H., Wilson, P.A., 2000. Cenozoic Deep-Sea Temperatures and

Global Ice Volumes from Mg/Ca in Benthic Foraminiferal Calcite. Science 287, 269–272.

Lipps, J.H., 1970. Plankton Evolution. Evolution 24, 1–22.

Liu, Z., Pagani, M., Zinniker, D., DeConto, R., Huber, M., Brinkhuis, H., Shah, S.R., Leckie, R.M., Pearson, A., 2009. Global Cooling During the Eocene-Oligocene Climate Transition. Science 323, 1187–1190. doi:10.1126/science.1166368

Liu, Z., Tuo, S., Zhao, Q., Cheng, X., Huang, W., 2004. Deep-water Earliest Oligocene Glacial Maximum (EOGM) in South Atlantic. Chinese Science Bulletin 49, 2190. doi:10.1360/04wd0228

Luciani, V., Giusberti, L., Agnini, C., Fornaciari, E., Rio, D., Spofforth, D.J.A., Pälike, H., 2010. Ecological and evolutionary response of Tethyan planktonic foraminifera to the middle Eocene climatic optimum (MECO) from the Alano section (NE Italy). Palaeogeography Palaeoclimatology Palaeoecology 292, 82–95. doi:10.1016/j.palaeo.2010.03.029

Magurran, A.E., 2004. Measuring Biological Diversity. Blackwell Science Ltd, Oxford, pp.256.

Martini, E., 1971. Standard Tertiary and Quaternary calcareous nannoplankton zonation, in: Farinacci, A. (Ed.), Proceedings of the Second Planktonic Conference, Roma, 1970. Edizioni Tecnoscienza, Rome, pp. 739–785.

McCune, B., Grace, J.B., 2002. Analysis of Ecological Communities. MjM Software Design, Gleneden Beach, Oregon, pp.300.

McIntyre, A., Bé, A.W.H., 1967. Modern coccolithophoridae of the Atlantic Ocean—I. Placoliths and cyrtoliths. Deep Sea Research 14, 561–597. doi:10.1016/0011-7471(67)90065-4

Miller, K.G., Wright, J.D., Katz, M.E., Wade, B.S., Browning, J. V, Cramer, B.S., Rosenthal, Y., 2009. Climate threshold at the Eocene-Oligocene transition: Antarctic ice sheet influence on ocean circulation. Geological Society of America Special Paper 452, 169–178. doi:10.1130/2009.2452(11)

Miller, K.G., Wright, J.D., Fairbanks, R.G., 1991. Unlocking the Ice House: Oligocene-Miocene oxygen isotopes, eustasy, and margin erosion. Journal of Geophysical Research Solid Earth 96, 6829–6848. doi:10.1029/90JB02015

Moebius, I., Friedrich, O., Edgar, K.M., Sexton, P.F., 2015. Episodes of intensified biological productivity in the subtropical Atlantic Ocean during the termination of the Middle Eocene Climatic Optimum (MECO). Paleoceanography 30, 1041–1058. doi:10.1002/2014PA002673

Moebius, I., Friedrich, O., Scher, H.D., 2014. Changes in Southern Ocean bottom water environments associated with the Middle Eocene Climatic Optimum (MECO). Palaeogeography Palaeoclimatology Palaeoecology 405, 16–27. doi:10.1016/j.palaeo.2014.04.004

Monechi, S., Buccianti, A., Gardin, S., 2000. Biotic signals from nannoflora across the iridium anomaly in the upper Eocene of the Massignano section: evidence from statistical analysis. Marine Micropaleontology 39, 219–237. doi:10.1016/S0377-8398(00)00022-0

Moore, T.C., Kamikuri, S., Erhardt, A.M., Baldauf, J., Coxall, H.K., Westerhold, T., 2015. Radiolarian stratigraphy near the Eocene–Oligocene boundary. Marine Micropaleontology 116, 50–62. doi:10.1016/j.marmicro.2015.02.002

Moore, T.C., Wade, B.S., Westerhold, T., Erhardt, A.M., Coxall, H.K., Baldauf, J., Wagner, M., 2014. Equatorial Pacific productivity changes near the Eocene-Oligocene boundary. Paleoceanography 29, 825–844. doi:10.1002/2014PA002656

Nannotax. Young, J.R. Bown P.R. Lees J.A. (Eds.), Nannotax3 website. International Nannoplankton Association. URL: http://ina.tmsoc.org/Nannotax3

Newsam, C., Bown, P.R., Wade, B.S., Jones, H.L., in press. Muted calcareous nannoplankton response at the Middle/Late Eocene Turnover event in the western North Atlantic Ocean. Newsletters on Stratigraphy.

Nocchi, M., Parisi, G., Monaco, P., Monechi, S., Madile, M., 1988. Eocene and early Oligocene micropaleontology and paleoenvironments in SE Umbria, Italy. Palaeogeography Palaeoclimatology Palaeoecology 67, 181–244.

doi:10.1016/0031-0182(88)90154-X

Norris, R.D., Wilson, P.A., Blum, P., Scientists, E. 342, 2014. Paleogene Newfoundland Sediment Drifts and MDHDS Test, in: Proceedings of the Integrated Ocean Drilling Program, 342: College Station, TX (Integrated Ocean Drilling Program). doi:10.2204/iodp.proc.342.2014

Ocean Drilling Stratigraphic Network. GEOMAR Research Center for Marine Geosciences. URL: www.odsn.de

O'Dea, S.A., 2013. Calcareous nannoplankton responses to early Paleogene climate change. PhD thesis, University of Southampton.

Okada, H., Bukry, D., 1980. Supplementary modification and introduction of code numbers to the low-latitude coccolith biostratigraphic zonation (Bukry, 1973; 1975). Marine Micropaleontology 5, 321–325. doi:10.1016/0377-8398(80)90016-X

Okada, H., Honjo, S., 1973. The distribution of oceanic coccolithophorids in the Pacific. Deep Sea Research 20, 355–374. doi:10.1016/0011-7471(73)90059-4

Pagani, M., Huber, M., Liu, Z., Bohaty, S.M., Henderiks, J., Sijp, W., Krishnan, S., DeConto, R.M., 2011. The Role of Carbon Dioxide During the Onset of Antarctic Glaciation. Science 334, 1261–1264.

Pagani, M., Zachos, J.C., Freeman, K.H., Tipple, B., Bohaty, S.M., 2005. Marked Decline in Atmospheric Carbon Dioxide Concentrations During the Paleogene. Science 309, 600–603.

Pälike, H., Lyle, M.W., Nishi, H., Raffi, I., Ridgwell, A., Gamage, K., Klaus, A., Acton, G., Anderson, L., Backman, J., Baldauf, J., Beltran, C., Bohaty, S.M., BownPaul, Busch, W., Channell, J.E.T., Chun, C.O.J., Delaney, M., Dewangan, P., Dunkley Jones, T., Edgar, K.M., Evans, H., Fitch, P., Foster, G.L., Gussone, N., Hasegawa, H., Hathorne, E.C., Hayashi, H., Herrle, J.O., Holbourn, A., Hovan, S., Hyeong, K., Iijima, K., Ito, T., Kamikuri, S., Kimoto, K., Kuroda, J., Leon-Rodriguez, L., Malinverno, A., Moore Jr, T.C., Murphy, B.H., Murphy, D.P., Nakamura, H., Ogane, K., Ohneiser, C., Richter, C., Robinson, R., Rohling, E.J., Romero, O., Sawada, K., Scher, H., Schneider, L., Sluijs, A., Takata, H., Tian, J., Tsujimoto, A., Wade, B.S., Westerhold, T., Wilkens, R., Williams, T., Wilson, P.A., Yamamoto, Y., Yamamoto, S., Yamazaki, T., Zeebe, R.E., 2012. A Cenozoic record of the equatorial Pacific carbonate compensation depth. Nature 488, 609–614.

Pälike, H., Norris, R.D., Herrle, J.O., Wilson, P.A., Coxall, H.K., Lear, C.H., Shackleton, N.J., Tripati, A.K., Wade, B.S., 2006. The Heartbeat of the Oligocene Climate System. Science 314, 1894–1898.

Palter, J.B., Lozier, M.S., 2008. On the source of Gulf Stream nutrients. Journal of Geophysical Research 113. doi:10.1029/2007JC004611

Pea, L., 2010. Eocene-Oligocene paleoceanography of the Subantarctic South Atlantic: Calcareous nannofossil reconstructions of temperature, nutrient and dissolution history. PhD thesis, University of Parma.

Pearson, P.N., Foster, G.L., Wade, B.S., 2009. Atmospheric carbon dioxide through the Eocene–Oligocene climate transition. Nature 461, 1110–1113.

Pearson, P.N., McMillan, I.K., Wade, B.S., Jones, T.D., Coxall, H.K., Bown, P.R., Lear, C.H., 2008. Extinction and environmental change across the Eocene-Oligocene boundary in Tanzania. Geology 36, 179–182. doi:10.1130/G24308A.1

Pearson, P.N., van Dongen, B.E., Nicholas, C.J., Pancost, R.D., Schouten, S., Singano, J.M., Wade, B.S., 2007. Stable warm tropical climate through the Eocene Epoch. Geology 35, 211–214. doi:10.1130/G23175A.1

Pearson, P.N., Ditchfield, P.W., Singano, J., Harcourt-Brown, K.G., Nicholas, C.J., Olsson, R.K., Shackleton, N.J., Hall, M.A., 2001. Warm tropical sea surface temperatures in the Late Cretaceous and Eocene epochs. Nature 413, 481–487.

Pelegrí, J.L., Csanady, G.T., Martins, A., 1996. The North Atlantic nutrient stream. Journal of Oceanography 52, 275–299. doi:10.1007/BF02235924

Perch-Nielsen, K., 1985. Cenozoic calcareous nannofossils, in: Bolli, H.M., Saunders, J.B., Perch-Nielsen, K. (Eds.), Plankton Stratigraphy. Cambridge University Press, Cambridge, pp. 427–554.

Persico, D., Fioroni, C., Villa, G., 2012. A refined calcareous nannofossil biostratigraphy for the middle Eocene-early Oligocene Southern Ocean ODP sites. Palaeogeography Palaeoclimatology Palaeoecology 335-336, 12–23.

Persico, D., Villa, G., 2008. A new Eocene Chiasmolithus species: hypothetical reconstruction of its phyletic lineage. Journal of Nannoplankton Research 30, 23–33.

Persico, D., Villa, G., 2004. Eocene–Oligocene calcareous nannofossils from Maud Rise and Kerguelen Plateau (Antarctica): paleoecological and paleoceanographic implications. Marine Micropaleontology 52, 153–179. doi:10.1016/j.marmicro.2004.05.002

Pinet, P.R., Popenoe, P., Nelligan, D.F., 1981. Gulf Stream: Reconstruction of Cenozoic flow patterns over the Blake Plateau. Geology 9, 266–270. doi:10.1130/0091-7613(1981)9<266:GSROCF>2.0.CO;2

Plancq, J., Mattioli, E., Pittet, B., Simon, L., Grossi, V., 2014. Productivity and sea-surface temperature changes recorded during the late Eocene-early Oligocene at DSDP Site 511 (South Atlantic). Palaeogeography Palaeoclimatology Palaeoecology 407, 34–44. doi:10.1016/j.palaeo.2014.04.016

Premoli Silva, I., Jenkins, D.G., 1993. Decision on the Eocene-Oligocene boundary stratotype. Episodes 16, 379–382.

Rabosky, D.L., Sorhannus, U., 2009. Diversity dynamics of marine planktonic diatoms across the Cenozoic. Nature 457, 183–186.

Roth, P.H., 1994. Distribution of coccoliths in oceanic sediments, in: Winter, A., Siesser, W.G. (Eds.), Coccolithophores. Cambridge University Press, Cambridge, pp. 199–218.

Salamy, K.A., Zachos, J.C., 1999. Latest Eocene–Early Oligocene climate change and Southern Ocean fertility: inferences from sediment accumulation and stable isotope data. Palaeogeography Palaeoclimatology Palaeoecology 145, 61–77. doi:10.1016/S0031-0182(98)00093-5

Scher, H.D., Whittaker, J.M., Williams, S.E., Latimer, J.C., Kordesch, W.E.C., Delaney, M.L., 2015. Onset of Antarctic Circumpolar Current 30 million years ago as Tasmanian Gateway aligned with westerlies. Nature 523, 580–583.

Scher, H.D., Bohaty, S.M., Smith, B.W., Munn, G.H., 2014. Isotopic interrogation of a suspected late Eocene glaciation. Paleoceanography 29, 628–644. doi:10.1002/2014PA002648

Scher, H.D., Bohaty, S.M., Zachos, J.C., Delaney, M.L., 2011. Two-stepping into the icehouse: East Antarctic weathering during progressive ice-sheet expansion at the Eocene-Oligocene transition. Geology 39, 383–386. doi:10.1130/G31726.1

Scher, H.D., Martin, E.E., 2006. Timing and Climatic Consequences of the Opening of Drake Passage. Science 312, 428–430.

Schneider, L.J., Bralower, T.J., Kump, L.R., Patzkowsky, M.E., 2013. Calcareous nannoplankton ecology and community change across the Paleocene-Eocene Thermal Maximum. Paleobiology 39, 628–647. doi:10.1666/12050

Schneider, L.J., Bralower, T.J., Kump, L.R., 2011. Response of nannoplankton to early Eocene ocean destratification. Palaeogeography Palaeoclimatology Palaeoecology 310, 152–162. doi:10.1016/j.palaeo.2011.06.018

Sepkoski, J.J., 1986. Phanerozoic Overview of Mass Extinction, in: Raup, D.M., Jablonski, D. (Eds.), Patterns and Processes in the History of Life. Springer-Verlag, Berlin, pp. 277–295. doi:10.1017/CBO9781107415324.004

Sexton, P.F., Norris, R.D., Wilson, P.A., Pälike, H., Westerhold, T., Rohl, U., Bolton, C.T., Gibbs, S., 2011. Eocene global warming events driven by ventilation of oceanic dissolved organic carbon. Nature 471, 349–352.

Sexton, P.F., Wilson, P.A., Norris, R.D., 2006. Testing the Cenozoic multisite composite δ^{18}O and δ^{13}C curves: New monospecific Eocene records from a single locality, Demerara Rise (Ocean Drilling Program Leg 207). Paleoceanography 21. doi:10.1029/2005PA001253

Shamrock, J.L., Watkins, D.K., 2012. Eocene calcareous nannofossil biostratigraphy and community structure from Exmouth Plateau, Eastern Indian Ocean (ODP Site 762). Stratigraphy 9, 1–54.

Sijp, W.P., von der Heydt, A.S., Dijkstra, H.A., Flögel, S., Douglas, P.M.J., Bijl, P.K., 2014. The role of ocean gateways on cooling climate on long time scales. Global and Planetary Change 119, 1–22. doi:10.1016/j.gloplacha.2014.04.004

Sluijs, A., Zeebe, R.E., Bijl, P.K., Bohaty, S.M., 2013. A middle Eocene carbon cycle conundrum. Nature Geoscience 6, 429–434.

Spencer-Cervato, C., 1999. The Cenozoic Deep Sea Microfossil Record: Explorations of the DSDP/ODP Sample Set Using the Neptune Database. Palaeontologica Electronica 2.

Theodoridis, S., 1984. Calcareous nannofossil biozonation of the Miocene and revision of the helicoliths and discoasters. Utrecht Micropaleontological Bulletins 32, 1–271.

Thomas, D.J., Zachos, J.C., Bralower, T.J., Thomas, E., Bohaty, S.M., 2002. Warming the fuel for the fire : Evidence for the thermal dissociation of methane hydrate during the Paleocene-Eocene thermal maximum. Geology 30, 1067–1070. doi:10.1130/0091-7613(2002)030<1067:WTFFTF>2.0.CO;2

Toffanin, F., Agnini, C., Fornaciari, E., Rio, D., Giusberti, L., Luciani, V., Spofforth, D.J.A., Pälike, H., 2011. Changes in calcareous nannofossil assemblages during the Middle Eocene Climatic Optimum: Clues from the central-western Tethys (Alano section, NE Italy). Marine Micropaleontology 81, 22–31. doi:10.1016/j.marmicro.2011.07.002

Tremolada, F., Bralower, T.J., 2004. Nannofossil assemblage fluctuations during the Paleocene–Eocene Thermal Maximum at Sites 213 (Indian Ocean) and 401 (North Atlantic Ocean): palaeoceanographic implications. Marine Micropaleontology 52, 107–116. doi:10.1016/j.marmicro.2004.04.002

Tripati, A., Backman, J., Elderfield, H., Ferretti, P., 2005. Eocene bipolar glaciation associated with global carbon cycle changes. Nature 436, 341–346.

Varol, O., 1998. Palaeogene, in: Bown, P.R. (Ed.), Calcareous Nannofossil Biostratigraphy. Kluwer Academic, London, pp. 200–224.

Via, R.K., Thomas, D.J., 2006. Evolution of Atlantic thermohaline circulation: Early Oligocene onset of deep-water production in the North Atlantic. Geology 34, 441–444. doi:10.1130/G22545.1

Villa, G., Fioroni, C., Persico, D., Roberts, A.P., Florindo, F., 2014. Middle Eocene to Late Oligocene Antarctic glaciation/deglaciation and Southern Ocean productivity. Paleoceanography 29, 223–237. doi:10.1002/2013PA002518

Villa, G., Fioroni, C., Pea, L., Bohaty, S., Persico, D., 2008. Middle Eocene–late Oligocene climate variability: Calcareous nannofossil response at Kerguelen Plateau, Site 748. Marine Micropaleontology 69, 173–192. doi:10.1016/j.marmicro.2008.07.006

Vonhof, H.B., Smit, J., Brinkhuis, H., Montanari, A., Nederbragt, A.J., 2000. Global cooling accelerated by early late Eocene impacts? Geology 28, 687–690.

Wade, B.S., 2004. Planktonic foraminiferal biostratigraphy and mechanisms in the extinction of *Morozovella* in the late middle Eocene. Marine Micropaleontology 51, 23–38. doi:10.1016/j.marmicro.2003.09.001

Wade, B.S., Houben, A.J.P., Quaijtaal, W., Schouten, S., Rosenthal, Y., Miller, K.G., Katz, M.E., Wright, J.D., Brinkhuis, H., 2012. Multiproxy record of abrupt sea-surface cooling across the Eocene-Oligocene transition in the Gulf of Mexico. Geology 40, 159–162.

Wade, B.S., Pearson, P.N., 2008. Planktonic foraminiferal turnover, diversity fluctuations and geochemical signals across the Eocene/Oligocene boundary in Tanzania. Marine Micropaleontology 68, 244–255. doi:10.1016/j.marmicro.2008.04.002

Wade, B.S., Bown, P.R., 2006. Calcareous nannofossils in extreme environments: The Messinian Salinity Crisis, Polemi Basin, Cyprus. Palaeogeography Palaeoclimatology Palaeoecology 233, 271–286. doi:10.1016/j.palaeo.2005.10.007

Wei, W., Villa, G., Wise, S.W., 1992. Paleoceanographic implications of Eocene-Oligocene calcareous nannofossils from Sites 711 and 748 in the Indian Ocean, in: Proceedings of the Ocean Drilling Program, Scientific Results. pp. 979–999.

Wei, W., Wise, S.W., 1990. Biogeographic gradients of middle Eocene-Oligocene calcareous nannoplankton in the South Atlantic Ocean. Palaeogeography Palaeoclimatology Palaeoecology 79, 29–61. doi:10.1016/0031-0182(90)90104-F

Westerhold, T., Röhl, U., Pälike, H., Wilkens, R., Wilson, P.A., Acton, G., 2014. Orbitally tuned timescale and astronomical forcing in the middle Eocene to early Oligocene. Climate of the Past 10, 955–973. doi:10.5194/cp-10-955-2014

Winter, A., Jordan, R.W., Roth, P.H., 1994. Biogeography of living coccolithophores in ocean waters, in: Winter, A., Siesser, W.G. (Eds.), Coccolithophores. Cambridge University Press, Cambridge, pp. 161–178.

Witkowski, J., Bohaty, S.M., Edgar, K.M., Harwood, D.M., 2014. Rapid fluctuations in mid-latitude siliceous plankton production during the Middle Eocene Climatic Optimum (ODP Site 1051, western North Atlantic). Marine Micropaleontology 106, 110–129. doi:10.1016/j.marmicro.2014.01.001

Witkowski, J., Bohaty, S.M., McCartney, K., Harwood, D.M., 2012. Enhanced siliceous plankton productivity in response to middle Eocene warming at Southern Ocean ODP Sites 748 and 749. Palaeogeography Palaeoclimatology Palaeoecology 326, 78–94. doi:10.1016/j.palaeo.2012.02.006

Young, J.R., Geisen, M.P.I., Probert, I., 2005. A review of selected aspects of coccolithophore biology with implications for paleobiodiversity estimation. Micropaleontology 51, 267–288. doi:10.2113/gsmicropal.51.4.267

Young, J.R., Geisen, M., Cros, L., Kleijne, a, Sprengel, C., Probert, I., Østergaard, J., 2003. A guide to extant coccolithophore taxonomy. Journal of Nannoplankton Research Special Issue, pp.125.

Young, J.R., Bergen, J.A., Bown, P.R., Burnett, J.A., Fiorentino, A., Jordan, R.W., Kleijne, A., Van Niel, B.E., Romein, A.J.T., Von Salis, K., 1997. Guidelines for coccolith and calcareous nannofossil terminology. Palaeontology 40, 875–912.

Young, J.R., Bown, P.R., 1997. Cenozoic calcareous nannoplankton classification. Journal of Nannoplankton Research 19, 36–47.

Zachos, J.C., Dickens, G.R., Zeebe, R.E., 2008. An early Cenozoic perspective on greenhouse warming and carbon-cycle dynamics. Nature 451, 279–283.

Zachos, J.C., Röhl, U., Schellenberg, S.A., Sluijs, A., Hodell, D.A., Kelly, D.C., Thomas, E., Nicolo, M., Raffi, I., Lourens, L.J., McCarren, H., Kroon, D., 2005. Rapid Acidification of the Ocean During the Paleocene-Eocene Thermal Maximum. Science 308, 1611–1615.

Zachos, J., Pagani, M., Sloan, L., Thomas, E., Billups, K., 2001. Trends, Rhythms, and Aberrations in Global Climate 65 Ma to Present. Science 292, 686–693.

Zachos, J.C., Quinn, T.M., Salamy, K.A., 1996. High-resolution (10^4 years) deep-sea foraminiferal stable isotope records of the Eocene-Oligocene climate transition. Paleoceanography 11, 251–266. doi:10.1029/96PA00571

Zeebe, R.E., Ridgwell, A., Zachos, J.C., 2016. Anthropogenic carbon release rate unprecedented during the past 66 million years. Nature Geoscience 9, 325–329.